ELECTROLUMINESCENT DISPLAYS BY SOL-GEL PROCESS

A thesis for the degree of Ph.D.

Presented to

DUBLIN CITY UNIVERSITY

BY

WENHUI. TANG, M. Eng.

SCHOOL OF ELECTRONIC ENGINEERING
DUBLIN CITY UNIVERSITY

RESEARCH SUPERVISOR

DR. DAVID C. CAMERON

TO

DAD, MUM

WIFE

BROTHER

DECLARATION

I hereby certify that this material, which I now submit for assessment on the programme of study leading to the award of Ph. D. is entirely my own work and has not been taken from the work of others save and to the extent that such work has been cited and acknowledged within the text of my work.

Signed: Tong Wenhui 唐文晖

Date: August 2, 1994.

CONTENTS

ACKNOWLEDGEMENTS VI
ABSTRACT VII

Chapter 1

INTRODUCTION

1.1 Displays 1
1.1.1 Electroluminescent Displays 1
1.1.2 Cathodoluminescent Displays 2
1.1.3 Cathode Ray Tube 2
1.1.4 Vacuum Fluorescent Displays 3
1.1.5 Plasma Displays 4
1.1.6 Light Emitting Diode 5
1.1.7 Liquid Crystal Displays 6
1.1.8 Electrochromic Displays 8
1.1.9 Electrophoretic Displays 8
1.1.10 Other Displays 8
1.1.11 Trend of Colour Displays 9
1.2 Comparison of Different Type Displays 10
1.2.1 Display Brightness 10
1.2.2 Display Operating Voltage 11
1.2.3 Resolution 11
1.2.4 Speed 11
1.2.5 Display Power Consumption 13
1.2.6 Operating Temperature Range 13
1.2.7 Visual Angle 14
1.2.8 Maximum Screen Size 14
1.2.9 Longevity 14
1.2.10 Efficiency 16
1.2.11 Driver 16
1.3 Electroluminescent Displays 17
1.3.1 Developing History of EL Displays 17
1.3.2 Current Status of EL Displays 20
1.3.3 Advantage of EL Displays Compare to Other Displays 23
1.3.4 Development of EL Displays in Future 24
1.4 Deposition Technology of Thin Films 25
1.4.1 Chemical Methods 25

1.4.1.1 Chemical Vapour Deposition 25
1.4.1.2 Spray Pyrolysis 26
1.4.2 Physical Methods 27
1.4.2.1 Evaporation 27
1.4.2.2 Sputtering 28
1.4.2.3 Reactive Ion Plating 30
1.5 Major Parameters and Characteristics of Thin Films 30
1.6 Objectives of the Project 32

Chapter 2

SOL-GEL TECHNOLOGY

2.1 Introduction 34
2.1.1 Historical Development of Sol-gel Science 34
2.2 Applications of Sol-gel Process 35
2.3 Theory of Sol-gel Process 39
2.3.1 Hydrolysis and Condensation 39
2.3.2 Gelation 41
2.3.3 Aging of Gels 42
2.3.4 Drying of Gels 42
2.3.5 Avoiding Fracture 43
2.3.6 Structural Evolution during Consolidation 44
2.3.7 Sintering of Gel 44
2.4 Film Formation 45
2.4.1 Physics of Film Formation 45
2.4.1.1 Dip Coating 45
2.4.1.2 Spin Coating 46
2.4.2 Precursor Structure 47
2.4.3 Deposition Conditions 47

Chapter 3

MEASUREMENTS OF THIN FILM CHARACTERISTICS

3.1 Introduction 49
3.2 Measurement of Thickness 51
3.2.1 Methods Using Interference Fringes of Equal Thickness 51
3.2.2 Ellipsometric Method 53
3.3 Measurement of Infrared 59
3.4 Measurement with Scanning Electron Microscopy 61
3.5 Measurement with Electron Microprobe 62
3.6 Measurement of Thin Film Photoluminescence 65
3.7 Electrical Measurement 67
3.7.1 Resistivity Measurement of Thin Films 68

3.7.2 Hall Effect and Carrier Concentration . . . 74
3.7.3 Conductivity Mobility . . . 75
3.7.4 Hall Effect and Mobility . . . 75
3.8 Measurement of Transmittance . . . 77
3.9 Measurement of X-ray Diffraction . . . 78
3.10 Measurements of Electroluminescence . . . 79
3.10.1 Measurement of Brightness . . . 79
3.10.2 Measurement of Optical Spectrum . . . 80
3.10.3 Measurement of Optical Output of EL Device . . . 80

Chapter 4

PHOSPHOR FILMS

4.1 Introduction . . . 82
4.2 Requirement of Luminescent Materials . . . 83
4.2.1 Choice of the Host Components . . . 84
4.2.2 Choice of the Activator . . . 85
4.2.3 Quenchers, or "Killers" of Luminescence . . . 85
4.3 Phosphor Materials . . . 86
4.3.1 Properties of Host Materials . . . 86
4.3.2 Some Properties of Host Phosphor ZnS . . . 89
4.3.3 Transition Metal Ions Mn^{2+} . . . 89
4.3.4 Rare Earth Ions . . . 92
4.3.5 Rare Earth Ions Tb^{3+} . . . 94
4.4 Relationship between Photoluminescence and Electroluminescence . . . 95

Chapter 5

BASIC SOL-GEL FILM DEPOSITION AND CHARACTERISTICS

5.1 Introduction . . . 97
5.2 ZnO Films Deposited Using the Sol-Gel Technology . . . 98
5.2.1 Experimental Procedure . . . 98
5.2.1.1 Solution Preparation . . . 98
5.2.1.2 Deposition Procedure . . . 99
5.2.2 Optical Measurements and Characteristics . . . 100
5.2.3 Electrical Measurements and Characteristics . . . 104
5.3 SiO_2 Films Deposited Using the Sol-gel Process . . . 109
5.3.1 Experimental Preparation of SiO_2 Films . . . 111
5.4 Al_2O_3 Films Deposited by the Sol-gel Process . . . 112
5.4.1 Experimental Preparation of Al_2O_3 Films . . . 113
5.5 Conclusions . . . 114

Chapter 6

TRANSPARENT CONDUCTING FILMS

6.1 Introduction 116
6.1.1 Tin Oxide 117
6.1.2 Indium Oxide 118
6.1.3 Zinc Oxide 119
6.2 Deposition of ZnO:Al Films 120
6.2.1 Introduction 120
6.2.2 Experiment Procedure 121
6.3 Structural Properties of ZnO:Al Films 122
6.4 Optical Properties of ZnO:Al Films 123
6.4.1 Optical Theory 123
6.4.2 Optical Properties 126
6.5 Electrical Properties of ZnO:Al Films 128
6.5.1 Electrical Theory 128
6.5.2 Electrical Properties 130
6.6 Conclusions 135

Chapter 7

LUMINESCENT FILMS

7.1 ZnS:Mn Phosphor Films 136
7.1.1 Deposition of ZnS:Mn Films 137
7.1.2 Characteristics of ZnS:Mn films 138
7.2 ZnS:Tb Phosphor Films 141
7.2.1 Deposition of ZnS:Tb^{3+} Films 142
7.3 Conclusions 143

Chapter 8

ELECTROLUMINESCENT DISPLAYS

8.1 Introduction 145
8.2 Structure of EL Displays 146
8.2.1 Structure of AC EL Devices 146
8.2.2 Structure of DC EL Devices 147
8.2.3 Colour EL Displays 147
8.2.4 Requirements of Every Layer of EL Displays 148
8.3 Theory of Electroluminescence 150
8.3.1 Principle of EL Devices 150
8.3.2 EL Mechanisms of Mn-Doped and Rare-Earth-Doped ZnS Thin Films 152
8.3.3 Hot Electron Processes in EL 152
8.3.4 Impact Processes in EL 153

8.3.5 Luminescence and Conduction Charge of DC EL Devices ... 154
8.3.6 Luminescence and Conduction Charge of AC EL Devices ... 155
8.3.6.1 Production of Electrons in EL Devices ... 155
8.3.6.2 Basic Principles of AC EL Devices ... 155
8.3.7 Luminescence and Conduction Charge in MIS EL Devices ... 157
8.3.8 Efficiency of Thin Film EL ... 158
8.3.9 Rate of Excitation and Ionization of Luminescent Centre ... 160
8.3.10 Concentration Quenching of Electroluminescence ... 161
8.3.11 Comparison of AC and DC EL Devices ... 162

Chapter 9

CHARACTERISTICS OF EL DISPLAY DEVICES

9.1 Structure and Fabrication of EL Devices in the Work ... 164
9.2 Characteristics of ZnS:Mn Thin Film EL Devices ... 164
9.2.1 Emission Spectrum of ZnS:Mn EL Devices ... 164
9.2.2 Brightness of EL Devices ... 166
9.2.2.1 Voltage-Brightness Relation ... 167
9.2.2.2 Function of Insulating Layer to Brightness of EL Devices ... 169
9.2.2.3 Function of Rise Time to Brightness of EL Devices ... 170
9.2.2.4 Concentration-Brightness Relation ... 170
9.2.2.5 Thickness-Brightness Relation ... 171
9.2.2.6 Driving Frequency-Brightness Relation ... 173
9.2.3 Luminescent Output of EL Devices ... 174
9.3 Characteristics of ZnS:Tb Thin Film EL Device ... 174
9.3.1 Emission Spectrum of ZnS:Tb EL Devices ... 175
9.3.2 Applied Voltage-Brightness Relation of ZnS:Tb EL Devices ... 175
9.3.3 Tb Concentration-Brightness Relation ... 175
9.3.4 Driving Frequency-Brightness Relation of ZnS:Tb EL Device ... 176
9.4 Conclusions ... 177

Chapter 10

CONCLUSIONS

10.1 Conclusions of the Work ... 180
10.2 Future Work ... 180

Appendix I **Boundary Layers** ... 183
Appendix II **High-voltage Drivers for EL Devices** ... 187

Reference ... 189

ACKNOWLEDGEMENTS

At the top of my list of acknowledgements I would like to thank Dr. David Cameron, My supervisor, for his advice and steadfast encouragement in the course of this work over three years. Without his instruction and excitement for the experiment and theories in this work I would not have continued and completed the work successfully.

I am grateful to Prof. Charles McCorkell of Electronic Eng. department and Dr. Brian Lawless and Dr. Colette McDonagh of Physics department for inspirational discussion and experimental instruction throughout this work. I would like to thank John Whelan, Conor Maguire, Liam Meany and Paul Wogan of Electronic Eng. department for their help.

I am grateful to Physics department and Chemistry department for allowing me to use their instruments.

I thank all those friends and classmates who patiently offered help in this work.

This thesis could not been written without the support of my beautiful and loving wife, Tiehong, who suffered through this work from several thousand miles.

My final and greatest debt is, of course, to my father, who has now supported and inspirited me in spirit through this work.

ELECTROLUMINESCENT DISPLAYS BY SOL-GEL PROCESS

ABSTRACT

Thin film electroluminescent displays are attractive commercially as well as scientifically and of technological interest in the design of large area, flat screen displays. The interest in developing reliable luminescent materials for applications on flat panel displays has produced a considerable research effort in this area. This effort has been directed to the techniques of film deposition as well as to the different types of materials and dopants used as active components on electroluminescent devices. Applications of ZnS and ZnS:Mn films in electroluminescent displays have been increasing examined. Mn-doped ZnS is one of the most studied materials for luminescent devices. Zinc sulphide is a semiconductor suitable to be used as host matrix for a large variety of dopants because of its wide energy band gap. The sol-gel process is now well accepted as a technology for preparing thin films. The advantages of the sol-gel process are that it is simple and inexpensive and has the general advantages of producing large area, high purity, homogeneous films at relative low temperatures.

Electroluminescent thin film display structures require the fabrication of insulators, transparent conductors and electroluminescent materials. In this project all of these materials have been produced using the sol-gel technique. Insulating films of silicon dioxide and aluminium oxide were fabricated from silicon and aluminium alkoxides respectively and their characteristics measured. Transparent conductors were produced from aluminium-doped zinc oxide using a zinc acetate precursor. The dependence of electrical characteristics upon aluminum concentration in the films and upon post-deposition heat treatment in vacuum was examined. The effect of changing the aluminum-to-zinc ratio from 0-4.5 at.% (atomic percent) and heat treatment temperature in vacuum have been thoroughly investigated. Resistivities of (7-10)$\times10^{-4}$ $\Omega\cdot$cm have been achieved for ZnO:Al films with Al/Zn 0.8 at.% heated to 450°C in vacuum. Transmittance in the visible region is above 90%. Similar results were obtained using aluminum chloride and aluminum nitrate as the aluminum precursor. Electroluminescent films of zinc sulphide were produced by a novel method involving sol-gel deposition of zinc oxide and a conversion technique where the films were annealed in a sulphiding atmosphere to produce zinc sulphide. The characteristics of these films were investigated using scanning electron microscopy, X-ray diffraction, infrared spectroscopy and optical transmission spectroscopy. Electroluminescent devices were fabricated using

manganese and terbium doped zinc sulphide and the luminescent characteristics of the displays were measured as a function of dopant concentration, applied voltage, driving frequency and insulator type.

It is has been demonstrated that the sol-gel technique is a simple, cheap method for the construction of electroluminescent displays.

Chapter 1

INTRODUCTION

1.1 Displays

Flat panel displays are becoming key devices of intelligent equipment as well as in information system and other applications such TV receivers and computers. They have been attractive over the years because of their inherent characteristics of low volume and light weight. With advance of displays technology, many kinds of flat panel displays can be listed. In the group of emissive flat panel displays, there are electroluminescent displays(EL), cathodoluminescent displays such as cathode ray tube (CRT), plasma displays, vacuum fluorescent displays (VFD), light emitting diodes (LED) and flat cathode ray tubes. In that of non emissive ones, there are liquid crystal displays (LCD) and electrochromic displays[1],[2],[3],[4]. At present with increase of commercial requirements and practical applications the demand for quality in flat panel displays has been very great with regard to viewing angles, high speed addressability, contrast ratio, luminance and power consumption.

1.1.1 Electroluminescent Displays

The electroluminescent display is a solid state device operated by electric field. According to current theory of electroluminescence, 'hot' electrons obtain energy from electric field and are released from the interface of the EL material layer and dielectric layer or conducting layer. The electric field within the EL cell is intense; over 10^6 V/cm. The hot electrons are accelerated by the electric field and collide with luminescent centres. This collision has a radiated photon as one of its results. The mechanism of EL materials and the principle of EL devices will be explained in the following chapters.

The EL display is a serious contender to replace the CRT in many applications. Computer displays, especially in portable and military applications, are expected to use EL displays. The EL display is reliable, very bright, has moderate power consumption, and has high resolution. EL displays have many good points. These properties, together with its light weight and very thin profile make it attractive for portable and ruggedized equipment. EL display is very rugged as it is a completely solid state structure. LCDs are liquid state devices, while both VFDs and plasma displays are gas state. Being a solid state device gives

EL displays the edge in mechanical ruggedness and allows them to operate over wider temperature ranges. All of these are desirable characteristics for a display used in portable, vehicular, or military service.

1.1.2 Cathodoluminescent Displays

In cathodoluminescence, when a beam of energetic electrons hits a solid, a fraction are backscattered. The remainder penetrate into the solid where they rapidly lose energy, mainly by causing bound electrons to be ejected from their parent ions. These secondary electrons in turn may generate further secondary electrons provided they have sufficient energy. The final stages in the secondary generation process consist of the excitation of electrons from states at the top of the valence band to those at the bottom of the conduction band. In cathodoluminescent materials electron-hole recombination and luminescent emission then takes place.

1.1.3 Cathode Ray Tube

The relative ease with which a beam of electrons can be directed and focused led to the early development and retention of the cathode ray tube as an important tool for the analysis of rapidly varying electrical signals as well as providing a versatile optical display devise. Electrons are derived by thermionic emission by heating a specially impregnated cathode surface and then focused onto the viewing screen by a series of metal electrodes held at various potentials. A grid for the control of the electron flow is usually also included. The electron beam is scanned across the viewing screen in a series of lines; when one line scan is completed the beam is rapidly switched to the start of the line below. The whole assembly is known as an 'electron gun'. Beam deflection is controlled by electrostatic or electromagnetic fields acting at right angles to the beam direction. Electrostatic deflection enables the highest beam deflection rates to be achieved, whilst electromagnetic deflection enables higher beam accelerating potentials to be employed, which results in a smaller spot size and higher screen brightness. When the beam strikes the viewing screen, radiation is generated by cathodoluminescence.

Colour displays for home video viewing are obtained using the 'shadowmask' principle. In this three electron guns are used; they are slightly inclined to each other so that their beams coincide at the plane of the shadowmask. Having passed through one of the holes in

shadowmask the three beams diverge and on striking the phosphor screen are again physically distinct. The phosphor screen consists of groups of three phosphor dots, placed so that when the three beams pass through a hole in the shadowmask they each hit a different dot. Each of the three phosphor dots emits one of the primary colours, so that any desired colour can be generated by the relative excitation intensities. Some of the more commonly used phosphors are zinc sulphide doped with silver, ZnS:Ag (blue), zinc cadmium sulphide doped with copper, $Zn_xCd_{1-x}S$:Cu (green), and yttrium oxysulphide doped with europium and terbium, Y_2O_2S:Eu,Tb (red).

A somewhat different method of CRT colour display has been developed within the last few years using the so-called 'penetration phosphors'. These utilize the variation in electron penetration depth that can obtained by varying the beam voltage.

In conclusion, the CRT provides a very versatile display which can readily cope with complex pattern. Its main disadvantages are its comparatively low screen area to volume ratio and the necessity for a high voltage power supply.

1.1.4 Vacuum Fluorescent Displays

Vacuum fluorescent displays based on low voltage cathodoluminescence were developed in Japan in the late 1960s. The displays consist of an oxide coated thermionic emitter in the form of a filament, and anodes mounted in a vacuum envelope. The anodes are coated with a low voltage phosphor, such as ZnO, which gives a bluish-green luminescence when bombarded with electrons of energy around 20eV, with an efficiency of from 5 to 10 lm/W. the filament is located in front of the anodes, but is run at a low temperature so that it is barely visible.

The effective resolution of a vacuum fluorescent displays is directly tied to the size of an individual vacuum fluorescent element. The speed of VFDs are very high. An individual element can be written or unwritten in less than 1 ms. The VFDs are available in the following colours, blue, blue-green, green, yellow, orange, amber, and red. These colours are produced by combination of differing phosphors in conjunction with a wide range of filters. The VFDs have wide viewing angles, long operating lifetime and low power consumption and operate in great temperature environments. But the high operating voltage level of VFDs is difficult to implement in the densely packed arrays necessary to attain high resolution information output.

1.1.5 Plasma Displays

Monochrome plasma displays have been developed for use in office and factory automation, and have played an important role in making equipment more compact. 640×480 and 640×400 panels have been developed as standard display devices for personal computers, and a 1280×1024 panel has been developed for workstation terminals. A 1.5 m-diagonal plasma display is the largest of the direct view display has been commercially available for use on the stork market since 1990, and a full colour display has been developed for use in HDTV. Plasma display, one of the oldest display technologies, still remains competitive for graph and video application in spite of its relatively high operating voltage. Plasma display devices utilise the light output of a cold cathode discharge. There are two processes for emission of photons in a gas, excitation of the atoms or molecules by electron bombardment giving radiation when they return to the ground state, and radiative recombination of ions and electrons; both represent efficient methods of producing light. The luminous efficiency is especially high for low voltage plasma.

Plasma displays depend on the glow produced when an electrical current is passed through a gas (usually neon). Free electrons and ionized gas atoms are present during the discharge. Under the influence of the external field the electrons acquire a high kinetic energy and when they collide with gas atoms (ions) they transfer this energy to the atoms, thereby exciting them into energy levels above the ground state. The atom may then lose energy radiatively and return to the ground state.

Colour in plasma displays is achieved by placing phosphors in plasma panels and exciting those phosphors with ultraviolet rays of gas discharge. A major problem with colour plasma displays is designing them to achieve high brightness and luminous efficiency. In addition, almost all plasma displays use light from negative glow, which is known to be considerably less efficient than light from the positive glow in a typical discharge region.

Basically the plasma panel consists of a two-dimensional array of discrete gas discharges which can be selectively addressed by cross-bar electrodes. In many designs the discharges are confined in separate cells formed by apertures in an insulating plate which is placed between two glass plates on which the orthogonal system of electrodes is mounted. The three plates are sealed together round the edges and filled with a gas mixture which is predominantly neon at a reduced pressure, 1×10^4-4×10^4 N/m^2.

The panels may be operated under AC conditions in which each set of electrodes acts

alternately as anodes or cathodes, under DC conditions in which one set of electrodes acts always as cathodes and the other as anodes. In the AC operation the electrodes need not be in contact with the gas but may be isolated from it by an insulating layer. Two drive modes may be distinguished: cyclic, in which each cell is illuminated only during the address pules; and storage, in which a cell once addressed remains on until it is erased some time later. AC plasma displays have the inherent characteristic of memory function due to the electrode structure. AC plasma displays have an excellent display quality, an especially high contrast ratio, a very wide viewing angle, and a capability of large area display in memory operation. Usually the life of AC plasma displays is longer than that of DC ones.

The basic plasma pixel needs to have a potential of at least 200 volts before it will work. The exact amount of voltage required depends on the panel's geometry, type of gas used, and gas's pressure. The level of power consumption is moderate, and slight more than the EL displays, but much less than a CRT of the same size. The plasma displays are among the brightest of the flat panel displays. Only the electroluminescent panel (ZnS:Mn) is brighter and more efficient at converting electricity to light. Plasma displays offer a high resolution, wide angles (120°-160°) and a very wide temperature operating range (-30°C to 55°C).

1.1.6 Light Emitting Diode

The basic structure of light emitting diode (injection luminescence) is that of a p-n junction diode operated under forward bias. Under forward bias, majority carriers from both sides of the junction cross the internal potential barrier and enter material at the other side where they are then the minority type of carriers and cause the local minority carrier population to be larger than normal. This situation is described as minority carrier injection. Ideally in a light emitting diode every injected electron takes part in radiative recombination and hence gives rise to an emitted photon. In practice the efficiency of the device is less than the ideal efficiency. The number of radiative recombinations that take place is usually proportional to the carrier injection rate and hence to the total current flowing. Radiative recombination in semiconductors occurs predominantly via three different processes, namely (1) interband transition, (2) recombination via impurity centres and (3) exciton recombination.

The requirements for a suitable LED material as follows: firstly, it must have an energy gap of appropriate width; secondly both p and n types must exist, preferably with low resistivities; and finally efficient radiative pathways must be present.

The LED is a current operated semiconductor device and a small consumer of power. The current determine the brightness of LED. Although LED has many advantages, there are many improvements and much work requied for a large area LED display.
Power consumption is moderate in LED dot matrix displays. It is comparable with small CRT displays and much greater than LCD displays used in the same type of applications.

1.1.7 Liquid Crystal Displays

Although liquid crystal materials have been known for 100 years, large scale applications for the materials in the form of electric displays did not occur until the mid 1970s when compact, attractive calculators and watches with liquid crystal displays reached the marketplace and soon became household item. Now low cost LCDs are being made by the hundreds of millions. Today, more sophisticated LCDs appear in such products as portable computers and hand-held colour TV sets; the fabled liquid crystal TV on a wall appears to be only a few years in the future.
Liquid crystal displays are one of the most important of the 'passive' types of displays. LCDs consume the least power of all common display devices because no light generation is required. There are two basic types of LCD available. These are (a) reflective, which requires front illumination, and (b) transmissive, which requires rear illumination. Most reflective types utilize ambient light for illumination with provision for secondary illumination via a small incandescent lamp or LED if ambient levels become too low. At the heart of all LCD devices is a cell formed between two glass plates each with a conductive coating. The cell is filled with a liquid crystal material.
The liquid crystal state is a phase of matter which is exhibited by a large number of organic materials over a restricted temperature range. When in the liquid crystal phase, there molecules can take up certain orientations relative both to each other and to the liquid crystal surface.
One of the most importance electrical characteristics of liquid crystal materials is that they show different dielectric constants $\varepsilon_{\parallel}$ and $\varepsilon_{\perp}$, depending on whether the external field is parallel to, or perpendicular to, the molecular axis. If $\varepsilon_{\parallel}>\varepsilon_{\perp}$ it is referred to as a positive material. In the nematic state the molecules are all arranged parallel to each other. There are two subdivisions of the nematic type of ordering: homeotropic ordering where the molecules are aligned perpendicular to a liquid solid interface and homogeneous ordering where the

molecules are aligned parallel to the interface. The application of an external electric field to a positive material will tend to make the molecules lie along the electric field since this will tend to minimize their energy. There is a possibility of changing the homogeneous type of ordering into a homeotropic type by the application of a field which is perpendicular to the surface. This transition is found to take place above a critical field (E_c). The most common liquid crystal display uses a 'twisted nematic' cell. When E=0 the molecules undergo a 90° rotation across the cell. When a beam of polarized light is incident on the cell the strong optical anisotropy of the liquid causes the polarization to undergo a 90° rotation. With a strong enough electric field across the cell, ie. $E > E_c$, the molecular alignments will have no effect on an incident polarized light beam. With no applied voltage the incident light is polarized, has its polarization direction rotated by 90° as it traverses the cell, passes through the second polarizer and is then reflected back along its path where the same process is repeated. With no field applied, therefore, the device reflects incident radiation and appears bright. When a field is applied the direction of polarization of light traversing the cell is not rotated and hence cannot pass through the second polarizer. Little light will be reflected from the device and it will appear dark. The amount of light reflected from an LCD is a function of applied voltage.

The transmissive LCD displays do not have the reflector, and must be provided with rear illumination, but otherwise they operate in a very similar fashion to the reflective displays.

The double layer supertwisted-nematic liquid crystal displays were developed by Seiko Epson[5]. Colour filters have been added to the structure of double layer supertwisted nematic liquid crystal displays for full-colour or multi-colour liquid crystal displays. Full-colour active matrix addressing liquid crystal displays have advanced very rapidly due to improvements in process technology. The active matrix LCD has diode or thin films transistor in each picture element and has features of high colour image quality. The active matrix LCDs have great viewing angles, low power consumption, high resolution and high speed suited for multiplex service. At present they are expensive due to complexity of manufacture.

Temperature is a critical factor in LCD operation. The LCD has a relatively narrow range of operating temperatures when compared with any other display technology. Generally, LCDs are intended for use at temperatures above freezing. The LC media is a liquid, and cooling it increases its viscosity, making it respond sluggishly to the electric field. At high

temperatures, the liquid crystals have sufficient thermal energy so that they will not hold their twist in the off state. If LCDs are stored at temperatures above 85°C they may be permanently damaged. One of the major advantages of all LCDs is their long lifetime but low power consumption and low driving voltage.

1.1.8 Electrochromic Displays

Electrochromic displays have also been attractive for low powered passive displays. They normally operate at low voltage of the order of a few volts and most have non-volatile memory so that their maintenance power is low. Their main asset is their appearance; they have a better colour contrast and wide viewing angle than the liquid crystal. Their main disadvantage is lack of threshold and narrow range of switching voltage making controlling and matrix addressing difficult. The phenomenon of electrochromism can be broadly defined as the changing of the light absorption properties of certain solid state materials by an externally applied electric field. The colour change usually remains after the field is removed and can only be bleached by reversing the polarity. Although first observed in the 1930s in alkali halides in connection with the production of colour centres in ionic crystals, electrochromism has not been extensively investigated and is still not well understood.

1.1.9 Electrophoretic Displays

In electrophoretic displays, charged pigment particles suspended in a liquid are attracted and deposited at the cathode under an electric field. If the particles are black suspended in a milky liquid and the cathode is in the form of transparent segments disposed on the front surface of a cell, then the appearance of the display will be a dark colour on a white background with wide viewing angle and good contrast.

1.1.10 Other Displays

There are one or two displays worth mentioning although their future exploitation is rather more doubtful. The ideas for active displays are electrochemiluminescence and the fluorescent dye. Electrochemiluminescence can be defined as the raising of molecules capable of luminescing to the excited state by electrochemical energy. The use of fluorescent dyes has been proposed. Europium chelate solution provides a bright red fluorescence when illuminated by ultraviolet radiation. For passive displays several ideas have been proposed

for moving particles or segments in either electrostatic or magnetic fields. The electroscopic displays are based on the idea of electroscope, i.e. the movement of a foil in an electrostatic field. Another device depending on electrostatic forces is the gyricon. Insulating spherical particles are coated on the two opposite hemispherical surfaces with material having different contact potential as well as colour. In contact with a dielectric liquid, in spherical cavities in an elastomer sheet, ionic double layers are set up with different charge densities associated with the two different hemispherical surface. Application of an external electrostatic field orientated the balls so that either the dark or light side of the spheres faces the observer.

1.1.11 Trend of Colour Displays

All flat panel displays such as plasma displays, electroluminescent displays and LCD displays were originally monochrome, but colour displays were strongly demanded and have been researched actively.

For electroluminescent displays, emissive materials for various colour have been actively researched, and red, green and bluish green phosphors with acceptable efficiency have been developed. But suitable blue phosphor has not been yet developed, which is the main barrier against realizing colour EL. A mosaic arrangement of EL layers for the three colours has been successfully obtained, but stacking three colour layers for high resolution is still under development.

In the case of plasma displays, the photoluminescent type has been developed , that is , UV-light is emitted by the discharge and phosphors for red, green and blue colour are excited by the UV-light, The surface-discharge AC plasma display is especially promising for its life time and simple structure which is suitable for large displays, and the problem of light efficiency has been improved recently[6]. Therefore, this panel is expected to be applied to the direct view, large size colour display such as HDTV.

As for LCD, colour was considered to be most difficult to obtain, but in 1981 the additive mixing system using a micro colour filter placed inside the LCD was proposed[7],[8]. This system was applied to the active matrix LCD and a small size colour television was made in 1983. Since then, the colour LCD has progressed rapidly, and portable colour television, colour view finder and colour display for lap top computers have put into practice. The problem of these LCDs is low transmission, typically 3%. Therefore, back lighting and a relatively big battery is necessary, which will become the largest problem for developing

future compact computers.

1.2 Comparison of Different Type Displays

Here the characteristics of various displays are compared. These displays are manufactured using CRT, LED, LCD, VFD, EL and Plasma display technology. Computer displays offer the widest variety of different display types. Computer displays use CRT, LCD, EL, and plasma panels in very large sizes and high resolutions. Amount and type of information to be displayed, operating environment, and power availability should be considered as main three factors for evaluating displays.

The following diagrams were obtained from literature[9] in which author, Mr. Perez, surveyed over 300 different manufacturers of electronic displays to obtain the information. From the diagrams the comparison for the fundamental characteristics of the displays can help us to know the development and trend of displays.

1.2.1 Display Brightness

Brightness is an important factor to consider in the choice of a display. Fig.1-1 shows the displays based on their brightness. Note that the LCD is not listed on Fig.1-1. This is

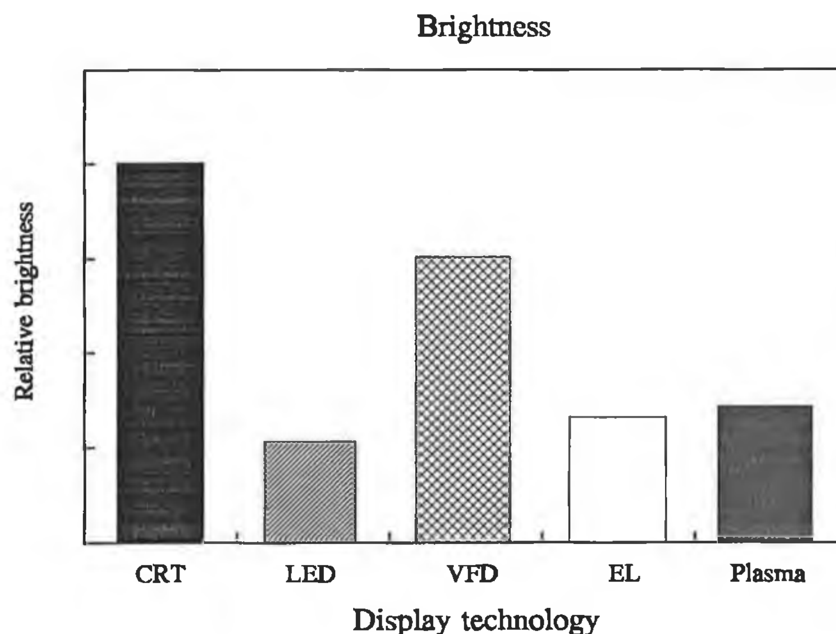

Figure 1-1 Relationship of brightness and display technology.

because the LCD is not a light producing display, but a light modifying display. Since LCDs use ambient light for modification, they function best in high levels of ambient light.

1.2.2 Display Operating Voltage

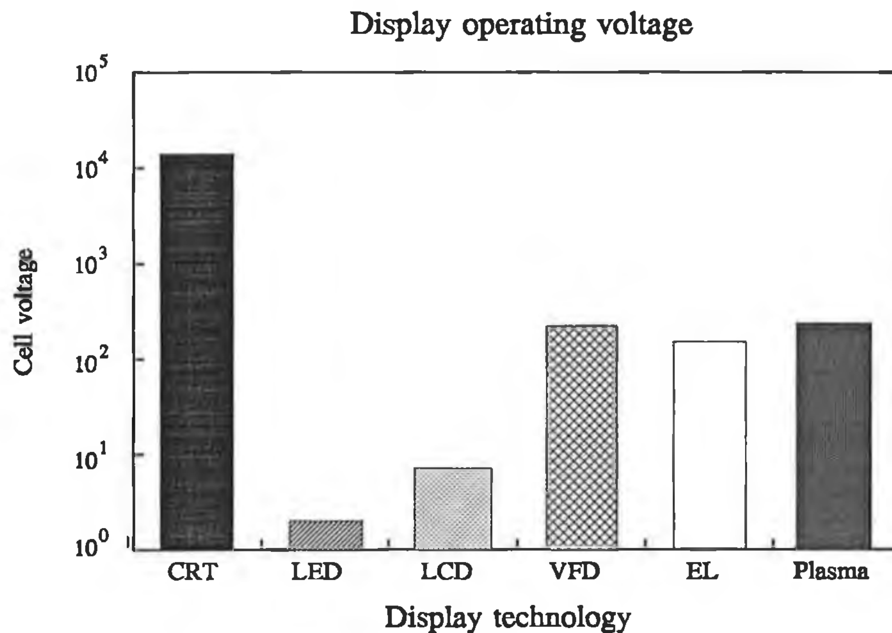

Figure 1-2 Relationship of display operating voltage and display technology.

Fig.1-2 shows the voltages required to operate a specific display technology. Operating voltages vary from over 20,000 volts in the CRT to less than 2 volts for the LED. Low voltage operation makes a display technology applicable to portable and battery operation.

1.2.3 Resolution

Fig.1-3 shows the resolution of various display technologies. The highest resolution belongs to the CRT. Plasma displays are the second. The resolution of both the EL and the LCD are limited by the resistance of transparent conducting electrode.

1.2.4 Speed

The question of speed in a display technology only becomes critical in higher resolution systems. Fig.1-4 shows the speed of various display technologies. The LED, CRT, VFD, EL and plasma display are capable of displaying entire pages of data in proper resolution without

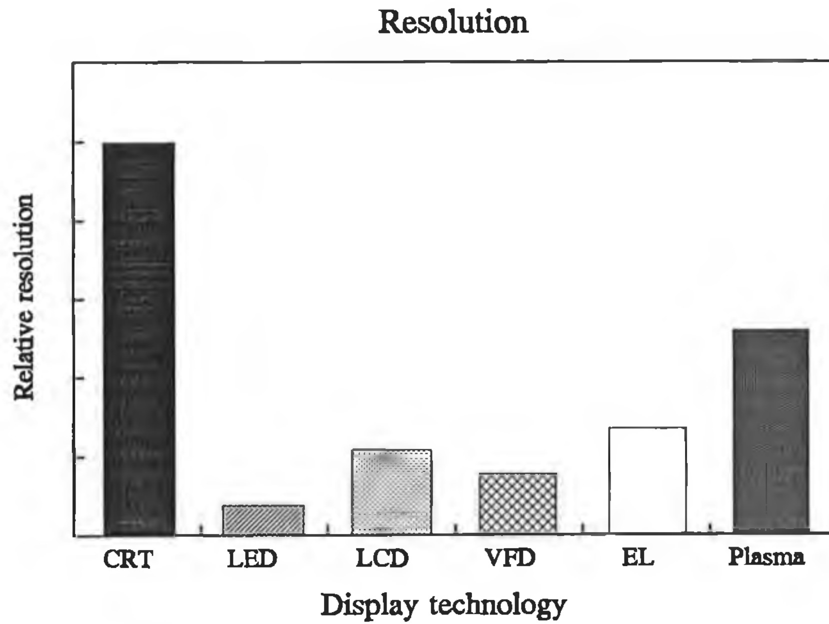

Figure 1-3 Relationship of display resolution and display technology.

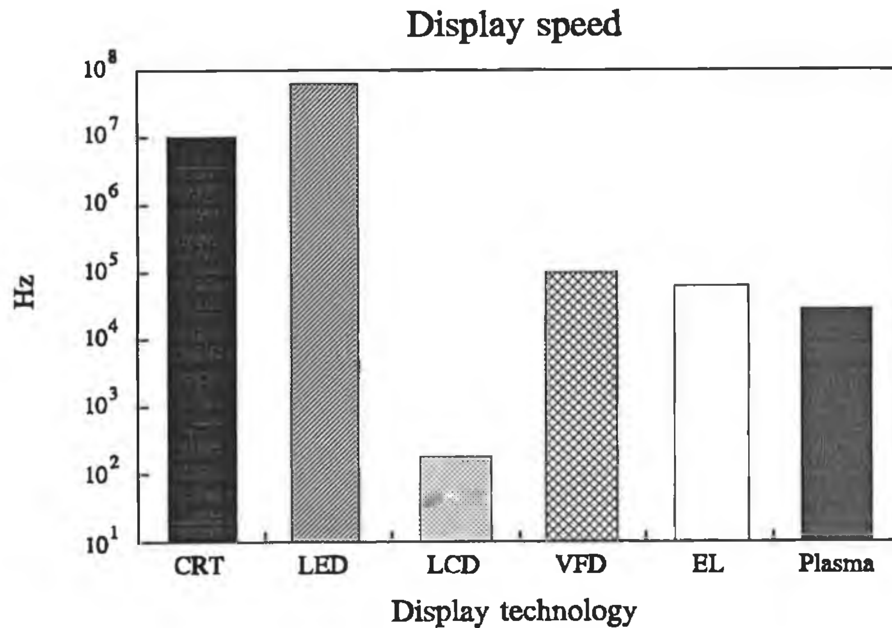

Figure 1-4 Relationship of display speed and display technology.

flicker. Because of the liquid phase construction and physics of the LC cell, the speed of LCD is very low with high resolution.

1.2.5 Display Power Consumption

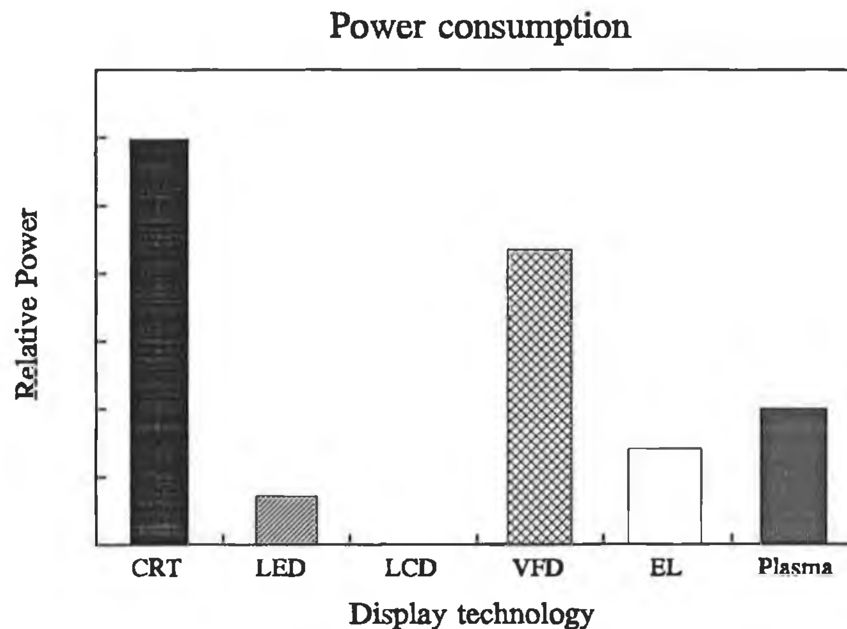

Figure 1-5 Relationship of power consumption and display technology.

Fig.1-5 is a bar graph comparing the power consumption of different display technologies. The y-axis of this graph shows the relative power consumption per unit of display area of each display technology in a normalized and linear fashion. The LCD's power consumption is so low that it dose not register on the graph. The LED remains the most efficient self-illuminating electric display device. For small scale or intermittent use, the LEDs can be used with batteries as power sources. Even so, the LED consumes many times the power of the LCD. At present the LCD remains the most practical display to consider for battery operation.

1.2.6 Operating Temperature Range

The question of temperature range is not critical for displays operated in a controlled environment, such as inside a building. If a display is to be operated in a vehicle, or outside as a portable, then temperature range is critical factor. Fig.1-6 shows the operating range of six different types of displays. The CRT offers the widest temperature operating range, followed by the VFD and LED. EL displays have a slightly wider operating range than plasma displays. The LCD has the narrowest temperature operating range of all displays so

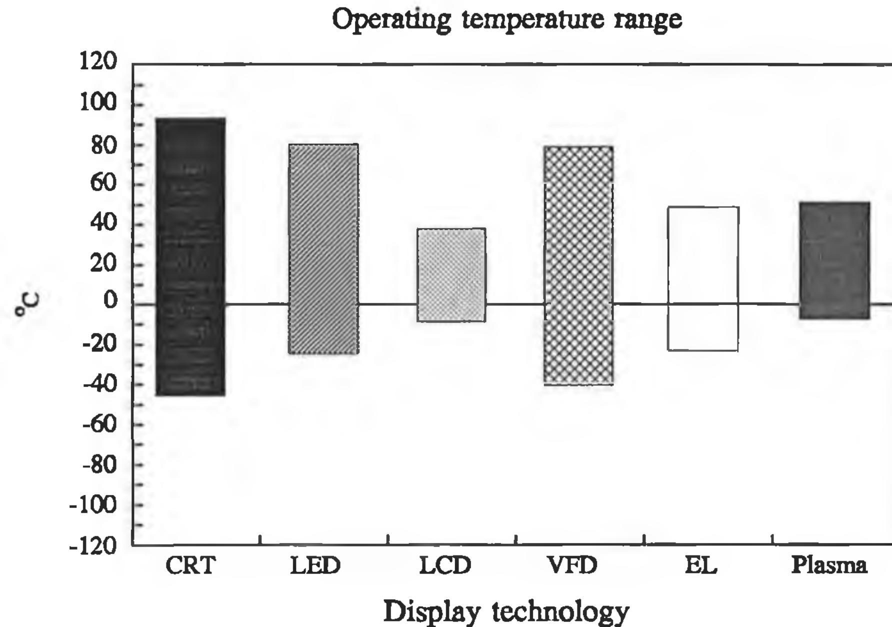

Figure 1-6 Relationship of display operating temperature range and display technology.

that it can be to difficult to use in an outside environment. If the limits of operating temperature are exceeded the display can be permanently ruined.

1.2.7 Visual Angle

Fig.1-7 illustrates the viewing angles of several display technologies. The plasma panel has the widest viewing angle, almost 160°. Although the viewing angle of an LED is wide it is a function of LED's lens. The narrow viewing angle of LCD has long been one of its major problems.

1.2.8 Maximum Screen Size

Fig.1-8 shows the maximum screen area that can be produced by the sample display technologies. The plasma panels are currently capable of producing gigantic displays with many times the area of the other types. These large area plasma panels are actually composed of smaller sub-panels. The CRT, VFD, LCD, and EL are all also available in large sizes. LED displays are generally only manufactured in smaller sizes.

1.2.9 Longevity

Fig.1-9 shows the longevity of various display types. Longevity is a factor in the economics

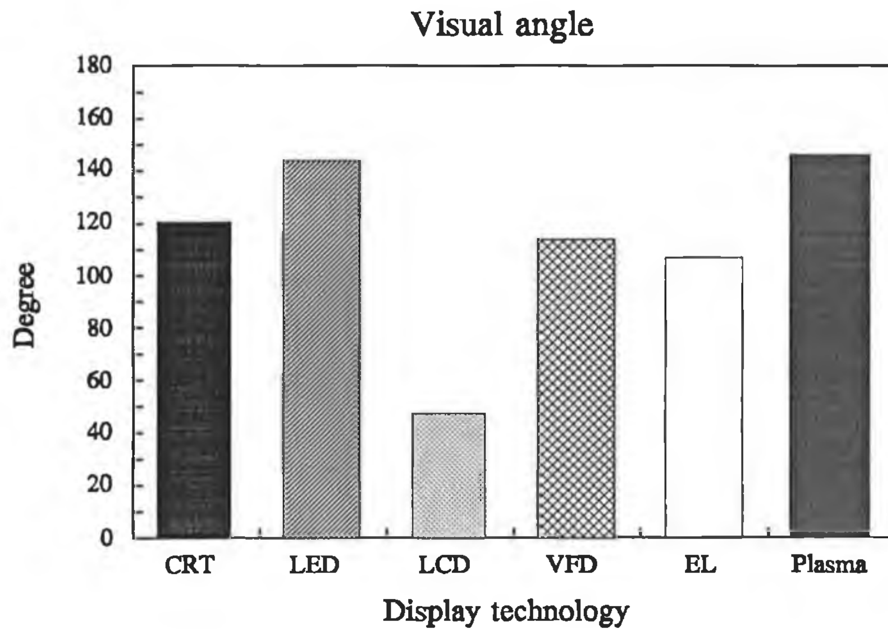

Figure 1-7 Relationship of display visual angle and display technology.

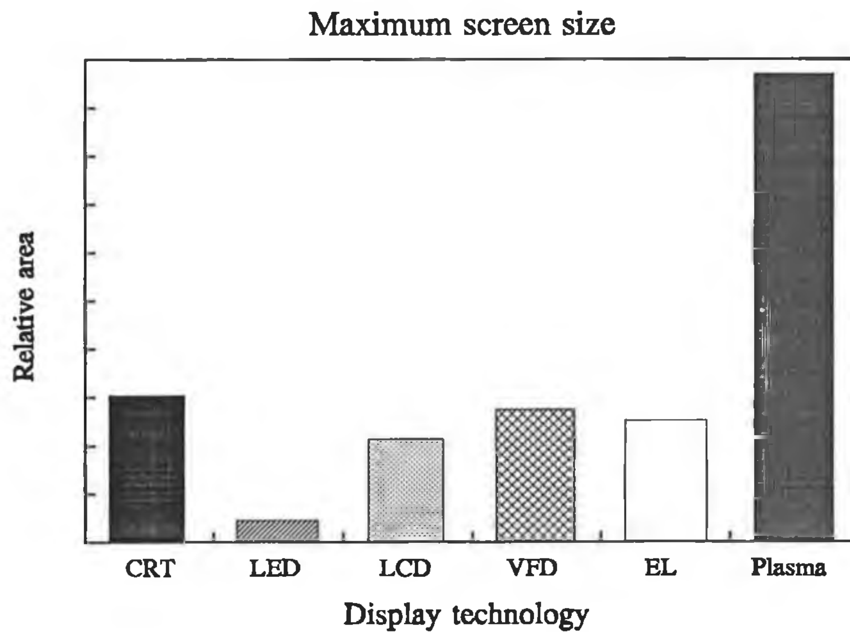

Figure 1-8 Relationship of display maximum screen size and display technology.

of electronic display use. The longer it lasts, the less often it has to be replaced. The longest lived display technology is the LED. The LCDs come next. With their low voltage, liquid

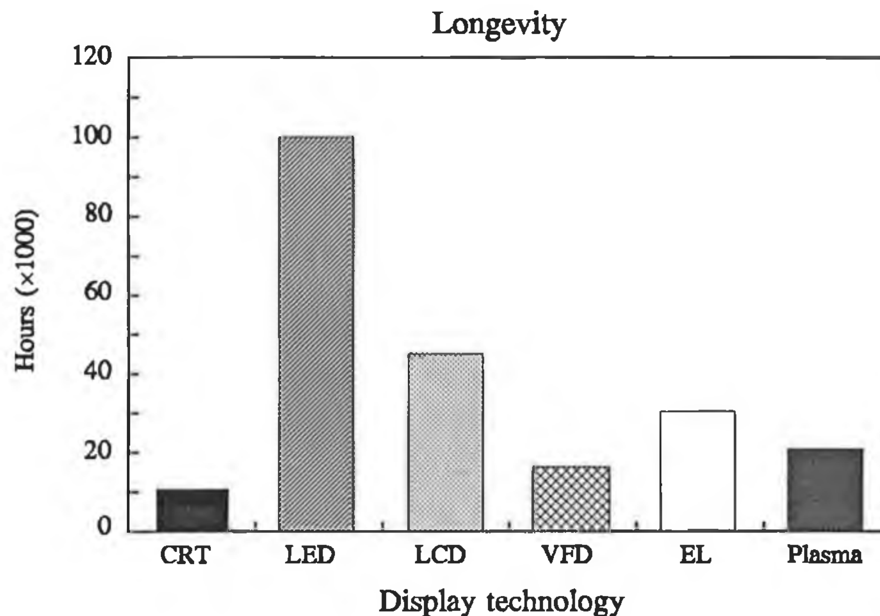

Figure 1-9 Relationship of display longevity and display technology.

phase operation, they will run for many years without losing their contrast. EL and plasma panels will last for several years of continuous operation. Since the EL is a relatively new solid state device it is very likely that this longevity figure will greatly increase in the future.

1.2.10 Efficiency

The high efficiency (lumens/watt), of the light emitting thin film phosphor layer does not require much power to generate light, relegating most of the power dissipated, to the drive circuits and their design. Plasma displays have an efficient light production mechanism (<.5 lumens/watt) and colour liquid crystal displays have colour filters with only ~20% transmissivity. Thus, both competing display light production mechanisms are inefficient. But with the thin film EL device, the total power is limited by the effectiveness of the energy-recovery of the drive circuits and the minimization of drive power by efficient circuit schemes.

1.2.11 Driver

LCD, LED, FVD, EL display and plasma displays are matrix displays, so their drivers produce complex waveform to drive the displays. FVDs, EL displays and plasma panels have

very complex high voltage waveforms passing through their drives. The drivers are semiconductor switches which can withstand the high voltages involved. These drivers have evolved into ICs specifically constructed just for this purpose. The higher the voltage output of drivers must be, the more expensive they are. In the meanwhile, power consumption of the drivers is also a problem.

1.3 Electroluminescent Displays

1.3.1 Developing History of EL Displays

Electroluminescent displays have been improved and developed for many years so various types of electroluminescent displays have appeared. Electroluminescent displays have developed by the improvement of phosphors, film deposition and the relative technologies used in fabrication of EL devices.

Electroluminescence discovered in 1936[10] was recognized as a new physical phenomenon. However, EL remained unexplored as far as devices were concerned, due to the immature development of both peripheral materials and technologies. In the early 1950's, EL attracted much interest for its practical use following the development of transparent electrode material with both high transparency in the visible light region and high electrical conductivity.

Worldwide research and development were actively done from the latter half of the 1950's to the first half of the 1960's. In this period the EL cell fabricated was called powder-type EL or dispersion type EL, because ZnS powder was bound with the appropriate polymer and was formed into a thin layer. The first target of its practical application was the realization of a new light source for wall illumination, and then as the next target, various optoelectronic devices were considered such as a light intensifier and a flat display panel. However, the brightness of the EL cell at that time was insufficient and too unstable for the practical use. The so-called half life, which is defined as the time when the brightness decreases to half of initial brightness, remained in the range of a few hundred hours to a thousand hours. In order to improve these points, the research on materials, panel configuration and fabrication process were energetically continued. However, the EL cell could not be essentially improved and could not secure the position as a general application of flat panel illumination, except in special applications such as an all-night lamp and an illumination lamp for measurement instruments in the ship's pilothouse.

For the application of the EL cell in a flat display panel, powder type EL was used only for displaying rigid patterns because of its poor contrast ratio due to the light scattering by powder of the active layer and above mentioned problems. So, powder type EL could not realize practical information panels which can display changing information. Thus, EL development gradually faded away toward the end of 60's.

A sign of emergence from the stagnation appeared in the following two papers presented in 1968. One paper presented by A. Vecht et. al.[11] showed that a DC drive of powder type EL panel is available by surface treatment of the phosphor powder. The other paper presented by D. Kahng[12] announced that thin film EL with high brightness could be attained using molecules of rare-earth fluoride as the luminous centres.

With the spread of information transaction equipment headed by computers, the information display device attracted growing interest as a man-machine interface, and the realization of flat display device in solid state was required in this period. Considering their cost and size, polycrystal EL devices had to be looked at again instead of mono-crystalline EL devices.

At the SID International Symposium in 1974, Inoguchi's paper[13] "Stable High Brightness Thin Film Electroluminescent Panels" announced that the problems such as low brightness and short life, which remained unsolved in the initial stage EL, could be solved at a stroke, and C Suzuki et. al.[14] also announced that this EL panel is capable of displaying moving TV pictures with half tone. M. Takeda et. al.[15] presented a paper "Inherent Memory Effects in ZnS:Mn Thin Film EL Devices". Analysing the success, the following three points from technical view point can be cited: (1) The development of process and deposition technologies of films improved the quality and the formation of II-VI compound semiconductor thin films. (2) The symmetrical device structure of the EL active layer sandwiched by insulating layer with high breakdown voltage, so-called double insulating layer structure was adopted in order to apply stably a sufficiently high voltage to the EL active layer and also in order to simplify the analysis of driving mechanisms and characteristics. (3) It was tried to eliminate the mobile ions such as the Cu^+ ion which can move easily under high electric field.

From the period of the initial stage EL development, there was a great demand to realize "Wall Hanging TV" as a large flat display panel with high brightness, viewable angle and so on without a vacuum tube, and the situation to date remains unchanged.

The thin film EL (TFEL) is expected to satisfy the above mentioned requirements. Large

information display devices with an X-Y matrix configuration can be re-evaluated as follows. First, concerning the contrast ratio of the display, the brightness of a selected pixel is required to be suitably high and the scattered light in non-selected pixel adjacent to the selected pixel must remain at a low level. In the TFEL consisting of all transparent thin films except back metal electrode, high contrast ratio can be easily obtained because of an essentially low light scattering level. Second, a distinct threshold and steep increase of brightness for the input is required for avoiding interference in X-Y matrix configuration. TFEL with a double insulating structure has no problem of such crosstalk in practical use because of a distinct threshold. Third, with respect to the response time, rise time is required within a selected period of refresh display cycle, fall time must be within one frame time. Luminescence of TFEL can respond sufficiently to the signal of a TV picture mode because the rise time is a few μsec, and fall time is a few msec in a general TFEL. Therefore, TFEL is suitable for the information display device with a large capacity.

As concerns future TFEL development, the most urgent and important subjects are full colouring in order to confirm a solid position in the flat display panel and to get a wider market including general consumer goods. The brightness of red and green colour EL have reached to practical level. But, the brightness and purity of blue colour have to make a further step.

In order to produce a full colour EL panel, it is important to first make fundamental research on EL materials of red, green and blue colours in well balanced brightness, and then efforts will be made to develop the panel structure and process technologies. It would be appropriate to get three primary colours using the same host material. For the moment, different host materials will be used in the present developing stage.

Monochrome thin film EL technology has established its position in the display market as an important flat panel technology. An increasing market share in the fast growing flat panel market is forecast for thin film EL in the future. There is, however, still a lot of further development potential in the thin film EL technology. It is quite obvious that reduction of power consumption, increase of luminance and improvements of colour thin film EL displays are needed. The prospects of growing tailored (or layered) colour phosphor film structures using modern thin film growth techniques open completely new perspectives. How fast the improvement of colour films will be realized depends more on innovations. Full colour thin film EL displays will have a much more simple structure than full colour LCDs and

consequently production costs can be expected to be lower, a fact that will be further enhanced as the display size become larger. The visual appearance will also be superior once sufficient luminance is achieved.

1.3.2 Current Status of EL Displays

The physical properties of EL devices need be understood for their development e.g. excitation and emission process, efficiency, concentration quenching and structure of EL. Many models and measuring techniques are used for supporting the basic theory. Many papers were published in six meetings of the International Workshop on Electroluminescence and in periodicals in recent years. At present much research theory is being studied for increasing the efficiency and improvement of EL devices.

EL displays can be divided into DC and AC EL displays whose structures are different. Generally AC structure is a three layers sandwich. The active layer is sandwiched between insulating layers. In order to increasing luminance and efficiency a multi layer structure of phosphor material layer has been developed for loss free carrier acceleration[16]. In order to widen spectrum of EL and realize white light for colour, multi-layer structures have been designed and researched[17],[18].

Monochrome ZnS:Mn thin film EL displays are available commercially. Considerable research efforts have already been made on colour thin film EL phosphor so that multi and full colour EL displays are also available in the future.

In order to realize colour displays, the basic structures (refer to description in later chapter 8) have been proposed to build multi-colour thin film EL displays. The first is a layered structure. This can be implemented either on a single substrate or on multiple substrates. The second type of structure is the patterned colour structure. This can be realized with either a patterned phosphor or a patterned filter approach. The patterned colour structure utilizes a single substrate and the standard electrode materials of monochrome thin film EL displays.

ZnS phosphors doped with rare earth ions produce luminescence with various colours, but one of the serious problems of rare earth doped ZnS thin films is the low solubility of rare earth ions into the ZnS lattice. Since rare earth ions are trivalent, they could be introduced into ZnS films with charge compensators to keep charge neutrality such as ZnS:TbF[19], ZnS:TbF_3 [20], [21], ZnS:TbOF[22] and ZnS:SmF[23]. With charge compensation luminance levels of ZnS:Tb were achieved [24], but the luminance is still

low.

Alkaline earth sulfides are more ionic than ZnS. The ionic radii of rare earth (IIIA) ions are very close to those of alkaline earth (IIB) ions compared with Zn (IIA) ions. In addition, the chemical nature of IIA and IIIA ions resemble each other. Rare earth luminescent centres are considered to be more effectively incorporated in these lattices without considering any solubility problem.

In table 1.1 some phosphors are summarised.

Table 1.1 Some phosphors and their EL spectra.

Phosphors	Colour
ZnS:Mn	Yellow-orange
ZnS:TbF	Green
ZnS:SmCl	Reddish-orange
ZnS:TmF	Blue
CaS:Eu	Red
SrS:CeK	Blue-green
ZnS:PrF	White
SrS:PrK	White
SrS:Ce,K,Eu	White

A range of phosphor colours is the key to colour EL displays. The development of new electroluminescent materials of white colour or various colours of red, green and blue is a final goal of EL researches both in fundamental and application. EL materials with rare earth ions as luminescent centres and II-VI compounds such as ZnS, CaS and SrS as host materials have been researched.

The specification for the minimum white areal brightness required for full colour display is 35 cd/m^2. Requirement of a white areal luminance of 50 cd/m^2 has been suggested by Pleshko[25]. In the long run HDTV may demand about 200 cd/m^2 of white luminance [26]. A patterned phosphor structure with equal fill factor for each colour requires a 26.5/65.8/7.7 luminance ratio for the red, green and blue primaries respectively assuming all

colours have TV CIE coordinates[27]. The following table 1.2 gives the pixel luminance values needed to achieve both the 35 and 50 cd/m^2 white real brightness targets assuming 0.22 fill factor for each primary colour.

Table 1.2 RGB pixel luminance requirements for colour displays.

Colour	Pixel luminance areal white=35 cd/m^2	Pixel luminance areal white=50 cd/m^2
Green	104 cd/m^2	150 cd/m^2
Blue	12 cd/m^2	17 cd/m^2
Red	42 cd/m^2	60 cd/m^2

ZnS:Tb is the most efficient green phosphor. Essentially equivalent green luminance values of about 70 cd/m^2 at 60 Hz drive have been achieved using ALE (atomic layer epitaxy) deposition[28]. Pure blue emission with sufficient luminance and efficiency is more difficult, but a blue luminance of 10 cd/m^2 has been achieved using a new ZnS/SrS:Ce multilayer phosphor structure. The highest red EL luminance has been achieved using thin film filter integrated into a ZnS:Mn thin film EL device. A luminance of 75 cd/m^2 was obtained at 60 Hz[29]. Although colour phosphor materials have been developed, further improvement of them is needed for increasing their luminance.

Deposition techniques and deposition conditions determine the crystal structure, surface and cross sectional morphologies and electric and optical characteristics of every layer in EL displays. The deposition methods of thin films are divided into physical methods and chemical methods. In the fabrication of ZnS:Mn EL displays, by the low temperature physical vapour deposition methods, thin columnar crystals with a zincblende crystal structure were obtained. By the high temperature CVD methods, large grain columnar crystals with a wurtzite crystal structure were obtained, and luminous efficiency is larger in CVD prepared EL devices[30]. The deposition and treatment temperature determine the characteristics of EL displays.

Monochrome displays and colour displays consist of multiple layers. Colour displays have more complex structures which include active layers, insulating layers, conducting layers and filters. Thickness and purity of every layer should controlled. Using physical methods the

former layers do not easily react during deposition of later films. In CVD methods the former layers may react with gases in deposition of later layer at high temperature so that the characteristics of the former layers change. In general physical methods need vacuum equipments so they are expensive. Chemical methods usually are less expensive and do not use large high vacuum equipment for a large area display.

The advantages of EL displays make them useful in many applications. Sharp, Planar and Finlux have developed the EL display industry continually. Sharp has developed and produced the highest pixel count EL display to date: an 1152x900 array and also began regular deliveries of 640×480, 16 grey scale state of art display. Planar systems also introduced several new products including some low energy displays[31].

In general, the attainment of high efficiency and luminance, multi and full colour EL displays depends upon research on basic theory and new materials, improvements of materials characteristics, structure design and processing and deposition technology.

1.3.3 Advantage of EL Displays Compare to Other Displays

EL displays have many advantages that other displays have not. In displays many characteristics of EL displays are currently moderate compared with other types. If they are improved EL displays will replace other displays in many areas.

EL displays have the following advantages:

a. EL has excellent viewability.

b. EL is fast.

c. EL is solid state.

d. EL is inherently easy to produce.

e. EL has good luminous efficiency.

f. EL has good resolution

g. EL is long life.

h. EL displays have a relative simple structure.

No other technology has the inherent capabilities that characterize EL.

The monochrome product performance will be improved in the following area:

a. Increased brightness.

b. Reduced power.

c. Decreased electrode resistance.

d. Elimination of the circular polarizer as a means of contrast enhancement.

e. Reduction in operating voltage.

The present development of LCD displays has made great progress in commercial products. The thin film EL flat panel display technology has great potential. There are good reasons to anticipate that the power consumption of thin film EL displays can be decreased to a level sufficiently low for battery operation. Improvement in the performance of the primary colour phosphors is still needed so that commercial display requirements can be satisfied. When compared to production costs and investments of corresponding LCDs, thin film EL colour display are expected to be very competitive because of a simple device structure.

1.3.4 Development of EL Displays in Future

An ideal electroluminescent device should be bright, efficient, available in a range of colours, cheap, long-lasting, robust and preferably made of non-toxic material. For addressable displays there may be additional requirements such as fast enough response and the existence of a drive threshold.

Power consumption, screen resolution, number of grey scales and number of the colours are required to follow the market. Battery operated pc (personal computer) products will be an increasing percentage of the growing portable pc market, lower power is a solved problem at present for requirement of market. In addition, for lower power colour display, thin film EL technology has a unique opportunity. It is the only flat panel display technology for which, there could be no appreciable difference in the power required for the multicolour display, as compared to the monochrome display, for the same brightness levels, if the efficiencies were at the required level.

The growth in screen information of personal computers is required now for many applications such as CAD (computer aided design). In the past, this has been driven primarily by the convenience of having a screen which can display a full page of information. In addition, the requirement for the number of grey scale for monochromatic displays and the number of colours for colour displays has also been increasing. For the lower cost monochrome displays, grey scales to simulate colour and to provide smoothness of shading has been driving the increase in requirements. For colour, smoothness of shading more than colour differentiation has driven the number of colour up, especially for applications such as CAD.

1.4 Deposition Technology of Thin Films

Thin film technology is simultaneously one of the oldest arts and one of the newest science. Thin film science and technology play a crucial role in the high tech industries that will bear the main burden of future. While the major exploitation of thin films has been in microelectronics, there are numerous and growing applications in telecommunications, optical electronics, coatings of all kinds, and in energy generation and conservation strategies.

Methods of preparing thin films may be divided essentially into two main groups, namely, chemical methods and physical methods. Physical methods such as sputtering and vacuum evaporation can result in the formation of very pure and well-defined films, but they requires lowered pressure in the working space and make use of vacuum techniques. Chemical methods are deposition technologies of films under chemical reaction conditions. Chemical methods have the ability to produce a large variety of films and coatings of metals, semiconductors, and compounds in either crystal or vitreous form, possessing high purity and desirable properties. Furthermore, the capability of controllably creating films of widely varying stoichiometry makes chemical methods applicable to many fields among deposition techniques. Other advantages include relatively low cost of equipment and operating expenses, suitability for both batch and semicontinuous operation, and compatibility with other processing steps.

The fabrication of EL displays, light emitting diodes, liquid crystal displays, plasma displays, vacuum fluorescent displays and electrochromic displays requires conductive films, transparent and conductive films, luminescent or fluorescent films as well as dielectric and insulating layers. The qualities and characteristics of films and displays and the process of fabrication relate to the methods of film deposition.

1.4.1 Chemical Methods

Chemical and electrochemical methods include electrolytic deposition, electroless deposition, anodic oxidation, chemical vapour deposition and so on, but only some of them have been used in fabrication of EL displays.

1.4.1.1 Chemical Vapour Deposition

Chemical vapour deposition (CVD) is widely used method in semiconductor technology for preparation of thin films of high purity and is the process of chemically reacting a volatile

compound of a material to be deposited, with other gases, to produce a nonvolatile solid that deposits atomistically on a suitably placed substrate. It consists of surface reaction, on a solid surface, involving one or more gaseous reacting species. To carry out such deposition, several types of chemical reactions are available. One of them is pyrolysis; another is photolysis of gaseous compounds. With new technology and for some purposes chemical vapour deposition is classified into atmospheric-pressure CVD (APCVD), low-pressure CVD (LPCVD), metalorganic CVD (MOCVD), photo-enhanced CVD (PHCVD), plasma-enhanced CVD (PECVD), laser-enhanced CVD (LECVD), electron-enhanced CVD and so on which promises many interesting and useful applications in the thin film deposition processes and techniques.

1.4.1.2 Spray Pyrolysis

Spray pyrolysis involves spraying of solution, usually aqueous, containing soluble salts of the constituent atoms of the desired compounds onto heated substrates. Whether or not the process can be classified as CVD depends on whether the liquid droplets vaporize before reaching the substrate or react on it after splashing. The technique is very simple and is adaptable for mass production of large-area coatings for industrial applications. Various geometries of the spray set-ups are employed, including an inverted arrangement in which larger droplets and gas phase precipitates are discouraged from reaching the substrate, resulting in films of better quality. The size of the droplets and their distribution affect the uniformity of the surface.

1.4.1.3 Dip technique

The dip technique consists essentially of inserting the substrate into a solution containing hydrolysable metal compounds and pulling it out at a constant speed into an atmosphere containing water vapour. In this atmosphere, hydrolysis and condensation processes take place. Finally, the films are hardened by a high temperature cycle to form transparent metal oxides. Any hydrolysable compound including halides or nitrates but preferably metalorganics are suitable for this process. The important control parameters are the viscosity of the solution, the pulling speed and the firing temperature. The rate of heating also needs to be controlled to avoid cracking of the films. The technique has been used commercially to deposit large-area coatings (about 10-12 m^2) for a multitude of applications[32]. The

dip technique will be discussed in the following chapter.

From this brief survey it is already clear that the majority of chemical methods of preparation of thin films are only applicable to a small group of materials. Some of methods are excellent and are frequently used in many technologies and applications. It is worth mentioning that for industrial purposes relatively simple methods were developed which allow deposition of thin or thick films of large-area such as spraying, spray-pyrolysis and dip coating.

1.4.2 Physical Methods

Physical deposition of films is the physical processes. The objective of these processes is controllably transfer atoms from a source to substrate where film formation and growth proceed atomistically. The main properties are

1. Reliance on solid or molten sources
2. Physical mechanisms (collisional impact or evaporation) by which source atoms enter the gas phase
3. Reduced pressure environment through which the gaseous species are transported
4. General absence of chemical reactions in the gas phase and at the substrate surface (reactive PVD processes are exceptions).

1.4.2.1 Evaporation

Vacuum and also reactive evaporation using different sources have been employed to deposit various films. The important control parameters are the evaporation rate, substrate temperature, sources-to-substrate distance partial pressure. Vacuum evaporation is currently the most widely used method for the preparation of thin films. The method is comparatively simple, but it can in proper experimental conditions provide films of extreme purity and, to a certain extent, of preselected structure.

The process of film formation by evaporation consists of several physical stages:

(1) transformation of the material to be deposited by evaporation or sublimation into the gaseous state;

(2) transfer of atoms (molecules) from the evaporation source to the substrate;

(3) deposition of these particles on the substrate;

(4) their rearrangement or modifications of their binding on the surface of the substrate.

Atoms or molecules are liberated by heating from every material in its solid or liquid phase and that in a closes system a certain equilibrium pressure, which is called the saturated-vapour pressure, is established at a given temperature. The dependence of this pressure on temperature is rather strong.

(a) Direct evaporation

Thin films have been deposited by thermal, electron beam or laser beam evaporation of sources for thin film deposition.

(b) Reactive evaporation

Reactive evaporation of films has been achieved by the vacuum evaporation of the corresponding metal, alloy or other material sources in an reactive material atmosphere onto substrates heated to a certain temperature.

(c) Activated reactive evaporation

In the activated reactive evaporation (ARE) method, the reaction between the evaporated species and the gases is activated by establishing a thermionically assisted plasma in the reaction zone. A dense plasma is generated in the reaction zone by employing a thoriated tungsten emitter and low voltage anode assembly. The technique has been used to deposit excellent quality films.

(d) Post-treatment of metal or alloy films

Thin films of metal or alloy evaporated can be improved by the post treatment of the respective metal films or alloy films.

1.4.2.2 Sputtering

Sputtering is one of the most extensively used techniques for the deposition of films. Both reactive and non-reactive forms of d.c. and r.f. sputtering, and recently, magnetron and ion beam sputtering have been used. Regardless of the type of sputtering, however, roughly similar discharges, electrode configurations, and gas-solid interactions are involved.

(a) Sputtering

Sputtering is a process operating an atomic or molecular scale whereby an atom or molecule of material is ejected when the surface is struck by a fast incident particle. The momentum of incident atom is transferred to the atoms in the target material and this momentum transfer can often lead to the ejection of a surface atom -the sputtering process. In order for the sputtering process to be efficient, the incident particle also has be of atomic dimensions.

(b) Reactive sputtering

In some cases, gases or gas mixtures other than Ar are used. Usually this involves some sort of reactive sputtering process in which a compound is synthesized by sputtering a metal target in a reactive gas to form a compound of the metal and the reactive gas species. Reactive sputtering is also used to replenish constituents of compound targets lost by dissociation. Elevated substrate temperatures or a post-deposition heat treatment results in changes of microstructure, which depend primarily on the sputtering rate and sputtering pressure and conditions. The dynamics of the reactive sputtering process has been studied in detail and the conditions which determine the appearance of various phases in films, and hence control the stoichiometry, have been identified.

(c) Ion beam sputtering

Ion beam sputtering processes were invented to provide independent control of the deposition parameters and, particularly, the characteristics of the ions bombarding the substrate. Ion beams are used in thin film deposition in two main ion source configurations. In the dual-ion-beam system, one source provides the inert or reactive ion beam to sputter a target in order to yield a flux of atoms for deposition onto the substrate. Simultaneously, the second ion source, aimed at the substrate, supplies the inert or reactive ion beam that bombards the depositing film. Separate film thickness rate and ion current monitors, fixed to the substrate holder, enable the two incident beam fluxes to be independently controlled.

In the second configuration, an ion source is used in conjunction with a deposition material source. The process, known as ion-assisted deposition, combines the benefits of high film deposition rate and ion bombardment. The energy flux and direction of the ion beam can regulated independently. Unlike r.f. sputtering, ion beam sputtering involves minimal intrinsic heating and electron bombardment and hence constitutes a low temperature deposition method.

(d) Chemical sputtering

Chemical sputtering involves the reaction of an excited neutral or ionized gas with a surface to form volatile compounds. This technique is mainly used for plasma treatment of organic surfaces and for etching in plasmas. However, it is sometimes a factor in film deposition. When targets containing reactive anions are sputtered, some of these anions are sputtered as secondary ions and accelerated toward the substrates where chemical etching reactions can occur.

1.4.2.3 Reactive Ion Plating

Reactive ion plating is a promising alterative to high temperature deposition processes. The technique is essentially a reactive evaporation or magnetron sputtering of metals alloys, aided by a low power r.f. discharge directed towards the substrate. The resulting bombardment of energetic ion or atoms provides energy to the surface of the substrate and of the growing film, obviating the need for substrate heating. The presence of ionized reactive species also facilitates their reaction with the evaporated or sputtered atoms. The influence of various control parameters such as negative substrate bias, residual gas composition and deposition rate on the properties of films is important factor of film quality.

Perhaps the chief advantage of ion plating is the ability to promote extremely good adhesion between the film and substrate. A second important advantage is the high "throwing power" when compared vacuum evaporation. This results from gas scattering, entrainment, and sputtering of the film, and enables deposition in recesses and on the area remote from the source substrate line of sight. Relatively uniform coating of substrates with complex shapes is thus achieved. Lastly, the quality of deposited films is frequently enhanced. The continual bombardment of the growing film by high energy ions or neutral atoms and molecules serves to peen and compact it to near bulk densities.

1.5 Major Parameters and Characteristics of Thin Films

The desired material characteristics of the deposited films will be in most cases the decisive factor for the selection of a preferred deposition technology. In many, if not most, instances the characteristics of a thin film can be quite different from the bulk volume ratio. In addition, the morphology, structure, physical and chemical characteristics of the thin film can also be quite different from those of the bulk materials. The surface and /or interface properties of the substrate to be coated can influence thin film characteristics drastically due to surface contamination, nucleation effects, surface mobility, chemical surface reactions, adsorbed gases, catalytic or inhibitory effects on film growth, surface topography, and crystallographic orientation, and stress effects due to thermal expansion mismatch.

The major physical and chemical parameters of thin films of EL displays to be considered can be listed as follows:

Electric:

Conductivity for conductive films

Resistivity for resistive films

Dielectric constant

Dielectric strength

Dielectric loss

Stability under bias

Polarization

Permittivity

Electromigration

Radiation hardness

Thermal:

Coefficient of expansion

Thermal conductivity

Temperature variation of all properties

Stability or drift of characteristics

Thermal fusion temperature

Volatility and vapour pressure

Mechanical:

Intrinsic, residual, and composite stress

Adhesion

Density

Fracture

Morphology:

Crystalline or amorphous

Structural defect density

Conformality/step coverage

Planarity

Microstructure

Surface topography

Crystallite orientation

Optical:

Refractive index

Absorption

Spectral characteristics

Dispersion

Chemical:

Composition

Impurities

Reactivity with substrate and ambient

Thermodynamic stability

Etch rate

Corrosion and erosion resistance

Toxicity

Hygroscopicity

Impurity barrier

Gettering effectiveness

Stability

1.6 Objectives of the Project

The interest in developing reliable luminescent materials, and deposition technology and EL device structure for applications on flat panel displays has produced a considerable research effort in this area. This effort has been directed on film deposition techniques as well as on different types of materials and dopants usable as active components on electroluminescent devices. Applications of ZnS and ZnS:Mn films in electroluminescent displays have been studied more and more. Mn-doped ZnS is one of the most studied materials for luminescent devices. Zinc sulphide is a semiconductor suitable to be used as host matrix for a large variety of dopants because of its wide energy band gap. The luminescent properties of this material doped with Mn have proved to be adequate for electroluminescence applications. Manganese is generally incorporated in the ZnS lattice as a Mn^{2+} ion in substitutional sites. The excitation and decay of this ion produces a yellow luminescence at approximately ~590 nm associate with a transition between energy levels.

Thin films of zinc sulphide have been prepared by a wide variety of techniques, including reactive evaporation, RF sputtering, DC and ion beam sputtering, chemical vapour deposition, atomic layer epitaxy and spray pyrolysis. The above methods usually required complex equipment or vacuum condition. Compared to conventional thin film forming processes the

sol-gel film formation requires considerably less equipment and is less expensive, and is an efficient and simple method for the deposition of large area metal oxide film. The method of conversion of ZnO films is simpler and less expensive and yields large area, pure, homogeneous and controllable dopant concentration zinc sulphide films.

Electroluminescent display devices consist of several films which include phosphor film, insulating films and transparent conducting film. In order to realize the electroluminescent devices using the sol-gel process, the first thing is to complete the deposition of the phosphor film.

Because of the limitation of deposition technology a fabrication method for large area, cheaper and superior characteristic EL displays is an unsolved problem. Because of the advantages of the sol-gel process it was chosen as deposition method in fabricating a large area and less expensive EL display.

The objective of this work was completed with the deposition of several films:

(1) Electroluminescent layer:

Deposit ZnS, doped Mn ion ZnS and doped rare earth ion ZnS films and measure the characteristics of EL films.

(2) Insulating films:

As insulating film of EL device Al_2O_3 and SiO_2 were deposited respectively. The insulating films have a good dielectric properties and deposited easily in manufacturing EL devices.

(3) Transparent conducting film:

The transparent conducting film ZnO:Al was chosen to be deposited in the work.

(4) Structure of EL device

The designed structure of EL devices should suit using the sol-gel process.

(5) Measurement of EL device

The characteristics of EL devices was measured. The characteristics include the EL spectra of phosphor materials and the relationship of brightness and applied voltage, driving frequency, Mn concentration, thickness of active layer and different insulating films.

In short, the objectives were to find a method for manufacturing the thin film EL display device using the sol-gel process. The depositions of several type films with the sol-gel technology and their properties were studied for the foundation of other applications.

Chapter 2

SOL-GEL TECHNOLOGY

2.1 Introduction

2.1.1 Historical Development of Sol-gel Science

A sol is a colloidal suspensions of solid particles in a liquid. The sol may be produced from inorganic or organic precursors and may consist of dense oxide particles or polymeric clusters. A gel is the substance where one molecule reaches macroscopic dimensions so that it extends throughout the solution. Sol-gel science has been researched for many years and the technology of sol-gel has been used in many areas.

The first metal alkoxide was prepared from $SiCl_4$ and alcohol by Ebelmen[33], who found that the compound gelled on exposure to the atmosphere. However, these materials remained of interest only to chemists for almost a century. It was finally recognised by Geffcken[34] in the 1930s that alkoxides could be used in the preparation of oxide films. This process was developed by the Schott glass company in Germany and was quite well understood, as explained in the excellent review by Schroeder[35].

Inorganic gels from aqueous salts have been studied for a long time. The network structure of silica gels was widely accepted in the 1930s, largely through the work of Hurd[36], who showed that they must consist of a polymeric skeleton of silicic acid enclosing a continuous liquid phase. The process of supercritical drying to produce aerogels (aerogel is one of dried gels which is dried by supercritical extraction of solvent.) was invented by Kistler[37] in 1932, who was interested in demonstrating the existence of the solid skeleton of the gel, and in studying its structure. Around the same time, mineralogists became interested in the use of sols and gels for the preparation of homogeneous powders for use in the studies of phase equilibria. Roy working in the ceramics community prepared homogeneous powders with these methods[38],[39]. That work, however, was not directed towards an understanding of the mechanisms of reaction or gelation, nor the preparation of shapes (monoliths). Much more sophisticated work, both scientifically and technologically, was being carried out in the nuclear-fuel industry, but it was not published until later[40],[41]. The goal of this work was to prepare small spheres (tens of μm in diameter) of radioactive oxides that would be packed into fuel cells for nuclear reactors. The advantage of the sol-gel processing was that it avoided generation of dangerous dust, as

would be produced in conventional ceramics processing, and facilitated the formation of spheres. The latter was accomplished by dispersing the aqueous sol in hydrophobic organic liquid, so that the sol would form into small droplets, each of which would subsequently gel. The ceramics industry showed more and more interest in gels in the late 1960s and early 1970s. Levene and Thomas[42] and Dislich[43] developed independently controlled hydrolysis and condensation of alkoxides for preparation of multicomponent glasses. Several companies made ceramic fibers from metalorganic precursors on a commercial basis [44], [45], [46]. Yoldas[47],[48] and Yamane et al.[49] produced monoliths by careful drying gel. This is a bit ironic in retrospect, as it is evident that monoliths are the least technologically important of the potential applications of gels.

The range of substrates that can be coated is not limited to the capability of withstanding a high firing temperature because of the associated low temperature for processing the gel. Thus it is possible to put an inorganic sol-gel coating on plastic. The majority of coatings have been applied by this technique in order to achieve some specific optical quality. The literature about coating solutions cites examples of more than 45 years ago. Much of the progress leading to commercial coatings has been pioneered by Schott in Germany.

Because it is possible to progress from sol to gel in a controlled manner, it is also possible to control the viscosity. This is extremely useful in the production of fibers. The expression is that solutions must exhibit spinnability in order to form fibers.

Great strides have been made in the past few years in understanding the fundamental aspects of preparing homogeneous multicomponent ceramics (crystalline and amorphous) from alkoxide-derived gels with the development of the technology that preceded the science of sol-gel process.

Sol-gel processing is now well accepted as a technology for preparing thin films, coating, fiber, monoliths, microsphere and fine powders.

2.2 Applications of Sol-gel Process

Applications for sol-gel processing derive from the various special shapes obtained directly from the gel state (e.g., monoliths, films, fibers, and monosized powders) combined with compositional and microstructural control and low processing temperatures. Compared to conventional sources of ceramic raw materials, often minerals dug from the earth, synthetic chemical precursors are a uniform and reproducible source of raw materials that can be made

extremely pure through various synthetic means. Low processing temperatures, which result from microstructural control (e.g., high surface areas and small pore sizes), expand glass-forming regions by avoiding crystallization or phase separation, making new materials available to the technologist. In the opposite sense, microstructural control results from low processing temperatures, since metastable porous structures created in solution are preserved, leading to applications in filtration, insulation, separations, sensors, and anti-reflective surfaces. The advantages of the sol-gel process are summarized:

1. Better homogeneity from raw materials.
2. Better purity of materials.
3. Low temperature of preparation which leads to:
    a. Conservation of energy;
    b. Minimization of evaporation losses;
    c. Minimization of air pollution;
    d. No reactions with containers, thus purity;
    e. Bypassing of phase separation;
    f. Bypassing of crystallization.
4. New non-crystalline solids outside the range of normal glass formation.
5. New crystalline phases from new non-crystalline solids.
6. Better glass products from special properties of gel.
7. Special products such as films.

Some disadvantages of the sol-gel methods are:

1. High cost of raw materials.
2. Large shrinkage during processing.
3. Residual fine pores.
4. Residual hydroxyl.
5. Residual carbon.
6. Health hazards of organic solution.
7. Long processing times.

Thin films benefit from most of the advantages of sol-gel processing just cited while avoiding these disadvantages; as of 1989, thin films are one of the few successful commercial applications. However even films suffer from cracking problems associated with attempts to prepare thick films (>1μm).

Sol-gel processes have been applied in producing films, fibres, monoliths, powders, composites, and porous media because of the potential advantages of sol-gel process.

Thin films and coatings

Films and coatings represent the earliest commercial application of sol-gel technology. Thin films (normally <1μm in thickness) formed by dipping or spinning use little in the raw materials and may be processed quickly without cracking, overcoming most of the disadvantages of sol-gel processing. In addition, large substrates may be accommodated and it is possible to uniformly coat both sides of planar and axially symmetric substrates such as pipes, tubes, rods, and fibers not easily handled by more conventional coatings. Since then, many new uses for sol-gel films have appeared in electronic, protective, membrane, and sensor applications.

Some applications of films and coatings:

1. Optical coatings
    - Coloured
    - Anti-reflective coatings
    - Optoelectronic
    - Optical memory
2. Electronic coatings
    - Photo anodes
    - High-temperature superconductors
    - Conductive
    - Ferroelectric-Electro-optic
3. Protective coating
    - Corrosion-resistant
    - Mechanical
        - Planarization
        - Scratch- and wear-resistant
        - Strengthening
        - Adhesion promoting
    - Passivation (electronic)
4. Porous coating

5. Miscellaneous coatings

Monoliths

Monoliths are defined as bulk gels cast into shape and processed without cracking. Monolithic gels are potentially of interest because complex shapes may be formed at room temperature and consolidated at rather low temperatures without melting.

Some applications of monolithic gels:

1. Optical glasses and fiber-optic preforms
2. Graded reflective index glass
3. Ultra-low expansion glass
4. Near net shape optical components
5. Aerogel transparent insulation
6. Substrates

Powders, grains and spheres

Potential advantages of sol-gel powders over conventional powders are controlled sized and shape, molecular scale homogeneity, and enhanced reactivity (lower processing temperature).

Some applications of gel-derived powders, grains and spheres:

1. High-temperature superconductors
2. Electronic
3. Refractory compositions
4. Waste immobilization
5. Abrasive grains
6. Nuclear fuel
7. Beads and microspheres

Fibers

Sol-gel methods may be used to prepare some fibers such as continuous, refractory, polycrystalline fibers that exhibit high strength and stiffness in addition to chemical durability.

Applications of gel-derived fibers:

1. Reinforcement
2. Superconducting

3. Electrolysis
4. Optical

Composites

Composites combine different types of materials to obtain synergistic properties unattainable by one material alone. Sol-gel processing can be used to form the matrix phase, the reinforced phase or phases (fibers, particles, etc.) or both in ceramic-ceramic composites. Because of inherently low processing temperatures, mixed organic-inorganic and ceramic-metal composites are also possible.

Applications of sol-gel composites:
1. Fiber-reinforced sol-gel matrix
2. Ceramic-ceramic or ceramic-metal
3. Glass or ceramic-organic

Porous gels and membranes

High surface areas and small pore sizes characteristic of inorganic gels are properties unattainable by conventional ceramic processing methods. These unique properties may be exploited in applications such as filtration, separations, catalysis, and chromatography.

Applications of porous gels and membranes:
1. Membranes
2. Porous glass substrates
3. Catalyst supports

2.3 Theory of Sol-gel Process

2.3.1 Hydrolysis and Condensation

A sol is a colloidal suspension of solid particles or polymers in a liquid. A colloid is a suspension in which the dispersed phase is so small (~1-1000 nm) that gravitational forces are negligible and interactions are dominated by short-range forces, such as van der Waals attraction and surface charges. If a monomer can make more than two bonds, then there is no limit on the size of the molecule that can be formed. If one molecule reaches macroscopic dimensions so that it extends throughout the solution, the substance is said to be a gel. The gel point is the time at which the last bond is formed that completes this giant molecule.

Thus a gel is a substance that contains a continuous solid skeleton surrounding, supporting and enclosing a continuous liquid phase. Gels can also be formed from particulate sols, when attractive dispersion forces cause them to stick together in such a way as to form a network. The sol-gel process uses inorganic or metal organic compounds as raw ingredients. In aqueous or organic solvents these compounds are hydrolysed and condensed to form inorganic polymers composed of M-O-M or M-O-M' bonds. For inorganic compounds hydrolysis proceeds by removal of a proton from an aqueous reaction to form a hydroxy (M-OH) or (M=O) ligand. Condensation reactions involving the hydroxy ligands result in inorganic polymers in which the metal centres are bridged by oxygens or hydroxyls.

The most commonly used metal organic compounds are metal alkoxides $M(OR)_x$. Where R is an alkyl group C_nH_{2n+1}. However, several factors have been known in sol-gel processing:

(1) The lower electronegativity of the transition metals causes them to be the more electrophilic and thus less stable toward hydrolysis, condensation, and other nucleophilic reactions.

(2) Transition metals often exhibit several stable coordinations. When coordinatively unsaturated, they are able to expand their coordination via olation, oxoation, alkoxy bridging, or other nucleophilic association mechanisms.

(3) The greater reactivity of transition metal alkoxide requires that they be processed with stricter control of moisture and conditions of hydrolysis in order to prepare homogeneous gels rather than precipitates.

(4) The generally rapid kinetics of nucleophilic reactions had led to further fundamental studies of hydrolysis and condensation reaction of transition metal alkoxides. Normally the alkoxide is dissolved in alcohol and hydrolysed by addition of water under acidic, neutral, or basic conditions.

A macromolecular oxide network is obtained through hydrolysis and condensation. The reactions are usually expressed as follows, Hydrolysis:

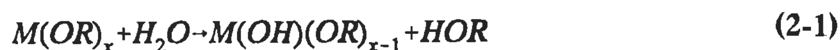

$$M(OR)_x + H_2O \rightarrow M(OH)(OR)_{x-1} + HOR \qquad \textbf{(2-1)}$$

Condensation:

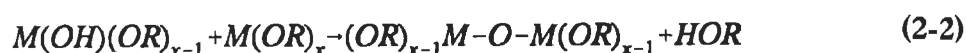

$$M(OH)(OR)_{x-1} + M(OR)_x \rightarrow (OR)_{x-1}M{-}O{-}M(OR)_{x-1} + HOR \qquad \textbf{(2-2)}$$

The overall reaction being:

$$M(OR)_x + \frac{x}{2} H_2O \rightarrow MO_{\frac{x}{2}} + xROH \qquad \textbf{(2-3)}$$

Chemical additives are always used in order to improved the process and obtain better materials. Acid or base catalysts can influence both the hydrolysis and condensation rates and the structure of the condensed product. Acids serve to protonate negatively charged alkoxide groups, enhancing the reaction kinetics by producing good leaving groups, and eliminating the requirement for proton transfer within the transition state. Hydrolysis goes to completion when sufficient water is added. The relative ease of protonation of different alkoxide ligands can influence the condensation pathway as demonstrated by consideration of a typical partially hydrolysed polymer. Usually base additions promote the hydrolysis. Condensation kinetics are systematically enhanced under basic conditions in some case.

The simplest method of preparation of multicomponent systems involves making a solution of all components as alkoxide precursors in a suitable organic solvent and then reacting the solution with water to form the oxide mix. The reaction can be represented as follow:

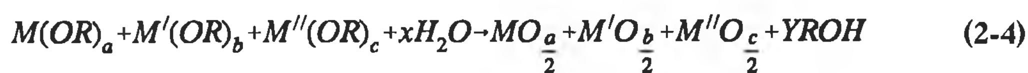

$$M(OR)_a + M'(OR)_b + M''(OR)_c + xH_2O \rightarrow MO_{\frac{a}{2}} + M'O_{\frac{b}{2}} + M''O_{\frac{c}{2}} + YROH \qquad \textbf{(2-4)}$$

Making multicomponent system coatings is easer in some cases and is more difficult in other cases. The reason for the difficulties is the different hydrolysis rates of various alkoxides.

2.3.2 Gelation

Gels are sometimes defined as "strong" or "weak" according to whether the bonds connecting the solid phase are permanent or reversible. The simplest picture of gelation is that clusters grow by condensation of polymers or aggregation of particles until clusters collide: links formed then between the clusters to produce a single giant cluster that is called a gel. The sudden change in rheological behaviour is generally used to identify the gel point in a crude way. The time of gelation is sometimes defined as corresponding to a certain value of viscosity; it may be defined as the time at which the solution loses fluidity. The reactions that produce gelation do not stop at the gel point. There is a substantial fraction of oligomers that are free to diffuse and react, and even the spanning cluster retains enough internal mobility to allow further condensation reactions. Therefore, the properties of a gel, such as elastic modulus and viscosity, continue to change after the time of gelation. The process,

known as aging, may result in substantial structural reorganization of the network, including coarsening of the pores or precipitation of crystals, or simply a stiffening of the network through formation of additional cross-links.

2.3.3 Aging of Gels

The chemical reactions that cause gelation continue long after the gel point, producing strengthening, stiffening, and shrinkage of the network. Processes of dissolution and reprecipitation may coarsen the pore structure, and separation may occur into mixtures of solid-liquid, liquid-liquid, or solid-solid phases. These changes have a profound effect on the subsequent processes of drying and sintering.

Gelation is a spectacular event, when a solution suddenly loses it fluidity and takes on the appearance of an elastic solid. The processes of change during aging after gelation are categorized as polymerization, coarsening, and phase transformation. Polymerization is the increase in connectivity of the network produced by condensation reactions. Coarsening or ripening is a process of dissolution and reprecipitation driven by differences in solubility between surfaces with different radii of curvature.

The condensation reactions that bring about gelation also result in syneresis i.e. spontaneous shrinkage of gel and progressive strengthening and stiffening of the gel during aging. Since the same mechanism is responsible for all of these phenomena, they depend in the same way on such factors as pH, temperature, and composition of the solution. In liquids in which the solid phase is soluble, dissolution and reprecipitation processes cause coarsening as the material is transported to a surface of lower curvature. This may result in loss of micropores, decrease in surface area, and stiffening through growth of interparticle necks.

2.3.4 Drying of Gels

The process of drying of a porous material can be divided into several stages. At first the body shrinks by an amount equal to the volume of liquid that evaporates, and the liquid-vapour interface remains at the exterior surface of the body. The second stage begins when the body becomes too stiff to shrink and the liquid recedes into the interior, leaving air-filled pores near the surface. Even as the air invades the pores, the drying continues to occur from the surface of the body. Eventually, the liquid becomes isolated into pockets and drying can proceed only by evaporation of the liquid within the body and diffusion of vapour to the

outside. The driving forces and transport mechanisms are important during the drying of gels, which affect the structure and quantity of the gel products. The driving forces for shrinkage include chemical effects, such as condensation reactions, and physical effects, such as capillary pressure. Fluid transport occurs through a pressure gradient or diffusion down a chemical potential gradient, and deformation of the network may involve elastic, plastic, or viscoelastic strains. As the liquid is removed by evaporation, the tension that develops in the pores produces a contraction of the network. When the pressure is not uniform warping and cracking of the gel may result.

2.3.5 Avoiding Fracture

Drying produces a pressure gradient in the liquid phase of a gel, which leads to a differential shrinkage of the network. When the exterior of the gel shrinks faster than the interior, tensile stresses arise that tend to fracture the network at the exterior. The material on either side of the crack can contract more freely, so it is favourable for the crack to grow into the drying surface. It seems odd that compression of the network by the liquid causes a fracture to occur. In fact, if the pressure in the liquid were uniform, the whole network would be isotropically compressed and the gel would shrink without the risk of cracking. However, the higher tension in the liquid at the exterior causes greater contraction of the network in that region. Since that contraction is inhibited by the slower-contracting interior, the network at the exterior is effectively stretched, and this promotes cracking. Thus, it is the differential contraction that produces macroscopic tension in the network and this leads to cracking. Cracking occurs when the stress in the network exceeds its strength. Fracture of brittle materials depends on the presence of flaws that amplify the stress applied to the body, i.e, if a uniform stress is applied to a body containing a long crack, the stress at the tip of the crack is related to the length of the crack and the uniform stress and failure occurs when that stress exceeds the strength of the material. Cracking is sometimes attributed to the existence of a pore size distribution in gel.

A variety of strategies have been employed to avoid fracture from drying stresses, including: developing gels with larger pores (having lower capillary stress and higher permeability); aging to increase the strength of the gel, as well as increasing the pore size; using chemical additives to lower interfacial energies or encourage diffusion within the pores; supercritical drying to eliminate entirely the liquid/vapour interfacial energy, thereby preventing fracture

and reducing shrinkage.

2.3.6 Structural Evolution during Consolidation

Surface tension forces created in a gel during solvent removal cause the network to fold or crumple as the coordination of the particles is increased. Porosity develops when, due to additional cross-linking or neck formation, the gel network becomes sufficiently strengthened to resist the compressive forces of surface tension. Thus the dried xerogel (xerogel is a dried gels which is dried by evaporation) structure will be a contracted and distorted version of the structure originally formed in solution. Structural evolution in crystalline systems may be dominated by effects of phase transformations which often occur in conjunction with dehydration or when metastable transitional phases are involved. In crystalline systems, microstructural evolution is dominated by phase transformations that accompany gel dehydration or that result from phase metastability. Both phase transformations and crystallization of amorphous systems may involve changes in the coordination numbers of the network-forming species. In transformations that occur by nucleation and growth, the addition of "seeds" that serve as multiple nucleation sites appears to be a viable approach to microstructural control.

2.3.7 Sintering of Gel

Sintering is a process of densification driven by interfacial energy. Material moves by viscous flow or diffusion in such a way as to eliminate porosity and thereby reduced the solid-vapour interfacial area. Amorphous materials are sintered by viscous flow and crystalline materials are sintered by diffusion, so the paths along which material moves, and the relationship between the rate of transport and the driving force are quite different[50]. Viscous sintering is driven by the energy gained by reduction in the surface area of the porous body. Given a microstructural model, it is possible to relate the change in surface area to the overall change in dimensions. As for viscous sintering, the driving force densification of crystalline materials is surface energy. One important respect in which crystalline and amorphous materials differ is that the plane of contact between crystals, called the grain boundary, has a specific interfacial energy. This energy reflects the fact that the crystal planes in the respective particles do not match perfectly at the boundary. The existence of the grain boundary energy means that the energy gained by eliminating porosity is partially

offset by the energy invested in creating necks between the grains. It is advantageous to sinter the gel while it is amorphous and then crystallize after complete densification. In gels, where the area is enormous, the driving force is great enough to produce sintering at exceptionally low temperatures, where the transport processes are relatively slow. The kinetics of densification of gels are complicated by the concurrent processes of dehydroxylation and structural relaxation. This leads to the remarkable result that faster heating permits complete densification at a lower temperature. For crystalline gels there are the further complications of grain growth and phase transformations.

2.4 Film Formation

Certainly one of the most technologically important aspects of sol-gel processing is that, prior to gelation, the fluid sol or solution is ideal for preparing thin films by such common processes as dipping, spinning, or spraying. Compared to conventional thin film forming processes such as CVD, evaporation, or sputtering, sol-gel film formation requires considerably less equipment and is potentially less expensive; however the most important advantage of sol-gel processing over conventional coating methods is the ability to control precisely the microstructure of the deposited film, i.e., the pore volume, pore size, and surface area.

2.4.1 Physics of Film Formation

2.4.1.1 Dip Coating

Dip coating is a method of the film deposition. The batch dip coating process can be divided into five stages: immersion, start-up, deposition, drainage, and evaporation. There are six forces in the film deposition region governing the film thickness and position of the streamline: (1) viscous drag upward on the liquid by the moving substrate, (2) force of gravity, (3) resultant forces of surface tension in the concavely curved meniscus, (4) inertial force of the boundary layer liquid arriving at the deposition region, (5) surface tension gradient, and (6) the disjoining or conjoining pressure[51]. In dip coating, the substrate is normally withdrawn vertically from the liquid bath at a speed U. When the liquid viscosity and substrate speed U are high enough to lower the curvature of the meniscus, the deposited film thickness t results from the balances of the viscous drag which is directly proportional to ($\eta U/t$) and to the gravity force ($\rho t g$)[52]:

$$t=C(\frac{\eta U}{\rho g})^{\frac{1}{2}} \qquad (2\text{-}5)$$

where the constant C is about 0.8 for newtonian liquids; η is liquid viscosity, ϱ is liquid density and U is substrate speed.

When the substrate speed and viscosity are low (often the case for sol-gel film deposition) this balance is modulated by the ratio of viscous drag to liquid-vapour surface tension r according to the relationship derived by Landan and Levich[53]:

$$t=0.94\frac{(\eta U)^{\frac{2}{3}}}{r^{\frac{1}{6}}(\rho g)^{\frac{1}{2}}} \qquad (2\text{-}6)$$

The thickness of coating layer depends on:

(1) the speed of withdrawal from the coating solution.

(2) the concentration of solution.

(3) the viscosity of solution.

(4) the angles of withdrawal.

(5) the surface tension of solution.

(6) the vapour pressure, temperature and relative humidity above the coating bath.

(7) the precise control of air velocity.

(8) the temperature of substrate and solution.

2.4.1.2 Spin Coating

Spin coating is also a method of film deposition. When a substrate is spun the solution on the substrate forms a film. Spin coating is divided into four stages: deposition, spin-up, spin-off, and evaporation. An advantage of spin coating is that a film of liquid tends to become uniform in thickness during spin-off and, once uniform, tends to remain so provided that the viscosity is not shear dependent and does not vary over the substrate. This tendency arises due to the balance between the two main forces: centrifugal force, which drives flow radially outward, and viscous force (friction), which acts radially inward. The final thickness of the film depends on the initial thickness, time between spin-up and spin-off, angular velocity, the evaporation rate in spin coating and liquid viscosity.

Besides the dip coating process, other techniques have been developed. Instead of withdrawing the parts from the solution the level of tank solution can be lowered and the substrate to be coated remain stationary.

Although the process and the chemical reaction initially appear simple, the dependency of various process parameters is complex. Great care in relation to these influences is required and so guarantee reproducible coating thickness and layer quality.

2.4.2 Precursor Structure

The size and extent of branching of the solution precursors prior to film deposition and relative rates of evaporation and condensation during film deposition control the pore volume, pore size, and surface area of the final film. The viscosity progressively increases due both to the increasing concentration and further condensation reactions promoted by increasing concentration. Although the underlying physics and chemistry that govern polymer growth and gelation are essentially the same for films as bulk gels, several factors distinguish structural evolution in the film. (1) the overlap of the deposition and evaporation stages establishes a competition between evaporation and continuing condensation reactions. In bulk systems, the gelation and drying stages are normally separated. (2) Compared to bulk systems, aggregation, gelation, and drying occur in seconds to minutes during dipping or spinning rather days or weeks. The short duration of the deposition and drying stages causes films to experience considerably less aging (crosslinking) than bulk gels. Fluid flow, due to draining, evaporation, or spin-off, combined with attachment of the precursor species to the substrate, impose a shear stress within the film during deposition. After gelation, continued shrinkage due to drying and further condensation reactions creates a tensile stress in the film.

2.4.3 Deposition Conditions

The overlap of the deposition and drying stages in dipping and spinning establishes a competition between evaporation and continued condensation reactions. Thus the porosity of the film depends on the relative rates of condensation and evaporation. During film formation the condensation rate can be controlled by varying the pH of the coating bath, evaporation rate can be controlled by varying the partial pressure of solvent in the coating ambient. The reduction in the condensation rate retards the stiffening of the film during deposition and drying: the precursors initially interpenetrate and then collapse by the high capillary pressure.

The response of particulate systems to changes in relative rates of condensation and evaporation depends on whether the particles are attractive or repulsive. If the particles are attractive, a reduction in evaporation rate is analogous to an increase in the condensation rates. It provides greater time for aggregation to occur, increasing the film porosity. Conversely, an increase in the evaporation rate is analogous to a reduction in the relative condensation rate, resulting in denser films. If the particles are repulsive, however, a reduction in the evaporation rate provides additional time for the particles to order. All of the particulate systems show an increase in refractive index (decrease in porosity) with withdrawal speed U while the "polymer" sample shows the opposite trend. Both increased shear rates and slower drying may contribute to the apparent ordering at high U. Molecular dynamics calculations indicate that repulsive particles tend to align in planes in shear fields[54]. The time required for alignment and registration of the sheets of repulsive particles is provided by slower drying of thick films compared to thin ones.

Both dipping and spinning establish shear fields that could influence the structure of the depositing film such as porosity, composition of rigid rod or linear polymers. The structures of films prepared from polymeric or particulate precursors by liquid-based coating methods depend on geometric factors such as precursor size and extent of branching or aggregation prior to deposition and concurrent phenomena during deposition. Unlike bulk gels, for most film formation methods the aggregation, gelation, and drying stages significantly overlap, establishing a time scale for aggregation or ordering, gelation, and aging that depends on the evaporation rate of the solvent, typically alcohol or water. Generally, this has the effect of producing denser structures than the corresponding bulk (monolithic) xerogels, because little aging can occur in the brief time span of film formation. Control of both the precursor structure and the deposition conditions result in precise tailoring of the film microstructure and properties: porosity, pore size, surface area, and refractive index.

Chapter 3

MEASUREMENTS OF THIN FILM CHARACTERISTICS

3.1 Introduction

Properties of thin films are determined by their morphology, chemical composition, the content and type of impurities in bulk and on the surface, the crystal structure of the bulk and surface, and the types and density of structure defects. Thus, all parameters should be known and controlled during preparation, deposition and post treatment for obtaining thin films of high quality and requirements.

The investigation of the physical properties of thin films which has become an independent and important branch in the physical science has progressed much during this century. This deals with systems which have only one common property, namely, that one of their dimensions is very small, though all other physical properties of such systems may be different, as well as methods of investigating then.

Usually, the physical characteristics of three-dimensional bodies are investigated. Their characteristic properties are often related to a unit volume, i.e., it is assumed that they are volume independent. This assumption is legitimate as long as the dimensions are "normal", i.e., more or less within macroscopic limits; but as so as one dimension becomes so small that there is considerable increase in a surface-to-volume ratio, this assumption is no longer valid. Further changes can be observed if the other two dimension also decrease. In practice, the physics and technology of thin films deal with films of between tenths of a nanometre and several micrometers.

The most conspicuous phenomena associated with thin films are optical ones, especially that of interference colours. The optics and its theory of thin films were advanced by many physical scientists. Thin films interference provide the means for exact measurement of thin films thickness and fundamental applications in optical and other fields.

From the beginning of this century the electric properties of thin films have been studied, from measurement of conductivity to the study of superconductivity, as well as the emission of electrons from thin films. This research has made extraordinarily rapid advances in recent years.

Detailed investigation of the structure of thin films and processes involved in their formation has been made possible by two physical methods, namely, electron microscopy and electron

diffraction. Electron microscopy enables us not only to study the morphology of the films, but also to observe the process of formation of film by deposition directly in the viewing field. The diffraction of electrons due to the wavelike nature of electrons passing through a crystal lattice was discovered by Davisson and Germer in 1927. The electron waves cancel or reinforce each other, depending on the direction of propagation, in such a way that after the impact of electrons upon a screen or photographic plate they give rise to a number of light spots. It is possible to discover from their positions and intensities whether a substance is amorphous, polycrystalline, or monocrystalline and, if necessary, what kind of lattice it has and how it is oriented. A special case of diffraction is low-energy electron diffraction (LEED). The basis of both phenomena is identical, the only difference being that low-energy electrons only penetrate to a depth of few atomic layers and therefore yield information only about the state and structure of an extremely thin layer at the surface of the sample and, accordingly, are suitable for the study of surface processes and properties.

By keeping the sample near room temperature and measuring the infrared absorption, spectra are obtained which are dependent on particular bonds. Infrared spectroscopy is most used for analysing organic compounds but is applicable to inorganic such as semiconductor analysis. The characteristics of thin films and the applications of thin film devices were determined using the following methods:

a. Optical measurement:

1. Transmittance
2. Infrared
3. Ellipsometry

b. Electrical measurement:

1. Four probes
2. Two probes
3. Hall effect

c. Crystal structure measurement:

1. X-ray diffraction
2. Scanning tunnelling microscopy (crystal grain size)

d. Morphology measurement:

1. Ellipsometry
2. Scanning electron microscopy (SEM)

3. Scanning tunnelling microscopy

e. Chemical composition and impurity measurement:

1. Infrared absorption
2. Electron microprobe
3. Photoluminescence

f. Thickness measurement:

1. Interferometry
2. Ellipsometry

3.2 Measurement of Thickness

3.2.1 Methods Using Interference Fringes of Equal Thickness

A variety of different optical methods for measurement of film thickness based on light interference in thin films exists. Visible light is an electromagnetic undulation with wavelengths ranging approximately from 400 to 800 nm. The interaction of two or more waves gives rise to interference phenomena; the intensity of the light in increased or reduced

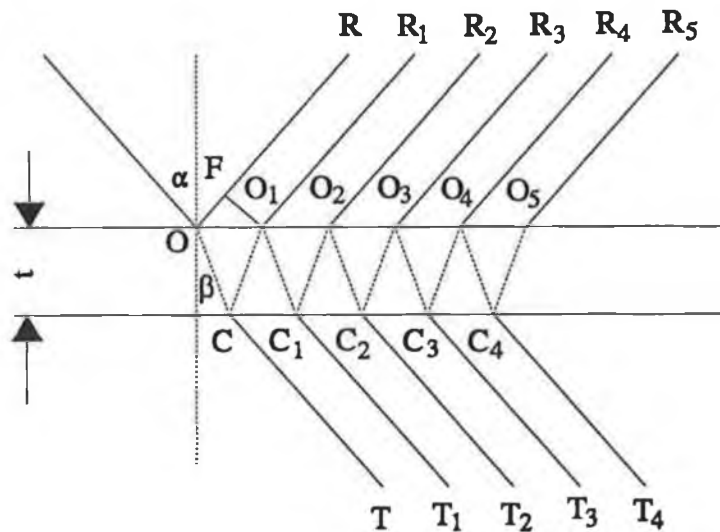

Figure 3-1 Schematic diagram for multiple beam reflection and transmission through a transparent film.

is certain directions.

Interference in thin films may be explained with the help of fig.3-1. A plane wave is impinging on a film of thickness t at an angle α. At interface, the wave is partially reflected and partially refracted at an angle β. The refracted wave is again partially reflected and refracted at the lower interface and the process is repeated successively, as shown in the diagram. The interference phenomenon depends on the difference in the optical paths of the interacting rays (the optical path and refractive index). Let us assume that the medium around the films is air ($n_{sub}=n_{amb}=1$) and that the film itself has refractive index n. The optical path difference of the OR and O_1R_1 ray is:

$$\Delta l=(OC+CO_1)n-OF=2t\sqrt{(n^2-\sin^2\alpha)}=(2k+1)\frac{\lambda_0}{2} \tag{3-1}$$

As the refractive index n is given by

$$n=\frac{\sin\alpha}{\sin\beta} \tag{3-2}$$

where k is an integer, λ_0 is the wavelength of the light in vacuum and t is the thickness of the film.

If the interference of monochromatic light is established on the thin film having the form of a wedge, the condition (Eq.(3-1)) for interference maxima and minima will be fulfilled for certain thicknesses, hence alternate dark and light parallel fringes will be observed. For film with irregular shape, the interference method, developed mainly by Tolansky, has become one of the standard methods for thin film measurement.

The layer on which the multiple beam interference takes place is formed by an air gap. Both surfaces are metal-coated with the same substance in order to obtain a high reflectance R ($\geq$0.94). In the system, interference fringes of equal thickness arise separated by $\lambda/2$ when viewed with a low power microscope. If both reflecting planes have a sufficiently high reflection coefficient and their spacing is small, then the interference fringes are very sharp (the thickness of dark fringes on a white background may be reduced to as little as $\lambda/100$). In the arrangement the fringes run parallel of the contact edge of the flats. At the site of the film step the fringes are displaced (Fig.3-2). If L is the fringe spacing, and ΔL the displacement of the fringes, then the film thickness is given by

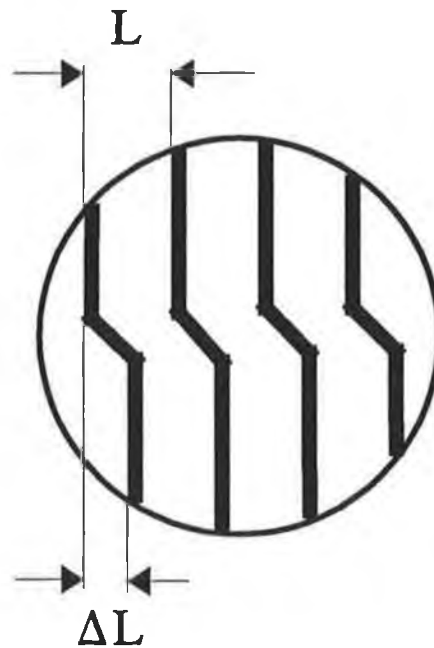

Figure 3-2 Interference fringes used for determining thickness of film.

$$t=\frac{\Delta L}{L}\frac{\lambda}{2} \tag{3-3}$$

where λ is the wavelength of the monochromatic light. It is necessary to coat the plate with the film as well as the opposite one with a layer possessing the same high reflection coefficient in order that phase shifts on reflection be the same at both sides of air wedge. If the system is executed carefully, it is possible to measure even ultrathin films with adequate accuracy. The accuracy of the interference method can be improved still further, theoretically to ±0.1Å, by using polarized light and photoelectric detection of intensity.

3.2.2 Ellipsometric Method

A thin film partially or wholly transparent on a high reflection plate affects the ellipticity of reflected light. The polarimetric of ellipsometric method is based on measuring the ratio of the amplitude of the reflected light polarized along the plane of incidence and that polarized perpendicularly and their phase difference at relatively large angles of incidence theoretically described by the Fresnel equations. By this method it is possible to determine the thickness, or optical constants of thin non-absorbing and homogeneous isotropic films on both non-absorbing and absorbing homogeneous substrates. The thickness may be calculated from the

data with the help of relatively complicated mathematical equations derive from the electromagnetic theory of light. The method has found a wide use only recently, the complicated calculation being carried out by computer.

Ellipsometers, or reflection polarimeters, are optical instrument which measure changes in the state of polarization of collimated beams of monochromatic polarized light caused by reflection from the surfaces of the sample at a known controllable state of polarization, and determining the differences between the states of polarization of the incident and reflected beams. From the measured differences caused by sample between the states of polarization of the incident and reflected beams, various properties of that reflecting surface can often be computed, as the follows:

A. For a bar surface (the 'substrate'), the real part n_s and the imaginary part k_s of refractive index, n_s+ik_s. The parameters n_s and k_s are called the optical constants of substrate.

B. For a substrate having known optical constants n_s and k_s, which is covered with a single transparent film, the film refractive index n_l; the zero-order film thickness t_l; the full-cycle film thickness ordl; and the first through ninth orders film thickness, t_l+ordl, t_l+2(ordl),..., t_l+9(ordl).

C. For a substrate having known optical constants and n_s and k_s, which is covered with a double-layer transparent film, the refractive indices n_u and n_l of the upper and lower films; the full-cycle thicknesses ordu and ordl of the upper and lower films; the full-cycle thicknesses ordu and ordl of the upper and lower films; the first through ninth orders of lower film thickness; t_l+ordl, t_l+2(ordl),..., t_l+9(ordl); and the first through ninth orders of upper film thickness, t_u+ordu, t_u=2(ordu, t_u+9(ordu).

Ellipsometry has the following advantages over other methods of measuring thickness:

1. It can measure film thicknesses at least an order of magnitude smaller than can be measured by other methods such as interferometry.

2. It can permit determination of the index of refraction of thin films of unknown thickness. Neither interferometry nor reflectometry permit this determination.

3. It can make measurements in optically-transparent environments such as air or liquids.

4. It does not require special conditions (such as vacuum, heat, or electron bombardment) that may change the optical properties of surface being studied, but does permit measurements under such conditions, if desired.

5. Nulling ellipsometers have the additional special advantage that the measured quantities

are usually azimuth angles (of rotation of the polarizing components), which can be measured with high resolution and accuracy. This almost completely eliminates effects caused by variations of intensity of the incident light beam, variations in total reflectance of the samples being measured, and variations in sensitivity of the detector-amplifier system used to measure the intensity of the reflected beam.

Basic Theory of Ellipsometry

Single-frequency harmonic oscillation can be represented by

$$E(t)=Ee^{i(\omega t+\epsilon)}=Ee^{i\omega t}e^{i\epsilon} \qquad \textbf{(3-4)}$$

where $e^{i\omega t}$ is time-dependent, and both E and $e^{i\epsilon}$ are time-independent.

The electric fields of the incident beam and the reflected beam can each be resolved into two orthogonal linearly-polarized components, one (the p components), with its electric field vector parallel to the plane of incidence, and the other (the s component) with its electric field vector normal to the plane of incidence. The p and s components of each beam may have different phases and different amplitudes. If the phase difference between the p and s components is either 0° or 180°, the beam is linearly polarized; all other phase differences will result in elliptical polarization. At phase differences of 90° or 270°, the major and minor axes of ellipse will be oriented parallel to the planes of polarization of the p and s components.

When a collimated beam of monochromatic polarized light is reflected from the surface, there generally occurs changes in the relative phases and the relative amplitude of the p and s components. These changes determine two angles Δ and Ψ, which are derived in the following paragraphs.

Reflection coefficients

The reflection of the p and s components of an incident beam from any surface can be described by defining a complex reflection coefficient r_p for the incident and reflected p components, and a complex reflection coefficient r_s for the incident and reflected s components, as follows:

$$r_p=\frac{E_p''(t)}{E_p(t)} \qquad \textbf{(3-5)}$$

$$r_s = \frac{E_s''(t)}{E_s(t)} \tag{3-6}$$

which can be simplified to give

$$r_p = \frac{|E_p''|}{|E_p|} e^{i(\epsilon_p'' - \epsilon_p)} = |r_p| e^{i\delta_p} \tag{3-7}$$

$$r_s = \frac{|E_s''|}{|E_s|} e^{i(\epsilon_s'' - \epsilon_s)} = |r_s| e^{i\delta_s} \tag{3-8}$$

where the amplitude attenuations caused by reflection are

$$|r_p| = \frac{|E_p''|}{|E_p|} \tag{3-9}$$

$$|r_s| = \frac{|E_s''|}{|E_s|} \tag{3-10}$$

and the changes in phase caused by reflection are

$$\delta_p = \epsilon_p'' - \epsilon_p \tag{3-11}$$

$$\delta_s = \epsilon_s'' - \epsilon_s \tag{3-12}$$

Equations of Ellipsometry

The complex reflection coefficients r_p and r_s defined are not separately measurable, but their ratio ϱ is defined as

$$\rho = \frac{r_p}{r_s} = \frac{|E_p''||E_s|}{|E_p||E_s''|} e^{i[(\epsilon_p'' - \epsilon_s'') - (\epsilon_p - \epsilon_s)]} \tag{3-13}$$

Simplifying further

$$\tan\Psi_i = \frac{|E_p|}{|E_s|} \tag{3-14}$$

$$\tan\Psi_r = \frac{|E_p^{//}|}{|E_s^{//}|} \tag{3-15}$$

$$\Delta_i = \epsilon_p - \epsilon_s \tag{3-16}$$

$$\Delta_r = \epsilon_p^{//} - \epsilon_s^{//} \tag{3-17}$$

and substituting these into Eq.(3-13) to obtain

$$\rho = \frac{\tan\Psi_r}{\tan\Psi_i} e^{i(\Delta_r - \Delta_i)} \tag{3-18}$$

Basic equation of ellipsometry

Equation (3-18) can be further simplified by defining the quantities

$$\tan\Psi = \frac{\tan\Psi_r}{\tan\Psi_i} \tag{3-19}$$

$$\Delta = \Delta_r - \Delta_i \tag{3-20}$$

and substituting them in Eq.(3-18) to obtain

$$\rho = \tan\Psi e^{i\Delta} \tag{3-21}$$

which is called the basic equation of ellipsometry. Note that both Δ and Ψ are angles. The angle Ψ may have any value between 0° and 90° and the angle Δ may have any angle between 0° and 360°.

Null ellipsometry

In the most common PRSA (Polarizer-Retarder-Sample-Analyzer) null ellipsometer configuration (Fig.3-3), an elliptically polarized light beam is incident on the sample. Its ellipticity and azimuth are chosen in such a way that the reflection at the sample surface just

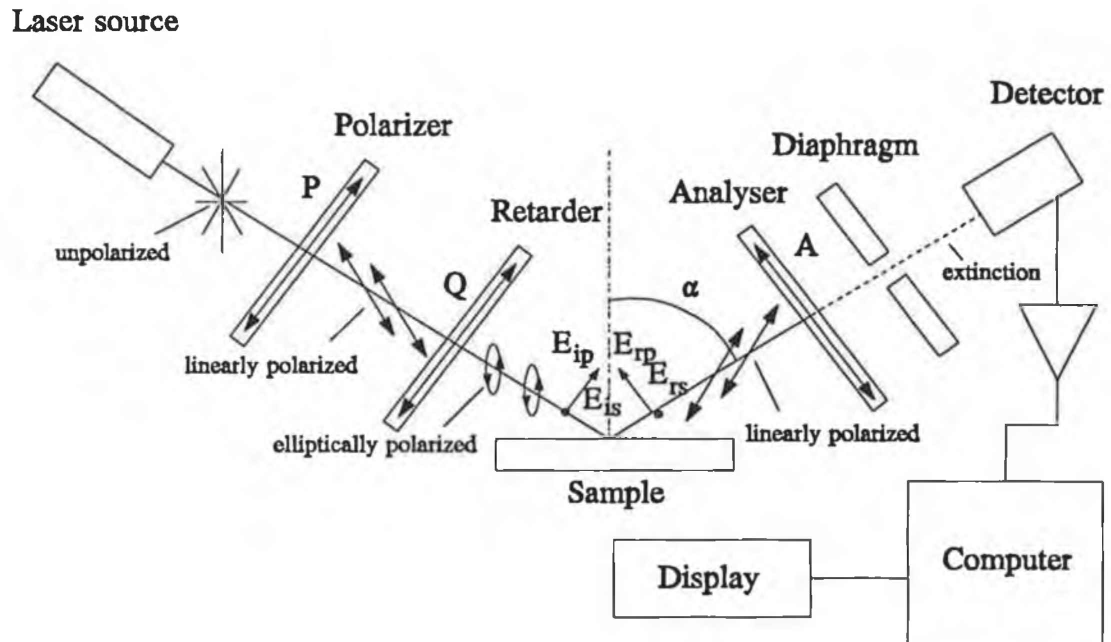

Figure 3-3 Basic ellipsometer schematic.

converts the beam to linear polarization. The elipticity of the incident beam is controlled by a polarizer with a variable azimuth which produces a linearly polarized wave. This wave subsequently passes through a retarder, a quarter-wave plate of a birefringent material. Depending on the relative positions of the transversal axes of the polarizer and the retarder, the resulting beam can be adjusted to any state of polarization between lineally and circular: The difference of the azimuth angles of the polarizer and the retarder defines the elipticity of the beam, while the azimuth of the retarder determines the azimuth of the polarization ellipse. A lineally polarized beam is reflected from the sample if and only if the elipticity of the incident light is exactly compensated for by the reflection at the sample. Only in this case, the reflected beam can be totally extinguished by a second polarizer, the analyzer. A measurement is done by alternating adjustments of the polarizer and analyzer azimuths for minimum intensity (retarder is normally kept at a fixed azimuth); it results in two independent sets of polarizer and analyzer azimuth readings for which extinction occurrence.

In the single-film model Δ and Ψ are each function of the angle of incidence α, the wavelength λ of the light, the refractive index n_a of ambient medium, the real part n_s and the imaginary part k_s of the substrate refractive index, the real part n_l and the imaginary part k_l of the film refractive index and on the film thickness t_l.

$$\Delta = F(\alpha, \lambda, n_a, n_s, k_s, n_l, k_l, t_l) \quad \textbf{(3-22)}$$

$$\Psi = G(\alpha, \lambda, n_a, n_s, k_s, n_l, k_l, t_l) \quad \textbf{(3-23)}$$

Since α, λ and n_a are known or entered by the operator, n_s and k_s can be found from the measurement and calculation of other sources. If the film is transparent (which means that k_l=0), the film thickness and refractive index n_l may be calculated from the results of a single Δ, Ψ measurement. Numerical techniques must be employed (which requires a computer) to determine n_l and t_l.

In the same theory the index and the thickness of the double films can be measured by the parameters of the substrate and first layer on the substrate.

3.3 Measurement of Infrared

Infrared technology has been used to analysis the composition of the materials. In my work, metal organic compounds transfer into inorganic substance, such as metal oxide. Infrared technology is a simple and efficient method for analysing composition of thin films and determining parameters of experiments.

As a first approximation, it is possible to separate the energy of a molecule into three additive components associated with (1) the rotation of the molecule as a whole, (2) the vibrations of the constituent atoms, and (3) the motion of the electrons in the molecule. In general pure rotational, vibrational, and electronic spectra are usually observed in the microwave and far-infrared, the infrared, and the visible and ultraviolet regions, respectively. This division into three regions, however, is to some extent arbitrary.

Through quantum mechanical considerations, the vibration of two nuclei in a diatomic molecule can be reduced to the motion of a single particle of mass μ, whose displacement q from its equilibrium position is equal to the change of the internuclear distance. The mass μ is called the reduced mass and is represented by

$$\frac{1}{\mu} = \frac{1}{m_1} + \frac{1}{m_2} \quad \textbf{(3-24)}$$

where m_1 and m_2 are the masses of the two nuclei. The kinetic energy is then

$$T=\frac{1}{2}\mu\dot{q}^2=\frac{1}{2\mu}p^2 \qquad \textbf{(3-25)}$$

where p is the conjugate momentum, $\mu\dot{q}$. If a simple parabolic potential function is assumed, the system represents a harmonic oscillator, and potential energy is simply given by

$$V=\frac{1}{2}Kq^2 \qquad \textbf{(3-26)}$$

here K is the force constant for the vibration. Then the Schrödinger wave equation becomes

$$\frac{d^2\psi}{dq^2}+\frac{8\pi^2\mu}{h^2}(E-\frac{1}{2}Kq^2)\psi=0 \qquad \textbf{(3-27)}$$

If this equation is solved with the condition that ψ must be single valued, finite, and continuous, the eigenvalues are

$$E_v=h\nu(n+\frac{1}{2})=hc\tilde{\nu}(n+\frac{1}{2}) \qquad \textbf{(3-28)}$$

with the frequency of vibration

$$\nu=\frac{1}{2\pi}\sqrt{\frac{K}{\mu}} \qquad \textbf{(3-29)}$$

or

$$\tilde{\nu}=\frac{1}{2\pi c}\sqrt{\frac{K}{\mu}} \qquad \textbf{(3-30)}$$

Here n is the vibrational quantum number, and it can have the value 0,1,2,3, ...
In diatomic molecules, the vibration of the nuclei occurs only along the line connecting two nuclei. In polyatomic molecules, however, the situation is much more complicated because all the nuclei perform their own harmonic oscillations. It can be shown, however, that any of these extremely complicated vibrations of the molecule may be represented as a supersition of a number of normal vibrations.
Infrared instruments may use either gratings or alkali-halide prisms for dispersion. The wavelength is then scanned by rotating the grating or prism, and detector output is recorded

on a strip chart. In order to afford greater sensitivity and to minimize the effects of atmospheric attenuation, a double-beam instrument is ordinarily used. That is, the beam splits and goes through two similar paths, except that one of them has provisions for inserting the sample. The light is chopped so that the signal processing can be AC signal. For high absorption, the signal-to-noise ratio may be very poor; so some variety of phase-sensitive detection is almost always used.

Most qualitative analyses will use only a strip-chart recording of relative transmittance vs. wavelength. However, for quantitative analysis the actual absorption coefficient α can be determined for one or more of bands. This is done through the equation

$$\frac{I}{I_0}=\frac{e^{-\alpha x}(1-R)^2}{1-R^2e^{-2\alpha x}} \qquad \textbf{(3-31)}$$

where I_0 is the intensity of the incident beam, I the intensity of the light transmitted, R the reflection coefficient, and x the sample thickness. This equation assumes normal incidence, parallel sides on the sample, and a surface finish adequate to prevent scattering (which usually means an optical finish).

3.4 Measurement with Scanning Electron Microscopy

Scanning electron microscopy (SEM) is an important and efficient method for the measurements of thin films. SEM can be used to detect qualities, morphology, crystalline grain size, thickness, etc. and to analyze the composition of the films with electron microprobe.

An electron microscope utilizes an electron beam (e-beam) to produce a magnified image of the sample. There are three principal types of electron microscopes: Scanning, transmission, and emission. In the scanning and transmission electron microscope an electron beam incident on the sample produces an image, whereas in the field-emission microscope the specimen itself is the source of electrons. A good discussion of the history of electron microscopy is given by Cosslett[55]. Scanning electron microscopy (SEM) is similar to light microscopy, with the exception that electrons are used instead of photons. This has two main advantages: much larger magnifications are possible since electron wavelengths are much smaller than photon wavelengths and depth of field is much larger.

De Broglie proposed in 1923 that particles can also behave as waves[56]. The electron

wavelength λ_e depends on the electron velocity v or the accelerating voltage V as

$$\lambda_e = \frac{h}{mv} = \frac{h}{\sqrt{2qmV}} = \frac{12.2}{\sqrt{V}} (\AA) \qquad \textbf{(3-32)}$$

The wavelength is 0.12Å for V=10,000 V. Hence the resolution of an SEM can be much higher than that of an optical microscope.

Electrons emitted from an electron gun pass through a series of lenses to be focused and scanned across the sample. The electron beam should be bright with small energy spread. The most common electron gun is a tungsten "hairpin" filament, emitting electrons thermionically with an energy spread of around 2eV. Tungsten sources have been replaced to some extent by lanthanum hexaboride (LaB_6) sources with higher brightness, lower spread (~1eV) and longer life, and field-emission gun with an energy spread of about 0.2 to 0.3 eV. Field-emission guns are about 1000× brighter than tungsten sources.

The incident or primary electron beam causes secondary electrons to be emitted from the sample and are ultimately accelerated to 10 to 20 kV. They are most commonly detected with an Everhart-Thornley (ET) detector[57]. The basic component of this detector is a scintillator material that emits light when struck by energetic secondary electrons accelerated from the sample to the detector. The light from the scintillator is channelled through a light pipe to a photomultiplier, where the light incident on a photocathode produces electrons that are multiplied creating the very high gains necessary to drive the CRT. High potentials of 10 to 12 kV are necessary for efficient light emission by the scintillator. For the electron beam not to be influenced by the high ET detector potential, the scintillator is surrounded by a Faraday cage at a few hundred volt potential.

3.5 Measurement with Electron Microprobe

The electron microprobe (EMP), also known as electron probe microanalysis (EPM or EPMA) was first described by Castain in 1948[58],[59]. The principle of the method consists of electron bombardment of the sample and X-ray emission from the sample. An EPM is usually a part of a scanning electron microscope equipped with appropriate X-ray detectors[60]. Of all the signals generated by the interaction of the primary electron beam with the sample in the SEM, X-rays are most commonly used for material characterization. The X-rays have energies characteristic of the element from which they originate leading to

elemental identification. The X-ray intensity can be compared to the intensity of the standard and this can be considered as a measurement of the amount of the element in the sample. The correlation, however, is not entirely straightforward. There are factors that tend to complicate the interpretation. The most important of these factors is the influence of other elements in the sample that absorb some of the X-rays generated by the primary electron beam and release other X-rays of their own characteristic energy, known as fluorescence. If the energy of the characteristic radiation from element A exceeds the absorption energy for element B in a sample containing A and B, a characteristic fluorescence of B by A will occur. Additionally not all X-rays leaving the sample are captured by the detector. The best accuracy in quantitative concentration determination is obtained if the standards can also be used but may lead to inaccuracies. Fortunately quantitative analysis is not always necessary; simple, qualitative, and semi-quantitative analyses are frequently sufficient.

EPM is not a true surface technique because X-rays are emitted from within the sample volume. A primary electron beam of typically 5 to 20 keV strikes the sample. The electron beam energy should be approximately three times the X-ray energy. X-rays are generated by electron bombardment of a target by two distinctly different processes: (1) deceleration of electrons in the Coulombic field of the atom core leads to formation of a continuous spectrum of X-ray continuum or Bremsstrahlung (German for braking radiation), sometimes called white radiation by analogy with white light of the visible spectrum. (2) The interaction of the primary electrons with inner-shell electrons. Incident electrons eject electrons from one of the inner atomic shells and electrons from higher-lying shells drop into the vacancies created by the ejected electrons. These are the characteristic X-rays. If the X-ray emission results from an L→K transition, the X-rays are known as $K\alpha$ X-rays. $K\beta$ X-rays are the result of M→K transitions, $L\alpha$ X-rays are due to M→L transitions, etc. There is but one K level, but the other levels are subdivided. The L shell is split into a triple fine structure, and the M shell has five levels. This leads to further subdivision of the nomenclature. For example, the $L_2 \rightarrow K$ transition is known as $K\alpha_2$, and the $L_3 \rightarrow K$ transition results in $K\alpha_1$ X-rays. Not all possible transitions occur with equal probability, and some are so impossible as to have earned the name "forbidden" transitions. For example, the $L_1 \rightarrow K$ transition does not occur.

X-ray detectors frequently lack the resolving power to separate X-ray lines close to one another (doublets). The unresolved doublets are measured in such cases as if they were a

single line. This indicated by dropping the subscript; the notation $K\alpha$ refers to the unresolved doublet $K\alpha_1$+$K\alpha_2$. Sometimes the term $K\alpha_{1,2}$ is used. The X-ray photon energy for an L→K transition in the EPM is

$$E_{EMP}=E_K(Z)+E_{1,2,3}(Z) \quad \textbf{(3-33)}$$

The energy between the K and L levels is much higher than the between the L and M levels, which in turn is higher than that between the M and N levels. For example, for silicon $E(K\alpha_1)$=1.74 keV. For most common EPM X-ray lines are the $K_{\alpha 1,2}$ the $K_{\beta 1}$, the $L_{\beta 1,2}$ and the $M_{\alpha 1,2}$. A graphical representation of all X-ray lines observed in high quality X-ray spectra in the 0.7 to 10 keV energy range is given by Fiori and Newbury[61]. A detailed discussion of both qualitative and quantitative EPM spectra interpretation is given in Goldstein et. al.[62]. The relationship between X-ray energy E and wavelength λ is

$$\lambda=\frac{hc}{qE}=\frac{12.398}{E}(\AA) \quad \textbf{(3-34)}$$

with E in keV. Both wavelength and energy are used in X-ray analysis.

The only possible outcomes of an ionization event involving the K shell are the emission of K-line X-ray photon or of an Auger emission. The fraction of the total number of ionizations leading to the emission of X-rays is the fluorescence yield. The sum of the probability of X-ray emission and that of Auger electron emission dominates for high Z materials. The two probabilities are about equal for $Z\approx 33$.

EPM utilizes the electron beam, focusing lenses, and deflection coils of an SEM. Only the X-ray detector is added, and many SEMs have EPM capability. Two different types of detectors are used: energy-dispersive spectrometers (EDS or EDX) and wavelength-dispersive spectrometers (WDS or WDXS). The two spectrometers complement each other, making it desirable to have both on an SEM. The EDS is commonly used for rapid sample analysis and the WDS for high-resolution measurements.

The energy of incident X-rays is determined in such semiconductor detectors by the number of electron-hole pairs those X-rays produce. Elements from Na to U can be detected with EDS. Lower Z elements are difficult to detect due to beryllium window that isolates the cooled detector from the vacuum system. Windowless systems allow lower Z elements to be detected. It is possible for X-rays from the sample absorbed in the Si detector to generate

Si $K\alpha$ X-rays that are subsequently absorbed in the detector. These X-rays, which do not originate from the sample, appear in the spectrum as the so-called silicon internal fluorescence peak.

WDS is based on an analysing crystal. X-rays from the sample are directed onto an analysing crystal. Only those X-rays that strike the crystal at the proper angle are diffracted through a polypropylene window into the detector, usually a gas proportional counter. The proportional counter consists of a gas-filled tube with a thin tungsten wire in the centre of the tube held at a 1- to 3-kV potential. The gas (usually 90% argon-10% methane) flows through the tube because it is difficult to seal the thin entrance window. An absorbed X-ray creates a shower of electrons and positive ions. The electrons are attracted to the wire and produce a charge pulse, much as electron-hole pairs are generated and collected in semiconductor detector.

X-ray diffraction is determined by Bragg's law

$$n\lambda = 2d\sin\theta_B \tag{3-35}$$

where n=1,2,3,..., λ is the X-ray wavelength, d the interplanar spacing of the analysing crystal, and θ_B the Bragg angle. The detector signal is amplified, converted to a standard pulse size by a single-channel analyzer, and then counted or displayed. The analysing crystals are curved to focus the X-rays onto the detector. More than one crystal is necessary to span an appreciable wavelength range.

WDS detectors are located at longer distances from the sample, giving them lower collection efficiencies than EDS detectors. WDS has higher energy resolution since only a small range of wavelengths is detected at one time, allowing greater peak-to-background ratios and higher count rates for individual elements. This gives approximately 1 to 2 orders of magnitude better sensitivity but makes the methods slow.

3.6 Measurement of Thin Film Photoluminescence

Photoluminescence (PL) provides a non-destructive technique for the determination of certain impurities in semiconductors. It is particularly suited for the detection of shallow-level impurities but can also be applied to certain deep-level impurities, provide that radiative recombination events dominate non-radiative recombination.

The sample is exited with an optical source, typically a laser with energy $h\nu > E_g$, generating

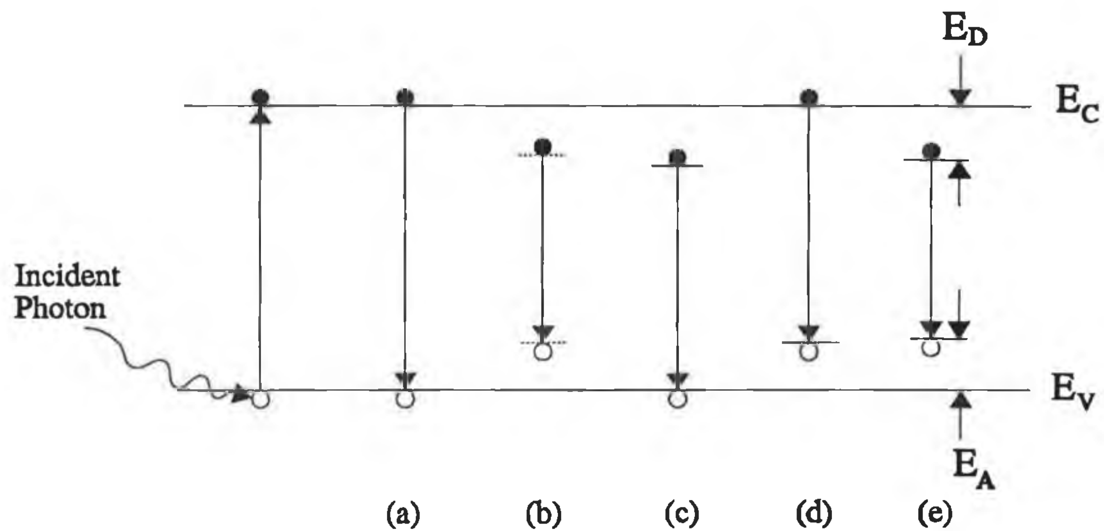

Figure 3-4 Radiative transitions observed with photoluminescence.

electron-hole pairs that recombine by one of several mechanisms. Photons are emitted for radiative recombination. For non-radiative processes photons are not emitted. For a good PL output one would like the majority of the recombination processes to be radiative. The photon energy depends on the recombination process illustrated in fig.3-4, where five of the most commonly observed PL transitions are shown. Band-to-band recombination [Fig.3-4 (a)] dominates at room temperature but is rarely observed at low temperatures in materials with small effective masses due to the large electron orbital radii. Exciton recombination is commonly observed. When a photon generates an electron hole pair, Coulombic attraction can lead to the formation of an excited state in which an electron and a hole remain bound to each other in a hydrogenlike state. This excited state is referred to as a free exciton (FE). Its energy, shown in fig.3-4 (b), is slightly less than the band-gap energy required to create a separated electron hole pair. An exciton can move through the crystal, but being a bound electron hole pair, both electron and hole move together and no photoconductivity results. A free hole can combine with a neutral donor [Fig.3-4 (c)] to form a positively charged excitonic ion or bound exciton (BE). The electrons combining with neutral acceptors also form bound excitons.

If the material is sufficiently pure, free excitons form and recombine by emitting photons.

The photon energy in direct band-gap semiconductors is

$$h\nu = E_g - E_x \tag{3-36}$$

where E_x is the excitonic energy. In indirect band-gap semiconductors, momentum conservation requires the emission of a phonon, giving

$$h\nu = E_g - E_x - E_p \tag{3-37}$$

where E_p is the phonon energy. Bound exciton recombination dominates over free exciton recombination for less pure material. A free electron can recombine with a hole on a neutral acceptor [Fig.3-4 (d)], and similarly a free hole can recombine with a neutral donor [Fig.3-4 (c)].

Lastly, an electron on a neutral donor can be recombine with a hole on a neutral acceptor, the well-known donor-acceptor (D-A) recombination, illustrated in fig.3-4 (e). The emission line has an energy modified by the Coulombic interaction between donors and acceptors

$$h\nu = E_g - (E_a + E_d) + \frac{e^2}{4\pi\varepsilon_0 \varepsilon r} \tag{3-38}$$

where r is the distance between donor and acceptor. The photon energy in Eq.(3-38) can be larger than the band gap for small E_a+E_d. Such photons are generally re-absorbed in the sample. The full width at half maximum (FWHM) for bound exciton transitions are typically ≤kT/2 and resemble slightly broadened delta functions. This distinguishes them from donor-valence band transitions which are usually a few kT wide. Energies for these two transitions are frequently similar, and the line widths are used to determine the transition type.

The optics in a PL apparatus are designed to ensure maximum light collection. The PL-emitted light from the sample is analyzed by a spectrometer and detected by a photodetector. PL radiation from shallow-level impurities can be detected with a photomultiplier tube.

3.7 Electrical Measurement

EL display usually consists of several films. Electrical properties of every layer determine the characteristics of EL display. Conductive film properties relate to the qualities of EL display so that it is significant to measure various electrical parameters of conductive films.

3.7.1 Resistivity Measurement of Thin Films

The resistivity of a semiconductor ρ is defined by

$$\rho = \frac{1}{q(n\mu_n + p\mu_p)} \qquad \textbf{(3-39)}$$

where n and p are the free electron and hole concentration, and μ_n and μ_p are the electron and hole mobilities, respectively. The resistivity can be calculated from the measured carrier concentrations and mobilities. In order to determine the resistivity in this manner, both carrier concentrations and both mobilities must be known. For extrinsic materials in which the majority carrier concentration is much higher than the minority carrier concentration, it is generally sufficient to know the majority carrier concentration and the majority carrier mobility. The carrier concentration and mobility are generally not known, however. Hence an alternative resistivity measurement technique must be used. These techniques range from contactless, through temporary contact to permanent contact techniques.

The four-point probe technique is one of the most common methods for measuring the semiconductor resistivity because the two-point probe methods are much more difficult to interpret. The total resistance between the two probes is given by

$$R_T = \frac{V}{I} = 2R_c + 2R_{sp} + R_s \qquad \textbf{(3-40)}$$

where R_c is contact resistance at each metal probe/semiconductor contact, R_{sp} is the spreading resistance under each probe and R_s is the semiconductor resistance. Neither R_c and R_{sp} can be accurately calculated so that R_s can not be accurately extracted from the measured resistance.

A solution to this dilemma can be found in the use of four probes. Two probes carry the current and the other two are used for voltage sensing. The four-point probe was originally proposed by Wenner[63] in 1916. This measurement technique is referred to in Geophysics as Wenner's method. It was adopted for semiconductor wafer resistivity measurements by Valdes in 1954[64].

The resistivity of thin film is:

$$\rho = \frac{2\pi V/I}{1/s_1 + 1/s_3 - 1/(s_1+s_2) - 1/(s_2+s_3)} \tag{3-41}$$

usually in units of ohm-cm, with V measured in volts and I measured in amperes. For most four-point probes the probe spacings (s_1, s_2 and s_3) are equal with $s=s_1=s_2=s_3$, and Eq.(3-41) reduces to:

$$\rho = 2\pi s(V/I) \tag{3-42}$$

Semiconductor wafers are not semi-infinite in extent in either the lateral of the vertical dimension. Eq.(3-41) must be corrected, for finite geometries. For an arbitrarily shaped sample the resistivity is given by

$$\rho = 2\pi s F(V/I) \tag{3-43}$$

where F is a correction factor that depends on the sample geometry. F corrects for edge effects, for thickness effects, and for probe placement effects, and it is usually a product of several independent correction factors. For sample thicknesses greater than the probe spacing, the simple, independent correction factors contained in F of Eq.(3-43) are no longer adequate due to interactions between thickness and edge effects. Fortunately the sample thickness is generally smaller than the probe spacings, and the correction factors can be independently calculated.

Four-point probe correction factors have been calculated by various techniques. The following correction factors are for collinear or in-line probes with equal probe spacing, s. The correction factor F is written as a product of three separate correction factors

$$F = F_1 F_3 [\ln(2) F_2/\pi] \tag{3-44}$$

Each of these factors can be further subdivided. F_1 corrects for sample thickness, F_2 corrects for lateral sample dimensions, and F_3 corrects for placement of probes relative to sample edges. A parameter that must be corrected, for most practical measurement conditions is the sample thickness since semiconductor wafers are not infinitely thick. Their thicknesses are usually on the order of the probe spacing or less introducing the correction factor[65]

$$F_1 = \frac{t/s}{2\ln[\sinh(t/s)/\sinh(t/2s)]} \tag{3-45}$$

for a non-conducting bottom wafer surface boundary, where t is the wafer or layer thickness. When $t \leq s/2$, for very thin samples for which $F_2=F_3=1$ we obtain from Eq.(3-43), (3-44) and (3-45)

$$\rho=\frac{\pi t}{ln2}\frac{V}{I}=4.532t\frac{V}{I} \quad (3\text{-}46)$$

Thin layers are often characterized by their sheet resistance ρ_s expressed in units of ohms per square. The sheet resistance is given by

$$\rho_s=\frac{\rho}{t}=\frac{\pi}{ln2}\frac{V}{I}=4.532\frac{V}{I} \quad (3\text{-}47)$$

subject to the constraint $t \leq s/2$. The sheet resistance is frequently used to characterize thin semiconductor sheet or layers, such as diffused or ion implanted layers, polycrystalline silicon, and metallic conductors.

The collinear probe configuration is the most common four-point probe arrangement. Arrangement of the points in a square has the advantage of occupying a smaller area since the spacing between the points is only s, whereas in a collinear configuration the spacing between the outer two probes is 3s. However, the square arrangement is more commonly used, not as an array of four mechanical probes but rather contacts on a square semiconductor samples. Occasionally it is difficult to provide a sample in a square format. In fact sometimes the sample is irregularly shaped. The theoretical foundation of measurements on irregularly shaped samples is based on conformal mapping developed by van der Pauw [66],[67],[68]. He showed how the specific resistivity of a flat sample of arbitrary shape can be measured without knowing the current pattern, if the following conditions are met:

(1) the contacts are at the circumference of sample,

(2) the contacts are sufficiently small,

(3) the sample is uniformly thick, and

(4) the surface of the sample is singly contacted, i.e., the sample does not contain any isolated hole.

Consider the flat sample of a conducting material of arbitrary shaped, with contacts 1, 2, 3 and 4 along the periphery as shown in fig.3-5 and fig.3-7 to satisfy the conditions above. The resistance $R_{12,34}$ is defined as

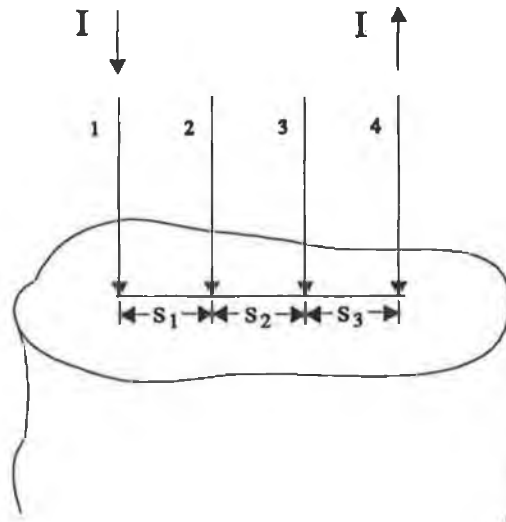

Figure 3-5 A collinear four-point probe.

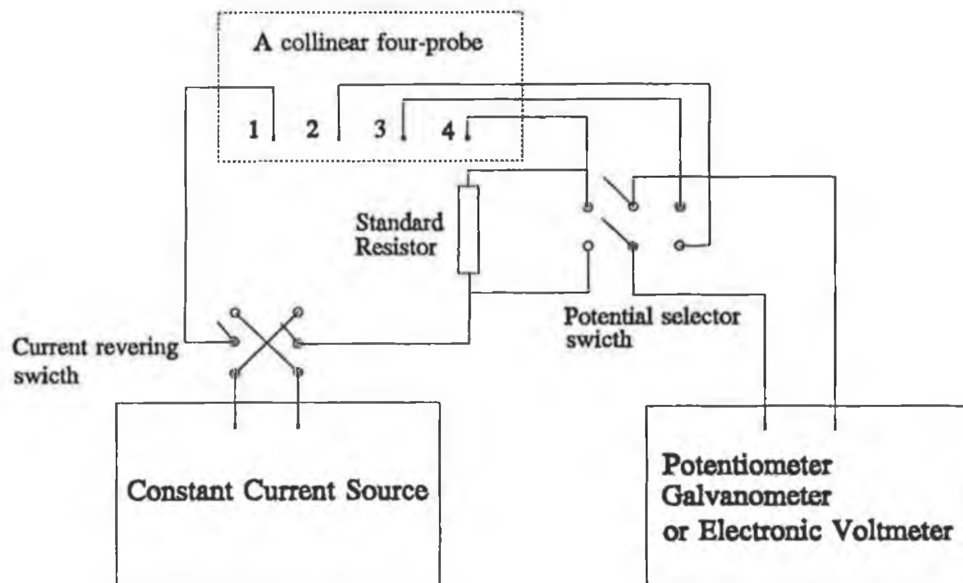

Figure 3-6 Measurement circuit for four-point probe.

$$R_{12,34} = \frac{V_{34}}{I_{12}} \tag{3-48}$$

where the current I_{12} enters the sample through contact 1 and leave through contact 2 and

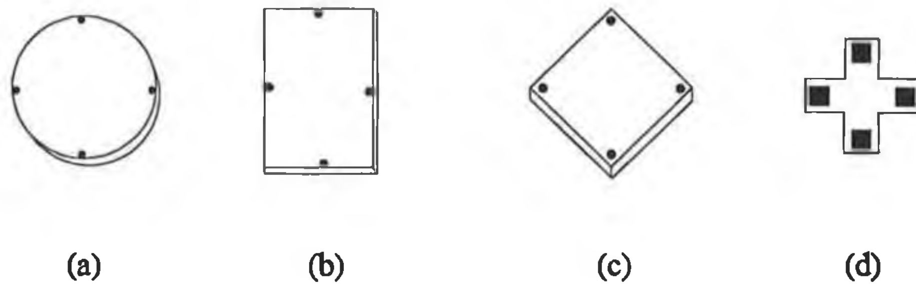

Figure 3-7 Typical symmetrical circular (a), rectangle (b) and square sample geometries and a cross resistance test structure.

$V_{34}=V_3-V_4$ is the voltage difference between the contacts 3 and 4. $R_{23,41}$ is defined similarly. The resistivity is given by

$$\rho=\frac{\pi T}{ln2}\frac{R_{12,34}+R_{23,41}}{2}F \qquad (3\text{-}49)$$

where F is a function only of the ratio $R_r=R_{12,34}/R_{23,41}$, satisfying the relation

$$\frac{R_r-1}{R_r+1}=\frac{F}{ln2}arcosh(\frac{\exp[(ln2)/F]}{2}) \qquad (3\text{-}50)$$

The function F on the right side of Eq.(3-50) depends only upon R_r.

For a symmetrical sample such as a circle or a square, R_r and F=1. This allows Eq.(3-50) to simplified to give the resistivity as

$$\rho=\frac{\pi t}{ln2}R_{12,34}=4.532tR_{12,34} \qquad (3\text{-}51)$$

The sheet resistance is given by

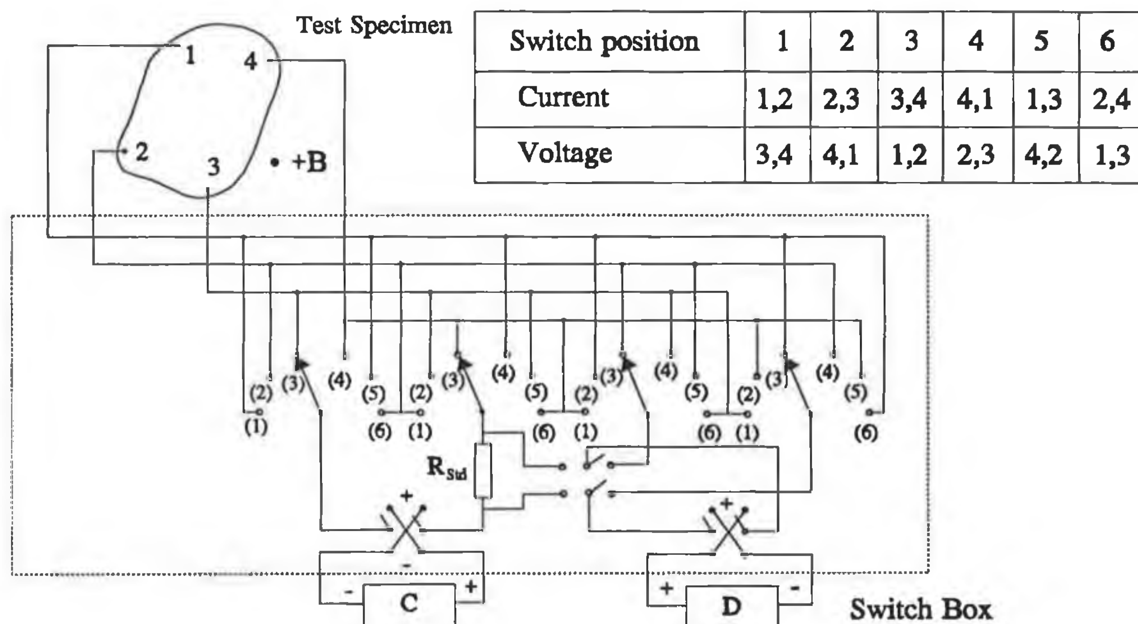

Switch position	1	2	3	4	5	6
Current	1,2	2,3	3,4	4,1	1,3	2,4
Voltage	3,4	4,1	1,2	2,3	4,2	1,3

Figure 3-8 Measurement circuit for van der Pauw structure. C=constant current supply, D=electrometer or potentiometer/galvanometer, R_{std}=standard resistor.

$$\rho_s=\frac{\pi}{ln2}R_{12,34}=4.532R_{12,34} \quad (3\text{-}52)$$

similar to the four-point probe expression.

The van der Pauw equations are based on the assumption of negligibly small contacts located on the sample periphery of the sample. The influence of non-ideal contacts has been calculated. The error so introduced can be eliminated by the use of the clover-leaf configuration. Such configurations make sample preparation more complicated and are therefore undesirable, so square samples are generally used. One of the advantages of van der Pauw structure is the small sample size compared with the area required for four-point probe measurements. Van der Pauw structures are therefore preferred for integrated circuit technology. For simple processing it is preferable to use the circular or square sample geometries. For such structures it is not always possible to align the contacts exactly.

Measurement circuits

The basic four-point probe measurement circuit is simple. One implementation recommended is shown in fig.3-6 and fig.3-8. The double pole switch allows voltage measurements for both

current directions. The resistance for the two current directions are measured, and the average resistance is calculated.

3.7.2 Hall Effect and Carrier Concentration

Those aspects of the Hall effect pertaining to carrier concentration measurements are discussed here. A more complete treatment of Hall effect, including a derivation of the appropriate equations, can be found in the following. The key feature of Hall measurements is the ability to determine the carrier concentration, the carrier type, the resistivity, and mobility with a relatively simple measurement.

The Hall theory predicts the Hall coefficient R_H as[69]

$$R_H=\frac{r(p-b^2n)}{q(p+bn)^2} \qquad \textbf{(3-53)}$$

where $b=\mu_n/\mu_p$ and r is the scattering factor that lies between 1 and 2, depending on the scattering mechanism in the semiconductor. For lattice scattering $r=3\pi/8=1.18$, for ionized impurity scattering $r=315\pi/512=1.93$, and for neutral impurity scattering r=1[70]. The scattering factor is also a function of the magnetic field and the temperature. In the high magnetic field limit $r\rightarrow 1$. The scattering factor can be determined by measuring R_H in high magnetic field limit, i.e., $r=R_H(B)/R_H(B=\infty)$ where B is the magnetic field.

For extrinsic p-type material, where $p \gg n$, the above Eq.(3-53) reduces to

$$R_H=\frac{r}{qp} \qquad \textbf{(3-54)}$$

or

$$p=\frac{r}{qR_H} \qquad \textbf{(3-55)}$$

and for extrinsic n-type, where $n \gg p$, it becomes

$$R_H=-\frac{r}{qn} \qquad \textbf{(3-56)}$$

or

$$n=-\frac{r}{qR_H} \quad (3\text{-}57)$$

The above Eq.(3-56) and (3-57) show that a knowledge of Hall coefficient leads to a determination of the carrier type as well as the carrier concentration.

3.7.3 Conductivity Mobility

The conductivity of semiconductor σ is given by

$$\sigma=\rho(\mu_n n+\mu_p p) \quad (3\text{-}58)$$

For reasonably extrinsic n-type semiconductors n>p, and the electron mobility from Eq.(3-58) is

$$\mu_n=\frac{\sigma}{qn}=\frac{1}{qn\rho} \quad (3\text{-}59)$$

Measurement of the conductivity and the carrier concentration was one of the first means of determining the semiconductor mobility, namely the conductivity mobility.

3.7.4 Hall Effect and Mobility

The Hall effect was discovered by Hall in 1879 when he investigated the nature of the force acting on a conductor carrying a current in a magnetic filed[71].

The Hall coefficient R_H is defined as

$$R_H=\frac{tV_H}{BI} \quad (3\text{-}60)$$

giving

$$p=\frac{1}{qR_H} \quad (3\text{-}61)$$

A similar derivation for n-type samples gives

$$n=-\frac{1}{qR_H} \quad (3\text{-}62)$$

When both holes and electrons are present, then the Hall coefficient becomes[72]

$$R_H=\frac{(p-b^2n)+(\mu_nB)(p-n)}{q[(p+bn)^2+(\mu_nB)^2(p-n)^2]} \tag{3-63}$$

This expression is relatively complex and depends on the mobility ratio $b=\mu_n/\mu_p$ and on the magnetic field strength B. For $B\rightarrow 0$

$$R_H=\frac{p-b^2n}{q(p+bn)^2} \tag{3-64}$$

and for $B\rightarrow\infty$

$$R_H=\frac{1}{q(p-n)} \tag{3-65}$$

with t in meters, V_H in volts, B in Teslas (T) (1 T=1 Weber/m^2=1 V·s/m^2), and I in amperes, the Hall coefficient has the units m^3/C. If, as is frequently done, the magnetic field is expressed in Gauss (G)(1 T=10^4 G), t in centimetres, V_H in volts, and I in amperes, then

$$R_H=\frac{10^8tV_H}{BI}cm^3/C \tag{3-66}$$

The Hall mobility $\mu_H$is defined by

$$\mu_H=\frac{|R_H|}{\rho}=|R_H|\sigma \tag{3-67}$$

The Hall mobility is not identical to the conductivity mobility.

$$\mu_H=r\mu_p,\mu_H=r\mu_n \tag{3-68}$$

for extrinsic p- and n- type semiconductors. Hall mobility can differ significantly from conductivity mobility since r is generally larger than unity. For most Hall-determined mobilities, r is taken as unity, but this assumption should be carefully specified. For lattice scattering $r=3\pi/8=1.18$, for ionized impurity scattering $r=315\pi/512=1.93$, and for neutral impurity scattering r=1. In the high magnetic field limit $r\rightarrow 1$. The scattering factor can be determined by measuring R_H in high magnetic field limit, i.e., $r=R_H(B)/R_H(B=\infty)$.

With van der Pauw method the Hall coefficient can be given by

$$R_H = \frac{t\Delta V_{34}}{2BI} \quad (3\text{-}69)$$

where $\Delta V_{34} = V_{34}(\text{for } +B) - V_{34}(\text{for } -B)$ with I flowing into terminal 1 and out of terminal 2.

3.8 Measurement of Transmittance

Optical transmission or absorption of transparent, insulating and emission films in EL display devices influences directly characteristics of the EL devices. Impurities in films determine the spectra in uv-visible range and properties of films. Optical transmission or absorption measurements are routinely used to determine the properties of the films.

During transmission measurements light is incident on the film, and the transmitted light is measured as a function of wavelength. The transmittance T of a film with identical front and back reflection coefficient and light incident normal to the film surface is given by

$$T = \frac{(1-R)^2 e^{-\alpha d}}{1 + R^2 e^{-2\alpha d} - 2Re^{-\alpha d}\cos(\phi)} \quad (3\text{-}70)$$

where $\phi = 4\pi n_1 d/\lambda$, α is the absorption coefficient, and the reflectance R is given by

$$R = \frac{(n_0 - n_1)^2 + k_1^2}{(n_0 + n_1)^2 + k_1^2} \quad (3\text{-}71)$$

The absorption coefficient is related to the extinction coefficient k_1 by $\alpha = 4\pi k_1/\lambda$.

There are two basic instrumentation approaches to measure the transmission spectrum. The more traditional one is based on the use of a monochromator; the more recent and now more popular one is based on an interferometer. The monochromator selects a narrow band of wavelengths $\Delta\lambda$ from source of radiation. The spectral band is centred on a wavelength λ that can be varied. The monochromator can be thought of as a tunable filter with a band pass $\Delta\lambda$ and a resolution $\Delta\lambda/\lambda$. For a transmittance measurement, light from source S enters the monochromator through a narrow entrance slit. The light rays should be made parallel for optimum performance by passing the light through a collimating lens. When the light falls on the prism or grating, it is dispersed; that is, the prism or the grating breaks the light into

its spectral components. A prism disperses and refracts white light by virtue of having a wavelength-dependent refractive index. Short wavelength light is refracted more than long wavelength light. A grating consists of many equidistant parallel lines inscribed on a polished substrate (glass or metal film on glass) with typically between 10000 and 50000 line or grooves per inch. The dispersed light depends on the groove spacing and on the incident angle. Two advantages of gratings over prisms are 1) high resolution and dispersion and 2) a dispersion that is almost constant with wavelength. The chief disadvantage are that gratings are slightly less rugged, and they generate slight more scattered light, particularly at short wavelengths. Frequently optical light is detected by optoelectronic detector and output signal from the detector is processed by using lock-in or signal-averaging techniques.

The basic optical component of Fourier transform (FT) spectrometers is the Michelson interferometer. Light from a source is collimated and incident on a beam splitter. An ideal beam splitter creates two separate optical paths by reflecting 50% of the incident light and transmitting the remaining 50%. Although the light from the source is incoherent, when it is split into two components by the beam splitter, the component are coherent and can produce interference phenomena when the beams combined. The measured quantity in FT is the interferogram. It contains not only the spectral information of the source, but also the transmittance characteristics of the sample. The spectral response can be calculated from interferogram using the Fourier transformation

$$B(f) = \int_{-\infty}^{\infty} I(x)\cos(2\pi x f)dx \tag{3-72}$$

The effects of the source and the background are eliminated by making one measurement without the sample and one with the sample. Storing the two interferograms in a computer allows the ratio of the two to be calculated, thereby eliminating the background. A computer is used for FT and signal processing, which has made the technique so powerful.

3.9 Measurement of X-ray Diffraction

X-rays are generated when high energy electrons strike some other material. Several sharp peaks will be superimposed on a background. The wavelength of the peaks is characteristic of the target material, while the minimum wavelength and general shape of the continuous spectrum are primarily functions of the energy of the impinging electrons. For electron-

acceleration voltages corresponding to minimum wavelengths longer than those of the characteristic peak (line), no lines will occur. Diffraction is the phenomenon most used. Constructive interference, i.e., a peak in x-ray intensity, will occur when

$$n\lambda = 2d\sin\theta \quad (3\text{-}73)$$

where n is the order, λ the x-ray wavelength, d the spacing between two consecutive scattering planes. This is Bragg's law and is the basis for crystal diffractometers. Provisions are made to allow the θ and 2θ angles to be quite precisely set, and for applications, a gear train is provided to rotate simultaneously the crystal by θ and detector arm by 2θ. Beam-width control is by slits, and wavelength control is by using a combination of a characteristic line of the chosen target material and the absorption edge of specific filter material. If a material with known lattice spacings is examined, the orientation can be determined by matching the d with previously calculated spacings for various orientations. If provisions can be made for observing the material from many directions and measuring the spacings for several orientations, they can be compared with tables of known spacings and the sample composition determined.

3.10 Measurements of Electroluminescence

3.10.1 Measurement of Brightness

Brightness or luminance is a measure of the flux emitted from the surface of EL display devices. Brightness of EL devices is an important property of EL devices. Quality and characteristics of EL displays are evaluated by measurements of brightness of EL devices. The relationships of brightness vs. applied voltage, brightness vs. frequency and brightness vs. Mn concentration of ZnS:Mn films as well as the brightness of EL devices with different insulating films are examined in this work. The system used in the brightness measurement consists of optometer, EL device driver and EL devices sample. EL driver consists of a generator and an amplifier. The generator produces a sine signal and a pulse signal whose pulse width can be adjusted. The output voltage of the amplifier can be adjusted from 0-300V. Fig.3-9 shows the schematic diagram of the brightness measuring system. The optometer is an instrument used to measure brightness. The UDT model 380 dual channel optometer was used in the measurements. The UDT model 380 dual channel optometer is a powerful optical measurement tool used in conjunction with a UDT detector head. The

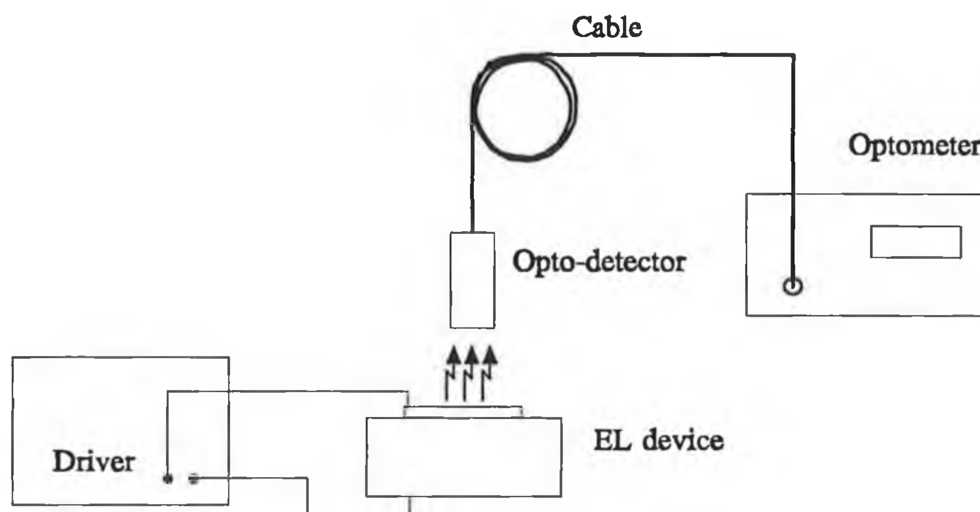

Figure 3-9 Schematic diagram of the brightness measuring system for electroluminescent display devices.

instrument allows selection of calibration, wavelength, or linear/logarithmic measurements.

3.10.2 Measurement of Optical Spectrum

Fig.3-10 shows the system of optical spectrum measurement for EL display devices. As in fig.3-9 above, the driver of EL device consists of a generator and a high voltage amplifier. The system used to measure the spectra consists of an optical fibre, optical lens, a monochromator whose uv-visible range is 200-900nm, an optoelectronic detector which consists of photomultiplier tube with silica windows , an electron circuit and a computer. The computer controls the monochromator, i.e. the range of spectra, the electronic circuit and the supply voltage of photomultiplier tube, ie. the gain of signal, and processes the signal.

3.10.3 Measurement of Optical Output of EL Device

Optical output is measured using an optoelectronic detector with a large area, a wide spectral range, low noise, fast response and low capacitance, an amplifier and a storage oscilloscope. The optical signal is received by the detector, amplified and stored in storage oscilloscope.

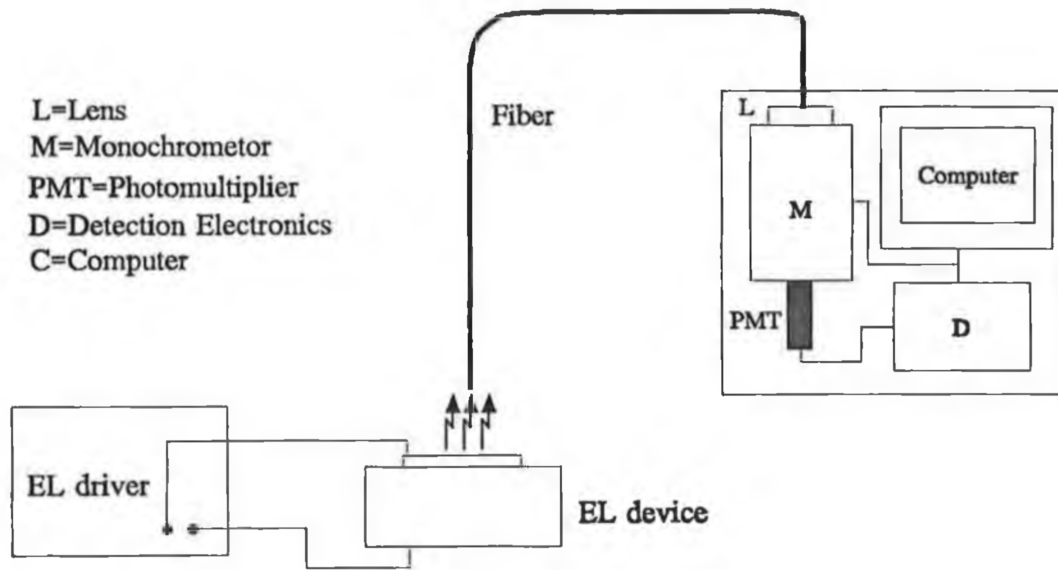

Figure 3-10 Schematic diagram of electroluminescent emission spectrum measuring system for EL display devices.

Chapter 4

PHOSPHOR FILMS

4.1 Introduction

In this chapter we shall be concerned with the luminescence from inorganic solid materials, i.e., in the emission of electromagnetic radiation in visible range. Luminescence emission involves radiative transition originates on some excited electronic level, and after the emission of a photon a lower electronic level is occupied.

An emitting solid is a much more complicated electronic system; it consists of a very large number of atoms (or ions), each one interacting with many of its neighbours. The energy levels of the solid are characteristic not only of the constituent atoms or ions, but also of the way in which the atoms or ions combine together in the material and impurities and defects may have a strong effect on the luminescence properties. A material must have a reasonably large energy between adjacent energy levels if it is emitting luminescence. Consequently it is found that inorganic luminescence solids are either large band gap semiconductors or insulators, since both of these are characterized by filled electron band separated by a sufficiently large gap from an adjacent unfilled electron band. In the ZnS semiconductor, the band gap corresponds to the energy of an ultraviolet photon, and visible luminescence is not expected from the pure material. Impurity atoms and defects, however, are always present, and these may produce electron levels separated by a gap which corresponds to a photon of visible light. The luminescence from ZnS semiconductor is almost always associated with such impurity atoms and defects.

High field collision excitation electroluminescence has been extensively investigated since the original work of Destriau. Most of these investigations have been on zinc sulphide host material doped with luminescent centre materials. Electroluminescent display having ZnS:Mn phosphors are finding increasing commercial use for displaying graphic and character information. Although such EL display has been found to have many advantages, such as light emitting, high resolution, wide viewing angle, high operating speed and immune to temperature extremes, their performance is limited by the fact that they can only emit the yellow-orange light. To solve this problem, a considerable amount of research efforts has already been made on colour thin film electroluminescent phosphors, so that multi- and full-colour EL displays are available.

Research on different colour thin film EL phosphors originated with the pioneering studies at the end of 1960's[73]. Most of the research efforts undertaken since then have been concerned with ZnS host materials incorporating various rare-earth luminescent centres. As a result of these works, green EL with luminance level suitable for practical applications has been obtained from the ZnS thin film doped with Tb^{3+} luminescent centres. However, despite all the effort on these materials the maximum luminance achieved with red Sm^{3+} and blue Tm^{3+} luminescent centres is relatively low compared with the green Tb^{3+} centre[74].

In order to obtain efficient colour EL phosphors, many studies have thus been directed to new host materials as well as luminescent centres. It is found that the alkaline-earth sulfides, such as CaS and SrS doped with rare-earth luminescent centres are promising phosphor materials[75],[76],[77], especially for producing red, blue and white EL, which is applicable to thin film EL displays. Much fundamental research on these phosphors materials such as thin film deposition techniques, EL characteristics and EL excitation mechanisms have been carrier out in past few years.

Materials to be used as high field EL phosphors must be doped with luminescent centres which give luminescence in the visible spectrum. A very high field over 10^6 V/cm can be applied to the phosphor thin film to excite the luminescent centres. To satisfy this requirement, semiconductors with a fairly wide band gap should be used as host materials. ZnS is such one material which is already used as a host material for available ZnS:Mn EL displays and rare-earth doped colour EL phosphors. Other materials are alkaline-earth sulfides, such as CaS and SrS.

In order to realize colour EL displays some phosphor materials have been researched for colour displays. Table 4.1 summaries some phosphor materials.

Although research on colour phosphors has been made progress, the luminance level and efficiency are not still sufficient for practical applications. In order to improve the performance of these phosphors for EL display, further research should be made based on fundamental considerations of the physics of host lattice and luminescent centres.

4.2 Requirement of Luminescent Materials

For designing a good phosphor, several factors must be considered:

1) choice of the host components,

2) choice of the activator, and

Table 4.1 EL characteristics of some phosphor materials

Colour	Phosphor
Yellow-orange	ZnS:Mn
Yellow	ZnS:DyF_3
Green	ZnS:Tb, ZnS:TbF, ZnS:TbF_3, ZnS:TbOF
	ZnS:HoF_3
	ZnS:ErF_3
Red	ZnS:Sm,F
	ZnS:Sm,P
	ZnS:Sm,Cl
	CaS:Eu
	CaS:Eu,F,Cu,Br
Blue	ZnS:Tm
	SrS:Ce,F
Blue-green	SrS:Ce,K
White	ZnS:Pr,F, ZnS:Pr,K
	SrS:Pr,F, SrS:Pr,K, SrS:Ce,K,Eu
	CaS:Ce,K,Eu,

3) "killers" of luminescence.

4.2.1 Choice of the Host Components

In designing an efficient thin film EL phosphor, it was found that the inorganic host consists of one of several different cations combined with one of several different anions. The anion may be simple or it may consist of group of atoms. It should be apparent that both the cation and anion choice must be optically transparent, since the absorption-excitation process takes place. To satisfy the requirement, phosphors with fairly wide band gap should be used as host materials. The efficient host material should be have the best possible crystalline order to allow electron accelerated to obtain enough energy to excite luminescent centres. In order

for the activator atoms (or ions) to emit light efficiently, they should be incorporated in a substitutional lattice site, otherwise the excited centre will lose its energy non radiatively to a nearby lattice defect. In order to maintain the required good crystallinity, both the geometric size and the valence of the host cation with that of the dopant need to be matched. If there is a geometric mismatch, the dopant atoms will have to fit into a less efficient interstitial site and if there is a valence mismatch, this will have to be compensated by an additional co-activator ion. The phosphor should be miscible with activators for high luminescence. The physical and chemical stability of the phosphors is also one of important factors.

4.2.2 Choice of the Activator

In the design of phosphors, because of the limitations imposed by the ground state perturbation factor, certain cations are limited in specific valence states. It is pointed out that this type of activator dose not show strong absorption, but does show strong and efficient emission once it becomes excited. It is for this reason that they have been called "activators". One important point needs to be emphasized. All of the indicated valence states are stable states of that element. This brings us to a critical proposition, namely:

In choosing an activator, one must be able to form and stabilize the activator in the proper valence state within the host crystal in the required electronic configuration if efficient luminescence is to result.

It is apparent that there are other rules for phosphor design that need to be elucidated:

(a) The activator cation and the host cation need to be matched in size so as to obtain maximal efficiency in the produced phosphor. Mismatch creates strain in the lattice, and limits the actual solubility of the activator in the host lattice.

(b) The activator cation needs to be of the same valence state as that of the host cation. Otherwise, the activator will substitute into the lattice with the formation of cation vacancies (for charge-compensation). An alternative is the introduction of a compensating cation for the same purpose.

4.2.3 Quenchers, or "Killers" of Luminescence

Cations, having unpaired electron spins, function as quenchers of luminescence. Usually, these ions have electronic configurations which involve d-electrons. Note that some of these

cations can be optically active in proper valence state. In the wrong valence state, however, they function as quenchers. This observation has important consequences since the method of preparation thus becomes important. If these cations become stabilized in the wrong valence state, they become energy traps and dissipaters of excitation energy. These cations are essentially acceptors, even for resonant energy transfer. Since they cannot undergo an excitation transition because of ground state coupling to the local phonon modes, they function oppositely to the luminescence process. Many of them exhibit strong absorption bands at the frequencies of light commonly used for excitation of phosphors. Therefore, excitation energy is dissipated to the lattice by phonon processes, once it has been captured by this type of site.

An unwanted impurity affects deleteriously upon any given phosphor composition. To obtain a phosphor having a high degree of luminescent efficiency, a high degree of purity is mandatory.

4.3 Phosphor Materials

4.3.1 Properties of Host Materials

In order to be an efficient thin film EL phosphor, the host material should have the best possible crystalline order to allow electron acceleration a kinetic energy sufficient for impact excitation. In order for the activator atoms (or ions) to emit light efficiently, they should be incorporated in a substitutional lattice site, otherwise the excited centre will lose its energy non radiatively to a nearby lattice defect. In order to maintain the required good crystallinity, both the geometric size and the valence of the host cation with that of the dopant need to be matched. If there is a geometric mismatch, the dopant atoms will have to fit into a less efficient interstitial site and if there is a valence mismatch, this will have to be compensated by an additional co-activator ion. The table 4.2 give some pertinent data on the various EL host materials.

Table 4.3 give data on the geometric size and valence for common activator ions[78],[79].

The II-VI compounds exhibits properties which are intermediate between the covalent group IV elements and the III-V compounds on the one hand and the ionic I-VII compounds on the other. Almost all of the II-VI compounds can be prepared either in a hexagonal (wurtzite) structure or as cubic (zincblende) crystals. The interatomic distances are practically the same for compounds having both forms, which implies that their local environments and chemical

Table 4.2 Phosphor host lattice characteristics:

Material	Crystal structure	Lattice constant	Cation Radii (Å)	Bandgap eV
ZnS	Zincblende	5.409	0.74(Zn^{2+})	3.66
CaS	Rock salt	5.697	0.99(Ca^{2+})	4.41
SrS	Rock salt	6.019	1.13(Sr^{2+})	4.30
BaS	Rock salt	6.384	1.35(Ba^{2+})	3.78

Table 4.3 Dopant ion valence and size:

Ion	Valence	Ion size (Å)
Mn	+2	0.80
Tb	+3	0.93
Tm	+3	0.87
Sm	+3	1.00
Ce	+3	1.03
Eu	+2	1.09

bonding are nearly identical.

Each semiconducting material has its own unique physical, chemical, electrical and optical characteristics. Physical and optical properties such as crystal structure, lattice constant, energy gap, refractive index, lasing line which are important in the study of electroluminescent devices are given in table 4.4. Electronic properties of II-VI are given in table 4.5 [78],[79].

Although SrS and CaS have good geometric size and valence as host materials for some rare earth dopants, they are refractory materials and tend to react with moisture. The stoichiometry deviation and poor crystallinity of alkaline earth sulfide thin films result from their chemical instability and hygroscopic nature. This means the materials must be carefully handled to minimize exposure to a moisture containing atmosphere and implies high

Table 4.4 Some properties of II-VI compounds:

Properties	ZnS	ZnSe	CdS
Crystal structure	Z,W	Z,W	Z,W
Lattice constant (Å)	5.409(Z) a=3.806(4H) c=12.44(4H)	5.668(Z) a=4.01(W) c=6.54(W)	5.464(Z) a=4.1368(W) c=6.7167(W)
Thermal expansion coefficients (~300K)(10^{-6}/K)	6.14	7.2	4
Ionicity of bonds (%)	24	15	22
Energy gap (300K) (Ev)	3.66	2.67	2.38
Refractive index	2.49 (4400Å)	2.61 (5890Å)	2.506 (6000Å)
Lasing line (Å)	3290(4.2K)	4600(150K)	4897(4.2K) 4900(110K) 5270(300K)
Max melting point (°C)	1830	1520	1475

Table 4.5 Some electric properties of II-VI compounds:

Electric properties	ZnS	ZnSe	CdS
Dielectric constant static (ε_0)	8.9	9.2	10.3
Optical (ε_∞)	5.7	6.1	5.4
Mobility (cm^2/V•s) electron(μ_n) hole(μ_p)	 160 10	 600 40	 250 15
Effective mass electron(m^*_e/m_0) hole(m^*_h/m_0)	 0.34 0.58	 0.17 0.60	 0.208 0.80
Work function(ϕ)(Ev)	5.40	4.84	5.01
Electron affinity (χ)(Ev)	3.90	4.09	4.79

temperature processing. The processing of ZnS doped with rare earth ions is easier than that of CaS or SrS phosphor.

4.3.2 Some Properties of Host Phosphor ZnS

In the cubic structure of ZnS, the zinc sulfide is a direct gap semiconductor with the smallest energy gap at the centre of Brillouin zone(Γ). The topmost valence band(Γ_{15}) is split due to spin-orbit coupling into a fourfold (Γ_8) and a twofold (Γ_7) state[78],[79]. Hexagonal zinc sulfide is also a direct semiconductor with the smallest energy gap at the centre of the Brillouin zone (Γ) The topmost valence band (Γ_5+Γ_1) is split due to crystal field and spin-orbit coupling into three spin-degenerate states (Γ_9, Γ_7, and Γ_7). The energy gap is dependent upon the temperature.

The lattice parameter of the cubic structure is 5.40937Å (measured in 300 K) which depends on temperature. The lattice parameters of hexagonal structure are a(4H)=3.814Å and c(4H)=12.46Å. The distance (in Å) between its next neighbours of Zn ion is given below in table 4.6.

Table 4.6 The distance (in Å) between its next neighbours of Zn ion:

Zn-S	2.36	in cubic modification
Zn-Zn	3.82	in cubic modification
Zn-S	2.33	in hexagonal modification
Zn-Zn	3.12	in hexagonal modification

The covalent radii (in Å):

r_{Zn} 1.31

r_S 1.04

There are refractive index (cubic modification) of ZnS measured in different wavelength in table 4.7 [78],[79].

4.3.3 Transition Metal Ions Mn^{2+}

The transition metal ions enter substitutionally for positively charged ions in a variety of hosts. In the ZnS host material the transition metal ions are in sites which are surrounded by negatively charged sulphur ions. Because of the effect of the electrostatic crystal field of the neighbouring ions on the 3d electrons, the Mn^{2+} levels in an octahedral crystal field are split

Table 4.7 Refractive index of ZnS (cubic modification):

n	measuring wavelength λ (μm)
2.488	0.44
2.458	0.46
2.435	0.48
2.414	0.50
2.395	0.52
2.384	0.55
2.375	0.57
2.359	0.60
2.346	0.65
2.334	0.70
2.306	0.90
2.293	1.05
2.282	1.20
2.280	1.40

as shown in fig.4-1. All of these orbitals are even parity, since they belong to the $3d^5$ electronic configuration.

The excitation energies of the impurities in the semiconductors, as well as their donor and acceptor ionization energies, represent a combination of one-electron and many-electron multiplet, where the latter contribution becomes increasingly significant as localized states are formed. The neutral Mn^{2+} impurity in ZnS semiconductor has the $^6A_1$ ground state. This case (d^5) is unique in that all transitions are spin forbidden. The calculated multiplet structure for 3d impurity Mn in ZnS is shown in the literature[80], which is similar result to fig.4-1.

If the release of electrons depends only on the insulator-host matrix interfaces, all other processes depend on the host matrix and also on the luminescent centre. Host materials are characterized by a large energy gap between the highest filled electron band and the lowest empty electron band. This band gap corresponds to a photon of ultraviolet radiation. These

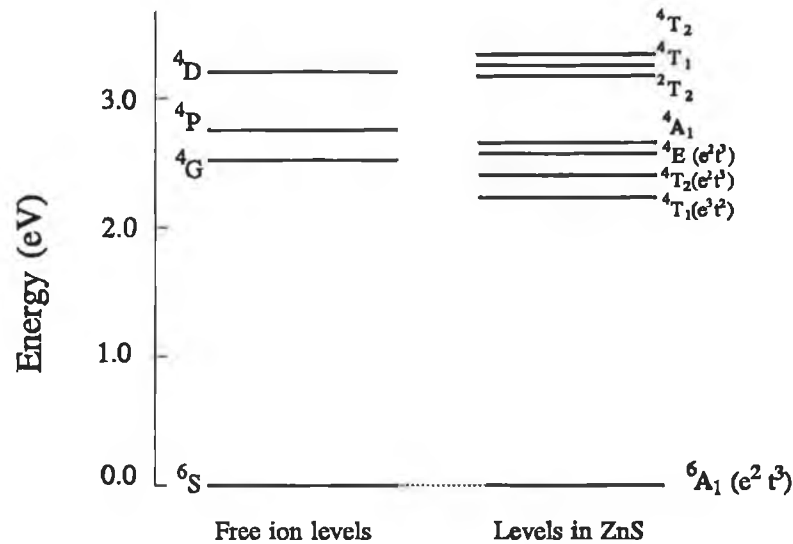

Figure 4-1 Energy levels of the free Mn^{2+}(3d) ion, and of Mn^{2+} in ZnS host material.

materials appear as transparent crystals, since they are unaffected by visible radiation and can be regard as optically inert. If the covalently bonded crystal is an electrical insulator, there is a large gap to the next higher vacant band which cannot be bridged by a photon of visible light, and so the material is optically inert and may make an excellent host material for the optically active dopant atoms or ions.

The optical activity of the transition metal ion can be understood by considering their ground state electronic configurations

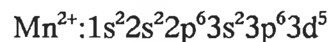

$$Mn^{2+}:1s^2 2s^2 2p^6 3s^2 3p^6 3d^5$$

Since the 3d shell requires 10 electrons to fill it, so each of the ions has a partially filled 3d shell. As a result they possess electronic levels close to the ground state, and the ions are optically active. Some of the low-lying energy levels of Mn^{2+} are seen in fig.4-1. The Mn^{2+} free ion levels are split up when the ion is placed in a host crystal, and visible as well as ultraviolet absorptions occur on the dopant Mn^{2+} ion. When the Mn^{2+} ion is raised to one of the higher excited states, it decays non-radiatively to the adjacent lower excited states until it reaches the lowest excited $^4T_1$ state. The 2.2 eV gap between this and the ground state is too large to be bridged by non-radiative decay, so the $^4T_1$ state decays radiatively by the emission of a yellow-orange photon. Fig.4-1 shows energy levels of the free $Mn^{2+}(3d^5)$ ion,

and of Mn^{2+} in a typical host material ZnS.

From data table 4.2 and table 4.3 it is known that why the ZnS:Mn combination is an efficient yellow orange emitting EL phosphor. It is seen that Mn has both the right valence and similar ionic size to the Zn atoms in the ZnS lattice and, therefore, Mn substitutes very nicely for the Zn atoms. In fact, Mn is miscible in ZnS lattice over a wide solid solution range. In comparison, the rare earth dopants have a valence of plus three and are too large to fit easily into the ZnS lattice.

4.3.4 Rare Earth Ions

The rare-earth ions are better luminescent centres in the phosphor materials for various colour. They have the general electronic configuration:

$$1s^2 2s^2 2p^6 3s^2 3p^6 3d^{10} 4s^2 4p^6 4d^{10} 5s^2 5p^6 4f^n$$

Rare-earth ions have a partially filled 4f shell of electrons. In contrast to the case of the transition metal ion, where the electrons in the partially filled 3d shell occupy orbits on the outside of the ion, 4f electrons in the rare-earth ion occupy inner orbits, since the filled 5s, 5p shells are outside the 4f shell. The 4f electrons, then, are shielded from the electric field of the neighbouring ions, and the effect of the crystal on the 4f electrons is small. The energy levels of the rare-earth ions do not vary greatly from one host material to another. In different hosts the energy levels of the trivalent ions are essentially in the same positions, but the splittings of the levels will be different, reflecting the different strengths and symmetries of the different crystal fields. Also, the strengths of the radiative transitions and the question as to whether or not luminescence is observed from a given level will depend in part on the symmetry of the crystal field. It should be remembered that, for each trivalent ion, the states with energies up to around 6eV belong to the same $4f^n$ configuration, and so these states have the same parity. States with the $4f^{n-1}5d$ configuration are over 6eV above the ground state, and these have the opposite parity to the ground state.

Divalent rare-earth ions can be incorporated in many hosts. In some cases the energy levels of divalent ions are obtained from the trivalent energy level diagram by looking up the appropriate $4f^n$ levels. Such, however, is not always the case, and the level assignment for divalent ions is not nearly as well understood as it is for the trivalent ions. One of the complicating factors is the fact that in divalent ions, the levels belonging to states with $4f^{n-1}5d$ configuration are often within 3eV of the ground state, and such levels give rise to broad

absorption transitions.

For divalent ions the low lying $4f^{n-1}5d$ states permit strong absorption transitions in the visible region from the ground $4f^n$ state. Furthermore, the 5d orbital is much more sensitive to the environment than the 4f orbital, and as a result, the $4f \rightarrow 5d$ transitions are broad. The presence of broad strong absorption bands causes a deep colour in these divalent crystals. They also allow efficient optical pumping of the divalent ion, which can result in strong luminescence from these ions.

Rare-earth materials are commonly used as a luminescent centre for colour thin film EL phosphors which are doped in the host material. The rare-earth ions have in common an open 4f shell, which is screened by the outer electrons in $5s^2 5p^6$ close shells. For this reason, the 4f electrons of rare-earth ions in the host materials are hardly influenced by crystal field. Two different types of luminescent transition can be observed for the rare-earth ions. One is f-f transition, which is parity forbidden. The other is parity allowed f-d transition. Some rare-earth ions emit visible light due to f-f transition. For example, Tb^{3+} ions show green EL and Sm^{3+} for red, Tm^{3+} for blue and Pr^{3+} for white EL. Eu^{2+} and Ce^{3+} ions produce luminescence due to f-d transition. Since the 5d electrons are affected most by the crystal field, the $f^{4n-1}5d$ excited energy levels depend on the host material. For this reason, emission colour varies by changing host lattices.

ZnS phosphors doped with trivalent rare-earth ions produce luminescence with various colours. The ZnS:Tm,F phosphor display show blue EL, which is the result of ${}^1G_4$-${}^3H_6$ transition at about 480 nm. The ZnS:Tb,F display shows green EL, which is dominated by the ${}^5D_4$-${}^7F_5$ transitions of Tb^{3+} ions occurring at 542 nm. The ZnS:Sm,F display shows orange-red EL due to ${}^4G_{5/2}$-${}^6H_J$ (J=5/2, 7/2, 9/2) transition of Sm^{3+} ions.

Although ZnS phosphors doped with rare-earth ions can produce luminescence with various colour, the luminescent intensities of the red ZnS:Sm,F and the blue ZnS:Tm,F are much lower than that of ZnS:Mn, and the solubility of rare-earth ions into ZnS lattice is low. Improvements have been sought for increasing luminescent levels and the solubility of ZnS phosphors doped with rare-earth ions to satisfy required standards of colour EL displays.

Alkaline-earth sulfides are more ionic than ZnS. The ionic radii of rare-earth (IIIA) ions are very close to the those of alkaline-earth (IIA) ions compared with Zn (IIB) ions. In addition, the chemical nature of IIA and IIIA ions resemble each other. Rare-earth luminescent centres, therefore, are considered to be more effectively incorporated in these lattices without

considering any solubility problem. These facts are likely to be very advantageous when one intends to dope the rare-earth luminescent centres in CaS and SrS phosphors are efficient, and have the possibility of colour thin film EL.

CaS and SrS thin films doped with Eu^{2+} and Ce^{3+} luminescent centres show the efficient EL due to $4f^{n-1}5d$-$4f^{n}$ transitions. The EL phosphors doped with Eu^{2+} centres show broad band emissions due to the $4f^6(^7F)5d$-$4f^7(^8S_{7/2})$ transition. The Ce^{3+} doped phosphors show broad band emissions due to the $5d(^2D)$-$4f(^2F_J)$ transition. White EL can be obtained by using SrS phosphors activated with Ce^{3+} and Eu^{2+} luminescent centres. SrS phosphors doped with Pr^{3+} show white EL and doped Tb^{3+} show green EL.

4.3.5 Rare Earth Ions Tb^{3+}

Rare earth Tb has been used for commercial products as luminescent centre of green EL phosphor. This is a very significant step forward for thin film EL displays since the luminance requirement of full colour display is predominantly in the green due to the eye's spectral response. The rare-earth ion Tb^{3+} is one of the most effcient luminescent centres in the phosphor materials for green colour. Tb^{3+} has the general electronic configuration:

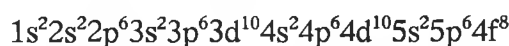

$$1s^2 2s^2 2p^6 3s^2 3p^6 3d^{10} 4s^2 4p^6 4d^{10} 5s^2 5p^6 4f^8$$

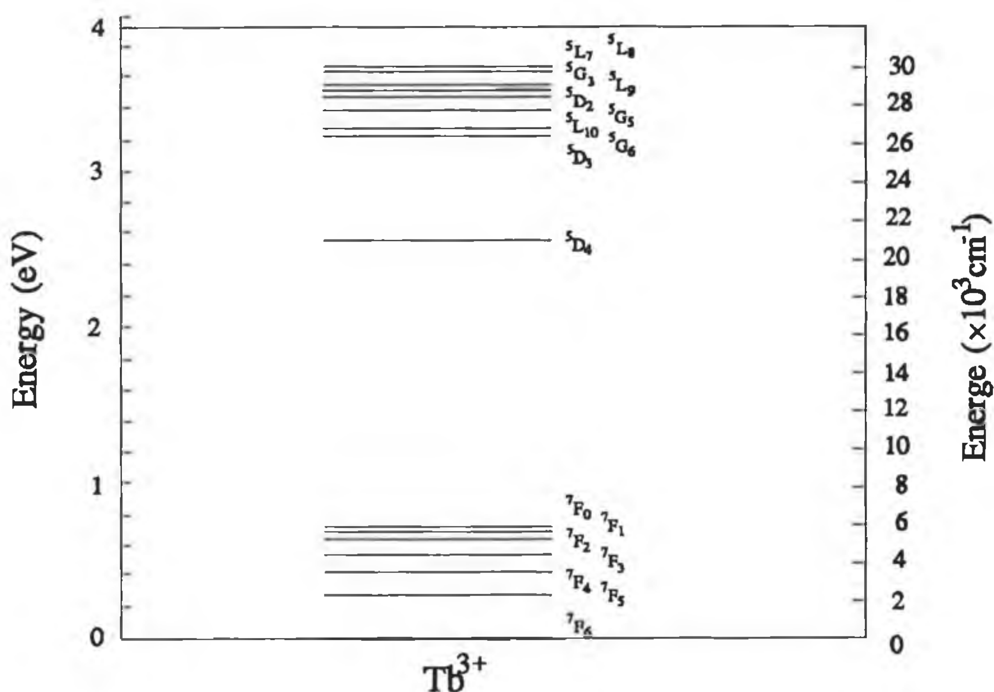

Figure 4-2 Energy levels for Tb^{3+}.

Fig.4-2 shows energy levels of Tb^{3+} resulting from theoretical predictions and comparison with experiment from literature[81].

The strong emission peaks at 490, 542, 590 and 625 nm correspond to the transition from $^5D_4$ to ^7F and emission peaks at 380, 420, 440 and 460 nm correspond to the transition from $^5D_3$ to ^7F of Tb^{3+} ion respectively. But because geometric size and valence charge of Tb^{3+} ions the luminance of ZnS:Tb can not be efficient.

When the charge compensation was considered it was found that TbF_3 was a more efficient dopant for ZnS than pure Tb. Tb-F and Tb-F_3 centres exist in ZnS with the Tb-F complex apparently the more efficient light emitting centre[82]. At low concentrations Tb-F complexes dominate. The Tb ions can be readily substituted for Zn site with an accompanied lattice imperfection. One F^- ion remains in the vicinity of the Tb^{3+} to provide charge compensation. However, at the high concentrations (4-6%) that are usually used to produce a high brightness green phosphor, the Tb^{3+} cannot be accommodated in the lattice substitutionally and therefore TbF_3 molecules go into the lattice interstitially or at grain boundaries. These latter centres are not as efficient as the Tb-F complexes, however, with annealing, it is possible to drive the excess Tb into the lattice substitutional sites with an accompanied decrease in F content and an increase of luminance.

The size difference between Tb ion and Zn ion result in an increased concentration of Tb for the optimum doping level. The Mn ion has a radius of 0.80Å while the Tb ion has a radius of 0.93Å which compare to a radius of 0.74Å for Zn. The large size of the Tb ions means it is more difficult to incorporate into the ZnS lattice without creating lattice defects. Since the Tb dopant does not experience luminance concentration quenching like the Mn dopant and, therefore, the optimum doping level is significantly higher.

In ZnS:TbOF phosphor, Tb^{3+} ion substitute for the Zn^{2+} site and F^- ions locate at an interstitial site to satisfy the need for charge compensation. O^{2-} ions substitute S^{2-} ions to relax lattice distortion. As a result, higher luminance level were achieved.

4.4 Relationship between Photoluminescence and Electroluminescence

Electroluminescence and photoluminescence are very different, but the fundamental processes seem to be connected to each other. The excitation, energy transfer and light emission are the fundamental processes of luminescence. Although the excitation and energy transfer processes are different in electroluminescence and photoluminescence, the emission is the

same. Photoluminescence is an effective method to study the characteristics of EL materials. In photoluminescence the monochromatic light is absorbed by luminescent centre with probability B_{if} to excite the luminescent centre from state i to f, then the centre relaxes to j state with probability T_{fj}, and then makes an emission transition to k state with probability A_{jk}. The emission intensity I_{jk} for photoluminescence is proportional to B_{jk}, T_{fj} and A_{jk}, as

$$I_{jk} \sim B_{if} T_{ff} A_{jk} \quad \textbf{(4-1)}$$

In direct impact excitation of EL an electron with enough energy excites the luminescent from initial state i to excitation state f, the excitation probability is proportional to the excitation cross-section σ of luminescent centre and energy distribution of electron in conduction band. The excited electrons relax from state f to j with probability T_{fj}, and the emission occurs with probability A_{jk}. σ is the function of the absorption probability B_{if} from state i to state f[83]:

$$\sigma(E_{if}, E) = \frac{114\pi^3 m^2 e^2}{n(n^2+2)^2} \frac{1}{E} \ln\left[\frac{E^{1/2}+(E-E_{if})^{1/2}}{E^{1/2}-(E-E_{if})^{1/2}}\right] B_{if} \quad \textbf{(4-2)}$$

where n is the refractive index, E_{if} the energy difference between i and f state, E the energy of electron.

Since the absorption, relaxation and emission processes take place in the luminescent centre, they are not influenced by an electric field, but they affect the emission intensity of EL.

The emission intensities of photoluminescence and electroluminescence are related to the absorption, relaxation and emission probabilities, so the efficient EL material should have the high probabilities. Information about spectra, emission efficiency and other properties of EL materials can be obtained from the PL characteristics of the materials. However, because of the different excitation and energy transfer processes between EL and PL, an efficient EL material may not be an efficient PL material and vice versa.

Chapter 5

BASIC SOL-GEL FILM DEPOSITION AND CHARACTERISTICS

5.1 Introduction

In general, deposition methods of thin films are divided into two groups, physical methods and chemical methods. Physical method includes mainly evaporation and sputtering. Chemical vapour deposition is usually used as deposition of films in chemical methods. In the physical methods vacuum equipments are required so deposition of films is relative expensive. Although chemical vapour deposition does not need a high vacuum system in some case, The deposition system is also expensive.

The physical deposition of films is processed in a bell jar and the chemical deposition is done in a chemical reactor. The size of the jar or the reactor controls the size of substrate. A large area deposition of films requires large scale, more complex and expensive deposition system. The characteristics of evaporation or sputtering sources, and the orientation and placement of substrates influence the ultimate film uniformity in physical vapour deposition. CVD is the process of chemically reacting a volatile compound of a material to be deposited, with other gases, to produce a nonvolatile solid that deposits atomistically on a suitably placed substrate. The deposited film or coating thickness uniformity depends on the delivery of equal amounts of reactants to all substrate surfaces. It is said that uniformity is confined by many factors such as substrate placement and position, reactive materials and gases flow, film growth rate and, temperature uniformity of environment and substrate.

The deposition of the film using the sol-gel process has many advantage. One of the most technologically important aspects of the sol-gel process is that, prior to gelation, the fluid sol or solution is ideal for preparing thin films by such common processes such as dipping, draining, or spinning. Compared to conventional thin film forming processes such as CVD, evaporation, or sputtering, sol-gel film formation requires considerably less equipment and is less expensive; however, the most important advantage of sol-gel process over conventional coating methods is the ability to control precisely the microstructure of the deposited film. Sol-gel process is an efficient and simple method for the deposition of a large area film.

In this chapter preparation of ZnO, SiO_2 and Al_2O_3 films is described, which is the fundamental of EL devices in the work.

5.2 ZnO Films Deposited Using the Sol-Gel Technology

The optical and electrical characteristics of ZnO films have attracted considerable attention in recent years because of their application in many fields. The resulting applications have already been widely studied for transparent electrodes [84],[85],[86], piezoelectric films for surface acoustic waves[87] and for detecting pressure and vibration[88],[89]. Although ZnO films can be deposited using many methods [90],[91],[92],[93],[94],[95], the deposition of a ZnO film is simpler and less expensive to apply by sol-gel process where the advantages are a higher purity, homogeneity and low temperature. A zinc oxide film is presently widely used in technology, in particular, in devices where its optical and electrical properties play a significant role. It is known that optical and electrical attributes of ZnO film are very sensitive to the technology of its preparation, which may be due to irregularities of stoichiometry[96]. Usually alkoxide used as a precursor in sol-gel process is hydrolysed easily, so it is difficult to be stored and bought. Some metal acetate compounds gelate under catalysis conditions. It may be pertinent to mention that the carboxylate of zinc acetate binds the metal in chelating bitentate[97]. Zinc acetate was selected as the precursor for ZnO films.

There are many applications of ZnO film which do require a cost-effective application technique such as dipping and air baking.

5.2.1 Experimental Procedure

5.2.1.1 Solution Preparation

A solution of ZnO precursor was made by dissolving zinc acetate $(Zn(CH_3CO_2)_2)2H_2O$ in anhydrous ethanol or methanol. Solutions of the solid were prepared in increasing concentrations to establish maximum solubility. After adding the zinc acetate powders to ethanol the solution was stirred on a magnetic heat plate and refluxed. Without acid additions the maximum concentration reached was 6% in ethanol and 12% in methanol.

The solutions were hydrolysed with 2 mol H_2O per mole of metal acetate by adding dropwise water dissolved in ethanol at 10 wt.% concentration together with roughly 5 wt.% lactic acid. Turbidity and precipitation occurred which was readily eliminated by introducing additional concentrated lactic acid until the turbidity permanently disappeared. By this procedure the stable solutions were prepared, as required to carry out the experiments described.

5.2.1.2 Deposition Procedure

Application of the coating was carried out by one of two techniques. Previous work showed that dipping was capable of producing controlled thickness sol-gel coatings in the work. The drain coating method was used in the work. In this case the substrate remains stationary, and the liquid is drained from the vessel. Some of the parameters in the fluid mechanics expression are changed, but the results are generally the same as dip-coating method. According to the theory of fluid mechanics[98], by assuming a velocity profile for laminar boundary layer which is the linear profile, the formula of solution film thickness was derived under the draining coating:

$$t=\left(\frac{\eta V_0}{g\rho}\left(1-e^{-\frac{12g}{V_0^2}x}\right)\right)^{\frac{1}{2}} \tag{5-1}$$

where t is the thickness of solution film, x is the vertical distance from initial surface to falling surface of solution, η is the viscosity, g is acceleration of gravity, the ϱ is the density of solution and V_0 is the falling velocity of solution surface. When x increases with low velocity, the thickness approximates to:

$$t=\left(\frac{\eta V_0}{g\rho}\right)^{\frac{1}{2}} \tag{5-2}$$

which is similar to the thickness of the dip-coating formula [99],[100].

The thickness of the coating layer depends on the velocity of solution level falling, the concentration of solution, the viscosity of solution, the surface tension of solution, the vapour pressure temperature and relative humidity above the coating bath. In fact for getting a homogeneous film with no cracking the thickness of the deposited liquid film on the substrate could not be too thicker in one coating. The average baked thickness was determined to be 40-60 nm in one coating. Thicker films needed multiple coatings.

Following the step after coating, the film must be dried. From the time the solution was applied to the time it took to gelate, the film remained steady, continuous and completely covering the surface. It was shown repeatedly that all shrinkage was taken up in the thin dimension and not in the plane of substrate.

For the purpose of outgassing, the drying temperature should be above 260°C. To go from a tacky gel to a hard gel usually takes some time. Water and solvent can remove through

interconnected pores which remain open at the surface until the coatings are fired to higher temperature. The coatings are more or less porous in all case. In order to shrink the pores the films were heated in a high annealing temperature.

After coating, the substrates were carefully introduced into a cold electrically heated furnace, where they were heated in circulating air to the desired temperature at the ramp rate of the furnace, about 10°C min^{-1}, where they were held for 1 hour at final temperature. Repeating the above process of dipping and heating substrates increased the thickness of ZnO film on the substrates. Fig.5-1 presents the flow diagram for ZnO films from preparation of solution to production of coated substrates.

5.2.2 Optical Measurements and Characteristics

After coating the film on the substrates the samples were annealed at different temperatures in the heating furnace for some time. The refractive indices and thicknesses of films on Si substrates and SiO_2 substrates were measured by an ellipsometry at a wavelength of 632.8 nm at room temperature. Approximate thicknesses were estimated initially with an interference method using the interference microscope. Transmittance in visible region was measured

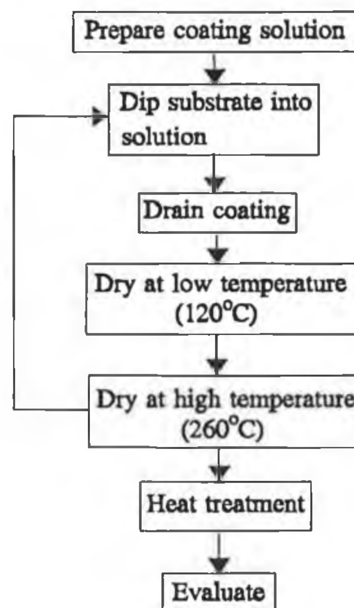

Figure 5-1 Flow diagram of the sol-gel process for depositing ZnO films.

using a Hewlett Packard 8452A UV-visible recording spectrophotometer.

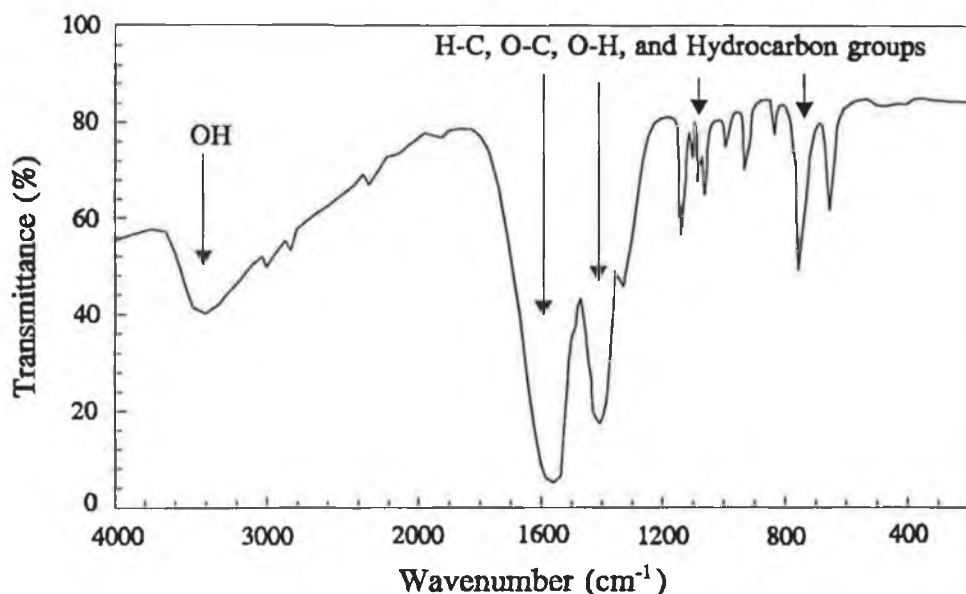

Figure 5-2 IR spectrum of the film at 120°C for preparing ZnO film.

The compositions of the deposited films depend on annealing temperature. A minimum temperature of 260°C was used to allow pyrolysis of the carbon-bearing molecules. The pyrolysis time is longer for thick films. The 260°C was not sufficient to ensure complete carbon and hydrocarbon groups removal. KBr was used as a substrate to confirm the IR peak of ZnO. Fig.5-2 shows the IR spectra of the film at 120°C. From fig.5-3 at a temperature of 260°C for 1 hour a large amount of hydrocarbon groups were removed, when the temperature is increased only the ZnO peaks exits while all the other hydrocarbon peaks disappear. Compared to the standard IR spectrum of ZnO the data suggests that a temperature of between 400-500°C would be ideal. There is abroad band at ~420 cm^{-1} in the standard IR spectrum.

The effect of anneal temperature on the index and the thickness of ZnO film was assessed. The measured refractive index by the ellipsometry for the film deposited directly on Si substrate revealed a range of 1.5-2.011 with anneal temperature, which is quite close to the bulk value of 2.08. Meanwhile measurement of film thickness was made. Fig.5-4 and fig.5-5 shows the effect of anneal temperature on the results of index and thickness.

The microstructure of the film can be further modified by heating. Heating initially densifies

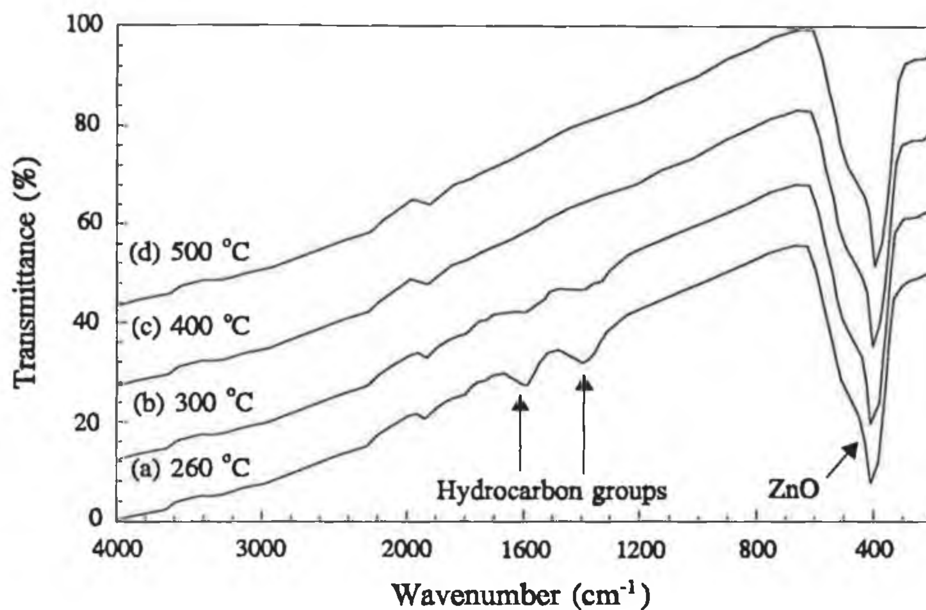

Figure 5-3 IR spectra of the film annealed at 260°C (a), 300°C (b), 400°C (c) and 500°C (d) for preparing ZnO film.

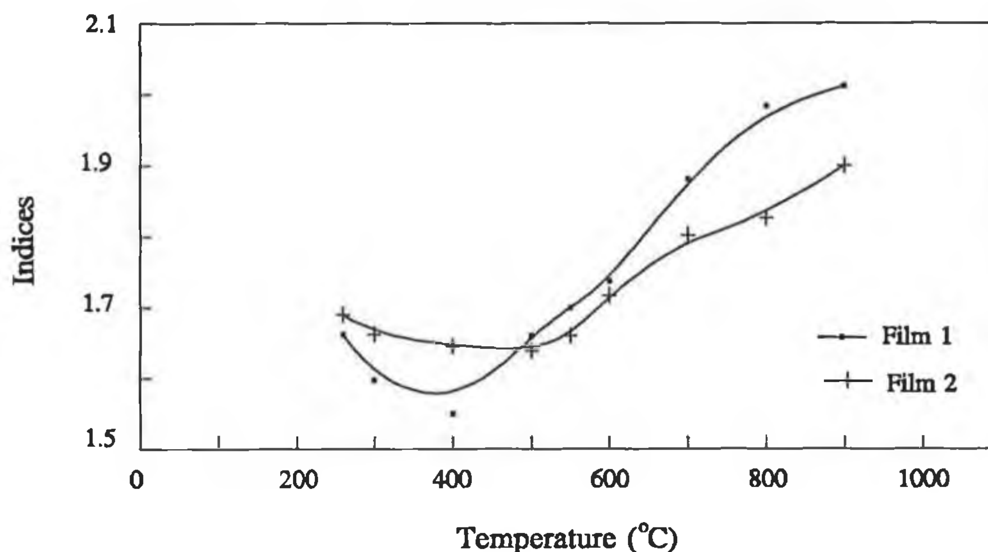

Figure 5-4 Indices of films change with an increasing of anneal temperature.

the skeleton and ultimately causes viscous sintering and complete densification. In geometrical models, the result of heating is a uniform reduction in pore size (and volume)

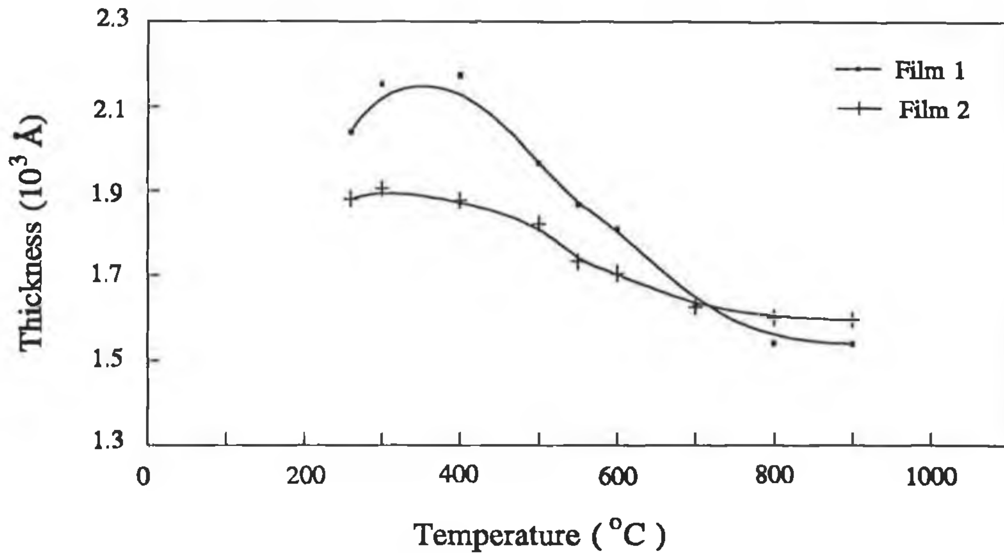

Figure 5-5 An increasing of annealed temperature leads to change of ZnO film thickness.

causing an increase in index.

Fig.5-4 shows the decreasing of indices with the increasing of heating temperature and fig.5-5 shows thickness was increased in a range of 260-400°C. It indicates that residual hydrocarbon groups and liquids escaped and that the pores were enlarged with increasing temperature, which resulted in the reduction of index and the expanding of thickness. The increasing of film index and the decreasing of film thickness with further increasing temperature above 400°C illustrates that pores shrunk and moved out gradually. In the range of 550-600°C, the largest rate of variations of index and thickness reveal that pores disappeared gradually in process of sintering by diffusion[101]. Fig.5-4 shows the index of original thicker film 1 arrive at 2.011 at 900°C which is close to the index of standard bulk ZnO, and the index of original thinner film 2 is 1.899. In variation of thickness film 1 is larger than that of film 2. At final film 1 is thinner film 2. The contraction of film thickness results in increasing of density and in increasing index. The more thickness contracts, the more index increases. Fig.5-6 shows the relationship between index and thickness, which are approximately linear under the same treatment conditions. The decreasing of one ZnO film thickness with temperature results in the increasing of the index, measurements being performed on one

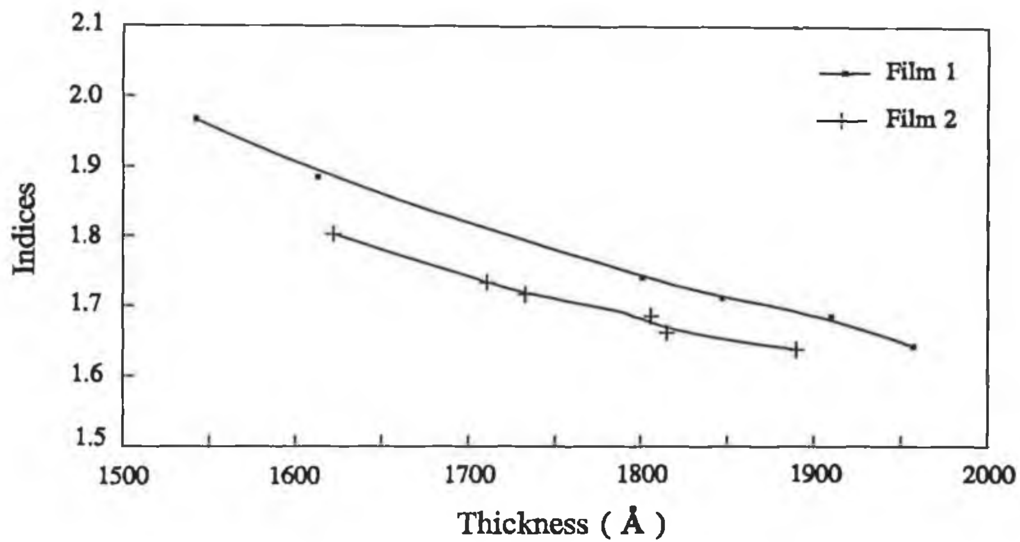

Figure 5-6 Indices depend on change of film thickness. The films were annealed at different temperatures.

sample. The approximate gradient (n/t) of curves of two samples are similar which indicate the decrease of thickness causes increase of index proportionally.

ZnO films were coated on several substrates in different thicknesses. They were then heated at 500°C for 1 hour and place back in the furnace at 550°C for 1 hour and their thickness and index were measured. The index of the thicker film was found to be larger than that of thinner one. Fig.5-7 shows the relationship between indices and thicknesses at 500°C (a) and 550°C (b).

Fig.5-8 and fig.5-9 shows that the increasing of index and the decreasing of thickness are proportional to heating time in furnace which indicates that pores of the film shrink continually with heating time.

5.2.3 Electrical Measurements and Characteristics

Standard capacitance-voltage C-V measurements are performed with a Boonton capacitance meter at a frequency of 1 MHz using a metal-insulator-semiconductor (MIS) structure with ZnO as the insulator.

Current-voltage I-V measurements were performed in order to determine the resistivity

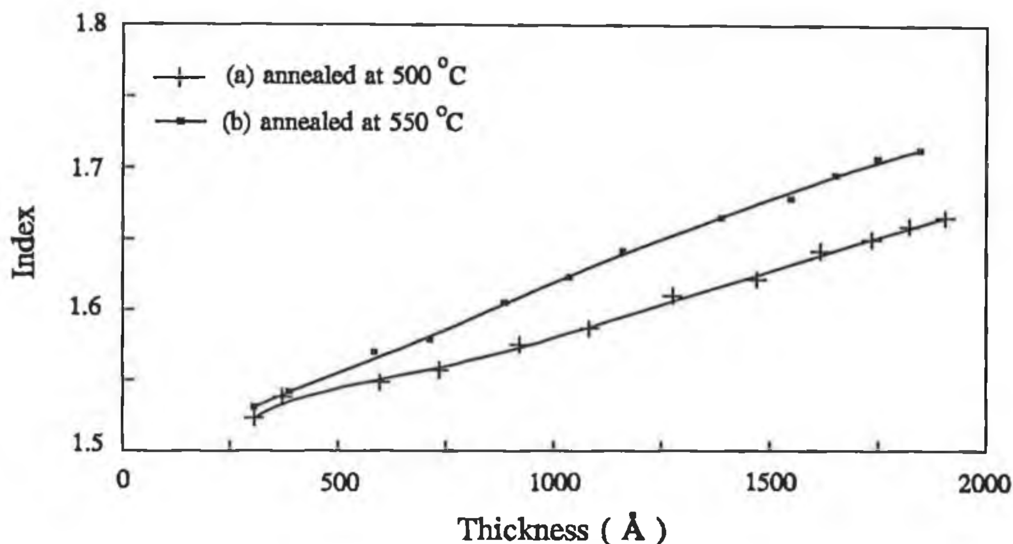

Figure 5-7 Relation of indices and thicknesses of different films. The films were annealed at (a) 500°C and (b) 550°C.

perpendicular to the substrate. The ZnO is sandwiched between aluminium or gold and Si substrate. Resistance measurements were recorded using a Keithley 614 and a Keithley 617 electrometers which have a high input resistance ($5\times10^{13}\Omega$). The electrical measurement was carried out using ZnO film deposited on highly doped silicon (type n), which exhibits metallic behaviour (3-5 Ω·cm) and used as a first electrode. The second electrode was evaporated aluminium coated by Edward Coating system or gold deposited by sputtering on ZnO films. In order to determine the sheet resistivity parallel to the substrate, the collinear four-point probe method was used. ZnO film was deposited on a silicon wafer covered with an SiO_2 layer. The sheet resistance is given by [102]:

$$\rho_s = \frac{\rho_\parallel}{t} = 4.532\left(\frac{V}{I}\right) \qquad (5\text{-}3)$$

ϱ_s is sheet resistance, $\varrho_\parallel$ is resistivity parallel to substrate, t is thickness of film.

Because of the photoconduction properties of zinc oxide, samples were sealed in a dark holder when the electrical measurement were being performed.

ZnO is an n-type semiconductor, in which carriers are due to excess zinc at interstitial

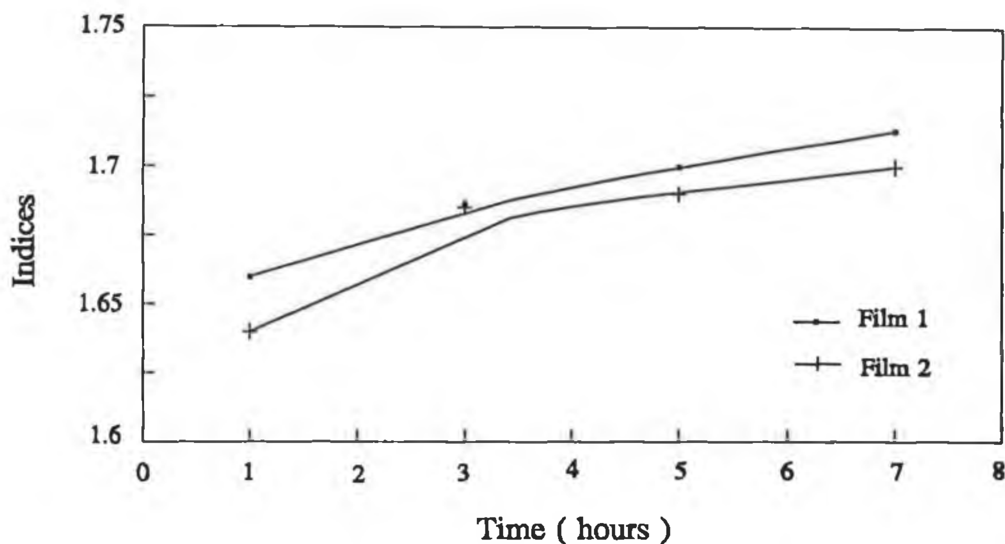

Figure 5-8 Indices of ZnO films depend on time of heat treatment.

positions acting as electron donors[103],[104]. They are formed according to the equilibrium:

$$ZnO \rightleftharpoons Zn_i^x + \frac{1}{2}O_2 \quad (5\text{-}4)$$

These interstitial atoms are ionized through two dissociation equilibria:

$$Zn_i^x \rightleftharpoons Zn_i^{\cdot} + e^- \quad (5\text{-}5)$$

$$Zn_i^{\cdot} \rightleftharpoons Zn_i^{\cdot\cdot} + e^- \quad (5\text{-}6)$$

Zn_i^x, $Zn_i^{\cdot}$ and $Zn_i^{\cdot\cdot}$ are a zinc atom, a monovalent and a divalent cation at an interstitial site, respectively, and e^- is a conduction electron.

It is characterized by oxygen desorption as temperature goes up and also by an electron release which is responsible for a conductivity increase. The resistance depends on the Zn_i^x concentration.

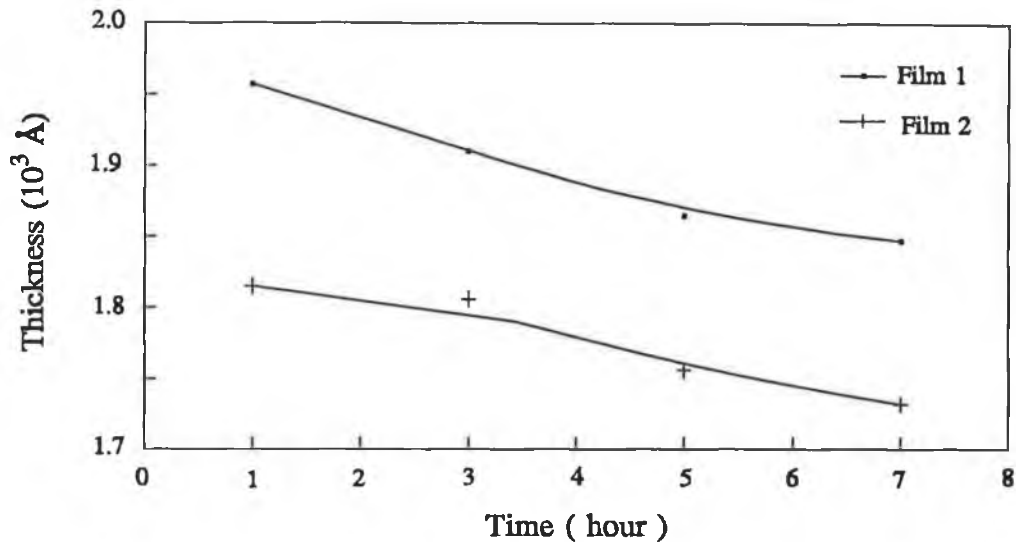

Figure 5-9 Thickness of ZnO film depends on time of heat treatment.

ZnO films usually are polycrystalline. Several conduction models for polycrystalline semiconductors can be found in the literature. Basic models are proposed by Volger[105] and Petritz[106]. In the Volger model, the polycrystalline material is divided into identical cubes (grains) consisting of two different materials: the bulk material at the centre of the cube, and the boundary material which surrounds this centre (grain boundary region). Generally, the grain boundaries of a polycrystalline semiconductor contain surface states due to defects or absorbed ions, which can trap free carriers from the bulk material. This results in band bending near the grain boundary and depletion of the boundary material. Thus the boundary region can be described electrically in terms of two back-to-back Schottky barriers. If the mechanism for conduction across the barriers is known, then expressions for the effective resistivity of the polycrystalline material can be derived. Basic assumptions thereby are that both the mean free path λ of the carriers and the Debye length L_D are small compared to the grain size.

The resistance of ZnO film depends on (1) Zn ion concentration, (2) microstructural properties of ZnO film, (3) quality of residual liquids and residue and (4) chemisorption of oxygen. Fig.5-10 shows that with increase of anneal temperature the resistivities decrease initially,

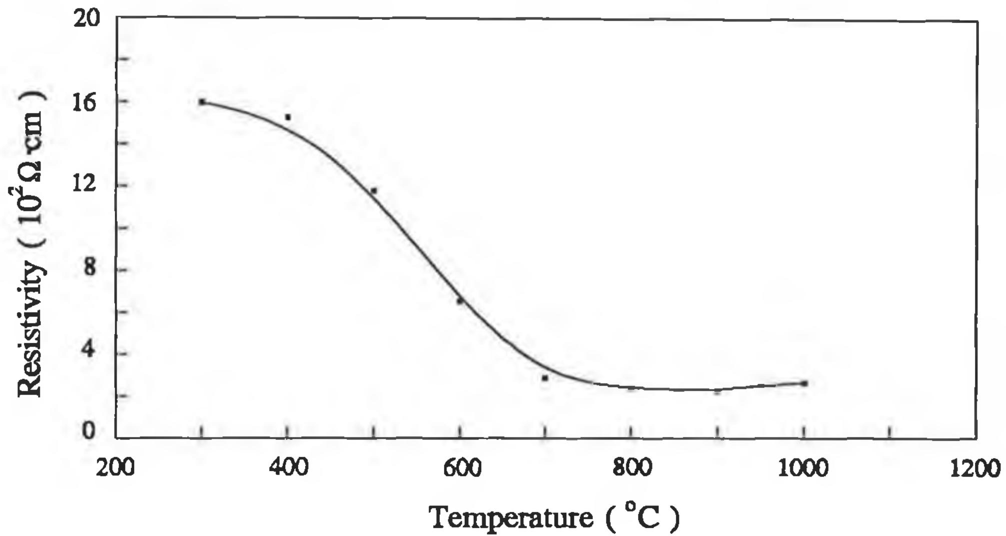

Figure 5-10 Resistivity of ZnO film depends on heat treatment temperature.

then increase slightly. This indicates that liquids and gases move out from pyrolysed film and the Zn ion concentration increases. At higher temperature Zn ions combine with oxygen in the air. Zn ion concentration lessens, which causes the increase of resistivities. With an increase of the anneal temperature the pores shrink therefore the volume of grain and interface between the grains changes.

The capacitance of ZnO films on Si substrates was measured. The capacitance changed when the voltage was applied to ZnO film. Fig.5-11 shows relation of capacitance and applied voltage. The film was annealed at 800°C and thickness is 2115Å.

The variation in the capacitance with bias is due to the combination of insulator capacitance and semiconductor substrate capacitance. When the diode is biased into accumulation the capacitance reaches a maximum determined by the insulator alone. From fig.5-11, the maximum capacitance is 1940 pF. The permittivity of the insulator can then be found from the equation

$$C_{ins}=\frac{\varepsilon_{ox}\varepsilon_{ins}A}{t} \qquad (5\text{-}7)$$

where A is the top area, t is the thickness of the insulator ε_{ox} is the permittivity of free space

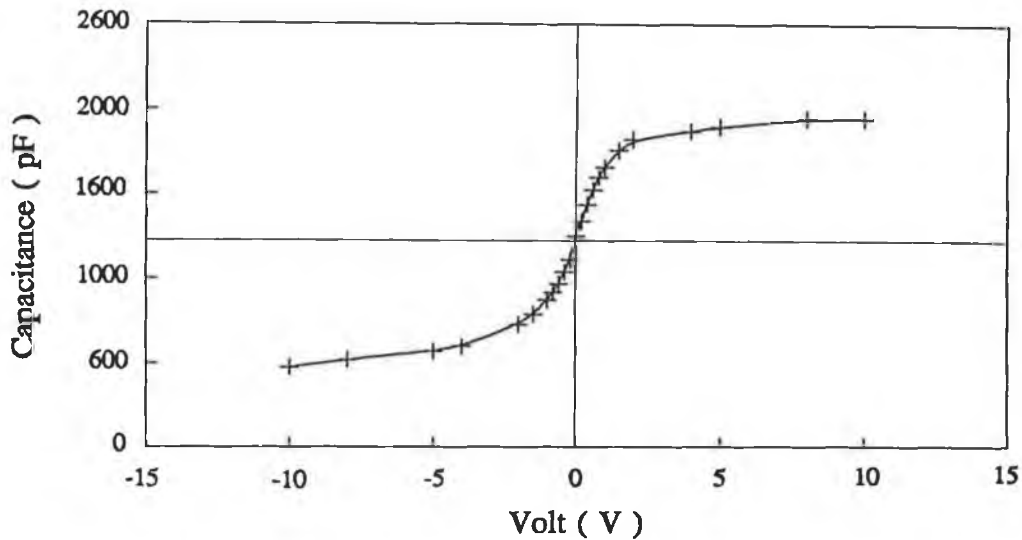

Figure 5-11 C-V characteristics of ZnO film on Si substrate were measured. The film was annealed at 800°C and thickness was 2115 Å.

and ε_{ins} is the permittivity of insulator.

This gave a value ε_{ins}=8.43 which compares with the theoretical value of 8.54 for bulk zinc oxide.

5.3 SiO_2 Films Deposited Using the Sol-gel Process

There has been considerable interest in the development of the sol-gel process for deposition of SiO_2 thin film. Although the optical properties required for anti-reflection or high-reflection coatings have received the most attention, there is also possible use of the sol-gel process for preparation of scratch resistant coatings, diffusion and oxidation barriers, and dielectric films. In fact, this method may be especially applicable in low-temperature processing and fabrication of microelectronic device such as deposition of field and gate oxides, passivation coatings, or interlayer dielectrics.

In depositing SiO_2 film by sol-gel technology, tetraethyl-orthosilicate (TEOS) is used most often, because it reacts slowly with water, and at equilibrium a complex silanol is formed, and in a one-quarter hydrolysed state has a shelf life of about six months. The clear TEOS liquid is the product of the reaction of $SiCl_4$ with ethanol. The colourless liquid, $Si(OC_2H_5)_4$, has

a density of about 0.9g/cm^3, is easy to handle safely, is extremely pure when distilled, and is available from several producers.

The two other ingredients that form the major volume of materials are alcohol and water. Industrial-grade ethanol and distilled water are used in most cases. The ethanol or other organic solvent serves as the mutual solvent for TEOS and water. The TEOS and water are immiscible, and only in the solvent can the two begin to react.

As soon as TEOS is dissolved in ethanol to make it soluble in water, the hydrolysation and condensation reactions begin. The chemical reactions are basically:

hydrolysis and esterification

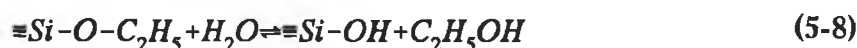

$$\equiv Si-O-C_2H_5+H_2O \rightleftharpoons \equiv Si-OH+C_2H_5OH \qquad \textbf{(5-8)}$$

alcohol condensation and alcoholysis

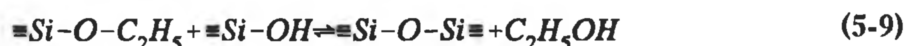

$$\equiv Si-O-C_2H_5+\equiv Si-OH \rightleftharpoons \equiv Si-O-Si\equiv +C_2H_5OH \qquad \textbf{(5-9)}$$

water condensation and hydrolysis

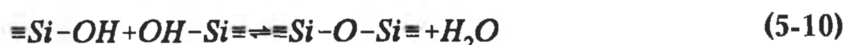

$$\equiv Si-OH+OH-Si\equiv \rightleftharpoons \equiv Si-O-Si\equiv +H_2O \qquad \textbf{(5-10)}$$

An acid is usually added to control the rates of these reactions. The temperature is maintained anywhere from -20°C to +80°C. This mixing takes between one and three hours, while the solution viscosity increases. Complete hydrolysis of $Si(OC_2H_5)_4$ to $Si(OH)_4$ would give silica acid. This does not occur. Instead, a condensation reaction takes place between a silanol and an ethoxy group to give a bridge oxygen or siloxane group, Si-O-Si. The intermediates, which remain soluble in the alcohol-water, are silanol, ethoxysilanols, and polysiloxanes.

The parameters that influence the chemical reactions are temperature, pH, amount of water, solvent, and precursor. In general, high temperatures speed up reactions. In terms of pH, low pH favours a polymerization scheme that gives linear molecules. To ensure that no organic residue results, the amount of water should be in excess of the amount calculated for complete reaction. In term of solvent, the complex compositions are easier to mix in longer-chain alcohols. In term of precursors, long chain organic groups give slower reaction rates and methyl groups give the fastest rates. In the case of silica, an acid catalyst gives a clear gel believed to be made up of linear chains, whereas a base catalyst gives a cloudy gel believed

to be made up of branched clusters which are almost particulate. An acid catalyst is preferred for the densest films. Presumably, the gel made up of chains can flow and cover easily the surface of the substrate during coating.

During drying, if the film is thick, it is easily cracked. This cracking is sometimes attributed to the existence of a pore size distribution in the gel. When larger pores are emptied by evaporation, the wall between adjoining pores is subjected to uneven stress that can cause cracking. It is reported that drying control chemical additives (DCCA) have been used to control the rate of hydrolysis and condensation, the pore size distribution, the pore liquor vapour pressure, and drying stresses to prevent cracking[107]. Without a DCCA a wide range of pore sizes and diameter of solids network are produced when gelation occurs. Addition of basic DCCA such as formamide produces a large sol-gel network with uniformly large pores. An acidic DCCA, such as oxalic acid, in contrast results in a somewhat smaller scale network after gelation but also with a narrow distribution of pores. Thus, either basic or acidic DCCAs can minimize differential drying stresses by minimizing differential rates of evaporation and ensuring a uniform thickness of the solid network that must resist the driving stress.

5.3.1 Experimental Preparation of SiO_2 Films

The silica sol was prepared by adding tetraethylorthosilicate (TEOS) into a mixture of ethanol, water and HCl (or an organic acid drying control chemical additive: oxalic acid (HO_2CCO_2H)) using a 2:1 molar ratio of water and TEOS. The pH of sol solution is set between 1~2. The 6~8:1 molar ratio of ethanol/TEOS was used in my experiment. The silica sol prepared was stirred in an ultrasonic reservoir.

The method of film deposition used is the drain coating method as the above mentioned. Thick films crack easily when applied to heat, but this can be avoided using a DCCA. The ratio of ethanol and TEOS determines the thickness of SiO_2 film. Depositing thin films can be achieved using a greater ratio of ethanol and TEOS.

SiO_2 thin films deposited on Si substrates were annealed at different temperatures with a temperature ramp rate of 5°C/min. The thin films of crack-free SiO_2 were obtained. IR spectrometer was used to monitor the composition of thin films. Fig.5-12 shows that thin films were annealed above 400°C and water and organic groups were removed from the thin films by analysing IR spectra. IR band were observed at the ~430, ~800, ~1080 and ~1220

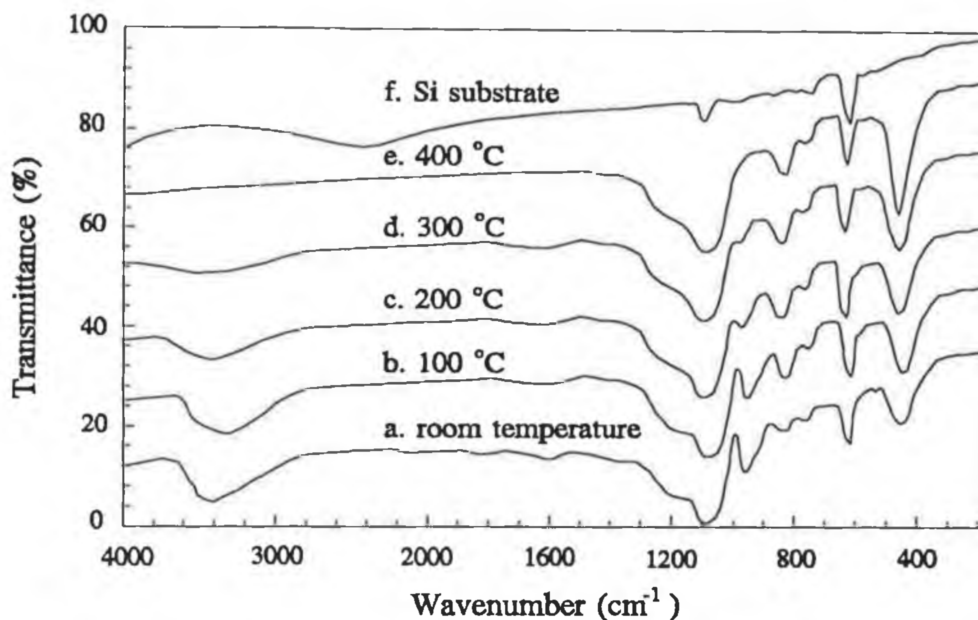

Figure 5-12 IR spectra of the film for preparing SiO_2 film by sol-gel process. films were deposited on Si substrate and annealed at various temperatures for 1 hour.

cm^{-1} bands. The ~1220 cm^{-1} and ~1080 cm^{-1} bands are assigned to LO and TO Si-O-Si asymmetric stretching modes respectively. The ~800 cm^{-1} vibration is associated with symmetric Si-O-Si stretching or vibrational modes of ring structures and the ~460 cm^{-1} is assigned to vibration of Si-O-Si banding mode. The C-H band in the 2800-3000 cm^{-1}, Si-OH bands at ~980 cm-1 and SiO-H broad bands centered near 3400 cm^{-1} are disappeared with an increasing annealed temperature. The SiO_2 film can be obtained using the sol-gel process and annealing at 400 °C from IR spectrum analysing.

In order to measure the dielectric constant and index of the SiO_2 films they were deposited on Si substrates. The films were annealed at 500 °C for 1 hour. The dielectric constant ε_{ins} of SiO_2 film in the work is ~4.104 which compares with the theoretical value of 3.96 for bulk silica. The index was ~1.42.

5.4 Al_2O_3 Films Deposited by the Sol-gel Process

Aluminium triethyl, $Al(C_2H_5)_3$, and aluminum isopropoxide, $Al(OHC(CH_3)_2)_3$, have often been used to prepare high purity alumina gels. Al_2O_3 coatings are applied to substrates in order to produce a physical property variation. Porous sol-gel coatings are an example of coatings

with several applications [108],[109],[110], [111],[112],[113]. High purity oxide formation as well as the presence of significantly large microporosity are inherent to sol-gel processing.

Fig.5-13 shows the most common method of producing transparent alumina gels. It consists of hydrolysing an aluminum alkoxide, $Al(OR)_3$, normally $Al(OPr^i)_3$, in a large excess of water (r=100-200) at 80-100°C, resulting in precipitation of fibrillar boehmite (AlOOH), followed by peptization with a mineral acid (HNO_3) to yield a stable particulate sol. Cold-water hydrolysis forms an amorphous precipitate that converts to bayerite upon ageing through a dissolution-recrystallization process. Gelation is generally achieved by increasing the concentration of the sol via boiling or evaporation. Yoldas observed that a minimum gel volume occurred with an acid:Al mole ratio of 0.07.

5.4.1 Experimental Preparation of Al_2O_3 Films

In my experiment, the solution was prepared from 75 moles of distilled water, one mole of aluminum isopropoxide $[Al(OC_3H_7]_3]$, and 0.15 of mole of nitric acid. After acidifying and heating the water to approximately 80°C, the aluminum isopropoxide was added slowly to the water, maintaining the temperature at approximately 80°C. Mixing using magnetic stirring

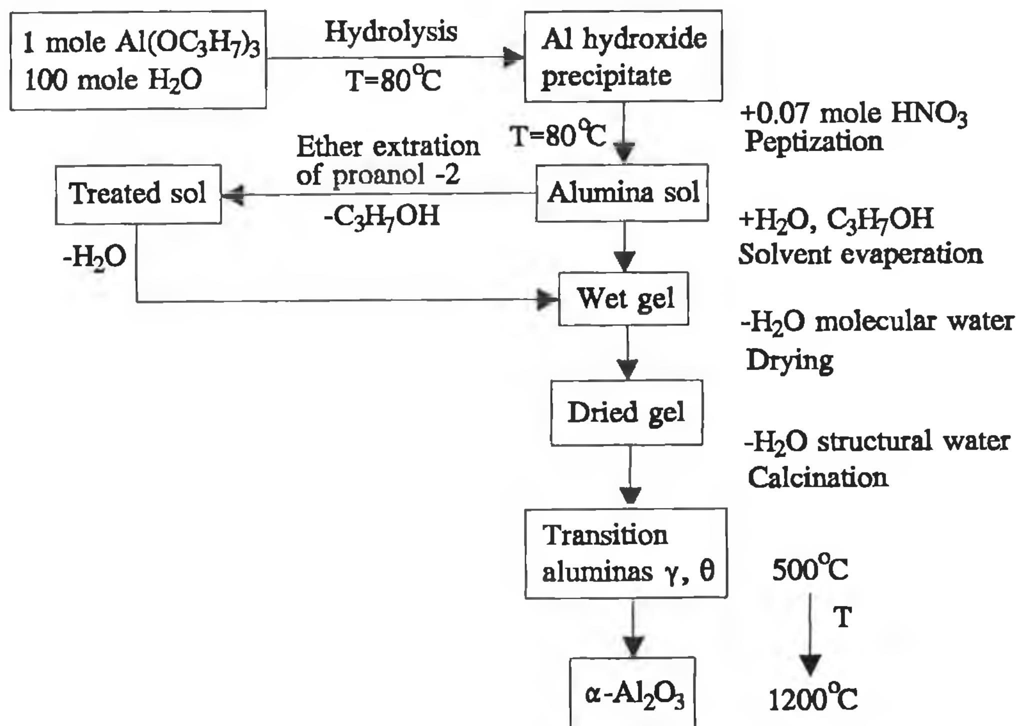

Figure 5-13 Flow chart of sol-gel process for preparing alumina.

was carried on throughout aluminum isopropoxide addition. Aluminum isopropoxide was added until a homogeneous solution was obtained, usually taking three to four hours. After complete mixing the solution was stored at 80°C in a sealed container until the application of the solution to substrate is performed.

Initial application of the coating to the substrate is accomplished via dipping. After dipping the substrates are dried at 70°C for one hour and then dried at room temperature for at least one day. After this drying period the coated substrates are fired to either 700°C, 800°C, 900°C or 1000°C at approximately 5°C/min, to obtain a once-coated sample. Thicker coatings were obtained by repeating this coat-dry-fire cycle several times.

At the gelling point the equivalent Al_2O_3 content of the system can be 4 to 25% by weight, depending on the concentration of solution. As a result, considerable shrinkage in size must occur during drying if the coherence is to be retained. Drying occurs in two stages: first, the gel shrinks to its final size of about 35 to 65% of the original dimensions (depending on concentration of solution), remaining transparent and non-porous; and, second, the gel is too rigid for further shrinkage to occur and begins to lose liquid internally with the formation of the porosity. The gel loses 23% of its weight and becomes opaque during this second stage. However, after drying complete transparency returns. Through evolved gas analysis of gel samples heated in nitrogen and air[114], the gas (or mixture of gases) released has a density less than air, and gas release is completed by 500°C. Oxygen from the atmosphere is apparently not required for pyrolysis. When gel samples are heated in vacuum, pyrolysis shifts to slightly lower temperatures. The evolving gases are essentially water with small amounts of organics.

The dielectric constant and index of the Al_2O_3 films were measured. The film were deposited on Si substrates. The measuring methods were same as for the measurements of ZnO films. The films were annealed at 500°C for 1 hour. The dielectric constant ε_{ins} of Al_2O_3 film in the work is ~9.28. The index was ~1.514.

5.5 Conclusions

The procedure of ZnO film deposited by the sol-gel process, the optical and the electrical properties of ZnO film are all described. We found that the structure and the properties of film depended on the precess of procedure and anneal temperature. Because of the amount of liquid and pyrolysis gases fleeing out of the film in the heat treatment process, which

causes many pores in the film to shrink, with a further increase in temperature pores shrink resulting in a decrease in the thickness and an increase of index. Resistivity of film depends mainly on Zn ion concentration and microstructure of the film.

The SiO_2 and Al_2O_3 films were prepared by the sol-gel process in order to be used as insulator. Their dielectric constants were measured respectively. The dielectric constant of SiO_2 film was ~4.104 and that of Al_2O_3 film was ~9.28.

Chapter 6

TRANSPARENT CONDUCTING FILMS

6.1 Introduction

Transparent conductors have found major applications in a vast number of active and passive electronic and opto-electronic devices such as solar cell windows, charge-coupled imaging devices and electroluminescent devices. Non-stoichiometric and doped films of oxides of indium, tin, cadmium, zinc and their various alloys, deposited by numerous techniques, exhibit high transmittance in the visible spectral region, high reflectance in the IR region and nearly metallic conductivity. The electrical as well as optical properties of these unusual materials can be tailored by controlling the deposition parameters.

The simultaneous occurrence of high optical transparency (more than 80%) in the visible region and low electrical resistivity (about $10^{-3}\Omega\cdot cm$ or less) is not possible in an intrinsic stoichiometric material. Partial transparency and fairly good transparent conductors may be obtained in thin films of variety of metals. The only way to obtain good transparent conductors is to create electron degeneracy in a wide band gap (greater than 3eV) oxide by controllably introducing non-stoichiometry and/or appropriate dopants. These conditions are very conveniently obtained in oxides of tin, indium, zinc, cadmium and their alloys in thin film form, and are prepared by a number of deposition techniques. Transparent conducting CdO films prepared by the thermal oxidation of sputtered cadmium reported firstly by Badeker[115] in 1907. Because of applications of transparent conductors the technological interest in them has grown tremendously. Numerous techniques for depositing several very useful transparent conducting oxides, notably antimony-doped tin oxide (ATO) or fluorine-doped tin oxide (FTO), tin-doped indium oxide (ITO) and aluminium-doped zinc oxide have been developed, some at a large-scale production level. A host of electronic, opto-electronic and mechanical applications based on transparent conductors have emerged. These thin film devices include the following: resistors; transparent heating elements for aircraft and automobile windows; antistatic coatings for instrument windows; heat-reflecting mirrors for glass windows and incandescent bulbs; anti-reflection coatings; selective absorber components in solar heat collector; gas sensors; electrodes for liquid crystal, electrochromic and ferroelectric photoconductor storage and display devices; solar cells; semiconductor /insulator /semiconductor (SIS) heterojunctions; protective and wear-resistant coatings for

glass containers.

With increasing sophistication of the active and passive devices based on transparent conductors, the need for improved electrical and optical properties and their understanding has been recognized for some time. In the last several years, the deposition techniques have undergone many changes. An understanding of the solid state physics of these materials has begun to emerge. As a result, it is now possible to tailor make various transparent conductors with a range of properties. A maximum solar transmittance of about 85%-95% with a minimum resistivity as low as about 7×10^{-5} $\Omega\cdot$cm is achievable, and still further improvements in the these parameters are expected to take transparent conductors into the semimetal regime.

The structural, electrical and optical properties of transparent conductors exhibit a marked scatter. The disposition conditions influence on the properties of these films. Resistivity and transmittance of films are important parameters. The phenomena of conductivity and transparency are quite strongly interrelated, leading to a certain trade-off between the two. The exact nature of this interdependence is dictated by the influence of various deposition parameters on electro-optical properties of these films.

In the following, a brief description of the properties of prominent oxide films will be presented.

6.1.1 Tin Oxide

A. Undoped tin oxide films

SnO_2 is the first transparent conductor to have received significant commercialization. A vast body of literature exists on the preparation, defect structure and electrical and optical properties of SnO_2 films. Under optimum conditions of deposition undoped SnO_2 films are generally polycrystalline (grain size, about 200-300Å) and retain the tetragonal rutile structure of bulk SnO_2. The n-type conductivity of undoped SnO_2 is primarily due to its non-stoichiometry. SnO_2 films are degenerate semiconductors, typically with carrier concentration $N\approx10^{19}$-10^{20} cm^{-3}, a mobility $\mu\approx$5-30 cm^2 V^{-1}s^{-1} and a resistivity $\varrho\approx10^{-3}$-10^{-2} $\Omega\cdot$cm. Shanthi et al.[116] have reported that annealing of SnO_2 films at 400°C in oxidizing or reducing ambient causes a large change in μ while N remains weakly affected. It is concluded that the chemisorption or desorption of oxygen, primarily from the grain boundaries, controls this behaviour and accounts for the lack of thermal stability of the electrical parameters. Pure

SnO_2 films exhibit a direct optical band gap of 3.87-4.3eV. The visible and near-IR transmittance is high (about 80%).

B. Antimony-doped tin oxide films

Doping of SnO_2 with antimony results in a large grain size (about 600Å) with no change in the lattice parameters[117]. Clearly, the dopant is incorporated substitutionally. The doping of SnO_2 with antimony gives rise to a donor level at 35meV[118] The resistivity and transmittance of the films vary with antimony concentrations. The resistivity decrease initially with increasing dopant concentration but starts increasing at still higher concentration. This is attributed to impurity scattering[119], precipitation of Sb_2O_5 or an increased disorder[120]. The optimum antimony concentration ranges between 0.3 and 3 mol.% [121],[122]. Typically, SnO_2:Sb films have $N \geq 10^{20} cm^{-3}$, $\mu \approx 15$-$30\ cm^2V^{-3}s^{-1}$ and $\varrho \approx 10^{-3} \Omega \cdot cm$ with T≈80%-90%. Randhawa et al.[123] have reported the best results for these films($\varrho \approx 5 \times 10^{-4} \Omega \cdot cm$ T≈95%) prepared by ARE.

C. Fluorine-doped tin oxide films

Fluorine-doped SnO_2 films are polycrystalline(grain size, about 400Å[124]) and retain the rutile structure with no change in lattice parameter[125]. These films exhibit strong orientation effects, with (200) planes parallel to the substrate.

The resistivity and transmittance of the films depends on fluorine concentration. These films generally have higher mobilities (about 25-50 $cm^2V^{-1}s^{-1}$) than SnO_2 or ATO films. N is typically about 5×10^{20}-$10^{21} cm^{-3}$ with $\varrho \approx 4.6 \times 10^{-4} \Omega \cdot cm$ and T≈80%-90%.

Numerous other dopants have been tried in SnO_2 films. These include phosphors, arsenic, indium, thallium, tellurium, tungsten, chlorine, bromine and iodine. These dopants do not affect the conductivity significantly, which is not entirely unexpected.

6.1.2 Indium Oxide

A. Undoped indium oxide films

Undoped indium oxide films are generally polycrystalline. Muller[126] has reported a typical grain size of about 100Å for reactively sputtered films. The superiority of In_2O_3 over SnO_2 films as transparent conductors is largely due to the higher mobility In_2O_3. In_2O_3 films prepared by various techniques have mobilities in the range 10-75 $cm^2V^{-1}s^{-1}$, with $N \approx 10^{19}$-$10^{20} cm^{-3}$, leading to $\varrho \geq 10^{-3} \Omega \cdot cm$. Better results are obtained after a reducing heat treatment which improves the conductivity[127]. A subsequent oxidizing heat treatment has found

to result in a decrease in conductivity.

In_2O_3 films exhibit a direct optical band gap which lies between 3.55 and 3.75eV and which has shown to increase with increasing carrier concentration[128]. The optical transmission in the visible and near-IR regions is about 75%-90%.

B. Tin-doped indium oxide films

ITO films retain the bulk structure of In_2O_3 but exhibit a slight increase in the lattice constant (10.118Å<a<10.31Å) which depends on the deposition parameters. The grain size ranges typically between 400Å and 600Å.

The resistivity of these films decreases initially with increasing tin concentration but starts increasing at still higher concentration, thus showing a behaviour similar to that of ATO films. These films have $N \approx 10^{21} cm^{-3}$ and μ lies in the range $15\text{-}40 cm^2 V^{-1} s^{-1}$ leading to ϱ in the range from 7×10^{-5} to $5\times10^{-4} \Omega \cdot cm$.

The direct optical band gap of ITO films is generally greater than 3.75 and exhibits an $N^{2/3}$ dependence owing to the Moss-Burstein shift[129]. The optical transmission in the visible and near-IR regions is high, reflection (average visible reflectance, about 10%) being the primary source of photon loss. The absorption in the visible region is typically about 2%.

Other dopants which have been studied for In_2O_3 films include titanium, antimony, lead and fluorine.

6.1.3 Zinc Oxide

ZnO is a technologically important material. The electrical and optical properties of pure and also doped bulk ZnO have been studied[130] extensively and reviewed[131]. Thin films of ZnO have been prepared by various techniques. ZnO has one of the largest electromechanical coupling coefficients of all non-ferroelectric materials, resulting in extensive use as transducers in surface acoustic wave devices and microwave delay lines.

A. Undoped zinc oxide films

ZnO films retain the bulk wurtzite structure and are composed of columnar crystallites with grain sizes in the range 50-300Å. Sputtered ZnO films have a strong c axis orientation, perpendicular or parallel to the substrate depending mainly on the substrate material, while the degree of preferred orientation depends on the deposition parameters. Films prepared by CVD and spray pyrolysis also exhibit a preferred c axis orientation.

Undoped ZnO films deposited by Webb et al.[132] using r.f. magnetron sputtering in an

$Ar\text{-}H_2$ mixture at $T_s \approx 75°C$ had a typical as-deposited resistivity of about $2\times10^{-3}\Omega\cdot cm$ ($N\approx10^{20}cm^{-3}$; $\mu\approx8cm^2V^{-1}s^{-1}$) and $T\approx90\%$. Significantly higher mobilities have been obtained for ZnO films deposited by ARE[133], leading to $\varrho\approx6\times10^{-4}\text{-}10^{-3}\Omega\cdot cm$ and $T\approx90\%$. CVD [134],[135] and sprayed pyrolysis have also been used to deposit transparent conducting ZnO films. The sprayed films, after annealing at about 400°C in an H_2 ambient[136] or vacuum[137], have $\varrho\approx10^{-3}\text{-}10^{-2}\Omega\cdot cm$ ($N\approx10^{18}\text{-}10^{19}cm^{-3}$; $\mu\approx20cm^2V^{-1}s^{-1}$) and $T\approx80\%\text{-}90\%$.

Oxygen chemisorption effects at the surface and grain boundaries of polycrystalline ZnO films affect the electrical parameters significantly[138].

B. Indium- and aluminium-doped zinc oxide films

ZnO films doped with trivalent cations such as indium and aluminium have been spray pyrolysed. Doping has been achieved by adding $AlCl_3$ and $InCl_3$ to the zinc acetate spray solution. The as-deposited films are polycrystalline (grain size, about 100Å) and retain the wurtzite structure. Whereas undoped ZnO films exhibit a strong preferred orientation with the c axis perpendicular to the substrate, no such orientation effects are observed for indium-doped films. High conductivity and transparency have been achieved in indium- doped films without any post-deposition heat treatment. As-deposited ZnO:In films(thickness, 0.6-0.8μm) with $N\approx5\times10^{20}cm^{-3}$, $\mu\approx15cm^2V^{-1}s^{-1}$, $\varrho\approx8\times10^{-4}\Omega\cdot cm$ and $T\approx80\%$ have been obtained.

There are several other binary and ternary metallic oxides having the potential to become visible transparent conductors such as Bi_2O_3, MoO_3 and so on, but much work must be done on them to decrease resistivity and increase transmittance.

6.2 Deposition of ZnO:Al Films

6.2.1 Introduction

Zinc oxide holds considerable promise as an optical transparent conducting material due to its wide band gap (~3.3eV), its amenability to defect or impurity doping, and other desirable properties such as low cost and non-toxicity[139]. Thin films of transparent conducting zinc oxide have been prepared by a wide variety of techniques, including reactive evaporation [140],[141], RF sputtering, DC and ion beam sputtering[142],[143], [144],[145], [146],[147],[148], chemical vapour deposition [149], [150], [151], [152] and spray pyrolysis [153],[154], [155], [156], [157],[158].

As an n-type semiconductor, the material can be effectively doped with an appropriate donor. Both stoichiometry and dopant impurities affect the electrical and optical characteristics to the point that ZnO can be either a near-insulator or a semi-metal. A potential low cost alternative to tin-doped indium oxide, ZnO films could be used as less expensive transparent electrode material for use as a window layer for solar cell devices and a transparent conducting layer for electroluminescent devices. For practical applications undoped ZnO films are inferior to indium- or tin- based oxide films. However doped films can be made to have very stable electrical and optical properties. The electrical properties of as-deposited films appear to be highly dependent upon the deposition methods, perhaps due to different stoichiometries and oxygen chemisorption on the surface of films and grain boundaries in polycrystalline ZnO films. Although ZnO:Al films can be deposited using many methods, the sol-gel process is simpler and less expensive and has the general advantage of producing high purity, homogeneous films at relatively low temperatures.

This chapter describes the preparation of aluminum-doped ZnO films by the sol-gel process and the optimization of aluminum-doped ZnO to produce highly transparent conductive films by controlling the dopant concentration and by annealing in vacuum.

6.2.2 Experiment Procedure

A solution of ZnO precursor was made by dissolving zinc acetate ($Zn(CH_3CO_2)_2 2H_2O$) in anhydrous ethanol or methanol. Solutions of the solid were prepared in increasing concentrations to establish maximum solubility. Without acid additions the maximum concentration reached was 6 wt.% in ethanol and 12 wt.% in methanol. To achieve aluminum doping, anhydrous aluminum chloride ($AlCl_3$) or aluminum nitrate ($Al(NO_3)_3 9H_2O$) was added to the solution. As various parameters involved in the process are mutually dependent on each other, only the doping concentration was changed. The doping concentration, i.e., aluminum/zinc atomic ratio in percentage (Al/Zn at.%), was varied from 0 to 4.5 at.% in the solution. The films were deposited as prescribed previously. Repeating the process of coating and heating substrates increased the thickness of ZnO:Al films on the substrates. Fig.6-1 presents the flow diagram for ZnO:Al films from preparation of solution to production of coated substrates.

The electrical resistivity and Hall coefficient of the films at room temperature were measured by Van der Pauw methods. A constant current source and electrometer (Keithley 614) having

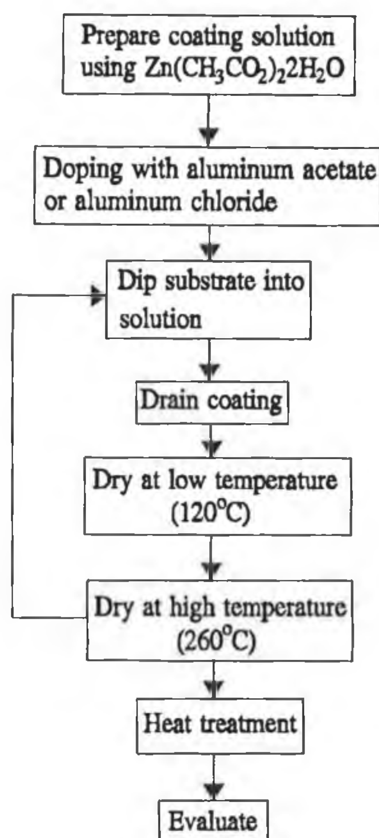

Figure 6-1 Flow diagram of the sol-gel process for depositing ZnO:AL films.

an impedance greater than $5\times10^{13}\Omega$ were used to measure the electrical and galvanomagnetic properties. The visible transmittance was measured using UV-240 and Hewlett Packard 8452A uv-visible recording spectrophotometers, which gave identical results. X-ray diffraction measurements were carried out on a Philips diffractometer using CuK_α (λ=1.542Å) as the source line. The films were treated in air or in a vacuum system at different temperatures.

6.3 Structural Properties of ZnO:Al Films

X-ray diffraction of ZnO and ZnO:Al films deposited by sol-gel process showed the annealed films to be polycrystalline. After annealing in air at 400°C, the films showed evidence of conversion from amorphous to polycrystalline structure with a degree of preferential orientation when a substrate of (100) silicon was used. In this case there was a tendency for the c-axis to be perpendicular to the substrate. Further annealing in vacuum led to no further increase in crystallinity or degree of orientation. Fig.6-2 shows the X-ray diffractograms of ZnO and ZnO:Al films.

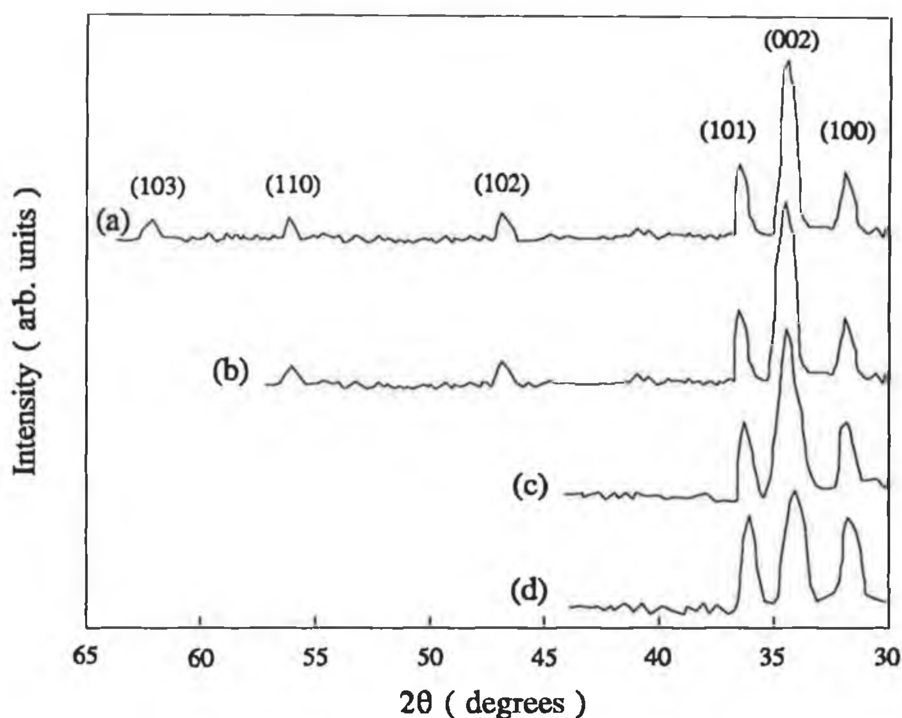

Figure 6-2 X-ray diffractograms for undoped air-annealed ZnO films (a) before and (b) after annealing in vacuum and ZnO:Al films with Al/Zn 0.8 at.% (c) before and (d) after annealing in vacuum.

6.4 Optical Properties of ZnO:Al Films

6.4.1 Optical Theory

A. Introduction

Zinc oxide and zinc-oxide-based transparent conductive films have recently gained much attention because they have a number of advantage over the more common indium and tin-based oxide films:

(1) consist of cheap and abundant elements, which may be contrasted with the more expensive Indium containing films.

(2) are nontoxic, whereas Cd-containing films have potential health hazards.

(3) are readily produced by sol-gel technology, which is currently preferred for large-scale architectural coatings.

(4) allow tailoring of the ultraviolet absorption, which is possible because the fundamental band gap of ZnO lies just at the end of the luminous spectrum.

The optical properties of Al-doped ZnO films, produced by sol-gel process, are analyzed. The observed band-gap widening can be understood quantitatively from an effective-mass model

for n-typed semiconductors. In principle, the optical band gap can be larger or smaller than the one of the undoped host material. A widening occurs since the lowest states in the conduction band are blocked; this is the well-known Burstein-Moss effect. Band-gap narrowing is associated with different many-body effects on the conduction and valence bands.

B. Optical Properties

The free electrons in the doped films modify some of the film's optical properties. In the infrared, the films behave like metals and have high reflectance. In the visible, however, the film are highly transparent, and their spectra are like those of dielectrics.

Spectral transmittance and reflectance data were used to evaluate the complex dielectric function $\varepsilon=\varepsilon_1+i\varepsilon_2$ for ZnO:Al.

A description of the electromagnetic properties can be achieved by taking the dielectric function to consist of additive susceptibilities according to[159],[160]

$$\varepsilon(\omega)=\varepsilon_1(\omega)+i\varepsilon_2(\omega)=1+\chi^{VE}(\omega)+\chi^{FC}(\omega)+\chi^{PH}(\omega) \qquad \textbf{(6-1)}$$

The susceptibilities are complex and frequency-dependent functions accounting for the effects of valence electrons(VE), free carriers(FC), and polar optical phonons (PH), A separation into parts representing different elementary excitations is useful if the χ's correspond to resonances in well separated frequency regions. χ^{VE} accounts for interband transitions. The resonance lies in the ultraviolet, with a band edge extending somewhat into the luminous range. χ^{FC} represents the free-electron gas, whose associated resonance lies at zero energy. The damping of this resonance leads to the susceptibility being complex to energies which can be as high as in near infrared. χ^{PH} is due to optical photons which couple to the transverse electromagnetic field. The resonances lie in the thermal infrared. From the above it is known that the ε is the function of wavelength λ lighted on the film.

The analysis is done in terms of the optical constants n and k, which are related to ε_1 and ε_2 by

$$\varepsilon_1=n^2+k^2 \qquad \textbf{(6-2)}$$

$$\varepsilon_2=2nk \qquad \textbf{(6-3)}$$

and the absorption coefficient α given by

$$\alpha = \frac{2\pi k}{\lambda} \tag{6-4}$$

C. Theory of Band-Gap Shifts

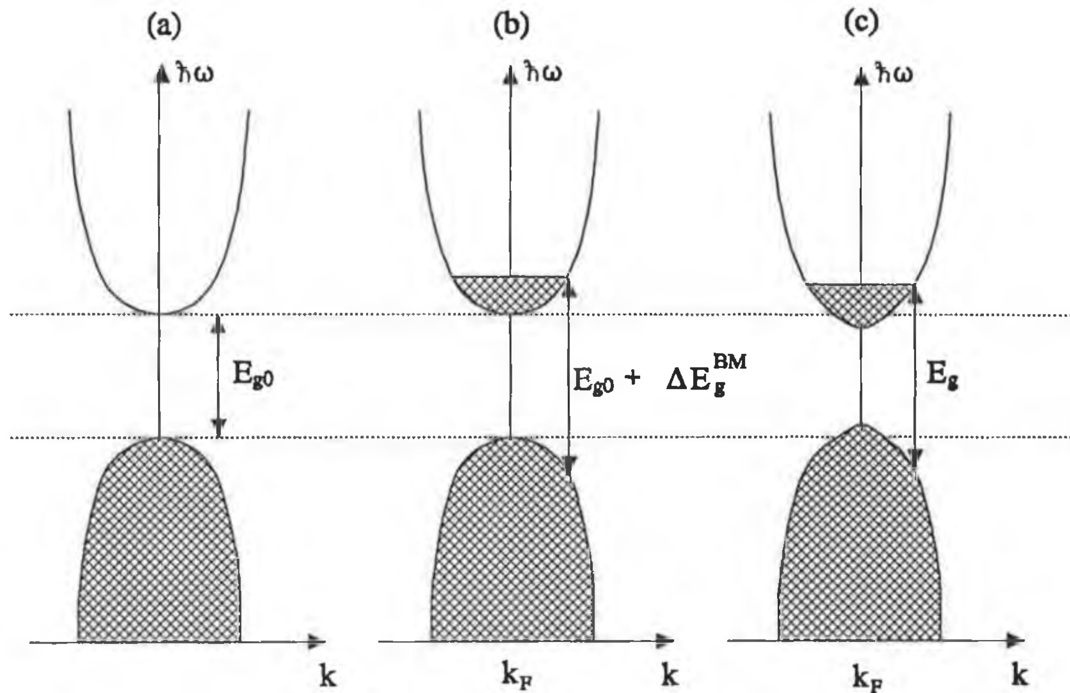

Figure 6-3 Schematic band structure with parabolic conduction and valence bands.

The optical gap is defined as the minimum energy needed to excite an electron from the valence band to the conduction band. In the pure, undoped crystal the optical gap equals the energy separation E_{g0} between the band edges, as illustrated for the case of isotopic and parabolic bands in fig.6-3 (a). In a heavily doped semiconductor, the donor electrons occupy states at the bottom of the conduction band. Since the Pauli principle prevents states from being doubly occupied and optical transitions are vertical, the optical gap is given by the energy different between states with Fermi momentum in the conduction and valence bands. This shown in fig.6-3 (b). The blocking of the low-energy transitions is known as the Burstein-Moss (BM) effect and enhances the optical gap by the energy

$$\Delta E_g^{BM} = \frac{\hbar^2 k_F^2}{2}[\frac{1}{m_e} + \frac{1}{m_h}] \tag{6-5}$$

where k_F is the Fermi wave vector, m_e is the effective mass for electrons in the conduction band, and m_h is the effective mass for holes in valence band. The band-gap widening is counteracted by a narrowing caused by the correlated motion of the charge carriers and by their scattering against ionized impurities. The ensuing effect on the optical gap is given, schematically, in fig.6-3 (c). The rest of this section is devoted mainly to quantitative assessments of band-gap narrowing.

In a nonpolar semiconductor, its electrons avoid each other for two different reasons: Electrons of equal spin avoid each other for statistical reasons, and all electrons -irrespective of relative spin- avoid each other because of Coulomb repulsion. Thus, effectively each electron is surrounded by an exchange and correlation hole which is lowers the energy of the electron, ie., the conduction band is shifted downwards. Furthermore, the electron density will relax around the impurities, which causes a lowering of the electron energies and additional downward shift of the conduction band. This latter shift is nonrigid because the interaction will in general give rise to a distorted band structure and band tailing. The valence band is also shifted. The hole is attracted by the donor electrons and tends to be surrounded by an enhanced electron density. This lowers the energy of the hole. The hole is repelled by the positively charged donor ions and has a tendency to avoid them, which causes a further downward shift of its energy. Thus even less energy is needed to create an electron-hole pair or is released when a pair is annihilated. In other words, the valence band is shifted upwards in energy[161].

In a polar semiconductor, or ionic insulator, there is a displacement of charge from one of the atomic species to the other, and hence the host atoms are charged. The displacement polarization modifies the self-energy shifts caused by many-body interactions. The details of the derivation of these shifts can be found in Ref.[162].

6.4.2 Optical Properties

All films with different doping concentration are highly transparent in the visible region. The free electrons in the doped films modify some of the film optical properties. In the visible, however, the films are highly transparent and their spectra are comparable to those of dielectric coatings. As shown in fig.6-4 and fig.6-5 the films have an average transmission of about 90% in the wavelength range of 0.40μm-0.9μm.

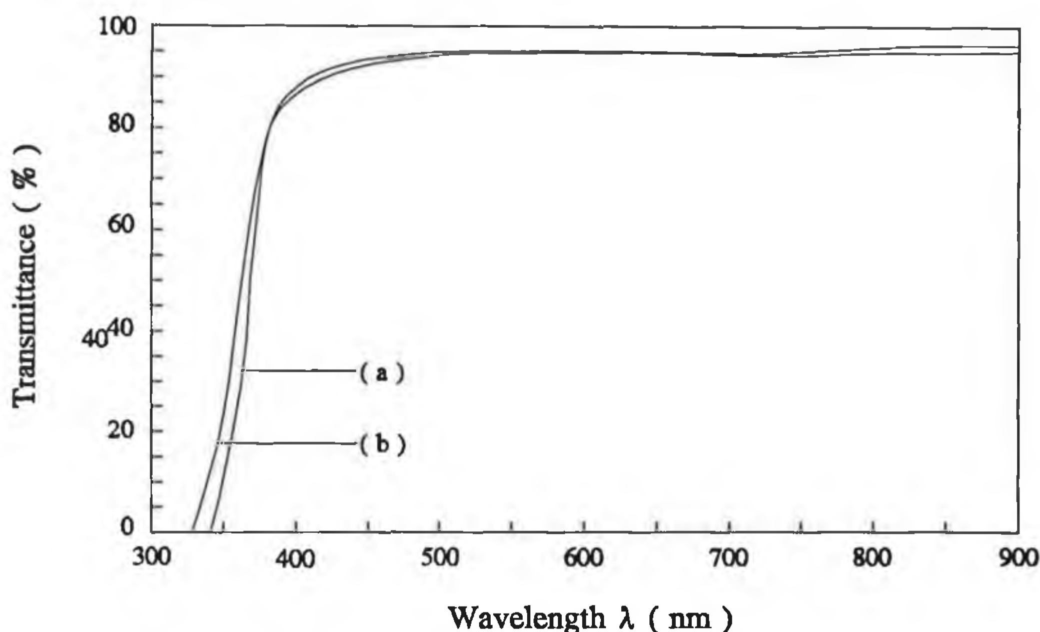

Figure 6-4 Comparison of optical transmission spectra for ZnO:Al films with Al/Zn 0.8 at.% (a) before annealing and (b) after annealing in vacuum.

The transmission spectrum for ZnO:Al films with Al/Zn 0.8 at.% both before and after annealing at 400°C in vacuum are shown in fig.6-4. Oxygen is chemisorbed on the ZnO surface and in the pores of the films as O_2^- by accepting an electron from occupied conduction band states. Heating of the surface leads to the desorption of oxygen with the increase of annealing temperature. From these results, the shift in the absorption edge can be ascribed mainly to the increase in carrier concentration due to the desorption of oxygen and the decomposition of Al_2O_3 leading to an increase of Al donors.

The spectra of undoped and aluminum doped ZnO films annealed in air at 400°C, then annealed in vacuum at 400°C are shown in fig.6-5. The shift of the absorption edge to a shorter wavelength was observed for films of increasing aluminum concentration which results in the increase of carrier concentration. A description of absorption edge shift as function of carrier density is given by Roth et al.[163]. Their findings show that the band-gap increase with increasing carrier concentration. Only part of the shift is explained by the Moss-Burstein theory [164],[165],[166], which relates the band-gap shift to the carrier concentration.

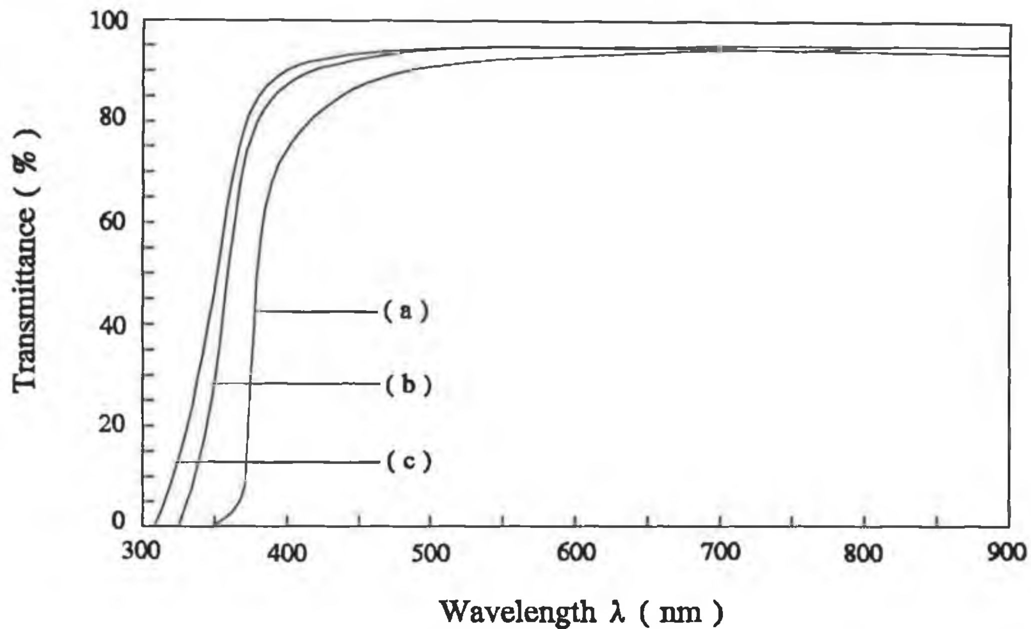

Figure 6-5 Comparison of optical transmission spectra for undoped ZnO film and ZnO:Al films with Al/Zn (b) 0.8 at.% and (c) 1.3 at.%.

6.5 Electrical Properties of ZnO:Al Films

6.5.1 Electrical Theory

In this section my studies on the electrical conductivity and Hall mobility of aluminium doped ZnO films prepared by sol-gel technique are reported. The films were heat treated in air and in vacuum.

It is known that the conductivity of semiconductor σ is given by

$$\sigma = q(\mu_n n + \mu_p p) \quad \text{(6-6)}$$

For reasonable extrinsic n-type semiconductors n>p, and electron mobility is

$$\mu_n = \frac{\sigma}{qn} \quad \text{(6-7)}$$

or in term of the resistivity ρ the majority carrier or conductivity mobility is

$$\mu_n = \frac{1}{qn\rho} \quad \text{(6-8)}$$

It is obvious that resistivity depends on carrier mobility and carrier concentration. Increasing

carrier mobility and/or carrier concentration leads to the decreasing of resistivity but increasing carrier concentration induces ionized impurity scattering, which influences carrier mobility. Microstructure of films also leads to changes of electrical properties. In polycrystalline semiconductors the effect between surface of grains is similar to barrier of diode so size and structure of grains also is one of the causes of modifying electrical properties. The absorption of oxygen and a form of impurity oxide between the surface of grains and the scattering on the grains lead to decreasing resistivity.

Carrier concentration of films increases with doping concentration except at higher doping concentrations, where it tends towards a saturation of carrier concentration because of limited solution of dopant in films. Such behaviour is expected as a result of substitutional doping of high valence impurity ions (Al^{3+}) at the host (Zn^{2+}) site creating one extra free carrier. As the doping level is increased, more dopant atoms occupy lattice sites of zinc atoms, and this results in more charge carriers (electrons). This process continues till the added dopant atoms find the available (Zn) lattice sites in the host semiconductor. However, after a certain level of doping, (Zn) lattice sites cannot be occupied by the dopant atoms. Instead, the dopant atoms occupy interstitial position in the form of oxide (Al_2O_3). Hence, the dopant atoms become ineffective as donors.

Mobility behaviour with dopant concentration of such polycrystalline extrinsic semiconductors is governed mainly by ionized impurity scattering and grain boundary scattering.

$$\frac{1}{\mu} = \frac{1}{\mu_{gb}} + \frac{1}{\mu_{IS}} \qquad (6\text{-}9)$$

Where μ is resultant mobility, μ_{gb} is mobility due to grain boundary scattering, μ_{IS} mobility due to ionized impurity scattering. The decrease in the carrier mobility can be due to:

1. poor structure of the film as reflected in the decrease of texture coefficient.
2. very slow increase followed by saturation in crystallite size which will halt the improvement in the mobility.
3. increase in the contribution of ionic impurity scattering.
4. segregation of Al dopant atoms at the grain boundaries in the form of Al_2O_3, which will increase the grain boundary barrier.

6.5.2 Electrical Properties

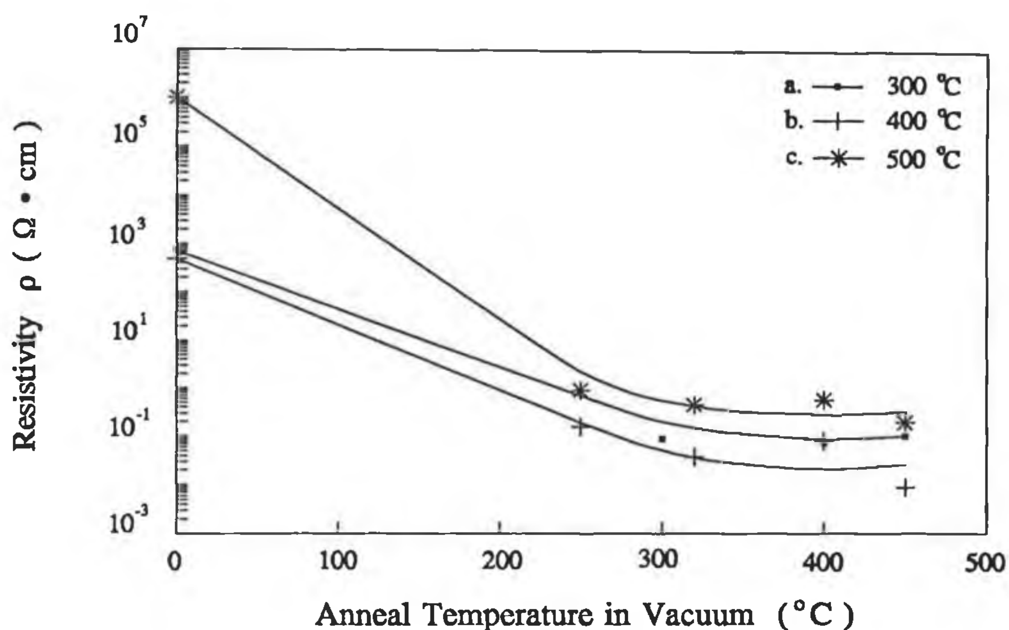

Figure 6-6 Resistivity dependence on anneal temperature in vacuum for ZnO:Al films with Al/Zn 1.5 at.%. The films were initially annealed at different temperature.

In the application of ZnO:Al films as a transparent conductor, especially in solid-state display devices, the electrical properties of the films must be the important factor. Therefore, the emphasis in the studies of transparent conducting films has been concentrated mainly on how to prepare low resistivity films.

To study the effect of annealing temperature and Al concentration on optical and electrical properties, a series of films with different Al/Zn atomic ratios were fabricated and annealed at various temperature. Fig.6-6 shows resistivities of the films with Al/Zn 1.5 at.% which were annealed initially at 300°C, 400°C and 500°C in air respectively, then annealed in vacuum. The results show that the film annealed at 400°C in air has the lowest resistivity. Fig.6-7 shows resistivities of the films with different Al concentration annealed in vacuum. The resistivities generally are lower with annealing at about 400°C. Fig.6-8 shows resistivities of the films with various Al concentration annealed at 400°C in air, at 250°C and at 400°C in vacuum respectively. The film with Al/Zn 0.8 at.% annealed at about 400°C exhibits the lowest resistivity ($\sim 7\times10^{-4}$ Ω·cm).

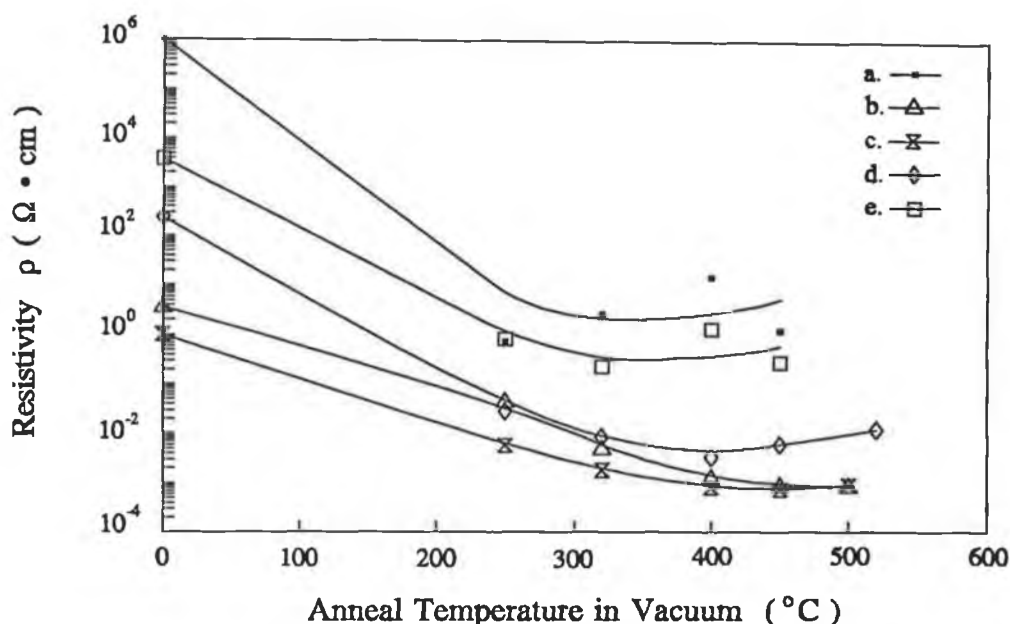

Figure 6-7 Resistivity dependence on anneal temperature in vacuum for the films with Al/Zn (a)0.0 at%, (b) 0.4 at.%, (c) 0.8 at.%, (d) 1.3 at.% and (e) 4.5 at.%.

The resistivity (ρ) is proportional to the reciprocal of the product of carrier concentration (n) and mobility (μ). Therefore, the decrease in resistivity during annealing in vacuum is attributed to an increase in n and/or μ resulting from an increase in donors and/or a decrease in scattering centres associated with the decomposition of Al_2O_3 and substitution of Al for Zn at the lattice site, and chemisorbed oxygen moving from the film surface, pores and grain boundaries.

Fig.6-9 shows that resistivity (ρ), carrier concentration (n) and Hall mobility (μ) of the film with Al/Zn 0.8 at.% depend upon anneal temperature in vacuum. The resistivity decreases with anneal temperature to 450°C and increases slightly 450-500°C. Carrier concentration increases largely to saturation. Hall mobility decreases slightly with temperature. The chemisorption of oxygen and the non-substitution of some Al^{3+} for Zn^{2+} sites result in low carrier concentration before heat treatment in vacuum. The chemisorption of acceptor oxygen on the ZnO:Al surface, in the pores of the film and between grain boundaries forms an electronic depletion layer which acts as a surface potential barrier and causes low mobility (μ). So we consider that the decrease of resistivity (ρ) during annealing in vacuum results from a change of carrier concentration (n) and mobility (μ) from decomposition of Al_2O_3 and

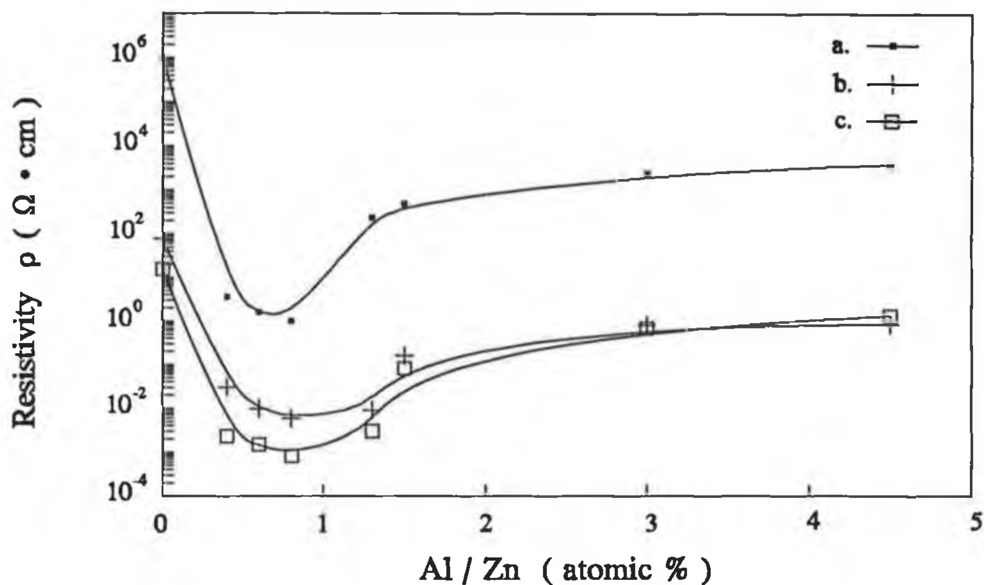

Figure 6-8 Relation between resistivity and Al concentration. The films were annealed at (a) 400°C in air, then at (b) 250°C and at (c) 400°C in vacuum respectively.

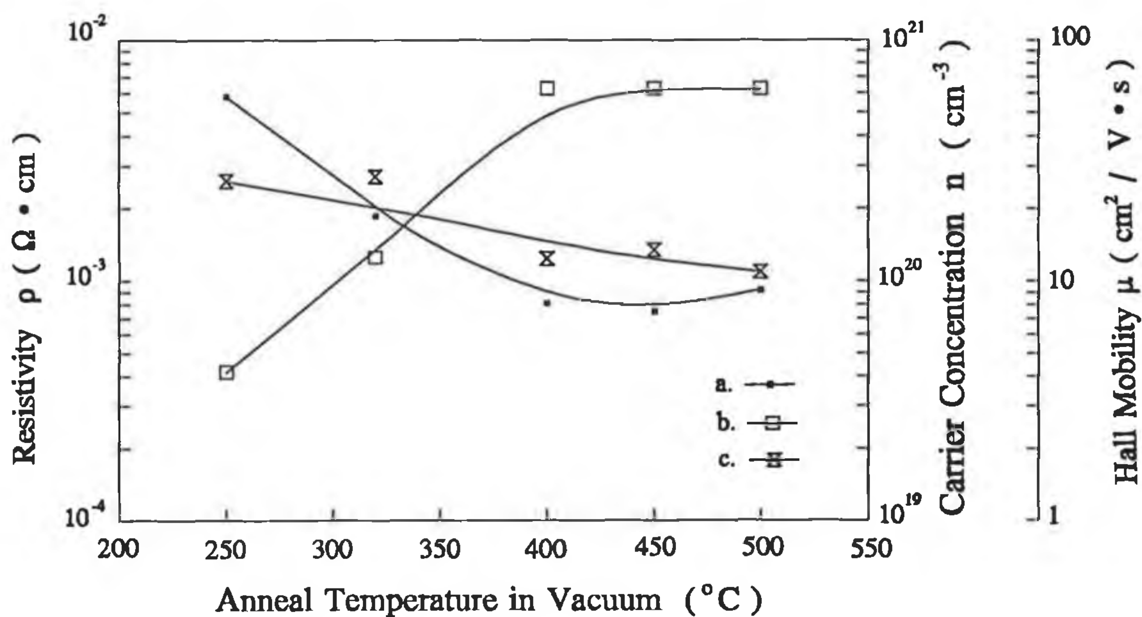

Figure 6-9 (a) Resistivity, (b) carrier concentration and (c) Hall mobility as a function of anneal temperature in vacuum for ZnO:Al film with Al/Zn 0.8 at.%.

desorption of oxygen from the ZnO:Al surface, pores and grain boundaries.

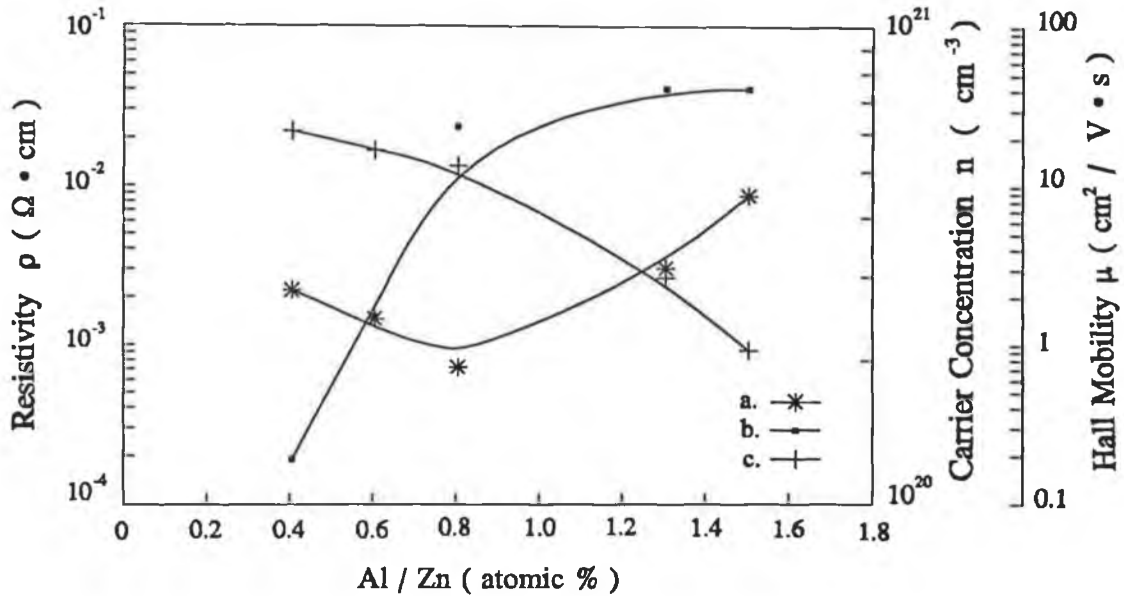

Figure 6-10 (a) Resistivity, (b) carrier concentration and (c) Hall mobility as a function of Al/Zn at.% ratio for ZnO:Al films annealed at 400°C in vacuum.

The relationships between resistivity (ϱ), carrier concentration (n), Hall mobility (μ) and Al concentration are shown in fig.6-10. The carrier concentration (n) of the film was found to increase with doping concentration except at higher doping concentration, where a tendency towards saturation was observed. Such behaviour was expected as a result of substitutional doping of Al^{3+} at the Zn^{2+} site creating one extra free carrier in the process. As the doping level is increased, more dopant atoms occupy lattice sites of zinc atoms, and this results in more charge carriers. However, after a certain level of doping, no more zinc sites can be occupied by dopant atoms because of the limited solubility of Al in the ZnO crystallites. The ionic radius of aluminum is smaller than that of zinc and therefore excess aluminum may occupy interstitial positions as suggested by Cossement and Streydio[167] leading to distortion of the crystal structure. High doping concentrations will therefore lead to ionized impurity scattering from the substitutional donors and also scattering from the interstitials. The aluminum atoms may also segregate to the grain boundaries in the form of Al_2O_3 which will increase the grain boundary barrier. Thus the doping concentration reaches a maximum when the substitutional doping of the zinc oxide by aluminum is maximum whereas the

mobility will continue to fall as more scattering and grain boundary barrier effects occur. The destruction of the films under treatment at high temperatures also causes the decrease of mobility and the increase of resistivity.

From the work of H. Kawamoto et al.[168] it is suggested that the decrease of stivity when annealed below 400°C was due to the formation of oxygen vacancies, whereas the increase at 400°C was mainly due to Al donors. After heat treatment at 400°C, the XPS feature occurring between those of Al_2O_3 (74.70eV) and Al (72.65eV) shifted and new peaks appeared which were attributed to Al_2O and AlO. Therefore the authors concluded that Al atoms substitute for Zn atoms in ZnO:Al films after heat treatment and they should act as Al donors.

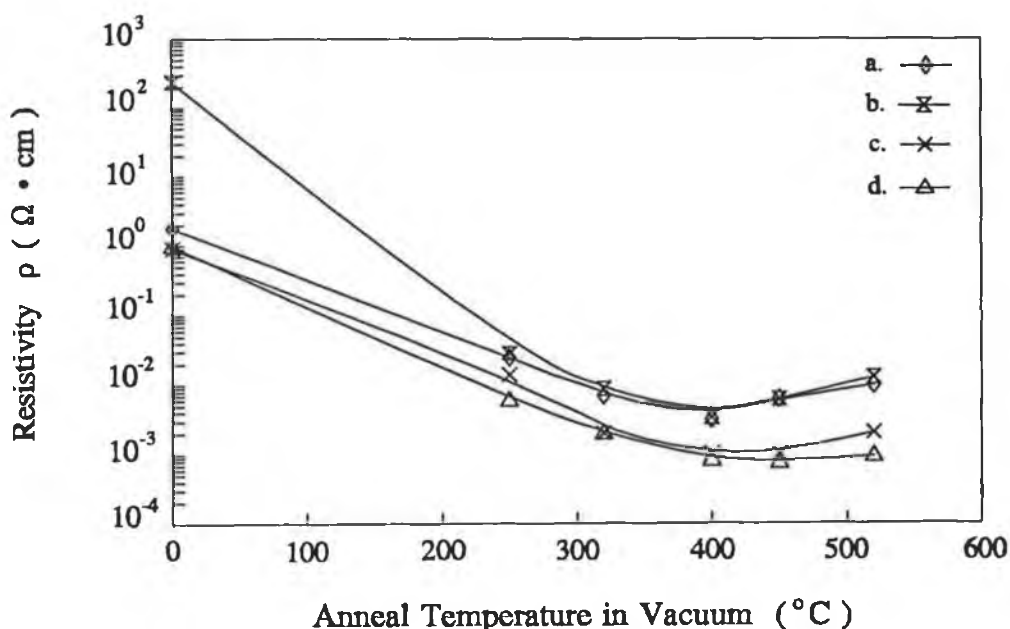

Figure 6-11 Comparison of resistivity for ZnO:Al films with Al/Zn (a) and (b) 1.3 at.% and (c) and (d) 0.8 at.% using aluminum nitrate and aluminum chloride as dopants respectively.

Aluminum chloride ($AlCl_3$) hydrolyses easily, therefore, aluminum nitrate ($Al(NO_3)_3 9H_2O$) which is more chemically inert and less expensive was selected as a dopant. Fig.6-11 shows that the resistivities of the films with Al/Zn 0.8 at.% and 1.3 at.% prepared using aluminum chloride and aluminum nitrate as dopant show very similar behaviour after annealing at 400°C in vacuum.

6.6 Conclusions

Highly transparent and conductive ZnO:Al films have been successfully deposited from zinc acetate and aluminum chloride or aluminum nitrate by the sol-gel process. The techniques developed for production of ZnO:Al films are relatively inexpensive and simple to implement and consequently should be amenable to large area production. It was found that the electrical properties such resistivity (ϱ), carrier concentration (n) and Hall mobility (μ), and optical properties such as transmittance and optical band-gap, were closely related to the annealing temperature in air and in vacuum and the aluminum concentration. The important results of the study so far can summarized as follows:

1. ZnO:Al transparent conducting films with transmittance above 90% and resistivity of about $(7\text{-}10)\times10^{-4}$ $\Omega\cdot$cm can be easily obtained.
2. Transparent conducting ZnO:Al films can be deposited by an inexpensive sol-gel technique from zinc acetate and aluminum nitrate or aluminum chloride solutions.

Chapter 7

LUMINESCENT FILMS

7.1 ZnS:Mn Phosphor Films

Undoped ZnS and Mn doped ZnS films were prepared by conversion of ZnO and Mn doped ZnO films which were annealed in H_2S. The films were deposited by the sol-gel process which is simpler and inexpensive and has the general advantage of producing thin films with a large area, molecular homogeneity, controllable dopant concentration and purity at relatively low temperatures. ZnS and ZnS:Mn films on silicon or glass substrates were obtained from annealing ZnO and ZnO:Mn films at 400-600°C in the H_2S atmosphere. ZnS films were characterized using scanning electron microscopy, x-ray diffraction, IR spectroscopy and transmittance spectroscopy.

Applications of ZnS and ZnS:Mn films in electroluminescent or cathodoluminescent displays[169],[170] have been attracting more and more attention, and ZnS films have been used as multilayer dielectric filters[171],[172] because of a large direct band (~3.6 eV) in the near-UV region. ZnS shows transparency from the mid-IR through the visible region, hence films may also be of use in optical phase modulation, IR antireflection coatings, light guiding in integrated optics[173],[174] and optical windows in the visible region, 3-5 μm and 8-12 μm[175].

Thin films of zinc sulphide have been prepared by a wide variety of techniques, including reactive evaporation [176], [177], RF sputtering, DC and ion beam sputtering [178],[179], chemical vapour deposition [180], [181], [182], [183], atomic layer epitaxy [184], dipping [185],[186], [187] and spray pyrolysis [188]. The above methods usually required complex equipment or vacuum condition. In contrast, the method of conversion of ZnO films is very much simpler and less expensive and yields large area, pure and homogeneous zinc sulphide films with controllable dopant concentration zinc sulphide films.

In this chapter, experimental results of ZnS and ZnS:Mn films produced by this method are described. The characterizations of polycrystalline ZnS films are performed by (scanning electron micrographs or by scanning tunnelling microscopic images), EDX, x-ray diffraction, ellipsometry, IR spectroscopy and UV-visible spectroscopy measurements.

7.1.1 Deposition of ZnS:Mn Films

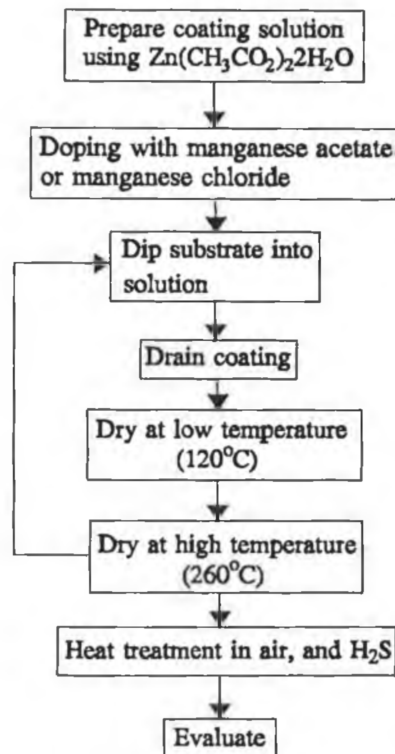

Figure 7-1 Flow chart of depositing ZnS:Mn films using the sol-gel process and conversion of ZnO:Mn film with H_2S.

A solution of ZnO precursor was made by dissolving zinc acetate ($Zn(CH_3CO_2)_2 2H_2O$) in anhydrous ethanol or methanol as described in Ch.5. To achieve manganese doping, anhydrous manganese chloride ($MnCl_2$) or manganese acetate ($Mn(CH_3CO_2)_2 4H_2O$) was added to the solution. The doping concentration, i.e., manganese/zinc atomic ratio in percentage (Mn/Zn at.%), was varied from 0 to 7 at.% in the solution.

Film deposition was carried out as described previously. Thicker films need multiple coatings. After coating, the substrates were loaded carefully into an electrically heated furnace, where they were heated in circulating air to the desired temperature at a rate of greater than 10°C min^{-1}. Repeating the above process of coating and heating substrates increased the thickness of ZnO:Mn films on the substrates. Fig.7-1 presents the flow diagram for ZnS:Mn films from preparation of solution to production of coated substrates.

Zinc oxide or zinc oxide doped with manganese films as deposited were annealed in a mixture of hydrogen sulphide, hydrogen and nitrogen (H_2S:H_2:N_2=10:1:9) in a horizontal tube furnace. The flow rate of the gas mixture was 40 cc min^{-1}. The temperature of the furnace was raised from room temperature to 400°C, 500°C, 550°C or 600°C at a rate of 20°C min^{-1}.

The furnace was maintained at the above temperatures for 60 min, 40 min, 30 min and 25 min, and then cooled down slowly in the mixture gas atmosphere. Fig.7-1 presents the flow diagram for ZnS:Mn films from preparation of solution, production of coated substrates to conversion of ZnS:Mn films.

The visible transmittance was measured using a Hewlett Packard 8452A uv-visible recording spectrophotometer. IR spectra at room temperature were obtained on a Perkin-Elmer 580 single beam scanning IR spectrophotometer at an instrumental resolution of 4 cm^{-1}. The measurements were recorded in the transmission mode over the range 198-4000 cm^{-1}. X-ray diffraction measurements were carried out on a Philips diffractometer using CuK_α (λ=1.542Å) as the source line. Film thicknesses and refractive index for ZnS were determined from a Rudoph Research AutoEL-III ellipsometry measurements at λ=632.8 nm. The surface topography (morphology) of the films was studied by scanning electron microscopy and scanning tunnelling microscopic images. Quantitative energy dispersive analysis of X-ray (EDX) was performed on a Philips SEM505 SEM with an electron beam energy of 20 keV. Spectra were analyzed on the SW 9100 system, which calculated the k-ratios from stored elemental standards.

7.1.2 Characteristics of ZnS:Mn films

Fig.7-2 shows X-ray diffraction patterns of ZnO films (a) deposited by the sol-gel process and ZnS and ZnS:Mn films (b) by conversion of ZnO and ZnO:Mn films. Analysis has indicated that undoped and lightly Mn-doped films are polycrystals, and are composed of mixed hexagonal and cubic crystallographic phases. Fig.7-2 displays the x-ray diffraction spectra obtained for the films. Diffraction peaks observed include the most intense features at ~28° 2θ which has overlapping contributions from the H (hexagonal) phase (002) at 28.49° 2θ, and the C (cubic) phase (111) at 28.56° 2θ. A second overlapping feature at ~48° 2θ has contributions from H phase (110) at 47.54° and from the C phase (220) at 47.51° 2θ. A third overlapping diffraction feature has the H phase contribution from (112) at 56.40° and the C phase contribution from (311) at 56.29° 2θ. Other H phase diffraction features from (100), (101), (102) and (103) appear at 26.9°, 30.5°, 39.62° and 51.8°, respectively, as shown in fig.7-2. No preferred crystallographic orientation is indicated by the data.

Uniform films of zinc sulphide, ranging in thickness from 0.1 to 1.0 μm, were readily prepared on silicon and glass substrates. The films adhered well to the two substrates. Film

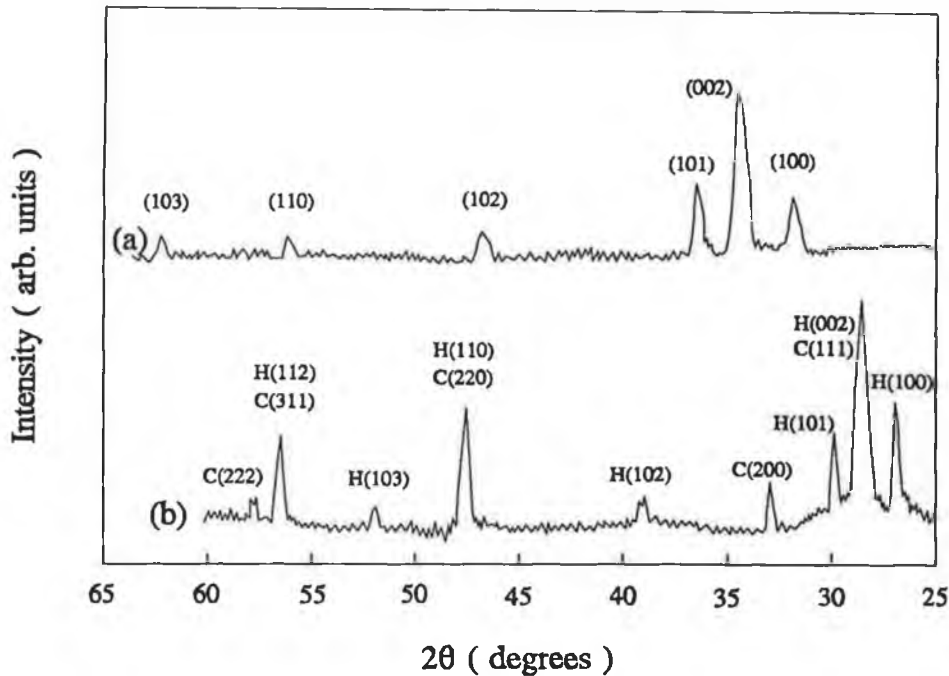

Figure 7-2 X-ray diffractograms for ZnO films (a) and ZnS films (b), which were annealed by sulphidation of deposited ZnO at 500°C in H_2S.

thicknesses and refractive indices for undoped ZnS and Mn-doped ZnS are determined by Rudoph Research AutoEL-III ellipsometry at λ=632.8 nm. The refractive index n shows variation with Mn doping in the films, ~2.10±0.02 for Mn/Zn 0.0at.%, ~2.13±0.02 for Mn/Zn 0.1 at.%, ~2.17±0.03 for Mn/Zn 0.5 at%, ~2.28±0.04 for Mn/Zn 1.0 at.% and ~2.31±0.03 for Mn/Zn 5.0 at.%. The refractive index n for undoped ZnS films is lower than that for bulk ZnS (n=~2.36 at λ=589.3 nm [189]) and ZnS thin films[190]. However, the value of the refractive index of the undoped ZnS films is close to the value reported by A.K. Arora and A. Mansingh[191]. The lower value of the refractive index is due to a lower density of as-deposited films because of porosity of the films, which is produced by outdiffusion of hydrocarbon groups and liquid during heat treatment. EDX analysis confirmed presence of ZnS with 49.8 atomic percent zinc and 50.2 atomic percent sulphur.

ZnS films are transparent in visible region. As shown in fig.7-3, the films have a maximum transmission of >90% at a wavelength of 0.9μm, but transmittance decreased at shorter wavelengths, particularly with increasing of Mn concentration. Optical transmission spectra of undoped and manganese doped ZnO and ZnS films are shown in fig.7-4. The increase in optical bandgap can also be seen from the cut-off wavelength.

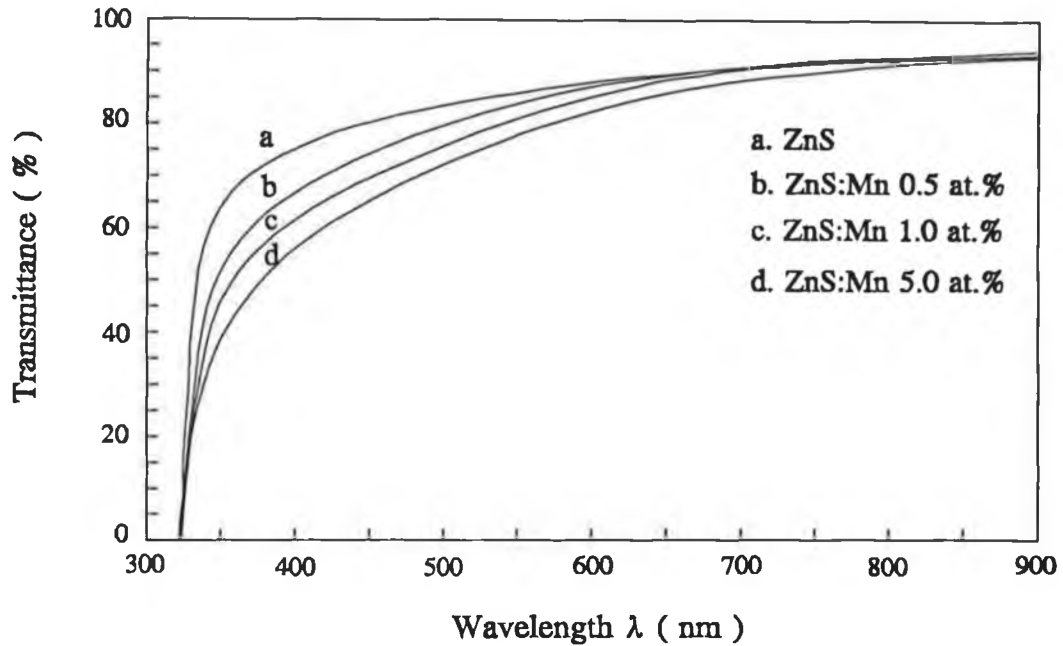

Figure 7-3 Comparison of optical transmission spectra for ZnS:Mn films with Mn/Zn: (a) 0.0 at.%, (b) 0.5 at.%, (c) 1.0 at.% and (d) 5.0 at.%.

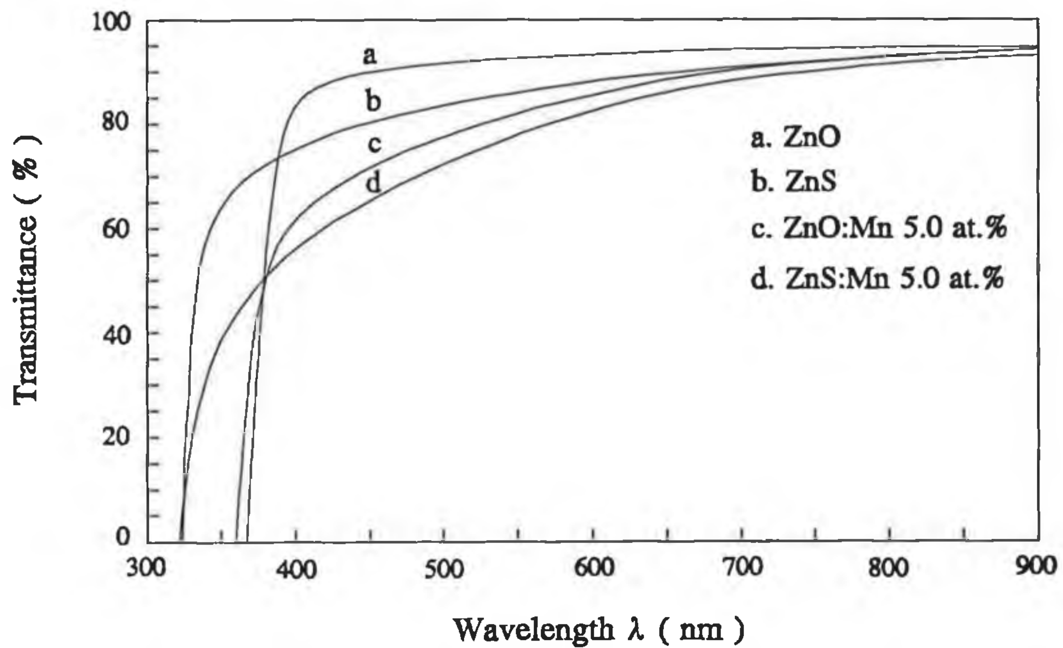

Figure 7-4 Comparison of optical transmission spectra for ZnO:Mn films with Mn/Zn: (a) 0.0 at.% and 5.0 at.% and ZnS:Mn films with Mn/Zn 0.0 at.% and 5.0 at.%.

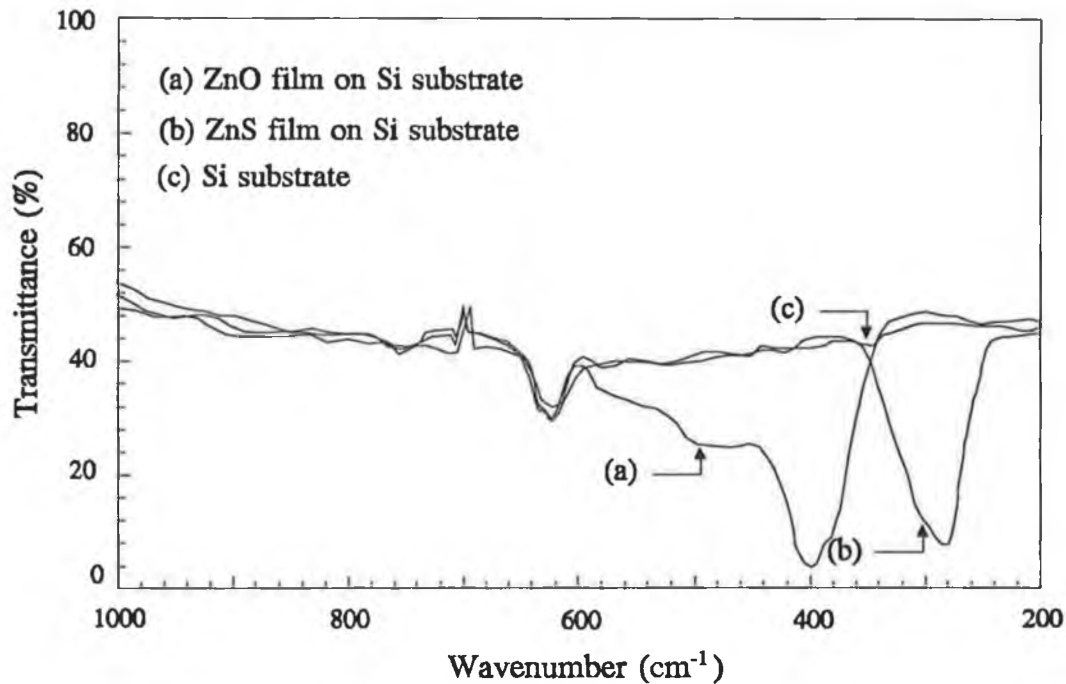

Figure 7-5 IR spectra of (a) ZnO film and (b) ZnS film on Si substrates and (c) Si substrate.

The IR spectra of silicon substrate and zinc oxide and zinc sulphide films on silicon substrates in the range from 198-1000 cm^{-1} are shown in fig.7-5. Zinc oxide films have a broad absorption band with peak at 420 cm^{-1}. After annealing in H_2S the IR peak of zinc oxide disappears and the IR peak of zinc sulphide films emerged at 280 cm^{-1}. Meanwhile, zinc oxide powder was annealed in a H_2S atmosphere. Similar results of IR spectra were obtained from pure zinc sulphide powder (99.9%) and zinc sulphide powder converted from zinc oxide powder. Infrared spectra of zinc sulphide films was also used as a means of confirming the completion of conversion of zinc oxide to zinc sulphide.

7.2 ZnS:Tb Phosphor Films

The best investigated rare earth dopant of ZnS certainly is Tb^{3+}. There are no reports about principally differing behaviours of other lanthanides. Mostly the rare earths have been added during deposition in the form of LnF_3. But more complex compounds and also metallic rare earths have been used. Many discussions about the possible complex centres developing either during deposition, during annealing in the preparation process, and/or during operation did not come to conclusive statements until now. The situation is very complicated by the

poor solubility of the 'large' ions, which need also a charge compensation, not to act as donors. The ZnS thin films doped with Tb^{3+} ion show efficient electroluminescence. Recently, the model of the Tb-F and Tb-OF complex centre was proposed as more efficient luminescent centre than the TbF_3 molecular centre.

For the Tb dopant, the situation is not so simple as for Mn. The Tb^{3+} ion is exited by impact of the kinetic electrons either in the $^5D_3$ or $^5D_4$ level. But the cross relaxation between an excited Tb^{3+} ion and another non excited Tb^{3+} ion is fast. Another fast relaxation process by phonons can also lead the Tb^{3+} excited from the $^5D_3$ level to the $^5D_4$. Therefore, at the end of the pulse, quite all the Tb^{3+} excited ions are in the $^5D_4$ excited state. The peak brightness of the $^5D_4$-->$^7F_4$ emission is at 545nm.

When the dopant content is increased, the sharp B(V) curves shift to higher voltage. The I_j/I_{max} ratio for the $^5D_4$-^7F_j band (j=3,4,5,6) did not depend on the applied voltage[192]. Certainly the ZnS lattice is disturbed by the TbF_3 dopant, in contrast to the Mn case. Therefore, the acceleration process of the carriers is affected by this dopant. But another mechanism can modify the acceleration process for high TbF_3 content, the active layer cannot be considered anymore as a semiconductor with the properties of ZnS. Until now, this aspect has not been investigated.

There are three reasons for concentration quenching in EL thin film devices doped with rare ions. When rare earth ion are introduced into ZnS, the lattice periodic field will be destroyed. (1) Some killers will be formed and lead to non-radiative energy transfer from RE ions to them. (2) The increase of scattering centre will result in the decrease of mean free path of hot electron and then the decrease of emission intensity because of the ionic radius of the RE ions. (3) The distance between RE ions will be decreased with increasing concentration. The interaction between them will result in energy transfer, i.e., cross relaxation.

7.2.1 Deposition of ZnS:Tb^{3+} Films

Fig.7-6 shows the flow diagram of depositing ZnS:Tb films. The process is similar to the process of depositing ZnS:Mn films. A solution of ZnO precursor was made by dissolving zinc acetate ($Zn(CH_3CO_2)_2 2H_2O$) in anhydrous ethanol. Solutions of the solid were prepared in increasing concentrations to establish maximum solubility. To achieve terbium doping, terbium acetate ($Tb(CH_3CO_2)_3$) was added to the solution. The doping concentration, i.e.,

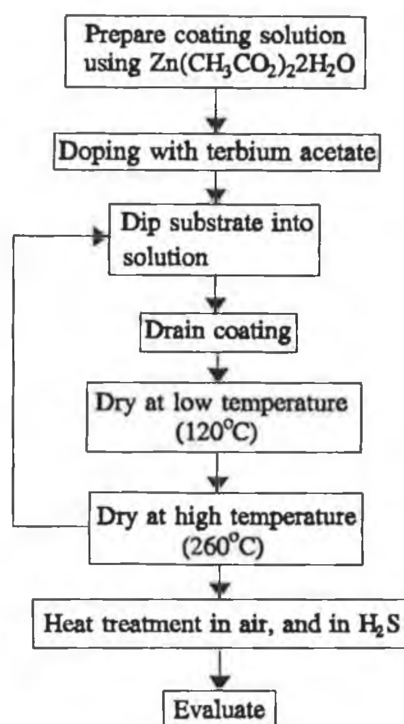

Figure 7-6 Flow chart of the sol-gel process for depositing ZnS:Tb films.

Terbium/zinc atomic ratio in percentage (Tb/Zn at.%), was varied from 0 to 4 at.% in the solution. The films were deposited as previously described.

Zinc oxide or zinc oxide doped with terbium films as deposited were annealed in a mixture of hydrogen sulphide, hydrogen and nitrogen (H_2S:H_2:N_2=10:1:9) in a horizontal tube furnace. The flow rate of the gas mixture was 40 cc min^{-1}. The temperature of the furnace was raised from room temperature to needed temperature at rate of 10°C min^{-1}. The furnace was maintained at the 500 °C for 60 min, cooled down slowly in the mixture gas atmosphere.

7.3 Conclusions

Thin polycrystalline ZnS:Mn films were grown on Si and glass substrates by the sol-gel process and conversion of ZnO:Mn with heat treatment in H_2S. Uniform films were obtained and the thickness of the films could be controlled in sol-gel process. The conversion of ZnO:Mn to ZnS:Mn depends on the time and the temperature of annealing in H_2S. Through analysis of x-ray diffraction, IR, and EDAX it is confirmed that ZnO:Mn films convert into ZnS:Mn films. X-ray diffraction analysis has indicated that undoped and lightly Mn-doped ZnS films are polycrystal orientated preferentially, and are composed of mixed hexagonal and cubic crystallographic phases. Transmittances and indices of films of ZnS doped with various

levels of manganese have been measured.

ZnS:Tb films were deposited by the sol-gel process and conversion of ZnO:Tb with H_2S. Zinc acetate ($Zn(CH_3CO_2)_2 2H_2O$) was used as the precursor and terbium acetate ($Tb(CH_3CO_2)_3$) was added to the solution as dopant. The doping content, i.e., terbium/zinc atomic ratio in percentage (Tb/Zn at.%), was varied from 0 to 4 at.% in the solution. The deposited ZnO:Tb films were annealed in a mixture of hydrogen sulphide, hydrogen and nitrogen so that they were converted into ZnS:Tb films.

Chapter 8

ELECTROLUMINESCENT DISPLAYS

8.1 Introduction

Thin film electroluminescent devices have been considered to be promising for large panel displays because of their many advantages. They have high brightness, long life, high resolution, completely solid state, large area and wide viewing angle, etc.. The development of the thin film EL devices must overcome some drawbacks, such as high driving voltage, lack of stable red and blue EL devices, reduce power consumption and develop efficient materials and deposition techniques for colour displays of practical application.

Intrinsic electroluminescence was discovered by Destriau *in* 1936[193] as an interesting new phenomenon that produced light by exposing phosphor materials to high electric fields, but no positive effort was made in developing the phenomenon into a practical device until engineers at Sylvania Electrical Products, Inc., developed the so-called "powder type" or "the dispersion type" EL panel which was demonstrated at a solid state conference at MIT in the spring of 1952. The immaturity in the fabrication techniques of transparent electrically conductive film was maybe one of the reasons why EL was not developed immediately after Destriau's publication. This drew considerable interest among a number of people, especially those working in illumination engineering and those working on luminescent materials.

During the period from 1950 to 1960, basic studies on the dispersion type EL device which consisted of activated phosphor powder dispersed in a layer of insulating substance were carried on very actively with the expectation that it would turn out to be a new light source for wall illumination. Although a number of devices were manufactured industrially around 1960, the meagreness in brightness, efficiency and lifetime appeared to be insurmountable. Thus, the fist generation of EL development gradually faded away.

In recent years advance in electronics and material science, requirement in commercials assisted and improved the new process technologies and device structures so that development of EL devices has been accelerated. Gradually the double insulating layer structure in EL devices has been more attractive and was payed more attention because of its high brightness with exceptionally high stability and long life, and the development of various kinds of deposition techniques.

8.2 Structure of EL Displays

8.2.1 Structure of AC EL Devices

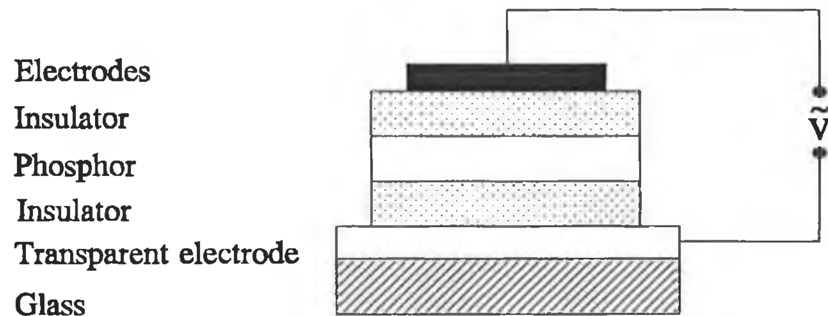

Figure 8-1 Schematic structure of the AC EL device.

Fig.8-1 shows the fundamental structure of EL device. Generally the device consists of a triple layer structure, namely, an active layer sandwiched between two insulating layers. Because of this sandwich structure, undesirable leakage current flowing through the device is prevented. Consequently, the device can keep a sufficiently high electric field for EL operation across the active layer without breakdown.

On the basis of the triple structure, a multiple layer structure of active layer and insulating layer has been developed to improve properties of EL devices such as efficiency of luminescence, characteristics of insulating and adhesive between thin films.

Materials and characteristics of these layers are as follows:

A. Transparent electrode: SnO_2, In_2O_3, In_2O_3:Sn or ZnO:Al. They should have high transmittance and high conductivity.

B. Insulating layers: High dielectric strength and high dielectric constant materials are desirable. SiO_2, Al_2O_3, $BaTiO_3$, TiO_2, Ta_2O_5, Y_2O_3, HfO_2 or Si_3N_4.

C. Active layer: ZnS:Mn, ZnS doped with rare-earth element, SrS doped with rare-earth elements and CaS doped with rare-earth element. They should have high brightness and

efficiency.

D. Rear electrode: Usually, formed by evaporated Al, Au or Ag film.

E. Protection layer: It is necessary to protect the device from humidity. An outer insulating layer of Si_3N_4 is a satisfactory protection layer.

8.2.2 Structure of DC EL Devices

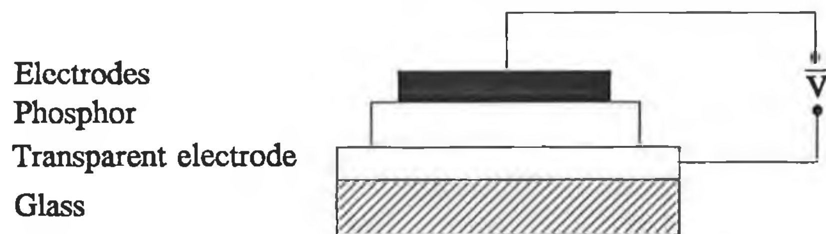

Figure 8-2 Schematic structure of the DC EL devices.

Fig.8-2 shows the fundamental of EL devices driven by DC. Usually the devices is composed of active layer between two electrodes. One is transparent electrode and other is rear electrode. Threshold of EL displays driven by DC is lower than that by AC, but Brightness of EL displays by AC is higher. Another structure of DC EL device includes an insulating layer between active layer and electrode. This structure improves the device characteristics.

8.2.3 Colour EL Displays

There are two basic structures that can be employed to build a multi-colour TFEL display. The first is a layered structure as shown in fig.8-3. This can be implemented either on a single substrate or on multiple substrates. In either case the structure makes use of the fact that the thin film layers are transparent and thus the light from a device can be transmitted

with low loss through the other device layers, provided all the intermediate electrodes are transparent.

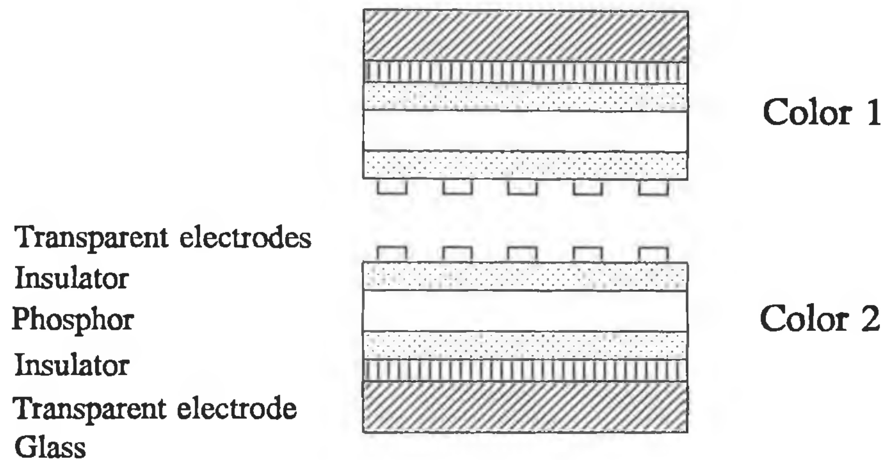

Figure 8-3 Layered colour structure of EL devices.

The second type of structure is the patterned colour structure. One idea is a stacked 3-colour display as shown in fig.8-4, a display, in which three independently operable displays are stacked above each other, on the same substrate. The other idea made public and demonstrated by Tanaka[194], relies on an unpatterned, laterally homogeneous 'white' emitter, parts of it being delegated to the 3 basic colours by colour filters as shown fig.8-5.

8.2.4 Requirements of Every Layer of EL Displays

High efficient and good quality EL displays depend upon characteristics of each of layers. Better physical and chemical properties of thin films in EL displays lead to high stability, high efficiency, high luminance and long life of EL displays. The fundamental requirements of every thin film in EL devices are:

1. Transparent layer should be high transmittance in visible range or required range and high conductive.
2. Insulator layer is high dielectric strength, dielectric constant and high optical transmittance.
3. Active layer should high efficient emission and emitting required light wavelength range

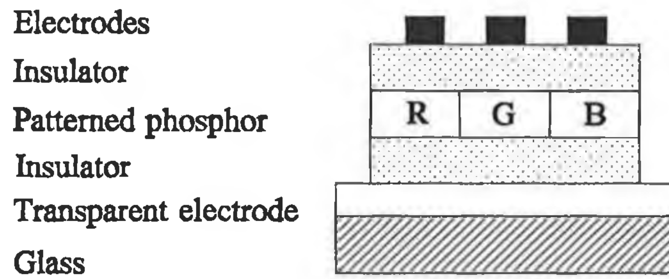

Figure 8-4 Colour EL device structure of patterned phosphor.

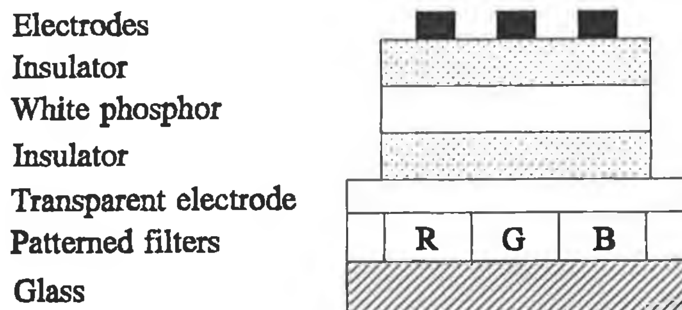

Figure 8-5 Colour EL device structure of Patterned filter.

and high transmittance and properties as mentioned in the chapter 4.

4. Rear electrode should be high reflective in uv-visible but good conductive. Aluminium is good conductor and reflects uv-visible light.

5. They should have good adhesion between films.

6. Good stability so that inter-reaction between layers does not take place during process of treatment.

7. Good reliability and stability of thin film and device parameters of such as electric, optic and mechanism.

8.3 Theory of Electroluminescence

8.3.1 Principle of EL Devices

Luminescence is the general term used to describe the emission of radiation from a solid when it is supplied with some form energy. Electroluminescence is the phenomenon of emission when the excitation results from the application of electric field (which may be either AC or DC).

When the energy input to the luminescing under electric field, the final stage in the process is an electron transition between two energy levels, E_1 and E_2 (E_2>E_1)in the luminescing material, with the emission of radiation of wavelength λ where

$$\frac{hc}{\lambda}=E_2-E_1 \quad \textbf{(8-1)}$$

Invariably E_1 and E_2 are part of two groups of energy levels so that instead of a single emission wavelength a band of wavelengths is usually observed.

Generally speaking phosphor materials depend for their action on the presence within the material of impurity ions which are called activators. These replace certain host ions on the crystal lattice. Unless the charge on the activator ion is identical to that of the host ion it replaces, then charge balance will be upset, and few will be able to enter the lattice. Improved solubility of activator in these circumstances may result from the introduction of further impurity atoms with different ionic charge. These are known as co-activators.

If the energy levels are those of the activator ion itself, this type of energy level system is referred to as characteristic. In the characteristic luminescence the excitation energy is usually transferred rapidly to the activator ion. The persistence of the luminescence is then

entirely due to the lifetime of the excited state level of the activator.

In the non-characteristics energy levels are those of the host lattice modified by the presence of the activator ions. In non-characteristic luminescent materials both activators and co-activators are usually present. These create acceptor and donor energy levels in the material, although in phosphors these levels are usually referred to as hole and electron traps respectively. Energy absorption within the solid creates excess electron-hole pairs and, as the hole trapping probability is usually much greater than the electron trapping probability, most of the excess holes quickly become trapped. Any electron that then finds itself in the vicinity of a trapped hole can recombine with it and generate luminescence. As the electrons migrate through the crystal, however, they themselves are subject to trapping. The electron traps could, of course, act as recombination centres were there appreciable numbers of free holes present, but the difference in trapping probability prevents this. Instead an electron may remain in its trap for some time before subsequently being released by thermal excitation. It may then go on to be retrapped or to recombine with a trapped hole.

Fig.8-6 presents electron-hole generation and recombination process in non-characteristic luminescent materials. (a) Electron-hole pairs are generated under excitation state. (b) The

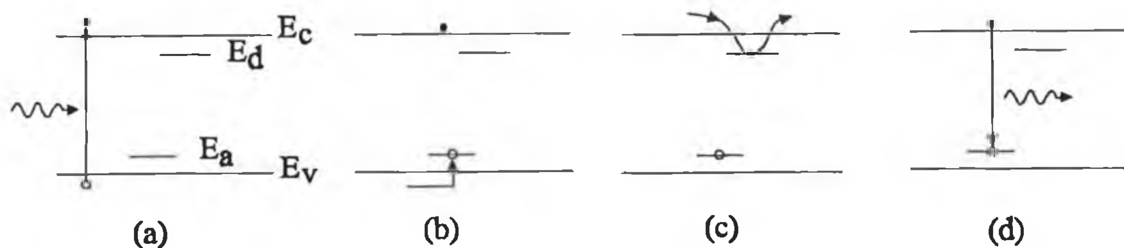

Figure 8-6 Electron hole generation and recombination process in luminescent materials.

holes are quickly trapped at acceptor sites. (d) Electrons may then recombine with these trapped holes, thereby giving rise to luminescent emission. (c) However, before such a recombination can take place, the electron itself may spend some time trapped at a donor site. In electroluminescent devices four main types of devices may be distinguished depending on the types of drive (AC or DC) and the character of active layer (powder or thin film). The first electroluminescent device to be extensively studied was the AC powder device which was proposed in 1936.

8.3.2 EL Mechanisms of Mn-Doped and Rare-Earth-Doped ZnS Thin Films

In electroluminescent devices, luminescent processes are divided three kinds:

1. electrical processes: release and acceleration of electrons by applied electric field;
2. excitation processes: excitation of the luminescent centre;
3. optical processes: radiative and non radiative deexcitations of this centre.

8.3.3 Hot Electron Processes in EL

Efficient luminescent radiation from electric power in electroluminescent devices needs an efficient conversion of electrical input into kinetic energy of the charge carriers, in order to impact-excite the luminescent centres strongly enough. When carriers travel through active film, they should possess energy above the excitation energy of the centres for efficient excitation.

The electronic energy distribution in ZnS:Mn films affects the luminescent efficiency of EL thin film devices. It is known that the light generation starts when there are electrons with kinetic energy above 2.2 eV, able to impact-excite the Mn centres. At the lower fields the electrons are not heated up efficiently, so the electrons are not able to excite the Mn centre. The Mn excitation yield is a function of electric field. Before arriving at concentration quenching, with electric field Mn excitation yield increases and leads to saturation. The saturation originates from the fact that at such high fields almost all electrons are heated up above 2.2 eV very rapidly and the field is able to keep them above this threshold. In the meanwhile, Mn excitation yield increases with thickness of luminescent thin films, indicating an excitation throughout the film at high fields. In lower Mn concentration the yield increases with Mn concentration.

8.3.4 Impact Processes in EL

Now it is important to find ways of producing light efficiently by passing an electrical current through a solid. In a solid one has the problem that the carriers can lose energy by the emission of phonons. Hence a high field is necessary so that the rate of energy gain from the field substantially exceeds the rate of loss to phonons.

Excitation processes affect the efficiency of EL device emission, so it is important to understand the processes.

1. Band-to-band ionization: Band-to-band impact ionization creates electrons and holes which can recombine radiatively through some centre. Another process is the two-step band-to-band impact ionization. An incident hot carrier ionizes a deep level by an electron transition to conduction band, and then another hot carrier raises an electron from the valence band to a deep level. The total effect is to produce free electrons and holes. In principle these can recombine radiatively at the same deep level or can interact with another centre to produce radiation. The cross-section and concentrations of luminescent centre and impact-ionizable centre affect the efficiency of luminescence. At sufficiently high fields virtually all the electrons are "hot", i.e. in the high density of states region, and the average cross-section depends only weakly on field. Centres with a high cross-section and high concentration are required in impact process involving deep centres.

2. Impact excitation: Impact excitation of the luminescent centre is a familiar process which occurs in ZnS:Mn electroluminescent devices and in some, but not all, rare-earth doped materials. The cross section is a main factor which depends on energy, velocity, distribution function of "hot" electron, band-structure of impact centre, interaction between "hot" electrons and impact centres and so on. The other factor in impact excitation is the concentration of the centres. For luminescent centres the limit can be set by solubility or concentration quenching. A frequent mechanism of concentration quenching is that the excitation energy diffuses through the assemblage of the luminescent centres to non-radiative centres.

The factors why ZnS:Mn is a better impact electroluminescent material than any other now known are:

a. Manganese has a very high solubility in ZnS. The concentration quenching limit can therefore be reached.

b. There is a high density of states 2-3eV above the bottom of the conduction band in ZnS. This allows nearly all electrons at high fields to have sufficient energy for exciting

manganese.

c. The band are flatter in this energy range, i.e. the electrons are slower than if the band were parabolic. Hence the exchange interaction is enhanced. (Direct processes are improbable because of the small oscillator strength for the optical absorption from the ground state) [195].

8.3.5 Luminescence and Conduction Charge of DC EL Devices

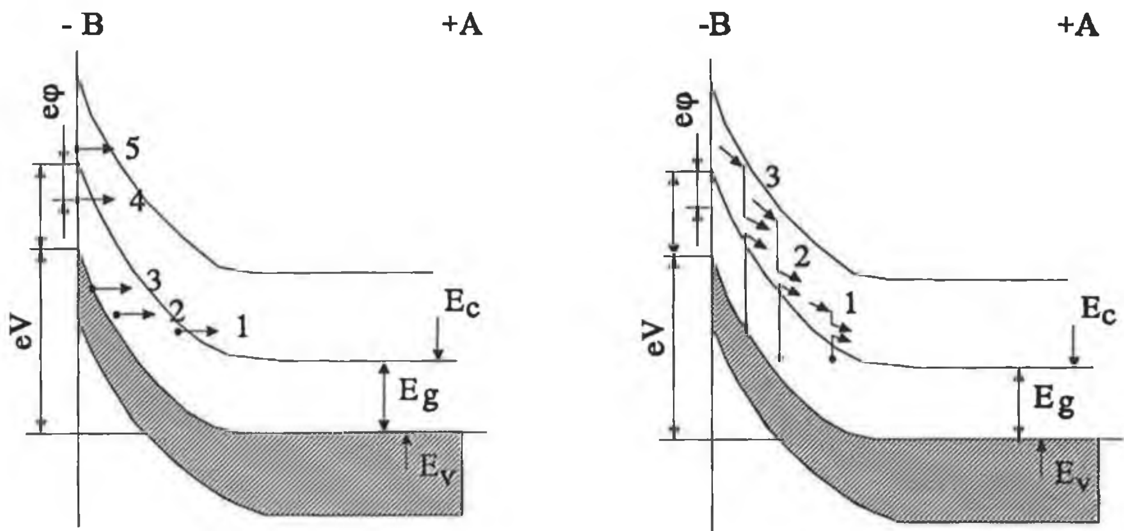

Figure 8-7 Energy band diagram of EL excitation of DC device.

In DC electroluminescent device the surface potential barrier is set up around the interface between electrode and semiconductor active layer. The electrode A of EL device is connected with positive of source and electrode B is connected with negative. If a positive voltage is applied to the electrode A, negative charge has to be pushed away from electrode B. This negative charge is obtained by fixed ionized acceptors (donors) which are exposed due to the holes that have been induced near the interface by the negative voltage at electrode. Since the semiconductor has a fixed amount of acceptor (donor) impurities per unit volume, a region of certain charge is created at interface. This region is called the 'depletion region' or 'space-charge region'. In the space charge region energy band is tilted or bent increasingly with the applied voltage. When the applied voltage arrives at a certain value, in the region change of

electric field is so great that free electrons, which are from crossing interface between electrode and semiconductor and ionized from donors or lattices, obtain energy and are speeded up. The moving electrons can excite new electrons from lattices and activators (luminescent centres). When electrons return to the ground state or empty acceptor levels radiation is emitted. Fig.8-7 shows energy band diagram of EL excitation of DC device.

8.3.6 Luminescence and Conduction Charge of AC EL Devices

8.3.6.1 Production of Electrons in EL Devices

Moving electrons in EL lead to luminescence. These can be:

1. Electrons crossing and passing by tunnel effect through potential barrier of dielectric film if the dielectric film is very thin.
2. Electrons generated from activators at host material under high electric field.
3. Donor electrons and electrons from occupied acceptor levels 'tunnelling' through the forbidden gap region into states of the same energy in the conduction band under high electric field. They can only do this if a considerable electric field is present thus causing the energy levels to be tilted.
4. Electrons produced from electron-hole pairs due to impact ionization of host material caused by high speed electron forced under high electric field.

8.3.6.2 Basic Principles of AC EL Devices

In AC electroluminescent device an active layer is suspended in a transparent binding medium of high dielectric constant and is sandwiched between two electrodes (one of which is transparent). Usually there is no complete conducting path between the electrodes so that DC excitation is not possible. When an alternating voltage, $V_0\cos(2\pi ft)$, is applied across the cell, however, light is emitted in the form of short bursts and occur once every half cycle. It is found that the integrated light output power P can be written in the form[196]:

$$P=P_0(f)\exp[-(\frac{V_1}{V_0})^{\frac{1}{2}}] \tag{8-2}$$

where V_1 is a constant and $P_0(f)$ is a function of frequency.

When an alternating voltage, $V_0\cos(2\pi ft)$, is applied to electrodes as shown in fig.8-8.

(a) At t_1, when the applied voltage is not too large, the electrons from shallow donor levels

move from - electrode to + electrode and a space charge region is created. Some moving electrons fall to valence band and some electrons are accumulated near active layer side of + electrode because of blocking of dielectric film.

(b) At t_2, with an increasing of applied voltage the space charge region is enlarged and change of electric field increase largely. Electrons through tunnel effect and from donors and acceptors accumulated in this region at the time positive voltage is applied to the electrode are accelerated and impact lattices, luminescent centres or activators. Electrons move towards the positive side and holes move to the negative side. Some electrons return to the ground state and acceptor levels in the moving process and emit radiation. The excited luminescent centres emit radiation because of electrons returning to the ground state. Some electrons are accumulated around the side of electrode and are recombine and return to the ground state, emitting radiation.

(c) At t_3, the applied voltage between two electrodes is being reduced. The distribution of electric field is complicated. When the electric field established by space charge is larger than the applied voltage, some electrons stored near the side of electrode move to other side. Some electrons probably recombine with holes moving from the other side to emit radiation, which is called secondary emission usually.

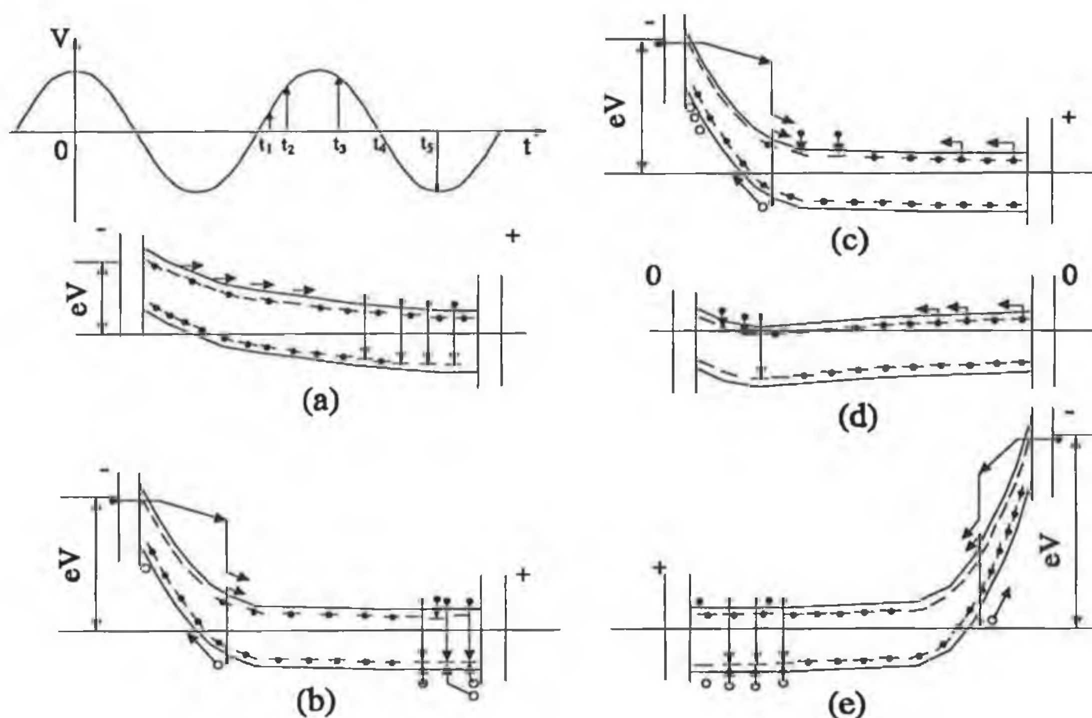

Figure 8-8 Energy band diagram of EL excitation of AC device.

(d) At t_4, the applied voltage is zero. Some electrons not being recombined move to space charge region to recombine with donor ions. After t_4, the applied voltage reverses.
(e) At t_5, the distribution of electric field reverse. A large amount of electrons recombine to emit radiation near the electrode.
The strongest emission from within the emission layer is found to take place from that side which is temporarily facing the cathode. A high electric field between the sides of the emission layer is sufficiently strong to enable electrons from occupied acceptor levels to 'tunnel' through the forbidden gap region into states of the same energy in the conduction band and accelerated electrons in conduction band to excite luminescent centres. It is only able to do this if a considerable electric field is present thus causing the energy levels to be tilted. Other electrons in the band are then able to fall into these vacated levels and emit radiation. Another possibility is that an electron moving in the electric field may acquire sufficient energy to enable it to excite an electron from the valence band to the conduction band. The resulting hole quickly becomes trapped at an impurity acceptor site thereby effectively emptying it for an electron. An electron in the conduction band can then make a radiative transition by falling into the empty acceptor level. In the emission layer containing activator (Mn^{2+}, Cu^{2+} or rare earth element ion) there is evidence that the activators themselves may be directly excited by the high energy electrons, radiation being emitted when the activator ions subsequently undergoes de-excitation.

8.3.7 Luminescence and Conduction Charge in MIS EL Devices

The single-insulated (MIS) EL devices have the structure of conductor/ insulator/ semiconductor/ conductor. One of conductors is a transparent or semi-transparent conductor and one of both is a rear electrode. An applied external field might cause carriers to be injected from the electrodes and/or generated in insulating layers which conduct through the insulating layers by the Poole-Frenkel effect, and to be injected into the ZnS layer by field-assisted tunnelling[197],[198]. By means of this process, a DC-like current would be created. In the (MIS) devices, carriers could be readily injected from the electrode because the ZnS layer is in direct contact with the electrode. The processes of release and acceleration of hot electrons, excitation and luminescence in MIS devices is similar to that in the doubly insulated devices. As a result of the conduction of charges near single ZnS-insulator interface, holes are accumulated near the cathodic interface and electrons near the

anodic interface. These accumulated charges caused a space-charge effect. This effect induces the energy band of the ZnS layer at the cathodic side to bend toward higher energy. This band-bending causes a decrease in the electric field at the cathodic side, resulting in insufficient electric field strength to either generate or to accelerate carriers. A crude estimation of the electric field induced by the space charges is shown below, in which it is assumed that the electric field state exists as in a plane along the ZnS-insulator interface. The accumulated charges Q can be expressed as

$$Q=\varepsilon\varepsilon_0 EA \qquad \textbf{(8-3)}$$

where E is the electric field, A is the area of the overlapping electrodes and ε_0 is the vacuum permittivity constant. ε is the dielectric constant of active layer ZnS.

If relaxation of the accumulated charges is slow, the electric field induced by the space charge will be superimposed on the electric field by the applied voltage. It would seem, therefore, (1) that a very large electric field is induced inside the ZnS layer, (2) that the electric field induced by the external field causes the release of the trapped charges, and (3) that the charges are mainly accelerated by the electric field induced by the space charge.

The luminescence caused by each applied pulse depends on the internal electric field induced by the charges accumulated, and not on the external electric field. The dominance of the fast variable current component in a high electric field is caused by these accumulated charges, which are a function of the average of the applied voltages.

Because in MIS devices there is no insulating layer between the electrode and the ZnS layer, carriers can be readily injected from the electrode or released from the ZnS layer, with the result that charges will not accumulate readily in variable electric field states near the ZnS-electrode interface. As a consequence, the internal electric field induced by space charge at the ZnS-electrode interface is weaker than the field generated at the ZnS-insulator interface. This would explain (1) why luminescence is weaker than the doubly insulated devices and (2) why the minute peak appears in the luminescence waveform after the applied pulse was turned off (fig.9-9).

8.3.8 Efficiency of Thin Film EL

Thin film EL devices rely on accelerating electrons or holes to sufficiently high energies that they can impact excite or ionized luminescent centres. Excited luminescent centres emit

radiative light and also decay non-radiatively. Efficiency is important in many ways. It may determine the required drive current or the maximum achievable brightness in particular devices. Many factors affect the efficiency of the EL devices in converting electrical energy into light.

Up to now AC thin film EL devices with ZnS:Mn as active layer are the most efficient devices and they are quite well understood in their basic physics. The conversion of electric input into light output is subject to several electro-optical processes which determine that total efficiency[199]:

$$\eta = \eta_{exc} \eta_{lum} \eta_{out} \tag{8-4}$$

where η_{exc} is the excitation efficiency of the Mn centres excited by impact of the kinetic electrons, i.e., the ratio of excited centres to the transferred charge across the active layer, η_{lum} stands for the radiative efficiency of an excited centre, i.e. the inner transitions of transition metals and rare earths, and η_{out} takes into account the outcoupling of the emitted photons.

The excitation efficiency η_{exc}, defined as the ratio of the number of the excited centres to the amount of the transferred charge, characterizes a series of different process:

1) the escape of carriers from the momentary insulator active layer cathode interface,

2) their acceleration under the applied electric field and

3) the impact excitation of the dopant.

Therefore η_{exc} will depend on the energy distribution of the electrons involved in the charge transfer and on the value of the impact cross section σ of the dopant and its concentration. As discussed in more detail in[200] the single factors are:

$$\eta_{exc} = \sigma N_L \tag{8-5}$$

$$\eta_{lum} = \frac{\tau}{\tau_r} \tag{8-6}$$

$$\eta_{out} \approx 0.1 d_s \tag{8-7}$$

where σ is electron impact cross section of an Mn^{2+} centre; the decay time of the Mn^{2+} luminescence:

$$\tau = \left(\frac{1}{\tau_r} + \frac{1}{\tau_{nonrad.}}\right)^{-1} \tag{8-8}$$

where τ_r is the decay time of radiation and $\tau_{nonrad.}$ is the decay time of non-radiation; d_s is thickness of the active layer. In principle both factors, η_{exc} and η_{lum}, could depend upon the concentration of excited centres N_L.

In ZnS:Mn film EL displays, improving on efficiency is difficult. Increasing Mn concentration causes problems with concentration quenching. The impact excitation cross-section can mostly not be increased. In a thin film EL device the operating field may be determined by the carrier generation process at the interface and so the field is not always optimum for the impact process. The conclusion is that improving on the efficiency of ZnS:Mn for impact excitation is difficult because it is difficult to increase the average cross-section and to increase the luminescent centre concentration. There is a possibility of increasing the cross-section by using impact ionization rather than excitation but then the effective radiative efficiency may decrease because the freed carriers can return to the ground state by non-radiative mechanisms, especially because generation occurs in a high field and recombination in a low field. In principle the impact and emission processes can be separated by having one set of centres with properties optimised for the impact process which then transfer energy by some mechanisms to another set of centres optimised for the emission process.

In EL high field devices a major factor limiting efficiency is that the hot carriers must travel a certain distance to interact with a luminescent centre and in this distance they acquire energy from the field, most of which is wasted.

8.3.9 Rate of Excitation and Ionization of Luminescent Centre

High field electroluminescence devices have been developed on an empirical basis. Quantitative theories of the mechanisms of high field electroluminescence are in a primitive state by the standards of semiconductor physics. The hot electron distribution, impact and ionization cross-section, the position of Mn^{2+} and rare-earth energy levels relative to energy gap affect directly on the characteristics of EL devices.

The rate of excitation or ionization R, which is related directively to light intensity, depends on a convolution of energy distribution and cross-sections[201]:

$$R=nN_L\sum_{\nu}\int_{BZ}\sigma(\nu,k)v(\nu,k)f(\nu,k,V,x)d^3k \qquad (8\text{-}9)$$

here n is the carrier density, N_L the concentration of centres which can be ionized or excited, ν a band index, k the carrier wave vector, σ the cross-section, V the velocity, and f is the distribution function which in general is a function of potential and position. A simple approximation to Eq.(8-9) can be used in terms of energy:

$$R\cong nN_L\int_0^{\infty}\sigma(E)\nu(E)g(E,\varepsilon)dE \qquad (8\text{-}10)$$

where the distribution function g depends on the local electric field ε.

8.3.10 Concentration Quenching of Electroluminescence

Mn^{2+} can be incorporated in the ZnS lattice up to very high concentrations, in fact up to complete miscibility[202]. As the yellow luminescence in this material is due to the excitation and decay of the Mn^{2+} ion, one would expect the intensity of luminescence to increase with Mn concentration. Such is not the case in practice. It is well known that the intensity of luminescence of ZnS:Mn increases initially until a certain optimum concentration of the activator, after which there is a drastic reduction in intensity. This typical behaviour is characteristic of the luminescent ZnS:Mn irrespective of the exciting mechanism. The physical basis of concentration quenching is, as yet, poorly understood.

Although ZnS:Mn based thin film electroluminescent display are commercially available to day, still many questions remain unanswered regarding the physical phenomena underlying their behaviour. One of these phenomena is concentration quenching: at a critical Mn concentration of about 1 mol% the luminescent efficiency of a ZnS:Mn layer suddenly drops. The process of concentration quenching in ZnS:Mn involves two processes: migration of excitation energy among Mn ions and energy transfer to traps in the form of red, infrared or non-radiative centre. This was suggested by Yang et al.[203] and Tornqvist[204].

According to the physical model suggested by M. Katiyar and A.H. Kitai[205], the fraction of excited Mn atoms is very low under normal condition. Therefore, it is assumed that if an Mn centre is excited it can transfer energy to another unexcited centre through a resonant non-radiative transfer process. A resonant transfer to a red, infrared or non-radiative

centre which will generally be a phonon-assisted transfer process due to energy mismatch. This will be true unless such a trap exists very near to a given Mn ion. Therefore, energy will migrate over Mn centres until it finds a trap in the form of red, infrared, or non-radiative centres very near to the excitation path. In other words, energy loss to a trap depends on the probability of finding a trap near the path of excitation. Trap concentration is independent of Mn concentration because emission at longer wavelength is not due to Mn pair or clusters[206]. An isolated Mn centre, capable of giving yellow emission, is referred to as a donor. An acceptor is a trap. Such a model explains:

(1) No significant change in absorption spectra corresponding to concentration quenching.

(2) Time delayed sensitized-luminescence of red centres.

(3) Non-exponential decay time measurements.

8.3.11 Comparison of AC and DC EL Devices

Because of different structures of DC and AC EL displays devices, the structure results in the different characteristics of EL devices. Comparison of the AC and DC EL devices contribute to the development and improvement of EL devices.

1. Structure

Fig.8-1 and Fig.8-2 show the fundamental structures of AC and DC EL devices respectively. The insulating film in EL device makes the changes of the properties.

2. Brightness

Brightness of AC EL devices is higher than that of DC devices. High quality and high dielectric constant insulating film leads to higher brightness.

3. Applied voltage

Because of insulating film the applied voltage of AC EL devices is higher than that of DC devices.

4. Efficiency

AC devices have higher efficiency than DC devices.

5. Power consumption

Power consumption of AC devices is lower than that of DC devices.

6. Longevity

Usually AC devices have longer lifetime than DC devices.

7. Driver

Because of lower voltage of driving DC EL displays the circuit of driver is simpler and its requirement is lower.

8. Manufacture technology

Manufacture technology of DC display is relatively simpler.

Chapter 9

CHARACTERISTICS OF EL DISPLAY DEVICES

9.1 Structure and Fabrication of EL Devices in the Work

Fig.9-1 shows the structure of EL device in the work. It is mainly composed of silicon substrate, insulating film (Al_2O_3 or SiO_2), phosphor film (ZnS:Mn or ZnS:Tb) and Au semitransparent film. The deposition of insulating films and phosphor films was the sol-gel process. Au film was deposited by sputtering.

The silicon substrate was cleaned using ethanol and distilled water firstly. Al_2O_3 or SiO_2 film was deposited on the Si substrate as described previously and annealed at 400-500°C in air. ZnS:Mn and ZnS:Tb films prepared by conversion of ZnO:Mn and ZnO:Tb film which were annealed in H_2S. ZnO:Mn and ZnO:Tb films were also deposited by the sol-gel process. Au film was sputtered lastly. The emission spectra were measured using the monochrometer of SOFIE Optical Instruments whose uv-visible range is 200-900 nm. Brightness was measured using the UDT model 380 dual channel optometer. Applied voltage of EL devices can be adjusted from 0-300V.

9.2 Characteristics of ZnS:Mn Thin Film EL Devices

Studies of Mn-doped ZnS film started rather early in the history of EL. Since 1960, Vlasenko et al. have continued their work on ZnS:Mn and have reported several interesting papers [207],[208],[209]. In 1974, Hanak reported on the DC EL properties in RF sputtered ZnS:Mn_x:Cu_x film[210]. Russ et al. reported in 1967 on a double insulating layer structure thin film EL device[211]. These studies seem to have been centred around the clarification of the physics of EL with less emphasis on prolonging the life of operation. In 1974, Inoguchi et al. reported an extremely long life and high brightness in devices which utilized EL in a thin film of ZnS:Mn with a double insulating layer structure[212]. Subsequently, in 1975, inherent memory function was found in the same structure[213].

9.2.1 Emission Spectrum of ZnS:Mn EL Devices

The EL device fabricated as fig.9-1 emits bright yellowish-orange light under DC high electric field excitation. This yellowish-orange light originates in the Mn^{2+} luminescent centre excited

1. semi-transparent gold electrode
2. ZnS:Mn luminescent layer 1200~2000 Å
3. aluminium oxide or silicon dioxide 500~800 Å
4. silicon wafer
5. back electrode (Al or Au)

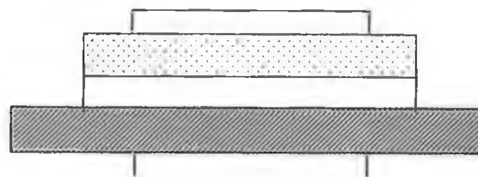

Figure 9-1 Schematic cross-section of electroluminescent device.

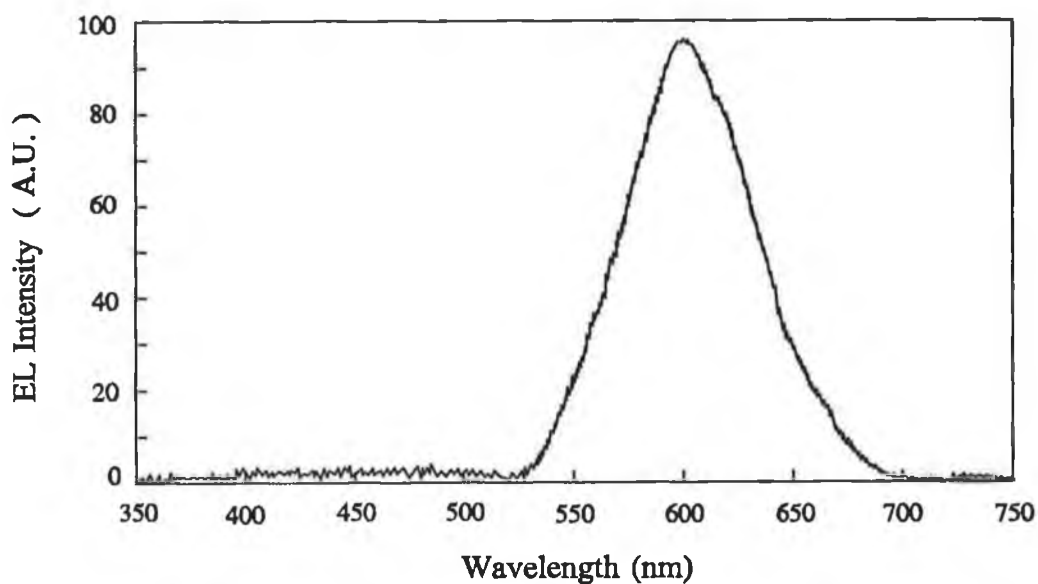

Figure 9-2 Electroluminescent emission spectrum of a ZnS:Mn EL device.

directly by hot electrons in ZnS layer, and has the spectrum shown in fig.9-2. This luminescence spectrum does not show any change with driving voltage and frequency.

9.2.2 Brightness of EL Devices

The good parameters of EL devices depend on the optimization of film properties. In designing EL devices the properties of every film of EL devices should br considered. Brightness of thin film EL display devices produced from transported charge ΔQ is related to parameters and properties of thin films[214]:

$$B=\beta\frac{\Delta Q}{A}d_p \tag{9-1}$$

$$\Delta Q=C_i(V-V_{th}) \tag{9-2}$$

where B is brightness, β phosphor figure of merit, A area of EL device unit, V_{th} threshold in the applied voltage, d_p thickness of phosphor layer, d_i thickness of insulating layer, C_p capacitance of phosphor layer and C_i capacitance of insulating layer.

Normal operating brightness is obtained with V_{mod} as the modulation voltage:

$$B_{op}=\beta\frac{C_i V_{mod}}{A}d_p \tag{9-3}$$

The capacitances are given by:

$$C_i=\frac{\epsilon_d\epsilon_0 A}{d_i} \tag{9-4}$$

$$C_p=\frac{\epsilon_p\epsilon_0 A}{d_p} \tag{9-5}$$

$$C_t=\frac{C_i C_p}{C_i+C_p} \tag{9-6}$$

At threshold, the voltage across the devices has reached the value providing a field E_t in the phosphor layer. It is easily shown that the relation between the device capacitance in the off state and the threshold voltage is given by

$$C_t=\frac{\epsilon_p\epsilon_0 A E_t}{V_{thr}} \tag{9-7}$$

9.2.2.1 Voltage-Brightness Relation

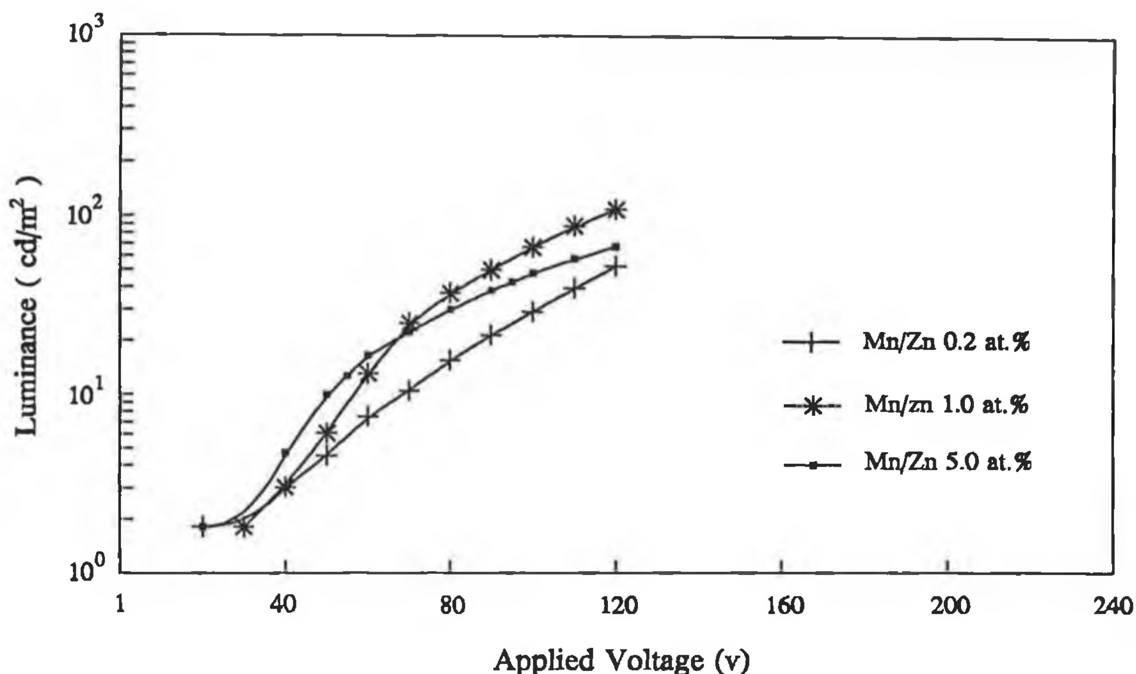

Figure 9-3 B-V characteristic of ZnS:Mn EL device with SiO_2 insulator and Au electrode connected with positive voltage.

Fig.9-3 shows the brightness curves by applying DC voltage as shown in fig.9-4. The brightness of thin film EL devices is extremely dependent on the applied voltage in the lower voltage region, and tends to saturate in the higher voltage region. When an Au film was connected to a positive electrode of DC source, electrons travel in ZnS:Mn film across insulator and impact luminescent centres. In the experiment it was found that when the value of applied voltage was over a certain limit, the Au film was burned out easily and brightness was weak. When Au film was connected to a negative pulsed source, brightness of EL increased very much. Fig.9-4 shows the brightness of EL devices with different Mn concentration with Al_2O_3 insulator. Fig.9-5 shows brightness of EL devices with Al_2O_3 or SiO_2 film as the insulator.

When a positive pules is applied to Si wafer, electrons are injected from Au film electrode, accelerated under high field and impact luminescent centres. Some electrons arrive at the interface of insulator-phosphor and accumulate near interface because of barrier of insulator. These accumulated electrons cause charge-space effect. This effect induced the energy band of the ZnS layer at side of insulator to bend toward higher energy. This band-bending causes

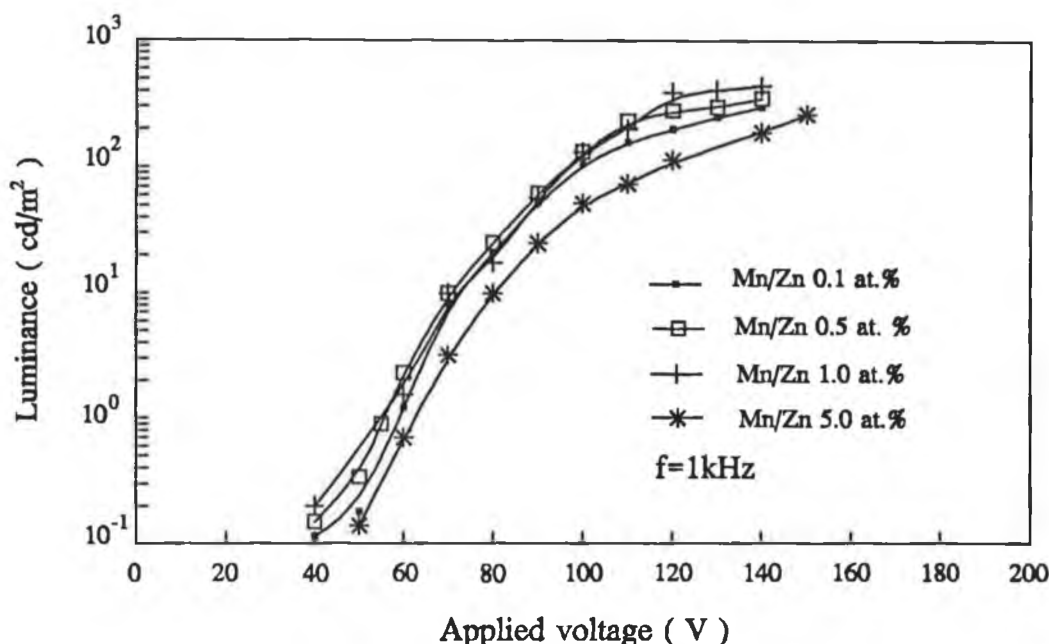

Figure 9-4 B-V characteristic of ZnS:Mn EL devices with Al_2O_3 insulator.

a decrease in the electric field at the insulator side. Electrons accumulated have a potential which depends upon value of applied voltage and properties of insulator such as dielectric constant and resistivity. When electrodes are short-circuited accumulated electrons are accelerated under internal field induced by space charge and impact luminescent centres. The luminescence caused by each applied pulse depends on the internal electric field induced by the charges accumulated in the pulse state, not on the external electric field. The electric field caused by the accumulated charges is a function of the average of the applied voltage. A large current leads to the breakdown of Au film electrodes. When the Au film was used as the positive electrode, electrons crossing insulator and through tunnelling from cathode enter ZnS:Mn film and impact luminescent centre. With an increase of applied voltage the number of electrons increases abruptly. This results in the burning of An film. In the period of the pulse electrons cross the active layer one time, so the effective emission occurs once per pulse. As the Au is connected to the cathode of the DC source electrons from the cathode enter active layer and excite the luminescent centres. Some electrons move towards insulator and are blocked by the insulating film resulting in the accumulation of electrons and building in space charge region. When the polarity of pulse inverts electrons are accelerated and impact luminescent centres under the internal field leading to radiation. The number of

electrons entering the active layer, i.e. current, is restricted by the electric field of space charge, which prevents from damage of the Au film. In the one period of pulse luminescent centres in active layer are excited by the accelerated electrons twice resulting in the two effective luminescence processes. In the meanwhile, the quality and characteristics of the dielectric film and the phosphor film affect the properties of EL devices.

9.2.2.2 Function of Insulating Layer to Brightness of EL Devices

The insulating layer plays an important role in realizing thin film EL displays with high brightness, high stability and high reliability. In order to reduce driving voltage and increase brightness, a high dielectric constant insulating material must be used. The properties of the dielectric materials are one of the important factors on the stability and reliability of the display. Two dielectric materials have been tested with idea of improving display performance, specially increasing the brightness, and lower the threshold voltage. Therefore the choice of dielectric material for use in thin film EL displays is very important. In this study, the electrical and optical performances of electroluminescent devices with Al_2O_3 and SiO_2 as insulating layers were researched.

The insulating layer is very important for bright electroluminescence in EL displays in that

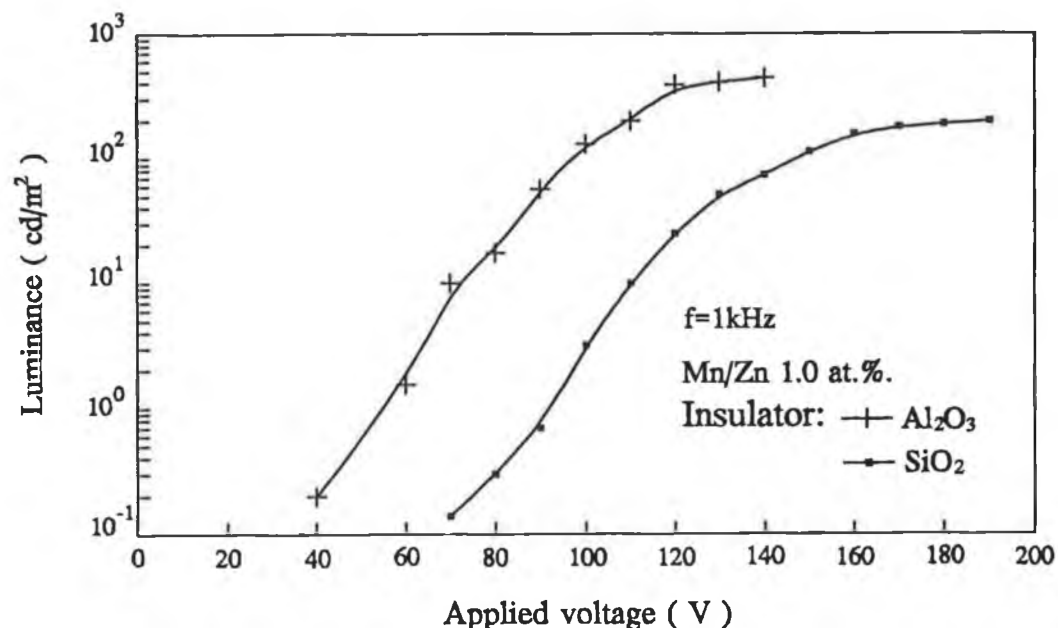

Figure 9-5 B-V characteristic of ZnS:Mn (Mn/Zn: 1.0 at.%) EL devices with Al_2O_3 or SiO_2 as insulator.

it allows accumulated charges to remain inside the ZnS layer. This accumulation will induce an electric field sufficient to accelerate carriers to excite luminescent centres as explained above. The properties of the insulating layer determine the quantity of accumulated carriers and the strength of the internal electric field. Brightness with applied voltage of EL devices using Al_2O_3 or SiO_2 as insulating layer is shown in fig.9-5. Table 9.1 shows the resistivity and dielectric constants of SiO_2 and Al_2O_3 films[215] and SiO_2 and Al_2O_3 films by the sol-gel process in the work.

Table 9.1 The resistivity and dielectric constant of Al_2O_3 and SiO_2.

Material	Resistivity (Ω•cm)	Dielectric constant	Measured dielectric constant
Al_2O_3	10^{12}-10^{13}	9-11	9.28
SiO_2	10^{10}-10^{15}	3.5-7	4.108

From literature[216], a high dielectric constant of insulating layer leads to a higher brightness, lower threshold voltage and reduction of applied voltage, which accords with our result. The properties of dielectric film can improve the properties of EL devices.

9.2.2.3 Function of Rise Time to Brightness of EL Devices

From measurement of brightness of EL devices, it was found that as the rise time became fast the luminance of EL devices increased, which was according to the literature[217]. The maximum value of field depends upon (1) the total charge transferred from cathode to anode by the tunnel current and (2) the rate at which the tunnel current builds up. The external and internal electric fields of EL devices and active layer, external circuit current and displacement current in insulator and active layer are the function of time. The luminance of EL devices depends on the electric fields and current in insulator and active layer. In addition, the current is related to EL devices properties such as capacitance of insulator and active layer.

9.2.2.4 Concentration-Brightness Relation

ZnS:Mn phosphors are well known to achieve maximum efficiency and maximum saturation brightness in electroluminescence at a Mn concentration of approximate 1.0 at.% in thin film

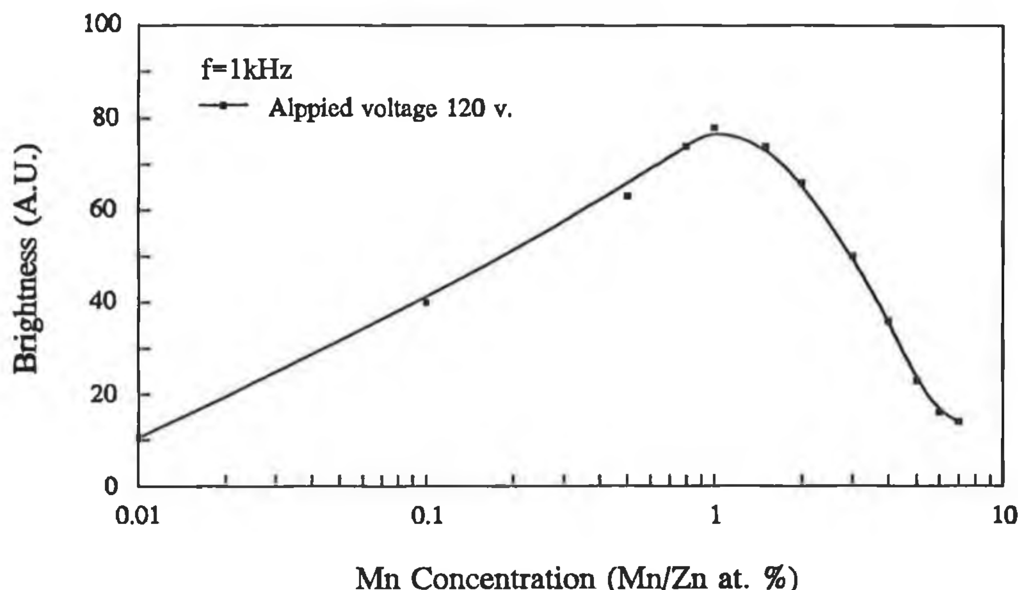

Figure 9-6 Relative EL brightness with Mn concentration of ZnS:Mn EL devices.

electroluminescent devices. At higher concentrations, brightness falls off due to some type of concentration quenching phenomenon in which nearby Mn centres are believed to couple energy away from a Mn site and direct it to a non-radiative site.

Thin film EL devices were systematically investigated for the change in EL characteristics due to a change in the Mn concentration. Results thus obtained are shown in fig.9-6. The applied voltage for all the measurements was 120v and frequency was 1kHz. It may be seen that initially the brightness increases with Mn content, up to approx. 1.0 at.%, beyond which there is a drop in the brightness.

9.2.2.5 Thickness-Brightness Relation

Fig.9-7 shows relation of brightness vs. thicknesses of active layer ZnS:Mn. The brightness increases initially with an increase in the thicknesse of active layer and then reaches a saturation point at a certain thickness. If thickness of active layer exceeds a certain limited thickness, brightness decreases. It is known that electrons from the interface of active layer are accelerated and move under high electric field, then some electrons impact luminescent centre emitting light and some impact the lattice producing new electrons, which leads to a multiple number of electrons. Lastly, some of the high speed moving electrons cause impact

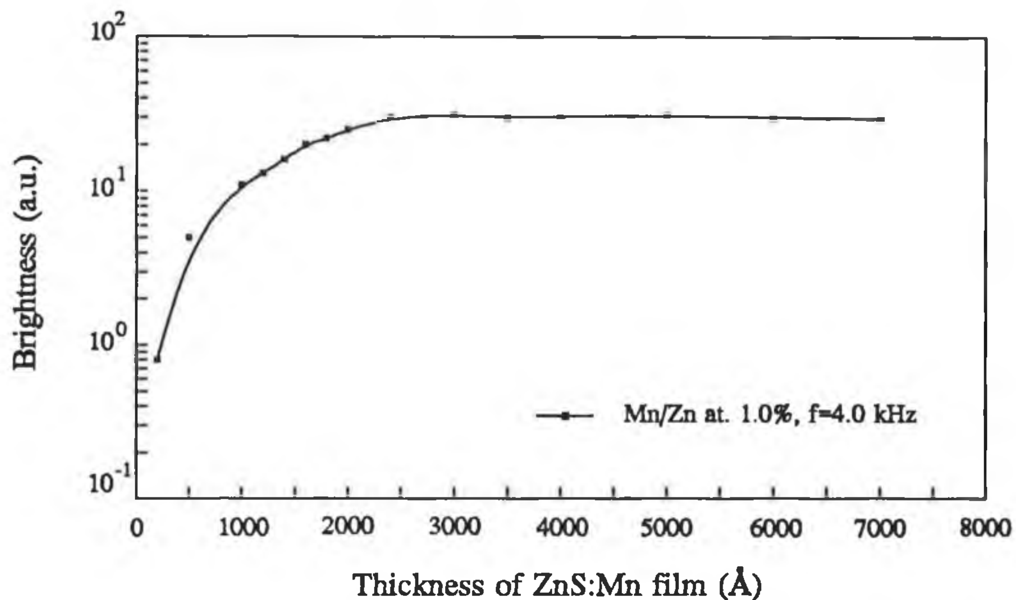

Figure 9-7 Dependence of ZnS:Mn thin film thickness on the maximum brightness at 100Hz driving condition. MIS structure is $Si/Al_2O_3/ZnS:Mn/Au$.

excitation of luminescent centres. Electrons obtain energy and are multiplied after moving distance, so brightness of very thin active layer is weaker.

Moving electrons lose energy and the speed of electrons decreases in long distance moving so that some of them can not excite luminescent centres. Efficiency of EL devices lessens with an increase in thickness.

In real device structure, the thickness of the active layer is necessarily finite and there is a storage of electrons in the insulator-semiconductor interface. This implies in any case a polarization field and, because the polarization is opposed to acceleration field, this may lead to field clamping at high charge transfer levels[218]. Under certain circumstances the polarization field becomes so important that a second light pulse at the trailing edge of electric pulse appears[219]. At high excitation levels, the charge transfer can diminish the internal field. This diminution of the field affects the acceleration mechanism of the electrons in such a way that the length needed to gain the necessary excitation energy becomes longer and the electron energy distribution may be altered significantly.

9.2.2.6 Driving Frequency-Brightness Relation

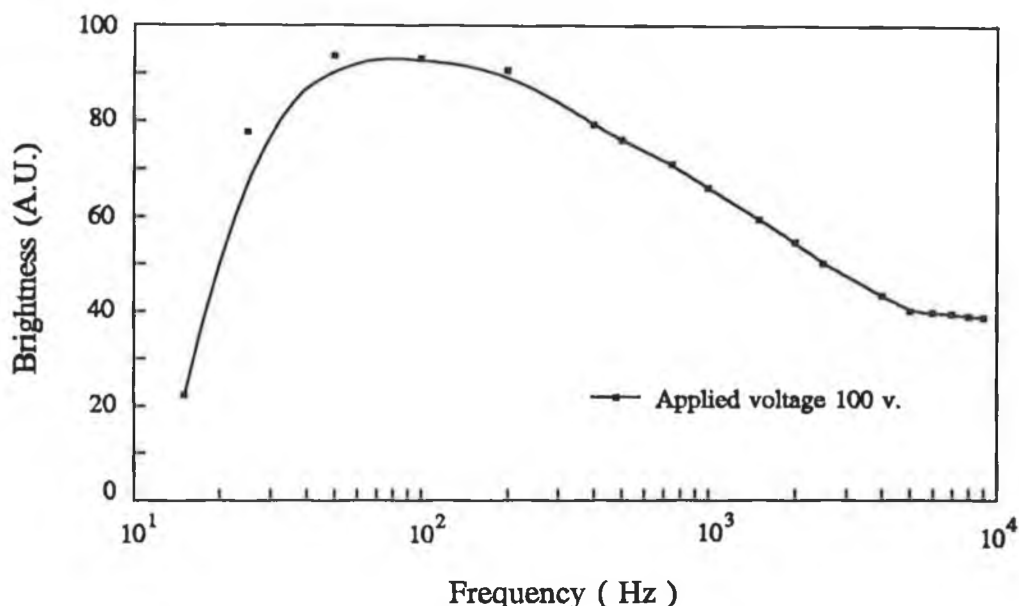

Figure 9-8 Relative EL brightness with applied voltage frequency of EL device.

Fig.9-8 shows that relative brightness of EL electroluminescent devices with Al_2O_3 insulating layer changes with applied voltage frequency. Brightness decreases with increase of frequency in the range of high frequency. As the frequency drops, the brightness reduces also. In the range of about 50-200 Hz brightness is maximum. Similar results were obtained in measurement of brightness of EL devices with SiO_2 insulator.

From Eq.(9-3) it is known that brightness of EL devices depends partly upon structure of EL device since capacitance of the device rely on the thicknesses of dielectric phosphor layers and properties of dielectric and phosphor layers.

The electrons are accumulated near interface of insulating film and phosphor film so that the space charge region is built. The building of space charge region needs time. In lower frequency lower brightness can be explained because the electrons are accelerated and impact luminescent centres, then accumulate near interface of insulator and phosphor layer for long time. The interval between output optical pulses is increased at lower frequency. In high frequency brightness should depend on the process of electrons accumulation, motion and impact with luminescent centres. Under high frequency external field, ineffective electron accumulation leads to low luminescent output. In the meanwhile, luminescent output also

depends upon the characteristics and structure of devices, materials of thin films such as crystal grain size and type of phosphor.

9.2.3 Luminescent Output of EL Devices

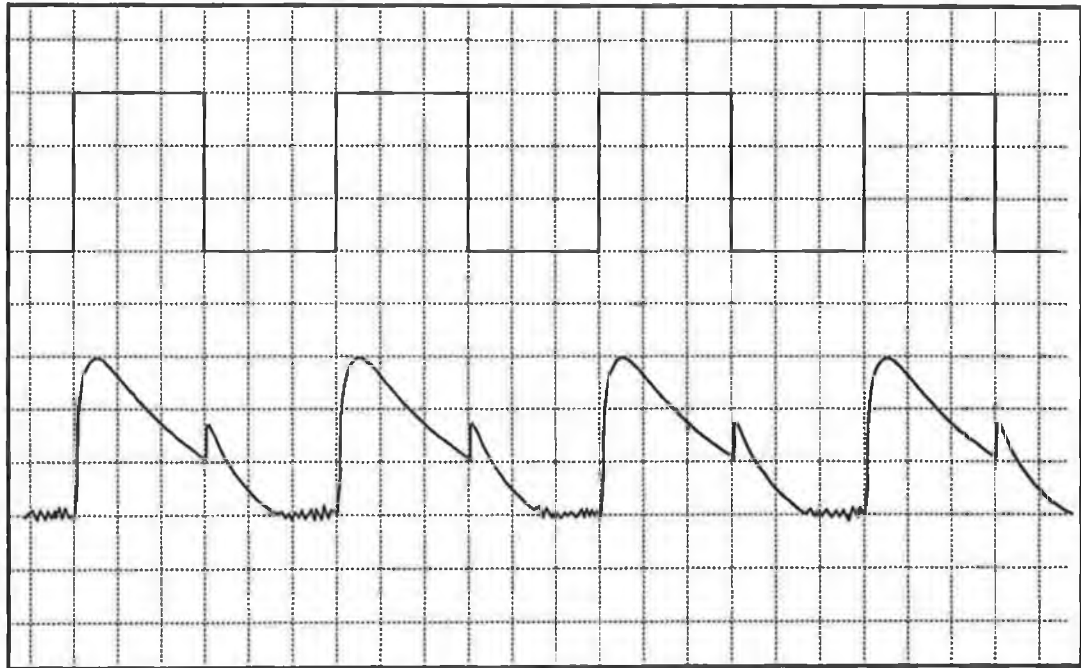

Figure 9-9 EL output waveform of EL devices.

Fig.9-9 shows the EL output waveform for the EL device. The excitation was done with a 100 Hz rectangular wave. As the polarity of applied voltage was changed, the leading edge of light emission changed abruptly. This is because the applied voltage causes the redistribution of internal electric filed, the electrons were injected, accelerated and impact luminescent centres under the applied voltage. The slow decay of light emission is considered to be due to reduction of internal field and electron speed and decrease of the number of electrons in active layer.

9.3 Characteristics of ZnS:Tb Thin Film EL Device

EL devices of ZnS thin film doped with rare earth ions to transition metal ions have been actively investigated in the past few years because they can yield various colours in the visible regions due to their internal transitions. Tb doped ZnS is the most promising phosphor after the ZnS:Mn film and produces green colour.

In my studies the EL device structures are Au/ZnS:Tb/Al_2O_3/Si or Au/ZnS:Tb/SiO_2/Si. The method of film deposition is the sol-gel process as described previously.

9.3.1 Emission Spectrum of ZnS:Tb EL Devices

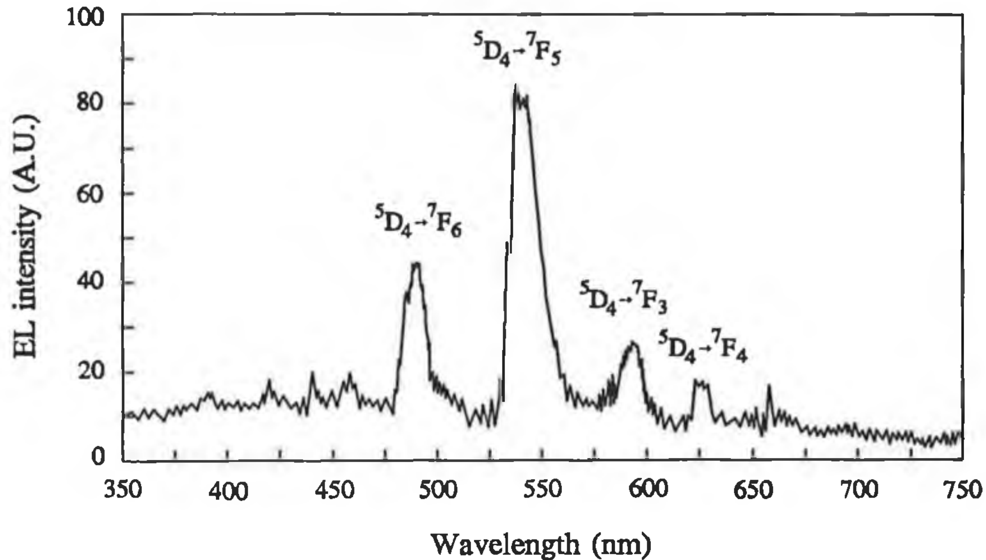

Figure 9-10 Electroluminescent emission spectrum of a ZnS:Tb EL device.

The EL intensity spectrum is shown in fig.9-19. Each peak of ~490 nm, ~542 nm, ~590 nm and ~625 nm corresponds to the transition of $^5D_4$-$^7F_6$, $^5D_4$-$^7F_5$, $^5D_4$-$^7F_4$ and $^5D_4$-$^7F_3$ respectively.

9.3.2 Applied Voltage-Brightness Relation of ZnS:Tb EL Devices

Fig.9-11 shows the typical luminance versus applied voltage characteristics of the ZnS:Tb devices with different insulators. The device with Al_2O_3 insulator has greater brightness and low threshold voltage than the device with SiO_2 insulator. This result is similar to that of the ZnS:Mn EL devices.

9.3.3 Tb Concentration-Brightness Relation

Fig.9-12 shows the dependence of the brightness on the Tb concentration of the devices with ZnS:Tb phosphor films. The Tb concentration of the ZnS:Tb devices varies 0.5-4 at.%. The applied voltage is 90v and the frequency is 1kHz. It is found that the brightness increases

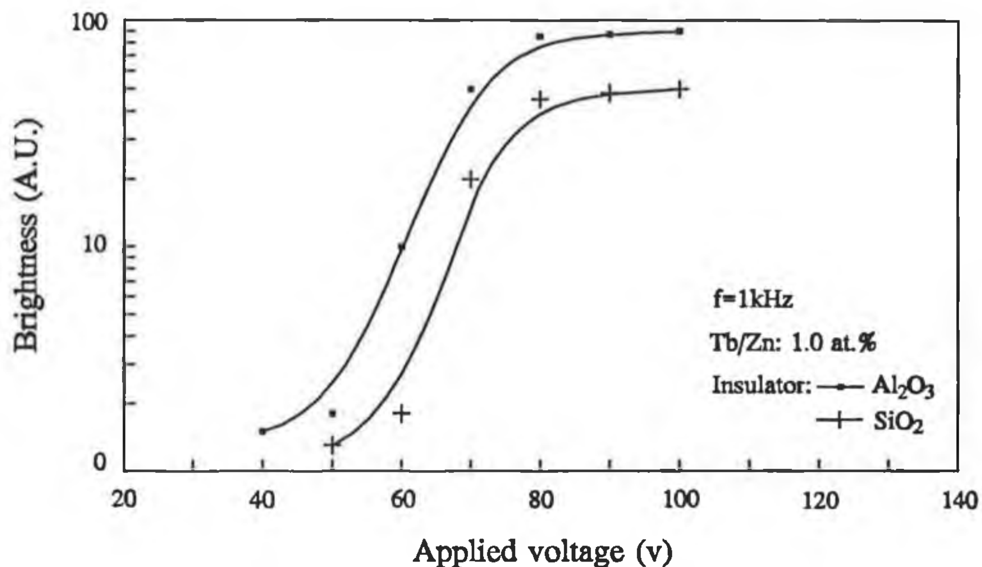

Figure 9-11 B-V characteristics of ZnS:Tb (Tb/Zn: 1.0 at.%) EL devices with Al_2O_3 or SiO_2 as insulator.

proportionally up to maximum around a Tb concentration region of ~1 at.%, and thereafter decreases gradually.

The interpretation of concentration is the difference geometric size and valence charge between Tb and Zn ion. The solubility of the Tb^{3+} ion in the ZnS is about 0.01 at.%, which is two orders of magnitude lower than the concentration to optimize the EL efficiency. It is, therefore, expected that when an excess of Tb is forced doped into ZnS film, lattice defects and impurity atoms are naturally produced to compensate the charge imbalance between Tb^{3+} and Zn^{2+} ions[220]. Consequently, various kinds of complexes are formed in the ZnS, and thus excitons are subject to nonradiative annihilation because of the poor crystal quality induced by the high density of imperfections.

9.3.4 Driving Frequency-Brightness Relation of ZnS:Tb EL Device

Fig.9-13 shows that relative brightness of ZnS:Tb thin film EL devices with Al_2O_3 insulating layer changes with applied voltage frequency. The brightness increases slowly up to maximum around 900 Hz, and thereafter decreases gradually. Similar results were obtained in measurement of brightness of EL devices with SiO_2 insulator.

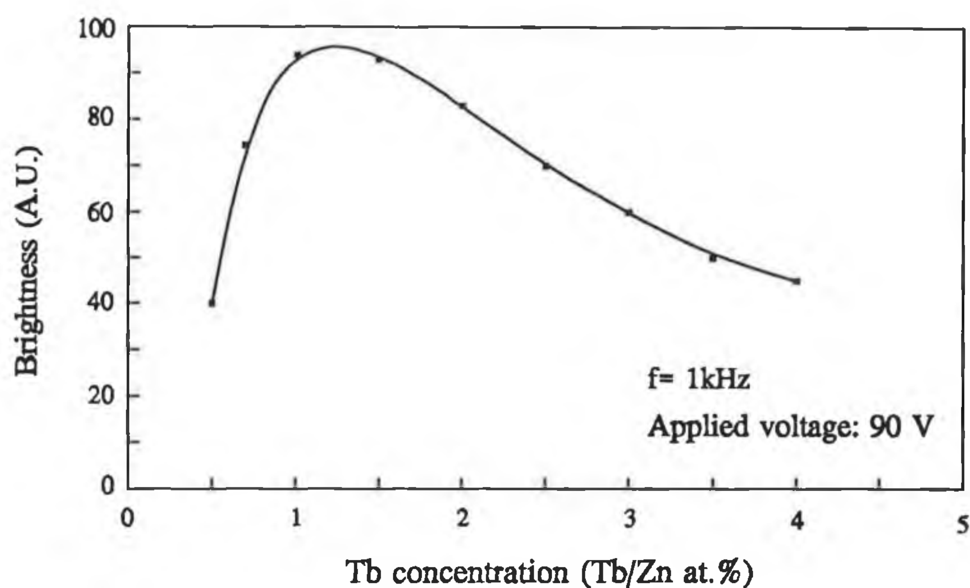

Figure 9-12 Relative EL brightness with Tb concentration of ZnS:Tb EL devices.

The structure of EL device and the properties of dielectric and phosphor films determine the brightness of EL devices since the capacitances of the device rely on the thicknesses of dielectric phosphor layers and properties of dielectric and phosphor layers.

9.4 Conclusions

Yellow light emitting ZnS:Mn films were prepared, which were converted from ZnO:Mn with heat treatment in H_2S. The ZnO:Mn films were deposited by the sol-gel process. Uniform films have been obtained with a Mn concentration in the sol-gel solution in the range of 0-7 at.%. The electroluminescent spectra showed emission peak at ~580-600 nm. It is proposed that this activation energy is associated with the energy required for a Mn atom to find and occupy a substitutional Zn site and form a Mn^{+2} luminescent centre. The dependence of the ~580-600 nm emission with the Mn concentration in the sol-gel solution is similar to that reported for films deposited by other techniques. The brightness of thin film EL devices is extremely dependent on the applied voltage in the lower voltage region, and tends to saturate in the higher voltage region. In this study, the electrical and optical performances of electroluminescent devices with Al_2O_3 and SiO_2 as an insulating layers were researched.

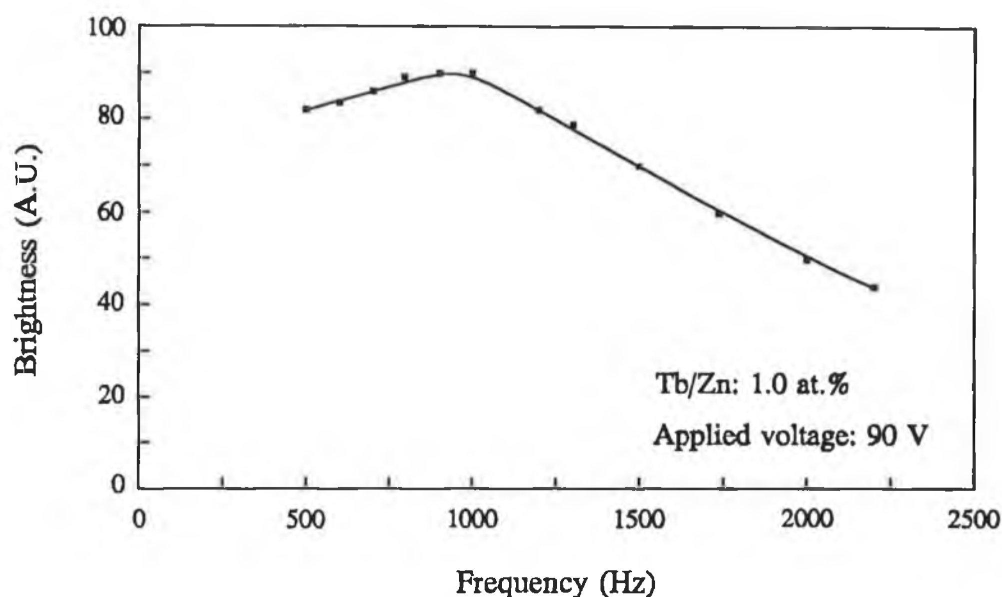

Figure 9-13 Relative EL brightness with applied frequency of ZnS:Tb EL device.

The brightness of EL devices with Al_2O_3 insulating film was greater than that with SiO_2 film in accordance with its higher electric constant. It was found that as the rise time of the applied waveform decreased the luminance of EL devices increased. The brightness increases initially with an increase in thickness of the active layer and then decreases with further increase of thickness. In the range of lower frequency, with an increase of frequency brightness increases. In the range of about 50-200 Hz the brightness is maximum. Brightness then decreases with further increase of frequency. The electroluminescent intensity initially increases as the Mn concentration increases and above certain concentrations (~1 at.% Mn in the solution), there is a quenching effect of the electroluminescence. This effect is similar to that reported to occur on samples deposited by other techniques[221].

The EL intensity Spectrum of ZnS:Tb film EL devices shows emission peaks at ~490 nm, ~542 nm, ~590 nm and ~625 nm. The results of typical luminance versus applied voltage characteristics of the ZnS:Tb devices with different insulator of Al_2O_3 or SiO_2 were obtained. The EL properties of the EL device with Al_2O_3 insulator present better than that with SiO_2 insulator. The brightness depends on Tb concentration of the devices with ZnS:Tb phosphor films. Tb concentration of the ZnS:Tb devices varies Tb/Zn 0.5-4.0 at.%. It is found that the

maximum brightness exits around a Tb concentration region of Tb/Zn ~1 at.%. The relative brightness of ZnS:Tb EL devices with Al_2O_3 insulating layer changes with applied voltage frequency. The EL device presents comparatively high brightness in the range of 500-1100 Hz, and in high frequency the brightness decreases gradually.

Chapter 10

CONCLUSIONS

10.1 Conclusions of the Work

The work described in this thesis has shown that the sol-gel technique is suitable for producing all the various layers necessary for producing an electroluminescent display. In order to complete the deposition of ZnS:Mn and ZnS:Tb phosphor films and ZnO:Al conducting film in the work the preparation of ZnO film was done. Solutions of ZnO precursor were made by dissolving zinc acetate ($Zn(CH_3CO_2)_2 2H_2O$) in anhydrous ethanol or methanol. The manganese acetate, terbium acetate, aluminium chloride and aluminium nitrate as dopant were added respectively into the solutions for preparing ZnS:Mn, ZnS:Tb and ZnO:Al films. It has been an demonstrated that transparent conductors of ZnO:Al can be produced, which achieve a minimum resistivity of $\sim 7\times10^{-4}$ Ω·cm when films with an Al content of Al/Zn 0.8 at.% are annealed at ~400°C in air and in vacuum. They also have high transmission of 90% in the visible region. The performance of these transparent conductors is similar to those produced conventionally by sputtering of indium tin oxide.

Electroluminescent films of ZnS have been produced by conversion of sol-gel deposited ZnO in an atmosphere of H_2S:H_2:N_2. It has been shown that complete sulphidation has taken place by structural and elemental analysis. These films can be doped with Mn and Tb to give a yellow and blue-green luminescence respectively. The maximum brightness occurred with a Mn content of Mn/Zn ~1.0 at.% and Tb content of Tb/Zn ~1.0 at.%. The results have shown that display structures using Al_2O_3 have a better performance than those using SiO_2 because of the higher dielectric constant of Al_2O_3.

These results demonstrated that a less expensive method of producing large scale electroluminescent displays is possible by using these techniques. This should allow the use of these displays for a wider range of purposes (eg. personal computer, TV, instrumentation panels, shop signs, etc.).

10.2 Future Work

Improvement and alternative of insulator material, conductor and dopant can lead to the improvement of EL device properties.

From the literature[222] some dielectric constants of materials are summarized in Table

10.1.

Titanium dioxide (TiO_2) has many interesting physical properties which make it suitable for thin film application, because of its good transmittance in the visible region, high refractive index and chemical stability. The high dielectric constant of TiO_2 (the largest ε among simple metal oxides) opens prospects for the use of TiO_2 thin films as insulators in EL displays. In order to prepare TiO_2 film, the solutions of doubly distilled titanium ethoxide ($Ti(OC_2H_5)_4$) or titanium butoxide ($Ti(OC_4H_9)_4$) in absolute alcohol with additional of a certain amount of water for hydrolysis and some HCl used as a catalyst are used.

Dielectric coating film consisting of ferroelectric crystal $BaTiO_3$ is useful as the film of high dielectric constant. $BaTiO_3$ can be prepared using mixtures of metal alkoxides and salts tend to be more complex due to the more facile hydrolysability of the alkoxides. Ti alkoxides and Ba acetate are used as precursors.

The transparent conducting films of In_2O_3 or SnO_2 doped with impurity can be deposited using the sol-gel technology and compared with the ZnO:Al films produced here. If the deposition of a transparent conductor is earlier than the deposition of insulating films and phosphor film in fabricating glass/ transparent conductor/ insulator/ active layer/ insulator/ Al conductor AC EL devices, the electrical properties can be measured with different temperature in air, in nitrogen or hydrogen sulphide to determine whether the film can be used in EL devices using the sol-gel process.

If the devices are manufactured using only the sol-gel process it is not easy. The mixture methods of sol-gel process with other deposition technologies should produce better AC EL devices. At same time, comparison of EL devices by various techniques may be done.

The suggested structure of the EL device is transparent conducting film / insulating film / phosphor film / insulating film / silicon substrate. As an electrode a silicon substrate can be

Table 10.1 Dielectric constants of some materials

Material	ε (1×10^6Hz)	Dielectric strength (V/cm)
Alumina	4.8-9.4	400-600
Titanates (Ba,Sr,Ca, Mg, and Pb)	12-12000	500-3000
Titanium dioxide	14-110	1000-2100

chosen because of its low resistivity. Al_2O_3, SiO_2, TiO_2 or $BaTiO_3$ can be deposited as an insulating film using the sol-gel process. ZnS:Mn or ZnS:Tb can be deposited as the phosphor film. SiO_2, TiO_2 or $BaTiO_3$ will be deposited as the insulating film in preference to the Al_2O_3 film, because the solvent of $Al(OR)_3$ is water which damages the ZnS:Mn film. The heat treatment should be carried out in nitrogen rather than oxygen may be necessary to prevent any influence on the ZnS phosphor film.

The above is only a suggestion and may not be realized experimentally. By these changes, which are based on the work carried out in this project, it may be possible to further improve the performance and case of manufacture of EL displays by the sol-gel process.

Appendix I

Boundary Layers[223]

In depositing film using the sol-gel process thickness of gel film is the most important parameter of deposited film. Most of the fluids possess relatively low viscosities, so that the Reynolds number $\varrho V_0 L/\eta$ of such flows, based on the approach velocity V_0, generally is quite high unless either the characteristic length L is very small or the flow velocity V_0 is very low. Reynolds number is probably the most important dimensionless parameter in fluid mechanics and presents the effects of viscosity on the flow. ϱ denotes fluid mass density, L denotes a characteristic length scale of the flow, V_0 denotes a typical flow speed and η is the coefficient of viscosity.

The flow at high Reynolds number implies that, at least over most of the flow field, inertial fluid forces are predominant over viscous forces; in other words, that the effect of viscosity is small over most of the flow field. However, at the fixed wall, the viscosity of the fluid causes the layer of fluid at the wall surface to stick to the wall; this layer of fluid has zero velocity relative to the surface. This boundary condition imposed on the flow, i.e., that the fluid velocity be equal to zero at the fixed surface, holds true for real fluids no matter how small the value of viscosity. Due to the shearing action of one fluid layer on the layer adjacent moving at a higher velocity, a velocity distribution is built up near the surface. It can be seen that large velocity gradients occur at the body surface; a small distance away from the surface, the flow velocity approaches asymptotically a free stream value.

It is thus possible, for the flow of low-viscosity fluids at high Reynolds numbers, to divide the flow field over a surface into two parts. The effects of viscosity can be confined to a thin layer in the vicinity of the surface, called the boundary layer. Outside the boundary layer, the flow can be treated as nonviscous. The method of dividing the flow has proven to be extremely useful in analysing the complex behaviour of real fluid flows. According to the method, the boundary layer is assumed thin enough so as not to affect the frictionless region of the flow. In fact, it can be assumed that there is no pressure variation in the direction normal to the surface in the boundary layer, so that the pressure variation throughout the boundary layer can be obtained from the frictionless flow solution outside the boundary layer. Flow in the boundary layer is in smooth layers, a particle of fluid in a given layer tending to stay in that layer. Flow in this portion of the boundary layer is laminar. Any slight

disturbance present in the flow is damped out by the action of viscous forces.

Shear stress in the laminar boundary layer is due to the sliding of one fluid layer over another. In this region of the flow, according to the definition of viscosity, shear stress τ_l is given by

$$\tau_l = \eta \frac{du}{dy} \quad \text{(I)}$$

In the following material, it will be assumed that the flow is steady and two-dimensional; that is, flow properties do not vary in the z direction. Furthermore, Incompressible flow (ϱ=constant), with no variation in physical properties such as η throughout the flow field. The latter assumption requires that significant temperature variations not be present in the flow. Gravitational forces is neglected. The radius of curvature of the body on which the boundary layer grows is assumed large enough so that centrifugal forces need not be taken into account (for a flat plate, the radius of curvature is infinite). Finally, the boundary layer will be assumed thin enough so that pressure does not vary in the direction normal to the wall surface.

Let x be the coordinate directed along the body surface, y the coordinate normal to the surface, with u the velocity component in the x direction and v the velocity component in the y direction.

For a steady flow, the continuity equation in the form is obtained

$$\frac{\partial u}{\partial x} + \frac{\partial v}{\partial y} = 0 \quad \text{(II)}$$

The momentum equation for steady flow is

$$\sum F = \iint V(\rho V \cdot dA) \quad \text{(III)}$$

or, in differential form,

$$\sum dF = V(\rho V \cdot dA) \quad \text{(IV)}$$

Momentum is a vector quantity. Therefore, for this two-dimensional flow, two momentum equations should be used, one in the direction and one in the y direction. However, as stated previously, the boundary layer is very thin; the velocity component in the y direction is very small in comparison with the velocity component in the x direction. In other words, the y

component of momentum is an order of magnitude less than the x component of momentum equation in the x direction.

Summing the forces in the x direction

$$\sum dF_x=(-\frac{\partial p}{\partial x}+\eta\frac{\partial^2 u}{\partial y^2})dxdy \qquad \textbf{(V)}$$

$$-\frac{\partial p}{\partial x}+\eta\frac{\partial^2 u}{\partial y^2}=\rho(u\frac{\partial u}{\partial x}+v\frac{\partial u}{\partial y}) \qquad \textbf{(VI)}$$

The equation is the momentum equation for the laminar boundary layer. In order to obtain a solution for flow in a laminar boundary layer, the equation must be solved in conjunction with the continuity equation.

The boundary conditions for the preceding equations are the following. At a fixed wall surface (y=0), the velocity components u and v are both equal to zero. At the outer edge of the boundary layer (y=δ), u approaches the free stream velocity V_0. The free stream velocity V_0 outside the boundary layer is given by the potential flow solution about the body in question. For a flow rate over a flat plate, the free stream velocity V_0 is constant along the plate; the Bernoulli equation for potential flow has the form

$$p_\infty+\frac{1}{2}\rho V_0^2=constant \qquad \textbf{(VII)}$$

so that there is no pressure variation outside the boundary layer.

According to the *Karman momentum integral method,* the momentum integral equation is derived.

$$\rho\frac{d}{dx}(\int_0^\delta u^2dy)-\rho U_\infty\frac{d}{dx}(\int_0^\delta udy)=-\delta\frac{dp}{dx}-\tau_0 \qquad \textbf{(VIII)}$$

where u and v are velocity components, p is pressure, ϱ is density of fluid, τ_0 is the fluid shear stress at the surface of a flat plate.

The equation constitutes the momentum integral equation. It is valid for both laminar and turbulent boundary layer flows.

According the boundary condition:

$u|_{y=0}=0$, $u|_{y=\delta}=V_0$,

$p=\varrho gx$, $dp=\varrho gdx$.

if

$$\tau_0=\eta(\frac{\partial u}{\partial y})_{y=0}=\eta\frac{V_0}{\delta} \quad \textbf{(IX)}$$

then

$$\frac{1}{6}\rho V_0^2\frac{d\delta}{dx}-\eta\frac{V_0}{\delta}+\delta g\rho=0 \quad \textbf{(X)}$$

we obtain the result:

$$\delta=(\frac{\eta V_0}{g\rho}(1-e^{-12\frac{g\rho}{V_0^2}x}))^{\frac{1}{2}} \quad \textbf{(XI)}$$

when V_0 is not too large and x increases:

$$\delta=\sqrt{\frac{\eta V_0}{g\rho}} \quad \textbf{(XII)}$$

Appendix II

High-voltage Drivers for EL Devices

In recent years, several types of flat display panels such as fluorescent indicator panels, plasma display panels or EL panels have been employed for miniaturization of equipment. For driving these panels, relatively high voltages and large currents are necessary. Therefore, hybrid ICs have so far been used as the drivers of these panels. However, along with the recent increase in the information density of display panels, driver circuit boards of lower cost, smaller size and simpler assembly have come to be required. To satisfy these requirements, monolithic driver ICs that have low-voltage logic circuits and multiple high-voltage output circuits have been developed[224],[225],[226].

High-voltage output circuits consists of high-voltage output stages and level shift circuits, which transfer the signals from low-level logic circuit to high-voltage output stage.

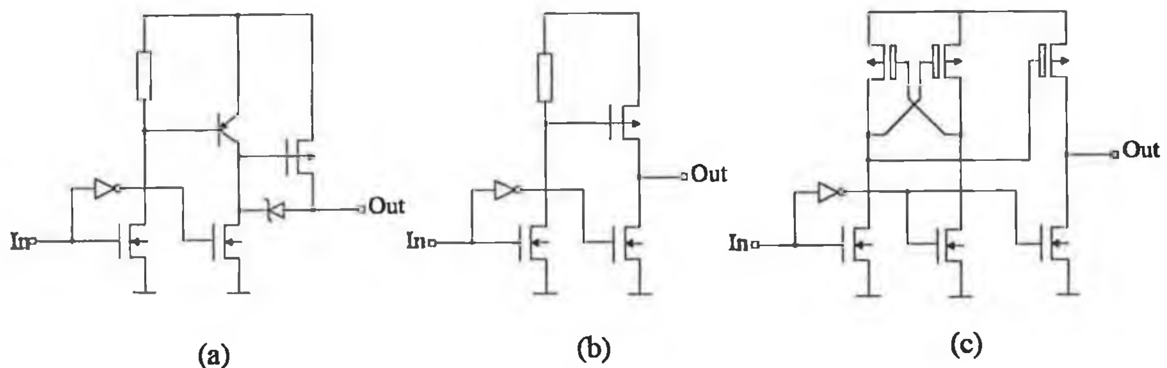

Figure I Several types of high-voltage output circuit construction.

Several types of high-voltage output circuit construction, which strongly depend on the device types, for example, a BiCMOS type output circuit, shown in fig.I (a), and a MOS type output circuit, shown in fig.I (b), have so far been used. Usage of a full complementary type level shift circuit, shown in fig.I (c), is effective to eliminate such static power dissipation and achieve high-speed operation. A problem is that the maximum rating of supply voltage is

limited at the gate oxide film dielectric breakdown voltage of PMOS because the PMOS gates in this type circuit are driven with high-voltage level equal to the supply voltage.

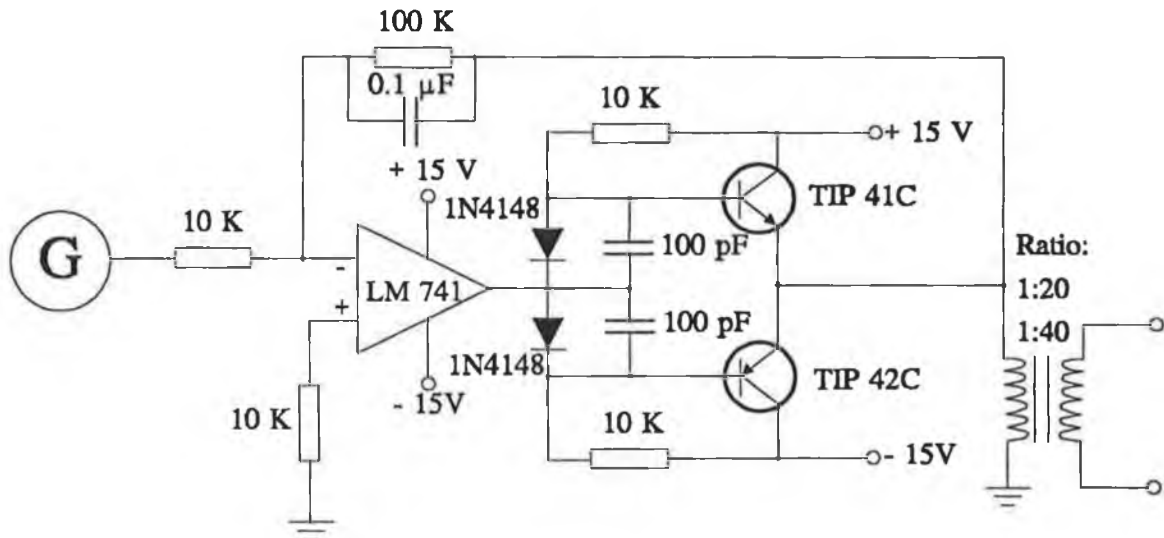

Figure II The amplifier circuit for high voltage.

A high voltage driver IC is the important device to determine the performance and the cost of EL display. With the recent progress in high voltage IC technology, a high voltage driver IC for EL display has been developed and put already practical use.

Fig.II is an amplifier circuit for the work reported here. The driving signal can be amplified to 20-50 times for driving the EL device.

Reference

1. *Society for Information Display 1988 Seminar Lecture,* vol. 1 and vol. 2.

2. T. Shinoda, *Optoelectronics-Devices and Technologies, 7* (1992) 231.

3. A. Sobel, *IEEE Trans. Plasma Sci., 16* (1991) 1032.

4. A. Mosley, *Displays, 14* (1992) 67.

5. K. Katoh et al., *Japan J. Appl. Phys. 26* (1987) 784.

6. T. Shinoda, M. Wakitani, T. Nanto, T. Kurai, N. Awaji, and M. Suzuki; *SID Symp. Digest,* (1986) 41.

7. T. Uchida, *Proc. 1st European display Res. Conf.,* (1981) 39.

8. T. Uchida, S. Yamamoto and Y. Shibata, *IEEE Trans. Electron Devices, 30* (1983) 503.

9. R.A. Perez, *Electronic Display Devices,* (1989).

10. G. Destriau, *J. Chem. Phys., 33* (1936) 620.

11. A. Vecht et. al., *Brit. J. Appl. Phys (J. Phys. D), 1* (1968) 620.

12. D. Kahng, *Appl Phys. Lett., 13* (1968) 210.

13. T. Inoguchi et. al., *74 SID International Symposium Digest,* (1974) 84.

14. C. Suzuki et. al., *74 SID International Symposium Digest,* (1974) 86.

15. *Proc. 6th Conf. of Solid State Devices (Tokyo),* (1974) 103.

16. R. Herrmann, G.O. Mueller and S. Sell, *Proc. of 5th International Workshop on Electroluminescence, Acta Polytechn. Appl. Phys. Ser. 170* (1990) 171.

17. S. Antonov and U. Sukharev, *Proc. of 5th Intern. Workshop on Electroluminescence, Acta Polytechn. Appl. Phys. Ser., 170* (1990) 127.

18. H. Kobayash, *Proc. of 6th intern. Workshop on Electroluminescence* (1992) 179.

19. A. Mikami, T. Ogura, K. Taniguchi, M. Yoshida and S. Nakajima, *J. Appl. Phys., 64* (1988) 3650.

20. N. Miura, H. Matsumoto and R. Nakano, *Jpn. J. Appl. Phys., 30* (1991) 288.

21. H. Matsumoto, S. Tanka and T. Yabumoto, *Jpn. J. Appl. Phys., 17* (1978) 1543.

22. K. Okamoto, T. Yoshimi and S. Miura, *J. Appl. Phys. 65* (1989) 1690.

23. R. Fukao, H. Fujikawa, M. Nakamura, Y. Hamakawa and S. Ibuki, *Proc. of the 4th Intern. Workshop on Electroluminescence,* Oct. 11-14, 1988.

24. K. Okamoto, T. Yoshimi, K. Nakamura, T. Kobayashi, S. Sato and S. Miura, *Jpn. J. Appl. Phys. 28* (1989) 1378.

25. P. Pleshko, *Proc. of 5th Intern. Workshop on Electroluminescence, Acta Polytechn. Scand., Ser. Appl. Phys., 170* (1990) 115.

26. R. Törnqvist, *Proc. of 5th International Workshop on Electroluminescence, Acta Polytechn. Appl. Phys. Ser. 170* (1990) 1.

27. H.A. Cole, *Basic Colour Television,* Oxford, New York, (1983).

28. G. Harkönen, K. Harkönen and R. Törnqvist, *SID 90 Digest,* (1988) 232.

29. R.T. Tuenge, *Proc. of the 6th Intern. Workshop on Electroluminescence,* May, 11-13 (1992) 173.

30. Y.A. Ono, *Proc. of 5th Intern. Workshop on Electroluminescence, Acta Polytechn. Appl. Phys. Ser., 170* (1990) 41.

31. J.M. Hurd, *Proc. of the 6th Intern. Workshop on Electroluminescence,* (1992) 3.

32. H. Dislich and E. Hussmann, *Thin Solid Films, 77* (1981) 129.

33. J.J. Ebelmen, *Ann., 57* (1846) 331.

34. W. Geffcken and E. Berger, *German Patent 736411* (may 1939).

35. H. Schroeder, *Phys. Thin Films, 5* (1969) 87.

36. C.B. Hurd, *Chem. Rev., 22* (1938) 403.

37. S.S. Kistler, *J. Phys. Chem., 36* (1932) 52.

38. R. Roy, *J. Am. Ceram. Soc., 39* [4] (1956) 145.

39. R, Roy, *J. Am. Ceram. Soc., 52* [6] (1969) 344.

40. R.M. Dell, *in Reactivity of Solids, eds.,* J.S. Anderson, M.W. Roberts, and F.S. Stone (Chapman and Hall, N.Y. 1972), 553.

41. J.L. Woodhead, *Silicates Ind., 37* (1972) 191.

42. L. Levene and I.M. Thomas, *U.S. Patent 3,640,093* (Feb. 8, 1972).

43. H. Dislich, *Angewandt Chemie, 10* [6] (1971) 363.

44. E. Wainer, *German Patent 1,249,832* (Apr. 11, 1968).

45. H.G. Sowman, *U.S. Patent 3,795,524* (Mar. 5, 1974).

46. S. Horikuri, K. Tsuji, Y. Abe, A. Fukui, and E. Ichiki, *Japanese Patent 49-108325* (Oct. 15, 1974).

47. B.E. Yoldas, *J. Mater. Sci., 10* (1975) 1856.

48. B.E. Yoldas, *J. Mater. Sci., 12* (1977) 1203.

49. M. Yamane, A. Shinji and T. Sakaino, J. *Mater. Sci., 13* (1978) 865.

50. R.H. Hopper and D.R. Uhlmann, *Mater. Sci. and Eng., 15* (1974) 137.

51. L.E. Scriven, *Better Ceramics Through Chemistry III,* eds. C.J. Brinker, D.C. Clark and D.R. Ulrich, (1988) 717.

52. L.E. Scriven, *Better Ceramics Through Chemistry III* eds. C.J. Brinker, D.E. Clark and D.R. Ulrich (1988) 717.

53. L.D. Landau and B.G. Levich, *Acta Physiochim, U.R.S.S., 17* (1942) 42.

54. J.H. Simmons, R.K. Mohr, and C.J. Montrose, *J. Appl. Phys., 53* (1982) 4075.

55. V. E. Cosslett, *Advances in Optical and Electron Microscopy, 10* (1988) 215.

56. L. de Broglie, *Compt. Rend., 177* (1923) 507.

57. T. E. Everhart and R. F. M Thornley, *J. Sci. Instrum., 37* (1960) 246.

58. R. Casting, Thesis, Univ. of Paris, France, 1948; *Advances in Electronics and Electron Physics, 13* (1960) 317.

59. K. F. J. Heinrich, *Electron Beam X-Ray Microanalysis,* Van Nostrand Rheinhold, New York, 1981.

60. K.F.J. Heinrich and E.D. Newbury, *Metals Handbook,* 9th Ed. (R.E. Whan, coord.), Am. Soc. Metals, Metals Park, OH, 10, (1978) 516.

61. C.E. Fiori and D.E. Newbury, *Scanning Electron Microscopy,* (1978) 401.

62. J.I. Goldstein, D.E. Newbury, P. Echlin, D.C. Joy, D.C. Fori, and E. Lifshin, *Scanning Electro Microscopy and X-ray Microanalysis,* Plenum, New York, 1984.

63. F. Wenner, *Bulletin of the Bureau of Standards, 12* (1915) 469.

64. L. B. Valdes, *Proc. IRE 42* Feb. (1954) 420.

65. J. Albers and H.L. Berkowitz, *J Electrochem. Soc., 132* (1985) 2453.

66. L.J. van der Pauw, *Phil. Res. Rep., 13* (1958) 1.

67. L.J. van der Pauw, *Phil. Tech. Rev., 20* (1958) 220.

68. R. Chwang, B. J. Smith and C.R. Crowell, *Solid-State Electron, 17* (1974) 1217.

69. R. A. Smith, *Semiconductors,* Cambridge University Press, Cambridge, (1959) Ch. 5.

70. A.C. Beer, *Galvanomagnetic Effects in Semiconductors,* Academic Press, New York, (1963) 308.

71. E.H. Hall, *Amer. J. Math., 2* (1879) 287.

72. R.A. Smiht, *Semiconductors,* Cambridge University Press, Cambridge, (1959) Ch. 5.

73. D. Kahng, *Appl. Phys. Lett., 13* (1968) 210.

74. H. Kohayashi, S. Tanaka, V. Shanker, M. Shiiki, T. Kunou, J. Mita and H. Sasakura, *Phys. Stat. sol. (a), 88* (1985) 713.

75. W.A. Barrow, R.E. Coovert and C.N. King, *1984 SID Intern. Symp. Degist Tech. Papers,* (1984) 249.

76. V. Shanker, S. Tanaka, M. Shiiki, H. Deguchi, H. Kobayashi and H. Sasakura, *Appl. Phys. Lett., 45* (1984) 960.

77. S. Tanaka, V. Shanker, M. Shiiki, H. Deguchi and H. Kobayashi, *1985 SID Intrn. Symp. Degist Tech. Papers,* (1985) 218.

78. K.H. Hellwege, O. Maelung, M. Schulz, H. Weiss, I. Broser, H. Landolt and R.E. Bornstein, *Semiconductors: Physics of II-VI and I-VII Compounds, Semiconducts, Semimagnetic Semiconductors,* Beilin, New York, Spring-Verlog (1982) 167.

79. O. Maelung, M. Schulz, W. Von der Osten, U. Rossler, H. Landolt and R.E. Bornstein, Semiconductors: *Instrinsic Properties of Group IV Elements and III-V, II-V and I-VII Compounds,* Berlin, New York, Spring-Verlog (1987) 61.

80. A. Fazzio, M.J. Caldas and A. Zunger, *Phys. Rev. B, 30* (1984) 3430.

81. S. Cotton, *Lanthanides and Actinides, Macmillan Physical Science Series* (1991) 29.

82. A. Mikami, T. Ogura, K. Tanaka, K. Taniguchi, M. Yoshita and S. Nakajima, *Jpn. Display, '86* (1986) 132.

83. J. Yu and Y. Shen, *J. Lumin., 40/41* (1988) 769.

84. D. Pier and K. Mitchell, *9th E.C. Photovoltaic Solar Energy Conf.*, 1989. 488.

85. J.F. Guillemoles, D. Lincot, P. Cowache and J. Vedel, *C.R. Acad. Sci. Paris, Ser. 11, 312* (1991) 1273.

86. S. Major, A. Baneerjee, K.L. Chopra and K.C. Nagpal. *Thin Solid Films, 143* (1986) 19.

87. R.M. White, P.J. Wicher. S.W. Wensel and E.T. Zellers. *IEEE Trans. Ultras. Ferroel. Freq.. Cont. UFFC, 34(2)* (1987) 163.

88. D.L. Polla, H. Yoon, T. Tamagawa and K. Voros, *IEEE Int Electron*. Der. Mtg., Washington, DC, (Dec. 1989) 495.

89. E.S. Kim and R.S. Muller, *IEEE Electron. Device Letters 8(10)* (1987) 467.

90. T. L. Tansley, D.I. Neely and C.P. Foley, *Thin Solid Films, 117* (1984) 19.

91. T. Minami, H. Nanto and S. Takata, *Thin Solid Films, 124* (1985) 43.

92. H. Watanable, *Jpn. J. Appl. Phys., 9* (1970) 43.

93. C.K. Lau, S.K. Tiku and K. M. Lakin, *J. Electrochem. Soc., 127* (1980) 1843.

94. P. J. Wright, R. j. M. Griffiths and B. Cockayne. *J. Cryst. Growth, 66* (1984) 26.

95. M. Tammenmaa, T. Oskinen, L. Hiltunen, M. Leskela and L. Niinesto, *Thin Solid Films, 124* (1985) 125.

96. R. R. nev'yantseva, T. D. Levitskaya, and B. I. Kidyarov, *Izv. Akad. Nauk SSSR, Neorg. Mater., 8, No. 3* (1972) 488.

97. R. C. Mehrotra, *Sol-gel Science and Technology Proc. of the Winter School on Glasses and Ceramics from Gels,* (14-19 Aug. 1989) 40.

98. J. E. A. John and W. L. Haberman, *Introduction to Fluid Mechanics, Pretice-Hell, Inc., Englewood Cliffs. New Tersey* (1980) 240.

99. L. E. Scriven, in C. J. Brinker, D. E. Clark and D. R. Ulrich (eds), *Better Ceramics Through Chemistry III, Materials Research Society, Pittsburgh, PA,* (1989) 717.

100. R. P. Spiers, C. V. Subaram and W. L. Wilkinson, *Chem. Eng. sci., 29* (1974) 389.

101. I. S. Semirikov, T. F. Tel'nykh, V. V. Kolchin, A. V. Vostretsova and G. S. Toropova, *Inorganic Materials, 20* (1990) 1251.

102. D. K. Schroder, *Semiconductor material and device characteristics, John Wiley & son, Inc.* (1990) 6.

103. F.R. Blom, F.C.M. Van De Pol, G. Bauhuis and TH.J.A. Popma; *Thin Solid Films, 204* (1991) 365.

104. F. Caillaud, A. Smith and J.F. Baumard; *J. of European Ceramic Society, 7* (1991) 379.

105. J. Volger, *Phys. Rev. 79* (1950) 1023.

106. R. L. Petriz, *Phys. Rev., 104* (1956) 1508.

107. L. L. Hench; *Science of Ceramic Chemical Processing;* (1986) 52.

108. B.E. Yoldas and T.W. O'Keefe, *Applied Optics, 25* [20] (1984).

109. C.J. Brinker and M.S. Harrington, *Solar Energy Mater., 5* (1983).

110. L.C. Klein, *12th Automotive Materials Conference,* University of Michigan. Ann Arbor, Michigan (1984).

111. B.E. Yoldas and T. W. O'Keefe, *Applied Optics, 18* (1979) 3133.

112. B.E. Yoldas and D.P. Partlow, *Thin Solid Films, 129* (1984) 1.

113. B.E. Yoldas and D.P. Partlow, *Applied Optics, 23* (1984) 1418.

114. B.E. Yoldas, *J. Mat. Sci., 10* (1975) 1856.

115. K. Badeker, *Ann. Phys., 22* (1907) 749.

116. E. Shanthi, A. Banerjee, V. Dutta and K.L. Chopra, *Thin Solid Films, 71* (1980) 237.

117. E. Shanthi, V. Dutta A. Banerjee and K.L. Chopra, *J. Appl. Phys., 51* (1980) 6243.

118. C.G. Fonstad and R.H. Redicker, *J. Appl. Phys., 42* (1971) 2911.

119. T. Arai, *J. Phys. Soc. Jpn., 15* (1960) 916.

120. A. G. Sabnis and L.D.Feisel, *J. Vac. Sci. Technol., 14* (1977) 685.

121. A. Rohatgi, T. Viverito and L.H. Slack, *J. Am. Ceram. Soc., 57* (1974) 278.

122. A.F. Carrol and L.H. Slack, *J. Electrochem. Soc., 123* (1976) 1889.

123. H.S. Randhawa, M.D. Matthews and R.F. Bunshah, *Thin Solid Films, 83* (1981) 267.

124. J.C. Manifacier, *Thin Solid Films, 90* (1982) 297.

125. E. Shanthi, A. Banerjee, V. Dutta and K.L. Chopra, *J. Appl. Phys., 53* (1982) 1615.

126. H.K. Muller, *Phys. Status Solidi, 27* (1968) 723.

127. J.C. Manifacier, L. Szepessy, J.F. Bresse, M. Perotin and R. Stuck, *Mater. Res. Bull., 14* (1979) 163.

128. V.I. Fistul and V.I. Vainshtein, *Sov. Phys.-Solid state, 8* (1967) 2769.

129. M. Mizuhashi, *Thin Solid Films, 76* (1981) 97.

130. F.A. Kroger, *Chemistry of Imperfect Crystals,* North-Holland, Amsterdam, (1964) Ch. 7, 16.

131. G. Heiland, E. Mollow and F. Stockmann, *Solid State Phys., 8* (1959) 193.

132. J.B. Webb, D.F. Williams and M. Buchanan, *Appl. Phys. Lett., 39* (1981) 640.

133. D.E. Brodie, R. Singh, J.H. Morgan, J.D. Leslie, L.J. Moore and A.E. Dixon, *Proc. 14th IEEE photovoltaic Specialists' Conf., San Diego, CA, 1980,* IEEE, New York, (1980) 468.

134. S.K. Ghandi, R.J. Field and J.R. Shelly, *Appl. Phys. Lett., 37* (1980) 449.

135. A.P. Roth and D.F. Williams, *J. Appl. Phys., 52* (1981) 6685.

136. J. Aranovich, A. Oritz and R.H. Bube, *J. Vac. Sci. Technol., 16* (1979) 994.

137. E. Shanthi, *Ph.D. Thesis,* Indian Institute of Technology, New Delhi, (1981).

138. A.P.Roth and D.F. Williams, *J. Appl. Phys., 52* (1981) 6685.

139. K.L. Chopra, S. Major and D.K. Pandya, *Thin Solid Films, 102* (1983) 1.

140. P. Petrou, R. Singh and D.E. Brodie, *Appl. Phys. Lett., 35* (1979) 930.

141. J.H. Morgan and D.E. Brodie, *Can. J. Phys., 60* (1982) 1387.

142. P.S. Nayar and A. Catalano, *Appl. Phys. Lett., 39* (1981) 105.

143. J.B. Webb, D.F. Williams and M. Buchanan, *Appl. Phys. Lett., 39* (1981) 640.

144. O. Caporaletti, *Solid State Commun., 42* (1982) 109.

145. H. Nanto, T. Minami, S. Shooji and S. Takata, *J. Appl. Phys., 55* (1984) 1029.

146. T. Minami, H. Nanto and S. Takata, *Jpn. J. Appl. Phys., 55* (1984) L280.

147. T. Minami, H. Nanto and S. Takata, *Thin Solid Films, 124* (1985) 43.

148. T. Minami, H. Sato, H. Nanto and S. Takata, *Jpn. J. Appl. Phys., 24* (1985) L781.

149. M. Ristov, R.J. Sinadinovski, I. Grozdanov and M. Mitreski, *Thin Solid Films, 124* (1985) 85.

150. O.F. Khan and P. O'Brien, *Thin Solid Films, 173* (1989) 95.

151. A.P. Roth and D.F. Williams, *J. Appl. Phys., 52* (1981) 6685.

152. R.D. Wieting and R.R. Potter, *US Patent 4,612,411.*

153. E. Shanthi, V. Dutt, A. Banerjee and K.L. Chopra, *J. Appl. Phys., 51* (1980) 6243.

154. J. Aranovich, A. Ortiz and R.H. Bube, *J. Vac. Sci. Technol., 16* (1979) 994.

155. C. Eberspacher, A.L. Fahrenbruch and R.H. Bube, *Thin Solid Films, 136* (1986) 1.

156. W.S. Lau and S.J. Fonash, *J. Electron. Mater., 16* (1978) 141.

157. J. Aranovich, A. Ortiz and R.H. Bube, *J. Vac. Sci. Technol., 16* (1987) 141.

158. S. Major and K.L. Chopra, *Sol. Energy Mater., 17* (1988) 319.

159. I. Hamberg and C.G. Granqvist, *J Appl. Phys., 60* (1986) R123.

160. G. Mahan, *Many Particle Physics,* Plenum, New York, (1981).

161. B.E. Sernelius, K.F. Berggren, Z. C. Jin, I. Hamberg and C.G. Granqvist; *Phys. Rev. B, 37* (1988) 10244.

162. B.E. Sernelius, *Phys. Rev. B, 36* (1987) 4878.

163. A.P. Roth, J.B. Webb and D.F. Williams, *Solid State Commun., 39* (1981) 1269.

164. T.S. Moss, *Proc. Phys. Soc. London B 67* (1954) 775.

165. E. Burstein, *Phys. Rev., 93* (1954) 632.

166. B.E. Sernelius, K.F. Berggren, Z.C. Jin, I. Hamberg and C.G. Granqvist, *Phys. Rev. B, 37* (1988) 10244.

167. D, Cossement and J. M. Streydio, *J. Cryst. Growth, 72* (1985) 57.

168. H. Kawamoto, R. Konnish, H. Harada, and H. Sasakura, *Springer Proceeding in Physics, Electroluminescence 38* (1989) 314.

169. T. Emma and M. McDonough, *J. Vac. Sci. Technol. A. 2* (1984) 362.

170. C. O. R. Mach, *Phys. Status Solidi A. 69* (1982) 11.

171. A. M. Ledger, *Appl. Opt. 18* (1979) 2979.

172. A. Preisinger and H. K. Pulker, *Jpn. J. Appl. Phys. Suppl. 2. Part 1* (1974) 769.

173. P. L. Jones, D. Moore and D. C. Smith, *J. Phys. E. 9* (1976) 312.

174. P. L. Jones. D. R. Cotton and D. Moore, *Thin Solid films. 88* (1982) 163.

175. W. L. Wolfe and G. J. Zissis, *The infrared Handbook, revised edition,* (1985) 7.

176. H. Kobayashi, S. Tanaka, V. Shanker, M. Shiiki, T. Kunou, J. Mita and H. Sasakura, *Phys. Solidi A 88* (1985) 713.

177. D. C. Morton, J. Koh, R. T. Lareau, R. I. Pleffer, S. Sun, S. Larach, M. Jusinki and C. Wrenn, *Proc. 9th Int. Display Res. conf., Kyoto,* (1989) 74.

178. T. E. Varitimos and R. W. Tustison, *Thin Solid Films, 151* (1987) 27.

179. S. Tanaka, S. Morimoto, K. Yamada, H. Kobayashi, Z. Zhang and X. Jiang, *J. Cryst. Growth, 117* (1992) 997.

180. S. Takata, T. Minami, T. Miyata and H. Nanto, *J. Cryst. Growth, 86* (1988) 257.

181. T. Shibata, K. Hirabayashi and H. Kozawaguchi, *Jpn. J. Appl. Phys., 26* (1987) L1664.

182. K. Hirabayashi and O. Kogure, *Jpn. J. Appl. Phys. 24* (1983) L484.

183. S. Fujita, T. Tomomura and A. Sasaki, *Jpn. J. Appl. Phys., 22* (1983) L583.

184. M. Tammenmaa, M. Leskelä, T. Koskinen and L. Niinitö. *J. Less-Commom Met. 126* (1986) 209.

185. Y. F. Nicolau and J. C. Menard, *J. Cryst. Growth, 92* (1988) 128.

186. Y. F. Nicolau, Mupuy and M. Brunel, *J. Electrochem. Soc., 137* (1990) 2915.

187. T. Maruyama and T. Kawaguchi, *Thin Solid Films, 188* (1990) 323.

188. R. D. Pick, H. Cui, R. Kershaw, K. Dwight and A. Wold, *Thin solid Films, 224* (1993) 221.

189. R. C. Weast, *CRC Handbook of Chemistry and Physics, 56thed.,* (1975) B-159 and E-129.

190. J. A. Dobrowolski, F. C. Ho and A. Waldrof, *Appl. Opt., 22* (1983) 3191.

191. A. K. Arora and A. Mansingh, *J. Phys. D 24* (1991) 1462.

192. A. Mikami, T, Ogura, K. Taniguchi, M. Yoshida and S. Nakajima; *J. Appl. Phys., 64* (1988) 3650.

193. G. Destriau, *J. Chem. Phys., 33* (1936) 620.

194. S. Tanaka el.al., *SID Degist,* (1988) 293.

195. J.W. Allen, *J. Lumin. 48 & 49* (1991) 18.

196. H. K. Henisch, *Electroluminescence,* Pergamon Press, Oxford, (1962) Sec. 1.3.1.

197. R.M. Hill, *Thin solid Films, 1* (1969) 39.

198. G. Vincent, A. Chantre and D. Bois, *J. Appl. Phys., 50* (1979) 5484.

199. R. Mach and G.O. Müller, *Phys Status Solidi, A 81* (1984) 609.

200. R. Mach and G.O. Müller, *Phys. Stat. Sol., (a) 81* (1984) 609.

201. J.W. Allen, *Proc. of the 4th Intern. workshop on Electroluminescence,* Oct. 11-14 (1988) 10.

202. R. Nitsche, *J. Cryst. Growth, 9* (1971) 238.

203. K.W. Yang, S.J.T. Owen and D.H. Smith, *IEEE Trans. Elec. Dev. ED-28* No. 6 (june 1981).

204. R. Tornqvist, *J. Appl. Phys. 54* (1983) 4110.

205. M. Katiyar and A.H. Kitai, *J. Lumin. 46* (1990) 227.

206. H.E. Gumlich, *J. Lumin. 23* (1981) 73.

207. N.A. Vlasenko, *Opt. Spect., 18* (1965) 260.

208. N.A. Vlasenko and A.M. Yaremko, *Opt. Spect., 18* (1965) 263.

209. N.A. Vlasenko, S.A. Zynio and Y.V. Kopytko, *Phys. Stat. Sol., (a) 29* (1975) 671.

210. J.J. Hanak, *Proc. 6th Intern. Vacuum Cong.,* Kyoto (1974) 809.

211. M.J. Russ and D.I. Kennedy, *J. Electrochem. Soc., 114* (1967) 1066.

212. T. Inoguchi, M. Takeda, Y. Kakihara, Y. Nakata and M. Yoshida, *74 SID Intern, Symp. Digest,* (1967) 84.

213. M. Takeda, Y. Kakihara, M. Yoshida, M. Kawaguchi, H. Kishishita, Y. Yamauchi, T, Inoguchi and S. Mito, *75 SID Intern, Symp., Sec. 7.8* (1975).

214. L.L. Hope, *Proc. of Intern. Workshop on Electroluminescnece,* Oct. 11-14 (1988) 246.

215. C.T. Hsu, J.W. Li, H. Liu, Y.K. Su and T.S. Wu, *J. Appl. Phys., 71* (1992) 1509.

216. C.G. Mueller, *Proc. of the 5th Intern. Workshop on Electroluminescence* Espoo Finland, Jun. 11-13, (1990) 13.

217. V.P. Singh, S. Krishna and D.C. Morton, *J. Appl. Phys., 70* (1991) 1811.

218. D.C. Krupka, *J. Appl. Phys., 64* (1972) 476.

219. E. Bringuier and A. Geoffroy, *Appl. Phys. Lett., 48* (1986) 1780.

220. A. Mikami, T. Ogura, K. Taniguchi, M. Yoshida and S. Nakajima; *J. Appl. Phys., 64* (1988) 3650.

221. H. Matsumoto, S. Tanaka and T. Yabumoto, *Jpn. J. of Appl. Phys., 17* (1978) 1543.

222. *Physical Properties of Materials for Engineer, Vol.3,* 214.

223. J.E.A. Jone and W.L. Haberman. *Introduction of Fluid Mechanics,* Prentice-Hall, Inc., Englewood Cliffs. New Tersey (1980) 240.

224. E. Habekotte, et al. *IEEE J., SC-16* (1981) 212.

225. H. Sakuma, et al., *86 SID Intern, Symp. Digest,* (1986) 184.

226. H. Hayama, et al., *IEEE CICC '87,* (1987) 431.